**Design of Lateral Support for Non-Integral Wing Walls of Culverts**

by

Herman Lester Lee, III

A thesis submitted to the Graduate Faculty of
Auburn University
in partial fulfillment of the
requirements for the Degree of
Master of Science

Auburn, Alabama
December 16, 2017

Keywords: culverts, earth pressure, instrumentation, LRFD design



Approved by

J. Brian Anderson, Co-Chair, Associate Professor of Civil Engineering
Robert W. Barnes, Co-Chair, Associate Professor of Civil Engineering
James S. Davidson, Professor of Civil Engineering

## Abstract

Traditionally, culverts are built with integral wing walls. This style of culvert has shown consistent issues at the joint where the wing wall frames into the culvert bodies due to differential settlement and inadequate reinforcement for the stresses that accumulate at this location. For the purpose of this study, three culverts were constructed utilizing a design in which the wing walls were completely separated from the culvert barrels and laterally supported by a tab that extends from the culvert.

During construction, each tab was instrumented with vibrating wire earth pressure cells to monitor the pressure that was induced within the tab. The wing walls were also instrumented to monitor movement relative to the culvert. This data was used to develop an LRFD design procedure that suggests a design load based upon the dimension of the wing wall along with the height and soil properties of the backfill.

Based upon their geometry and suspected loading conditions, it was suggested that the tabs extending from the culvert be designed as corbels in the manner laid out in the AASHTO LRFD Bridge Design Specifications. This suggestion was validated following a year of data collection at the three culvert sites. The observations made through this period also allowed for the conclusion that the studied culvert design was effective at mitigating the issues that occur when constructing the wing wall monolithically with the culvert.

## Acknowledgements

First and foremost, I would like to thank my incredibly supportive family, without whom I would not have been able to muster the drive to complete this undertaking. I would also like to thank my exceedingly patient and accommodating advisors, Dr. Anderson and Dr. Barnes, who worked with me for much longer than anticipated to get this research wrapped up and this thesis completed. A heartfelt “thank you” also goes out to the many friends, professors, and classmates who created a wonderful environment for me at Auburn to make my 7 years here some of the best of my life.

## Table of Contents

## List of Tables

## List of Figures

## List of Abbreviations

| | |
|---|---|
| AASHTO | American Association of State Highway and Transportation Officials |
| ALDOT | Alabama Department of Transportation |
| Caltrans | California Department of Transportation |
| DEMEC | Demountable mechanical concrete strain gauge |
| FHWA | Federal Highway Administration |
| LRFD | Load and Resistance Factor Design |
| NHI | National Highway Institute |

# CHAPTER 1: INTRODUCTION

## 1.1 Introduction

Traditionally, cast-in-place reinforced concrete box culverts are built integrally with their wing walls resulting in a monolithic structure. While this design is expedient due to being less formwork intensive, it results in a concentration of stress where the wing wall joins the culvert. As the structure settles, the difference in weight as well as bearing area of the two components leads to a differential settlement between the culvert barrels and the wing walls. This differential settlement, which can be exacerbated by scour, poor construction, and the out-of-plane flexibility of the wall, causes a moment to occur at the aforementioned concentration of stress. To explain this, the wing wall is considered to be a cantilevered beam which transfers moment to the body of the culvert. The flexure which results from the differential settlement creates tensile stresses in the extreme fibers which, in turn, lead to cracking, as shown in Figure 1-1. Depending on which element settles more quickly, this distress can occur at either the bottom or top of the junction and proliferate from there. This cracking reduces the effective cover of the reinforcement and can lead to a host of issues, such as corrosion, spalling, and in extreme cases, failure of the wing wall.

**Figure 1-1: Distress at Wing Wall Connection to Culvert (Minton, 2012)**

In order to mitigate this recurring problem, an alternative design, shown in Figure 1-2 and Figure 1-3, was proposed by Alabama Department of Transportation (ALDOT). In the proposed design, the wing wall is entirely separated from the culvert and supported on its own foundation. This allows for the two components to settle and deflect independently, eliminating the issues associated with differential settlement. To ensure the two structural elements continued to perform jointly in resisting the loads associated with backfill, a tab was added to each corner of the body of the culvert to serve as a horizontal bearing support for the wing walls. In this way, the wing walls still benefit from the lateral stiffness of the culvert, but restraint is removed from what was previously a concentration of stress. The result is a decrease in the probability of significant cracking, meaning a design with improved durability and longevity.

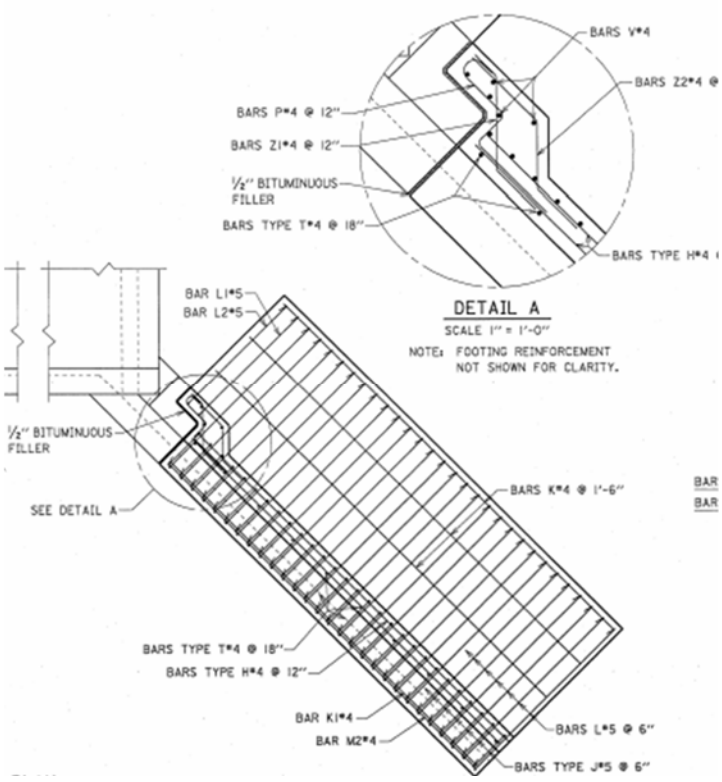


**Figure 1-2: Proposed Wing Wall Detail**

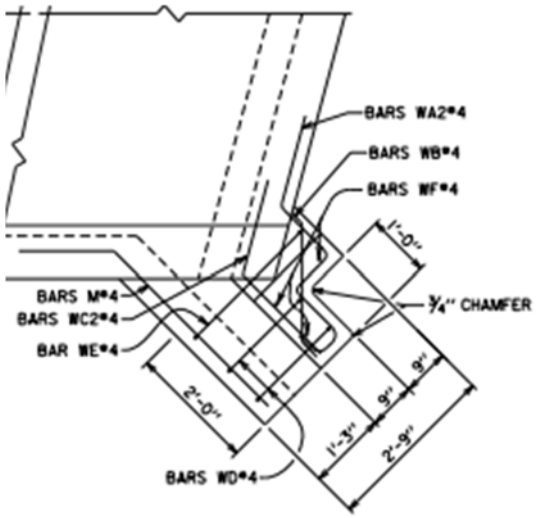


**Figure 1-3: Proposed Tab Detail**

## 1.2 Objective and Scope

The objective of this research project was to develop a recommended design procedure for the culvert tabs based on both the field observation of stresses induced within the tabs and the predictions of analytical computer models.

The scope of work encompassed in this thesis is as follows:

- Review of the existing literature related to both the stresses in culvert wing walls and their causes.
- Material testing of the concrete used for each culvert to determine representative moduli of elasticity and further refine the accuracy of the analytical computer models.
- Installation of earth pressure cells within the culvert tabs during construction to measure the resulting loads.
- Measurements of the pressure cells recorded periodically to detect patterns and determine representative magnitudes of load.
- Monitoring of gap width between the culvert tab and wing wall to track movement in two axes.
- Development of a design procedure to aid in the tab design of future culverts built in this manner.

# CHAPTER 2: BACKGROUND AND LITERATURE REVIEW

## 2.1 Overview

As stated in the research proposal, titled "Culvert Wing Tab Design Loads" and submitted to ALDOT by the Department of Civil Engineering at Auburn University in January of 2013, there is a dearth of published studies regarding the loading of culvert wing walls. As such, the goal of this literature review was to take a holistic approach toward understanding the various elements that must be considered as contributing factors to said loading. Furthermore, relevant background information was provided to add context to the purpose of this research study and introduce the thinking that went into the selection of procedures used.

This section is organized as follows:

First, culverts are discussed in general, with an explanation of their purpose and component parts, as well as a discussion on the justification for this research project. Because this research is focused solely on concrete culverts, this is followed by a discussion of concrete, with an emphasis on its various failure mechanisms. Then, as it is the primary source of the loading on wing walls, an explanation of earth pressure and the way its magnitude is estimated and measured is provided. Next, because the design procedure proposed in this thesis models the culvert tabs as corbels, a brief introduction to corbels is provided. Finally, a discussion of the rationale behind the LRFD factors chosen for the proposed design procedure is given.

## 2.2 Culverts

The Federal Highway Administration (FHWA) publication, *Hydraulic Design of Culverts*, defines a culvert as "a conduit which conveys stream flow through a roadway embankment or past some other type of flow obstruction." Because the hydraulic considerations in the design of a culvert allow for more substantial headwater than when designing a bridge, culvert installations typically feature a smaller opening than would a bridge in the same location, as illustrated in Figure 2-1. While the smaller opening allows for a smaller structure overall, it also raises concerns over potential debris and the passage of aquatic organisms that must be considered in the design of the culvert. The allowance of headwater also leads to concerns about potential flood damage (Schall, Thompson, Zerges, Kilgore, & Morris, 2012).

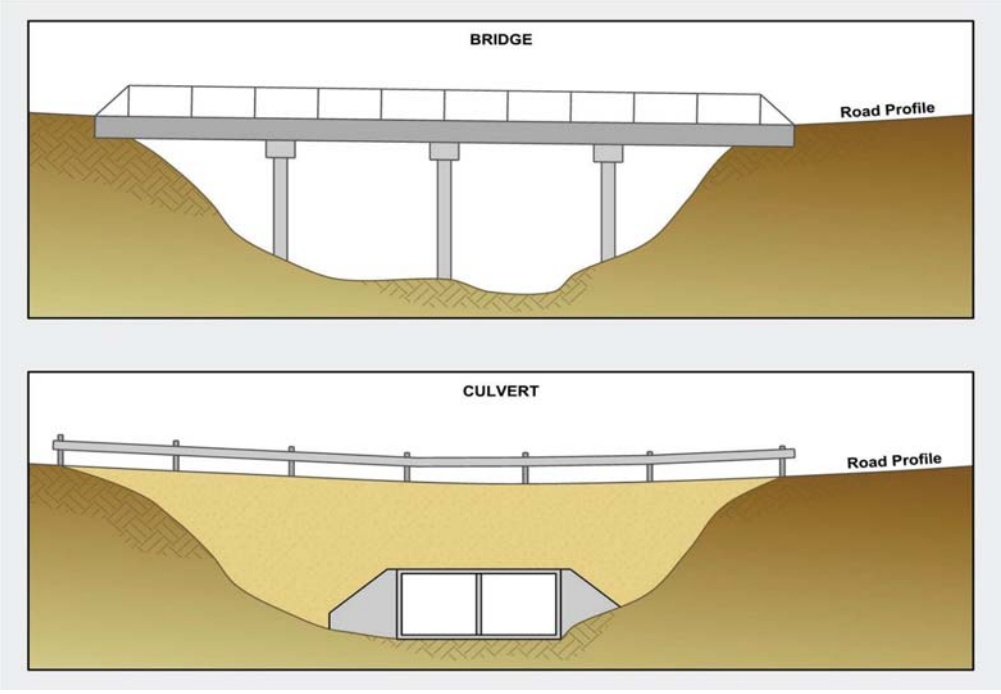


**Figure 2-1: Bridge versus Culvert (Schall, Thompson, Zerges, Kilgore, & Morris, 2012)**

If the considerations at a given location allow for the use of a culvert, however, the culvert tends to be the more economical option. This is due to both the construction and maintenance costs of culverts being less, in general, than they are for comparable bridges. It is important to note that the National Bridge Inspection Standards (NBIS) considers culverts that extend beyond 20 feet in span length to be bridges for the purposes of maintenance, which means that at this span length, some of the relative economy of a culvert over a bridge is lost (Schall, Thompson, Zerges, Kilgore, & Morris, 2012).

### 2.2.1 Culvert Materials

Culverts come in many variations and are thus adaptable to many applications. According to Schall, et al. (2012), the primary materials used for culvert construction are: "concrete (both reinforced and non-reinforced), corrugated metal (aluminum or steel), and plastic (high-density polyethylene [HDPE] or polyvinyl chloride [PVC]." Historically, materials such as clay, stone, or wood were also used, but this practice is much less common today. Typically, culverts are made entirely of one material. The selection of this material depends heavily on the required strength, cost of construction, and various hydraulic performance considerations (Schall, Thompson, Zerges, Kilgore, & Morris, 2012).

### 2.2.2 Culvert Shapes

While culverts are constructed in many varied shapes, these shapes are broadly divided into two main categories: closed conduit and open-bottom. Typical cross sections for closed conduit culverts are shown in Figure 2-2 while typical cross-sections for open-bottom culverts are shown in Figure 2-3.

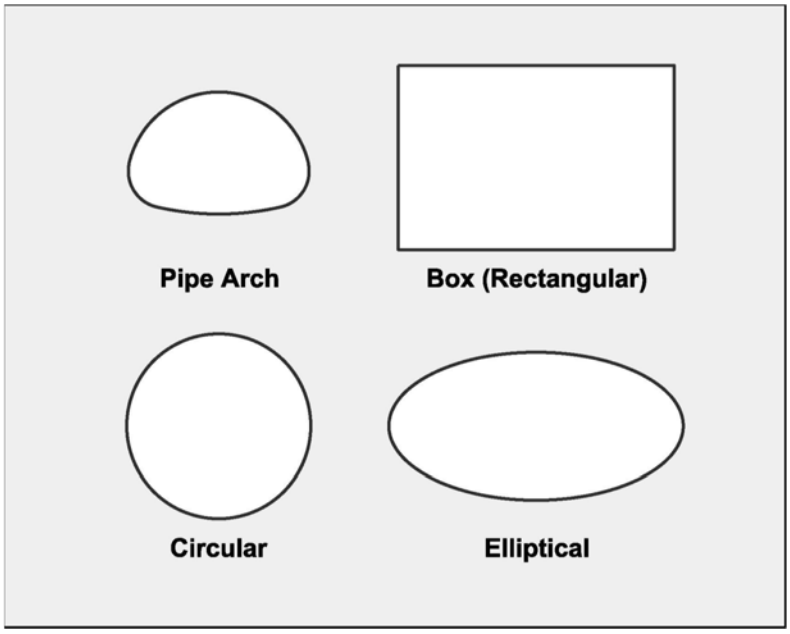


**Figure 2-2: Commonly Used Closed Conduit Shapes (Schall, Thompson, Zerges, Kilgore, & Morris, 2012)**

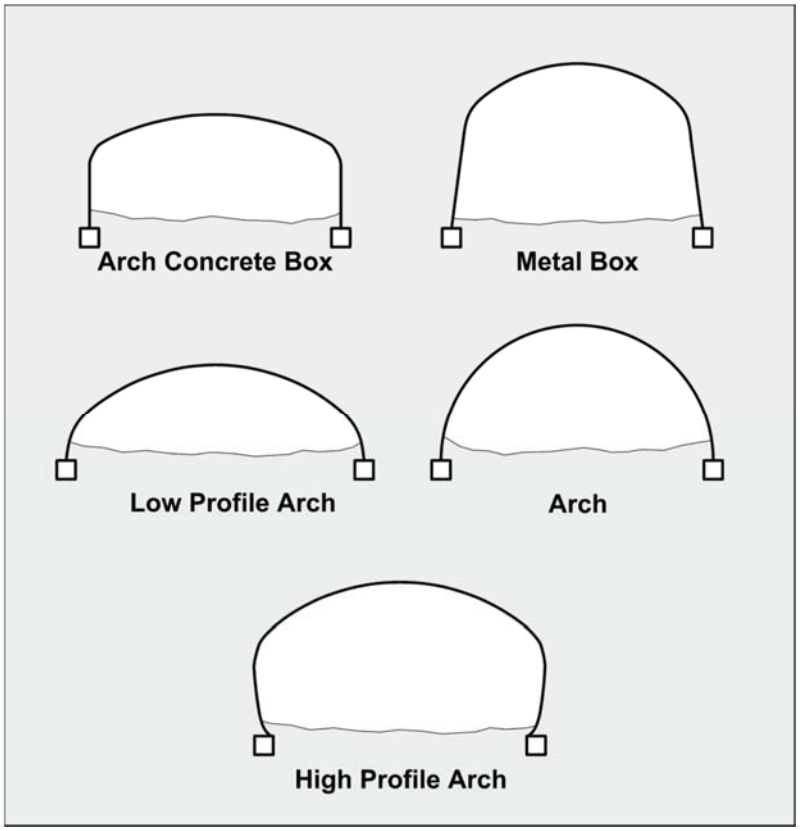


**Figure 2-3: Commonly Used Open-Bottom Shapes (Schall, Thompson, Zerges, Kilgore, & Morris, 2012)**

### 2.2.3 Reinforced Concrete Box Culverts

The three culverts constructed for the purpose of this research study were all cast-in-place reinforced concrete box culverts and therefore discussion of this type of culvert will be the focus of the remainder of this section. Information on the actual constructed culverts is found in CHAPTER 3: Constructed Culverts.

The primary components of a cast-in-place reinforced concrete box culvert are shown in Figure 2-4, which serves to provide context for the nomenclature used throughout this thesis.

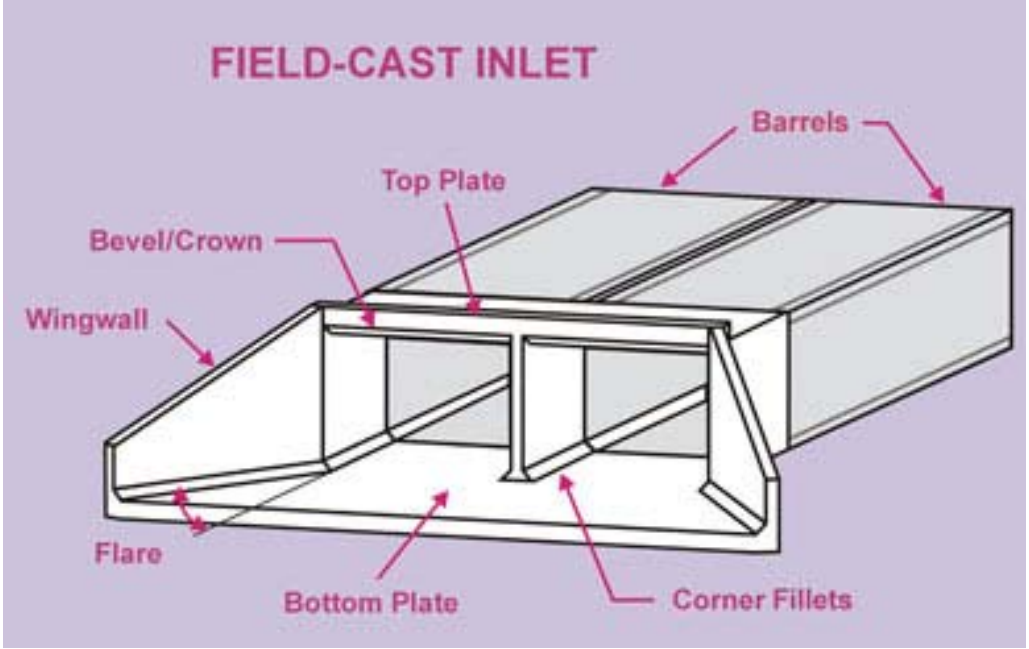


**Figure 2-4: Components of a Box Culvert (Kerenyi, Jones, Goeden, & Oien, 2005)**

#### 2.2.3.1 Wing Walls

Culvert barrels are typically narrower than the channel the culvert spans. This contraction of flow results in a loss of energy for the flow which can lead to the buildup of sediment at the culvert inlet, as well as potential damage to the culvert from other hydrological consideration. To address this, wing walls, shown in Figure 2-4, are typically constructed with a flare, or angle, relative to the path of travel of the culvert barrels. This flare, as well as the beveling of corners, makes the contraction of flow more gradual and, thus, reduces the aforementioned effects. The wing walls also serve as retaining walls that maintain the integrity of the subgrade for any roadway that passes over the culvert, as well as prevent backfill from obstructing the barrels of the culvert. (Schall, Thompson, Zerges, Kilgore, & Morris, 2012). If no flare is used, these walls are then referred to as head walls at the inlet of the culvert and end walls at the outlet. This is more typical for when

the culvert sits well below the finished grade of the roadway (Center for Dirt and Gravel Road Studies, 2004).

Figure 2-5 shows the appropriate terminology for the component parts of wing walls that are used throughout this thesis. The wing walls in this project were designed as long-heeled cantilever retaining walls, meaning the heel extends further than the toe.

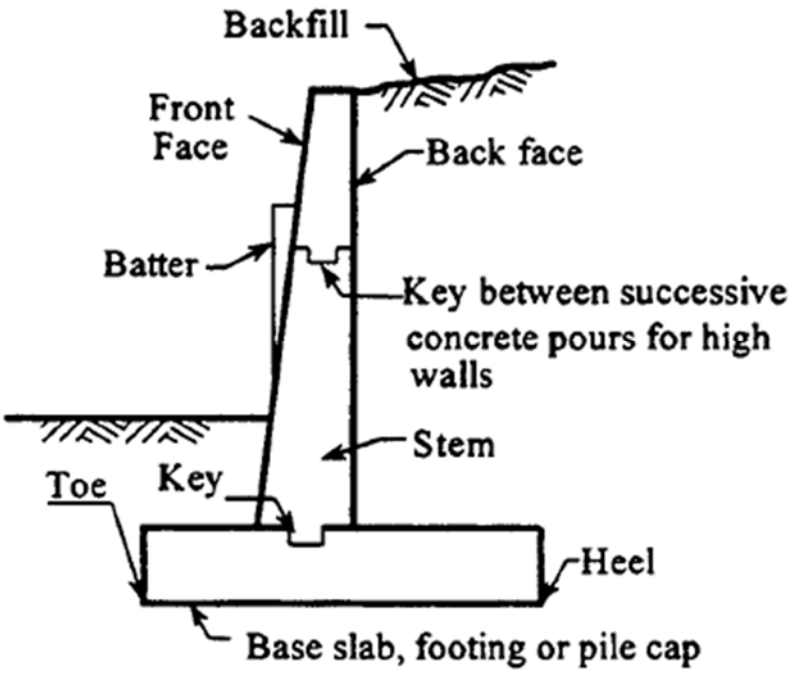


**Figure 2-5: Component Parts of a Cantilever Wing Wall (FHWA, 1999)**

#### 2.2.3.1.1 Non-Integral Wing Walls

The culverts constructed for the purpose of this project differ from the norm in that the wing walls were not placed integrally with the barrels of the culvert. Unlike cast-in-place culverts, precast culverts are segmented and assembled on site. As such, the wing walls in precast culverts are similarly not placed integrally; thus, some states have codes that provide guidance regarding the method of connection for wing walls to barrels. An evaluation of precast box culvert systems

performed by the University of Florida provided a review of these state specifications. Given below is a brief summary of some pertinent state requirements for non-integrally placed wing walls taken from the aforementioned evaluation (Cook & Bloomquist, 2002).

- Kansas requires all flared wing walls to be cast-in-place and have a special cast-in-place section for transition to the precast sections, although no explanation of the details of this transition is given.
- Louisiana uses standalone cast-in-place head walls with their precast culverts although no insight is given into the use of flared wing walls.
- Missouri requires that end components be integral with the barrels of the culvert
- Nevada requires that all end components be cast-in-place and mechanically connected to the barrels with dowels.
- Pennsylvania requires cast-in-place end components to be mechanically connected to the barrels with dowels.
- Tennessee requires cast-in-place end components to be mechanically connected to the barrels with dowels.
- Washington requires that all end components be mechanically attached to the barrels.

The above summary highlights that, even among culverts with non-integral wing walls, the three culverts constructed for this project were novel in that no mechanical connection to the barrels of the culverts was provided.

#### 2.2.3.1.2 Causes of Distress in Wing Walls

The impetus for this project was the frequent distress seen in wing walls at the location where they frame into the culvert barrels. A master's thesis by Minton (2012) discussed a thorough survey

of the box culvert crack conditions in the state of Alabama which concluded that the intersection of the culvert barrels and wing walls should be redesigned in order to mitigate the cracking at this location.

Ahmed, et al. (2002) found that soil settlement is the largest factor that leads to cracks in culverts. Figure 2-6 depicts how settlement can lead to damage in concrete structures. Figure 2-7 shows how differential settlement of the wing wall and culvert can lead to distress at the wing wall support. The dotted line in this figure represents he original location of the wing wall prior to settlement. As previously stated, the disparity of the masses of the culvert and wing walls, coupled with the difference in bearing areas, leads to a potential for differential settlement. This causes a concentration of stresses at the juncture of the culvert and wing walls, as well as throughout the wing walls. This is exacerbated by the disparity between the flexibility of the two members, as this juncture restrains the wing walls tendency toward out-of-plane deflection.

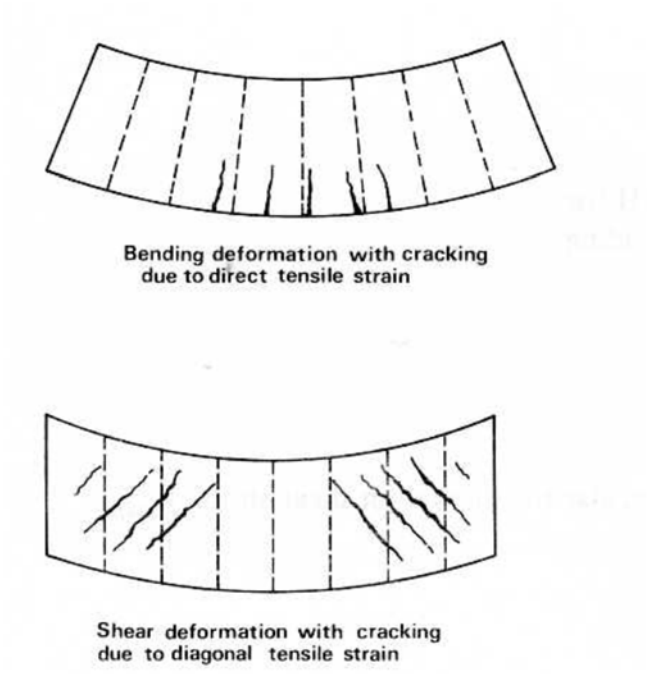


**Figure 2-6: Structural damage due to settlement (Burland & Wroth, 1974)**

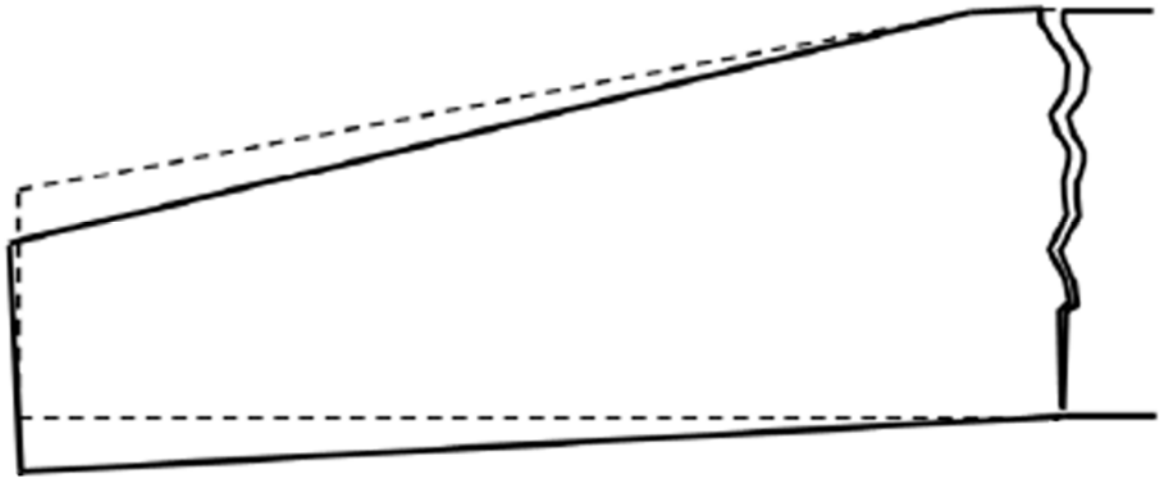

**Figure 2-7: Distress in support of wing wall (Minton, 2012)**

The separation of the wing wall and culvert through their foundation allowed for the free rotation of the wing walls with respect to the culvert. This removal of the restriction on motion alleviated the stresses associated with differential settlement as well as any possible stresses from drying shrinkage.

## 2.3 Concrete

Concrete is defined as "a hard strong building material made by mixing a cementing material (as Portland cement) and a mineral aggregate (as sand and gravel) with sufficient water to cause the cement to set and bind the entire mass" (Merriam-Webster, 2016). The final product of this mixture resembles a rocklike substance with significant strength in compression, but much lower tensile strength. Due to this tensile weakness, in most structural applications it is necessary to supplement the concrete with mild steel reinforcing bars which results in what is referred to as reinforced concrete (McCormac & Brown, 2014).

### 2.3.1 Mechanisms of Concrete Failure

As the goal of this research project was to address a common failure observed in the wing walls of the standard culvert design, it is important to understand the factors that contribute to this failure. There are many mechanisms through which concrete may fail, but this section will focus on those that are of concern to the project at hand and explain why the cracking that has been observed in the traditional culvert design is an issue that must be addressed.

#### 2.3.1.1 Embedded Metal Corrosion

According to the Portland Cement Association, the corrosion of embedded metals is the leading cause of concrete deterioration. The increase of steel volume that occurs due to precipitates from corrosion, shown in Figure 2-8, leads to increased internal stresses in the concrete which in turn can cause cracking (Portland Cement Association, 2014). The larger the ratio of concrete cover to reinforcing bar diameter, the larger the amount of corrosion required to induce cracking. The majority of cracks due to corrosion occur parallel to the reinforcing bars. In some cases, the corrosion causes a portion of the concrete cover to completely disengage from the concrete member, in what is called spalling (Emmons, 1993).

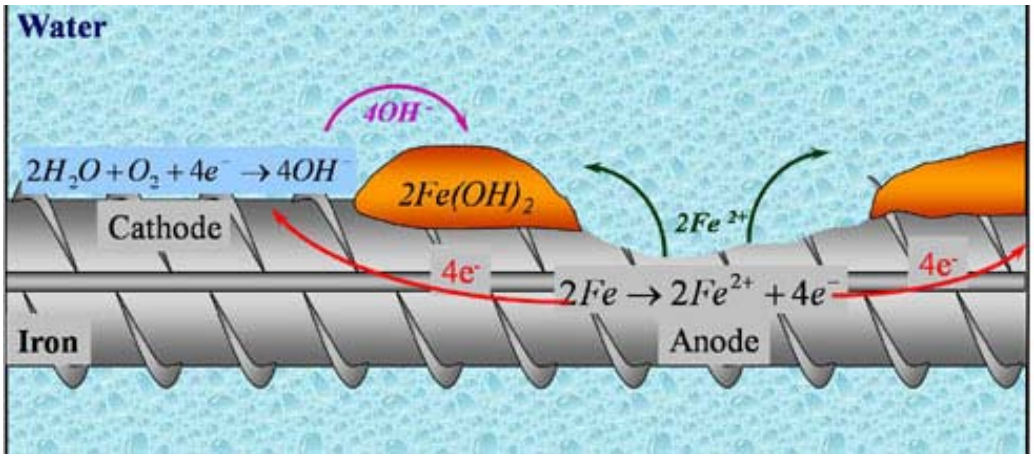


**Figure 2-8: Reduction in Steel Section (Portland Cement Association, 2014)**

While corrosion causes precipitates that increase the volume of the reinforcing steel, the diameter of the effective bar is reduced due to loss of effective bar cross-section, as shown in Figure 2-8, thus reducing the overall capacity of the member. Furthermore, the cracking and spalling that occur in the concrete reduce the effective cross section of the concrete which also reduces the compressive strength of that member (Emmons, 1993).

Excessive cracks in a concrete structure increase the amount of reinforcing steel exposed to corrosive environments and thus accelerate the deterioration of the overall structure, which illustrates one of the reasons that led to the redesign central to this research project.

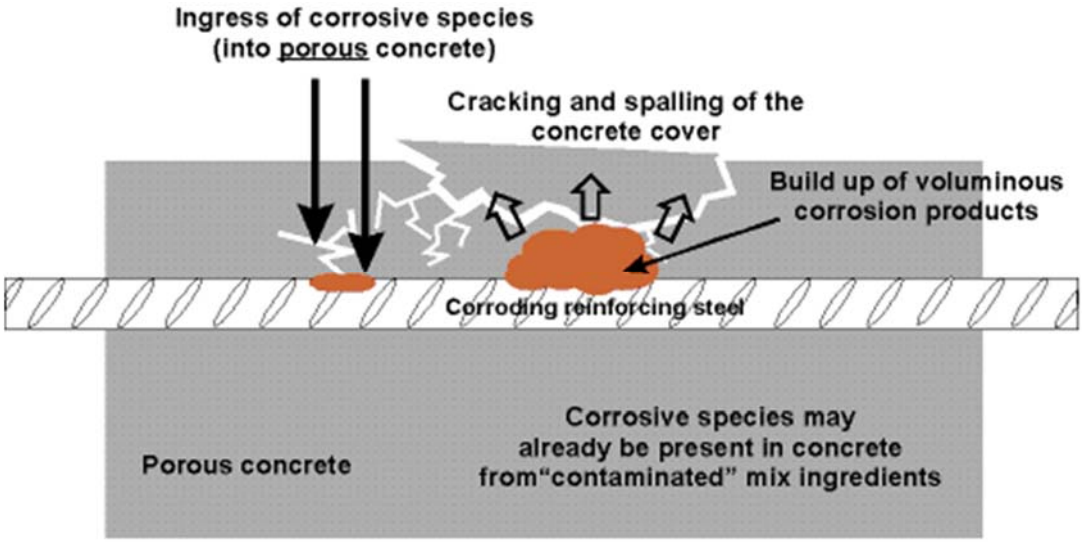


**Figure 2-9: Embedded Metal Corrosion (Tullmin, 2001)**

#### 2.3.1.2 Concrete Disintegration

Several environmental factors can lead to the disintegration of concrete. This disintegration is concerning on its own, but it also leads to a reduction in concrete cover of reinforcing steel. This, as previously discussed, increases the susceptibility of the reinforcing steel to corrosion. As

culverts will necessarily be exposed to water during their service life, these following mechanisms are of particular concern.

#### 2.3.1.2.1 Exposure to Aggressive Chemicals

There are five categories of aggressive chemicals that will attack various constituents of concrete: inorganic acids, organic acids, alkaline solutions, salt solution, and miscellaneous. Acids attack the concrete due to their reaction with the hydroxide present in the hydrated Portland cement. This reaction produces water soluble calcium compounds which are leached away allowing the aggregate to fall out. When limestone or dolomitic aggregates are used, the acid may actually completely dissolve them (Emmons, 1993).

#### 2.3.1.2.2 Freeze-Thaw Disintegration

Freeze-thaw disintegration only occurs if there is a cycle of freezing and thawing. Water populates pores within the concrete and proliferates through capillary action. As the water freezes, it expands and induces tension forces within the concrete that fracture the surrounding concrete matrix. This cracking allows more water to enter into pores and the issue propagates. Due to the poor thermal conductivity of concrete, the exterior of the concrete members is typically colder and, therefore, this issue generally starts on the exterior and works inward. This typically occurs on horizontal surfaces, or vertical surfaces at the waterline of water submerged structures (Emmons, 1993). This issue can be largely mitigated by ensuring that the concrete used has an appropriate air content. All concrete placed for the purpose of this project was tested for air content by ALDOT prior to placement (ALDOT, 2012). In areas where this is of particular concern, air-entraining admixtures can be used in the concrete mix design.

#### 2.3.1.2.3 Alkali-Aggregate Reaction

Certain aggregates, such as reactive forms of silica, react with potassium, sodium, and calcium hydroxide to create a gel around the reacting aggregates. When this gel is exposed to moisture it expands which then induces tensions forces within the concrete similar to the forces that occur during freeze-thaw cycles. Aggregate is typically tested to determine if it is reactive but there is no easy was to determine if the aggregate is reactive based solely on silica content (Emmons, 1993). ALDOT requires all aggregates used to come from approved sources that are subject to rigorous oversight (ALDOT, 2005).

#### 2.3.1.2.4 Sulfate Attack

Sulfates react chemically with the hydrated lime and hydrated calcium aluminate within the cement's paste. This reaction forms solid products with greater volume than the originally reacting agents. Precipitates, such as gypsum and ettringite, expand, pressurize, and disrupt the paste which causes disintegration and eventually deterioration. If sulfates are present in the clinker and the concrete reaches a high in-place temperature during very early stages of hydration, delayed-ettringite formation, which is another manifestation of sulfate attack, may occur, although it typically affects mass concrete or precast concrete members (Emmons, 1993).

#### 2.3.1.2.5 Erosion

Erosion may be caused by cavitation or abrasion. Cavitation occurs due to the formation of vapor bubbles that are generated by pressure changes within a high velocity water flow. The bubbles flow downstream and when they reach an area of higher pressure, they collapse and cause water to jet with extreme force at the surface below. This results in the erosion of the cement matrix which leaves harder aggregates in place. If the velocities of water in question are sufficiently high,

significant quantities of concrete may be eroded away. This is most easily avoided by producing smooth surfaces and avoiding protruding obstructions to flow. Abrasion is the erosion of the surface that is caused by rubbing and friction. This generally wears away the surface uniformly, including cement matrix and aggregate alike (Emmons, 1993).

#### 2.3.1.3 Moisture and Thermal Effects

The moisture content and temperature of both concrete and its surroundings have a significant impact on the development of stresses within concrete. Understanding how concrete will react to its environment is a crucial aspect of design and must be considered in order to minimize the concentration of stresses at undesirable locations within a structure. The following are some of the ways in which these issues can manifest.

##### 2.3.1.3.1 Drying Shrinkage

When exposed to the atmosphere, concrete naturally loses some water through evaporation, which causes the concrete to shrink. When the concrete is unrestrained, there is no buildup of internal stresses. When the member is restrained against deflection, however, this causes internal stresses to occur within the member. These stresses sometimes exceed the tensile strength of the concrete and cause cracking. Correctly placed reinforcement steel can be used to control the size of the cracks and distribute the stresses throughout the member (Emmons, 1993).

##### 2.3.1.3.2 Moisture Content Induced Volume Change

Concrete changes length based on moisture content, as evident in drying shrinkage. Moist concrete that dries out will shrink while dry concrete that encounters moisture will expand. This effect is evident during the course of seasonal changes, as a hot, humid summer will cause concrete to expand while a cold, dry winter will cause it to shrink. As discussed with drying shrinkage,

restraint against this volume change induces stress within the concrete and can lead to cracking (Emmons, 1993).

#### 2.3.1.3.3 Temperature Induced Volume Change

Concrete, like all materials, changes volume due to changes in temperature. As the temperature increases, so does the volume of concrete. Much like drying shrinkage, if a member is unrestrained, this does not cause any internal stresses to occur, but if a member is restrained against deflection, internal stresses will occur due to the change in volume (Emmons, 1993).

#### 2.3.1.3.4 Early Thermal Cracking of Freshly Placed Concrete

As concrete hydrates, its temperature increases to a certain peak temperature, dependent upon the ambient temperature when the concrete is placed. As it cools from this peak, it reaches a point of zero-stress. As it continues to cool, tension can occur within the member. This heating typically occurs within the first few hours of the concrete being placed, which means the concrete has not yet built up significant tensile strength. Thus, this tension within the member can cause cracking early within the life of the concrete. As stated, the zero-stress temperature is an artifact of the conditions when the concrete set and thus, the higher the environmental temperatures at the time the concrete sets, the greater the zero-stress temperature and the greater the potential temperature difference. For this reason, concrete placed in the summer exhibits more severe incidences of this stress mechanism. If the concrete later exceeds the zero-stress temperature, it can also induce compression forces within the member (Emmons, 1993).

#### 2.3.1.3.5 Thermal Movements in Existing Cracks

When cracks are already present, due to drying shrinkage for example, the movement of these cracks can allow for thermal change strain to be absorbed. This does, however, reduce the amount of movement at planned expansion joints (Emmons, 1993).

### 2.3.1.4 Load Effects

Structures are designed to support a certain load, be it self-weight or imposed load. Under these loads, concrete typically deflects, cracks, and even spalls. Different loading states and connections, however, may induce cracking in distinct patterns or locations as well as different magnitudes of deflection. This is due to the different associated load paths, points of concentration, end conditions, etc. Furthermore, if the structure is loaded beyond the design load, the associated distresses will be emphasized.

Cracking due to load effects can be caused by flexure, shear, or a combination of the two. In a simply supported span, flexural cracks occur around mid-span while the diagonal cracks that form from a combination of shear and flexure occur toward the supports. In continuous structures, flexural cracks also occur at the supports at the location of negative moment and diagonal shear cracks occur in the areas where there is a transition from negative to positive moment (Emmons, 1993).

### 2.3.1.5 Faulty Workmanship

Finally, even when environmental and material factors are accounted for, it is important to have a qualified team placing the concrete, as improper construction can lead to structural deficiencies. This is also an important consideration during the design phase of a structure, as increased complexity of a design increases the chances that the design will be executed poorly.

The following are common examples of ways in which faulty workmanship can negatively impact a structure.

#### 2.3.1.5.1 Improper Reinforcing Steel Placement

Reinforcing steel is designed to carry the tension that occurs within a member. If the steel is not placed correctly during construction, the tensile capacity of the member may be jeopardized. Furthermore, misplacement of the steel may create a situation with insufficient cover which in turn makes the steel more susceptible to corrosion. If the reinforcing steel is too congested, it may not allow for the concrete to flow through the grate and thus a void will occur around the reinforcing steel or there may again be insufficient cover. When a bend is present in a member, there may be insufficient development of the steel if the ends are placed too close to the exterior, which could in turn cause spalling to occur. Also, stirrups must be placed as designed or they may not pick up the intended forces which can lead to failure of a member (Emmons, 1993).

#### 2.3.1.5.2 Premature Removal of Forms

If the concrete has not reached its proper strength when formwork and shoring is removed, the premature loading of the structure can cause excessive compression and tension stresses which may cause cracking, excessive deflection, and possibly even collapse (Emmons, 1993).

#### 2.3.1.5.3 Segregation

Segregation, or insufficient mixing of the various sized aggregates within concrete, can occur due to over-vibration, improper handling of the concrete (such as pouring from too high an altitude above the desired level), or incorrectly batched concrete. The result is that larger aggregate settles at the bottom whereas the top portion of the concrete consists of excessive amounts of fines and

may have an excessive water-cement ratio. The placed concrete may lack the necessary strength and may not be sufficiently durable (Emmons, 1993).

#### 2.3.1.5.4 Improper Grades of Slab Surfaces

If a slab requires that it have certain slopes to aid in drainage, improper grading may slow this process and even allow liquid to pond at low points in the surface. This ponding allows time for water to saturate the concrete which in turn speeds along the distresses that coincide with moisture effects. Also, if the water is not drained as quickly as needed, it provides more time for the water to invade cracks and joints and again speeds along related distresses (Emmons, 1993).

#### 2.3.1.5.5 Construction Tolerances

If a member is cast out of tolerance, it may lack adequate cover for the reinforcing steel or adequate cross-section dimensions which can cause eccentric loading (Emmons, 1993).

## 2.4 Earth Pressure

The purpose of the culvert tabs that are the focus of this research was to provide an impediment to excessive rotation of the wing walls. These wing walls were designed as long-heeled cantilever retaining walls and as such, the primary lateral load of concern was that caused by the backfill. It was necessary to understand the methods used to estimate the magnitude of lateral earth pressures to develop a robust and flexible design approach. This section addresses both the manner in which lateral earth pressure is calculated and the manner in which field measurements of lateral earth pressure were recorded.

### 2.4.1 Lateral Earth Pressure

Section 3.11.5.1 of the American Association of State Highway and Transportation Officials (AASHTO) LRFD Bridge Design Specifications defines lateral earth pressure with AASHTO LRFD Equation 3.11.5.1-1, shown below as Equation 2-1:

$$p = k\gamma_s z \qquad \textbf{Equation 2-1}$$

Where:

p = lateral earth pressure (ksf)

k = coefficient of lateral earth pressure (dependent upon classification of pressure)

$\gamma_s$ = unit weight of soil (kcf)

z = depth below the surface of earth (ft)

The value of k is a ratio of the horizontal effective stress to the vertical effective stress induced by the backfill loading and is a function of the shear strength of the soil. As stated above, the selection of the design k value is dependent upon whether the pressure acting on the wall is classified to be in the at-rest, active, or passive condition, which is determined by the amount of deflection expected or allowed for the designed member. This also assumes there is no hydrostatic pressure on the wall.

The AASHTO LRFD Bridge Design Code allows for the use of either of two methods, one based on the Coulomb Theory and the other on the Rankine Theory, for calculating the value of k. The Coulomb Theory, which is based upon force equilibrium, is used by default in AASHTO, as it allows for there to be a frictional interaction between the soil and the face of the wall which

interferes with the development of the failure wedge within the backfill. Rankine theory does not account for this frictional interaction and thus should not be used when cohesive soils are used for backfill. Rankine theory, however, may be used for long-heeled cantilever walls, such as the ones studied in this project, and thus the two methods will be discussed (AASHTO, 2012).

What follows is an explanation of the distinctions between the pressure classifications and how the various values of k are calculated by the two methods.

#### 2.4.1.1 At-Rest Earth Pressure

The At-Rest Earth Pressure gives an intermediate magnitude of lateral earth pressure in comparison to the three classifications. It is appropriate to use at-rest earth pressure for rigid structures where deflection is not desirable. Typically, the addition of a backfill load would cause some sort of deflection or rotation of the wall and thus a portion of the lateral component of the load would be relieved. For the at-rest condition, however, it is assumed the total lateral component of the naturally occurring loads due to the weight of the overburden soils must be resisted (AASHTO, 2012).

For this condition, both Coulomb and Rankine methods calculate the coefficient of lateral earth pressure for normally consolidated soils using the Equation 3.11.5.2-1 from the AASHTO LRFD Bridge Design Specifications, shown below as Equation 2-2:

$$k_0 = 1 - sin\phi'_f \qquad \textbf{Equation 2-2}$$

Where:

$k_0$ = coefficient of at-rest lateral earth pressure

$\phi'_f$ = effective friction angle of soil (degrees)

For over consolidated soils, the coefficient can be modified using Equation 3.11.5.2-2 from the AASHTO LRFD Bridge Design Specifications, shown below as Equation 2-3:

$$k_0 = (1 - sin\phi'_f)(OCR)^{sin\phi'_f} \qquad \textbf{Equation 2-3}$$

Where:

OCR = overconsolidation ratio

However, the commentary in this section specifically states that it is common to not know the OCR with enough accuracy use Equation 2-3 (AASHTO, 2012).

#### 2.4.1.2 Active Lateral Earth Pressure

For both active and passive lateral earth pressures to be applicable, movement at the top of the wall is required. Approximate ratios of these required movements relative to wall height are given in Table C3.11.1-1 of the AASHTO LRFD Bridge Design specifications and reproduced below in Table 2-1:

**Table 2-1: Approximate Values of Relative Movements Required to Reach Active or Passive Pressure Conditions (AASHTO, 2012)**

| Type of Backfill | Values of $\Delta/H$ | |
|---|---|---|
| | Active | Passive |
| Dense sand | 0.001 | 0.01 |
| Medium dense sand | 0.002 | 0.02 |
| Loose sand | 0.004 | 0.04 |
| Compacted silt | 0.002 | 0.02 |
| Compacted lean clay | 0.010 | 0.05 |
| Compacted fat clay | 0.010 | 0.05 |

Where:

$\Delta$ = movement of top of wall required to reach minimum active or maximum passive pressure by tilting or lateral translation (ft)

H = height of wall (ft)

For the active case, the wall deflects away from the soil pressure. This does not impact the vertical stress related to the soil load, but decreases the horizontal stress to the minimum allowable without failure, according to the Mohr-Coulomb Failure Envelope, the equation for which is given below as Equation 2-4 (Coulomb, 1776):

$$\tau_f = c + \sigma \tan \phi'_f \qquad \textbf{Equation 2-4}$$

Where:

$\tau_f$ = shear stress at failure (ksf)

c = cohesion of soil (ksf)

$\sigma$ = normal stress (ksf)

For the active condition, the coefficient of lateral earth pressure for the Coulomb theory is given by Equation 3.11.5.3-1 in the AASHTO LRFD Bridge Design Specifications, shown below as Equation 2-5:

$$k_a = \frac{sin^2(\theta + \phi'_f)}{\Gamma[sin^2\theta \sin(\theta - \delta)]} \qquad \textbf{Equation 2-5}$$

In which $\Gamma$ is given by Equation 3.11.5.3-2, shown below as Equation 2-6:

$$\Gamma = \left[1 + \sqrt{\frac{\sin(\phi'_f + \delta)\sin(\phi'_f - \beta)}{\sin(\theta - \delta)\sin(\theta + \beta)}}\right]^2 \qquad \textbf{Equation 2-6}$$

Where:

$k_a$ = coefficient of active lateral earth pressure

$\delta$ = friction angle between fill and wall (degrees)

$\beta$ = angle of fill to the horizontal

$\theta$ = angle of back face of wall to horizontal

The notations of $\delta$, $\beta$, and $\theta$ are depicted graphically in Figure 3.11.5.3-1, reproduced below in Figure 2-10.

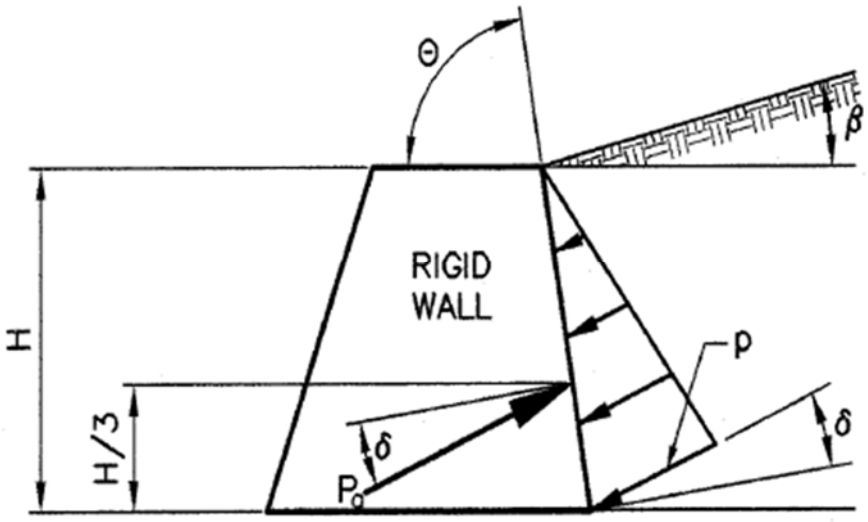


**Figure 2-10: Notation for Coulomb Active Earth Pressure (AASHTO, 2012)**

The value of $\delta$ can be determined using Table 3.11.5.3-1 from the AASHTO LRFD Bridge Design Specifications, which is reproduced below in Table 2-2.

**Table 2-2: Friction Angle for Dissimilar Materials (AASHTO, 2012)**

| Interface Materials | Friction Angle, δ (degrees) | Coefficient of Friction, tan δ (dim.) |
|---|---|---|
| Mass concrete on the following foundation materials: | | |
| • Clean sound rock | 35 | 0.70 |
| • Clean gravel, gravel-sand mixtures, coarse sand | 29 to 31 | 0.55 to 0.60 |
| • Clean fine to medium sand, silty medium to coarse sand, silty or clayey gravel | 24 to 29 | 0.45 to 0.55 |
| • Clean fine sand, silty or clayey fine to medium sand | 19 to 24 | 0.34 to 0.45 |
| • Fine sandy silt, nonplastic silt | 17 to 19 | 0.31 to 0.34 |
| • Very stiff and hard residual or preconsolidated clay | 22 to 26 | 0.40 to 0.49 |
| • Medium stiff and stiff clay and silty clay | 17 to 19 | 0.31 to 0.34 |
| Masonry on foundation materials has same friction factors. | | |
| Steel sheet piles against the following soils: | | |
| • Clean gravel, gravel-sand mixtures, well-graded rock fill with spalls | 22 | 0.40 |
| • Clean sand, silty sand-gravel mixture, single-size hard rock fill | 17 | 0.31 |
| • Silty sand, gravel or sand mixed with silt or clay | 14 | 0.25 |
| • Fine sandy silt, nonplastic silt | 11 | 0.19 |
| Formed or precast concrete or concrete sheet piling against the following soils: | | |
| • Clean gravel, gravel-sand mixture, well-graded rock fill with spalls | 22 to 26 | 0.40 to 0.49 |
| • Clean sand, silty sand-gravel mixture, single-size hard rock fill | 17 to 22 | 0.31 to 0.40 |
| • Silty sand, gravel or sand mixed with silt or clay | 17 | 0.31 |
| • Fine sandy silt, nonplastic silt | 14 | 0.25 |
| Various structural materials: | | |
| • Masonry on masonry, igneous and metamorphic rocks: | | |
| ○ dressed soft rock on dressed soft rock | 35 | 0.70 |
| ○ dressed hard rock on dressed soft rock | 33 | 0.65 |
| ○ dressed hard rock on dressed hard rock | 29 | 0.55 |
| • Masonry on wood in direction of cross grain | 26 | 0.49 |
| • Steel on steel at sheet pile interlocks | 17 | 0.31 |

The equation for the Rankine value for coefficient of active earth pressure is given below as Equation 2-7 (Rankine, 1857):

$$k_a = tan^2\left(45 - \frac{\phi_f'}{2}\right) \qquad \textbf{Equation 2-7}$$

It is typically assumed that the deflection at the top of retaining structures will be sufficient to develop the entirety of the active lateral earth pressure (AASHTO, 2012).

### 2.4.1.3 Passive Lateral Earth Pressure

As with active lateral earth pressure, passive lateral earth pressure requires movement of the structure to be activated. The magnitudes of this movement are significantly larger than those associated with active pressure. Approximate ratios of the required movement to achieve passive pressure relative to wall height are given in Table 2-1 above.

Unlike the active case, wherein the movement of the structure is away from the soil pressure, for the passive case, the structure moves into the soil. This does not impact the magnitude of the vertical stress, but the horizontal stress increases to the maximum allowable without failure, as discussed in section 2.4.1.2.

The Coulomb equation for the coefficient of passive lateral earth pressure is given below as Equation 2-8 (Coulomb, 1776):

$$k_p = \frac{cos^2(\phi'_f - \theta)}{\Gamma[cos^2\theta \sin(\theta + \delta)]} \quad \textbf{Equation 2-8}$$

In which Γ is given by the equation shown below as Equation 2-9:

$$\Gamma = \left[1 + \sqrt{\frac{\sin(\phi'_f + \delta)\sin(\phi'_f - \beta)}{\cos(\theta + \delta)\cos(\theta - \beta)}}\right]^2 \quad \textbf{Equation 2-9}$$

Where:

$k_p$ = coefficient of passive lateral earth pressure

$\phi'_f$ = effective friction angle of soil (degrees)

δ = friction angle between fill and wall (degrees)

β = angle of fill to the horizontal

θ = angle of back face of wall to horizontal

The notations of δ, β, and θ are depicted graphically in Figure 3.11.5.3-1 of the AASHTO LRFD Bridge Design Specifications, reproduced above in Figure 2-10. The value of δ can be determined using Table 3.11.5.3-1, which is reproduced above in Table 2-2.

The equation for the Rankine value for coefficient of passive earth pressure is given below as Equation 2-10 (Rankine, 1857):

$$k_p = tan^2\left(45 + \frac{\phi_f'}{2}\right) \qquad \textbf{Equation 2-10}$$

#### 2.4.1.4 Other Impacts on Lateral Earth Pressure

##### 2.4.1.4.1 Effect of Groundwater

Typically, the horizontal pressure along the wall varies linearly with depth and creates a linear distribution with an easily calculated resultant. When water is present, however, this is not the case, as the effective unit weight of the soil must be modified at any depth below the water table, thus resulting in a bilinear distribution. This is illustrated in Figure 2-11, reproduced from Section 2.5 of the FHWA Reference Manual for Retaining Structures.

It is typical to specify that a free draining backfill be used and to design the structure to include weep holes, which provide a path through the retaining structure for the water to drain and thus relieve the wall of the hydrostatic pressures that would otherwise build up along the face of the structure. In some instances, however, economic considerations lead to the use of locally sourced cohesive backfill without free draining properties and these hydrostatic pressures must then be accounted for in the design of the structure. In some cases, these hydrostatic pressures can far exceed the lateral earth pressure. It may also be undesirable to allow water to drain through the structure due to the impact on the settlement of adjacent structures (FHWA, 1999).

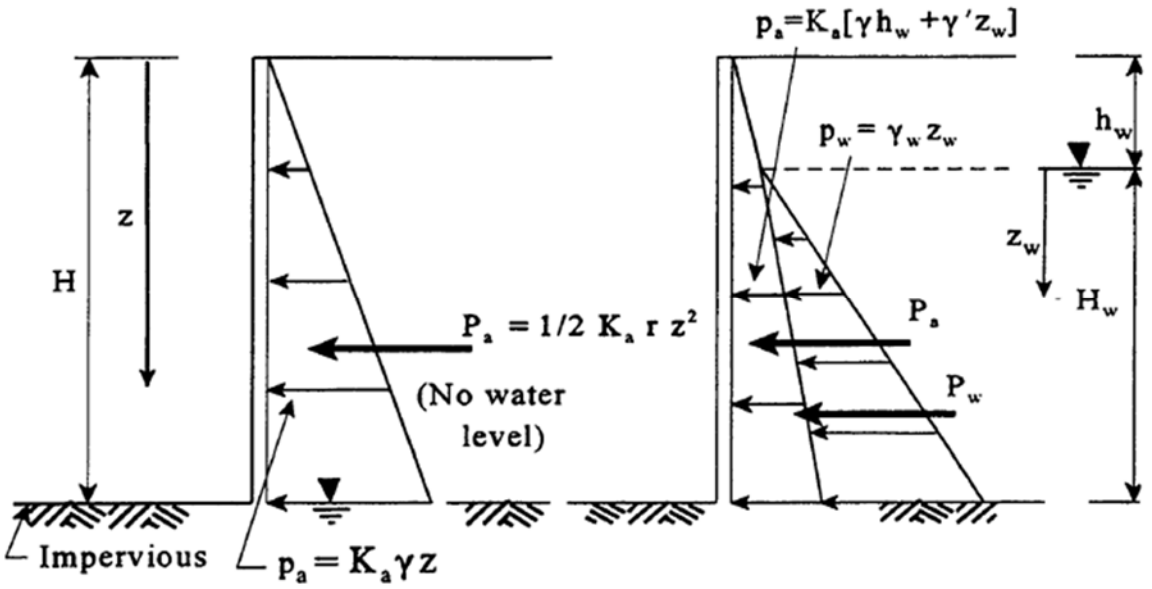


**Figure 2-11: Lateral Pressures for Static Groundwater Case (FHWA, 1999)**

#### 2.4.1.4.2 Effect of Surface Surcharge Loads

A retaining structure is responsible for the component of lateral load that results from the placement of any mass in addition to the soil backfill. Unlike the soil backfill, the impacts of these surcharge loads are often more difficult to conceptualize. These loads do not come into contact with the structure and the load path taken through the soil is uncertain, making this impact more difficult to estimate. In the case of evenly distributed surcharges that cover a significant area, it is typical to treat this mass as an equivalent height of additional backfill and calculate the lateral component accordingly. For other common surcharges, specifically point loads, line loads, and strip loads parallel to the wall, Section 2.6 of the FHWA Retaining Wall Manual (1999) has provided empirical methods, based on the work of French mathematician Joseph Valentin Boussinesq, through which their lateral components may be estimated. These methods are provided in Figure 2-12. Common examples of these surcharges relevant to this project include

highways, electric/communications towers, and construction equipment. Note that these methods were developed with the assumption of an unyielding wall which is conservative and yields nearly double the values calculated in an elastic half space, thus their applicability may vary from project to project (FHWA, 1999).

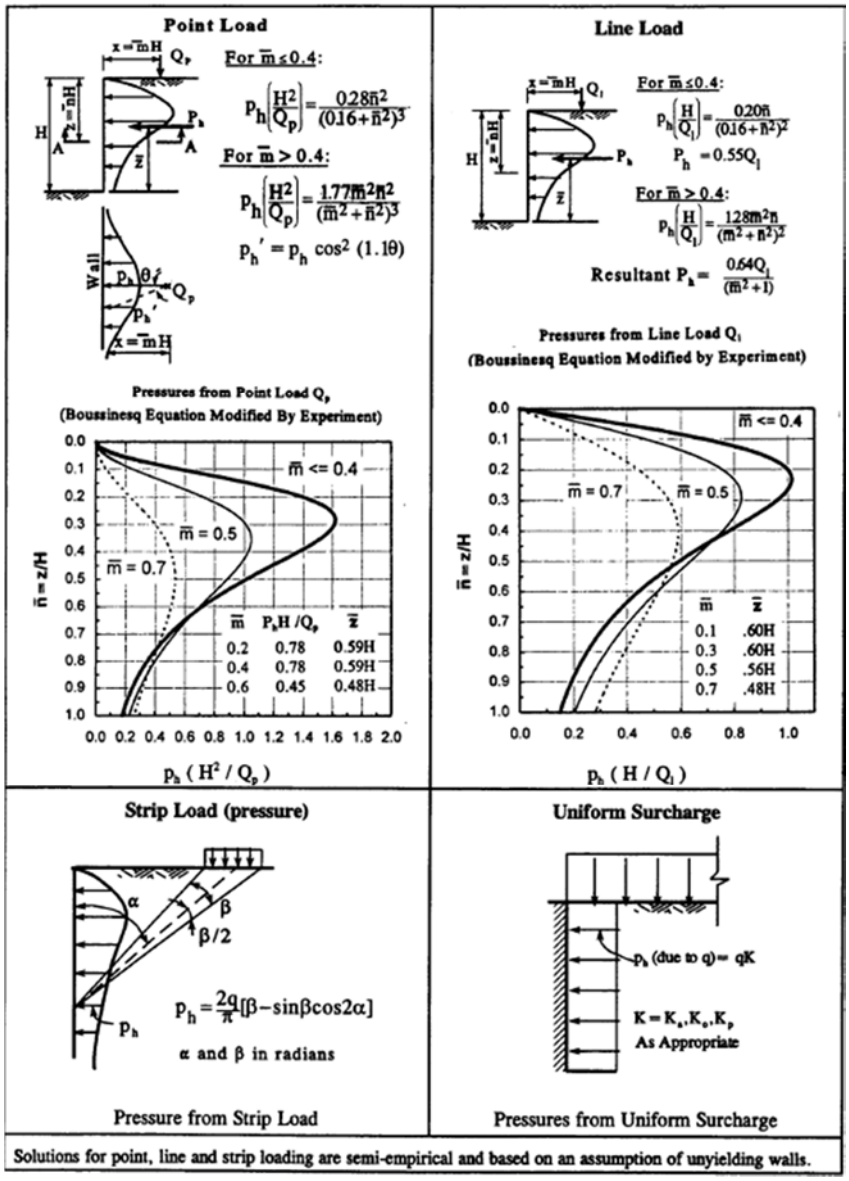


**Figure 2-12: Lateral Pressure Due to Surcharge Loads (FHWA, 1999)**

#### 2.4.1.4.3 Earth Pressures Due to Compaction

As it is necessary to compact the backfill in order to maintain the integrity of the road surface subgrade, it is important to consider the additional lateral load that results from this compaction. Because these loads can be substantial, it is common to specify lower compaction criteria for the area of backfill immediately surrounding the wall. Due to the inelastic nature of soil, some of this increased lateral load is present even after the compaction process is completed. The magnitude of this change is dependent upon the compaction equipment and methods used, as well as the rigidity of the wall (FHWA, 1999).

This increase of lateral load is most pronounced at the ground surface and by a depth of 18 feet, it has typically become negligible. This is evident in Figure 2-13, taken from Section 2.7 of the FHWA Retaining Wall Manual and used to calculate the impact of compaction on the magnitude of the lateral load. The dash-dot lines in Figure 2-13 represent the value of the At-Rest Earth Pressure and the solid lines represent the increased values due to compaction. The circled numbers on the solid lines are the values of $\bar{q}$ calculated using the equation given in the lower left corner of the chart. For values of $\bar{q}$ not given, it is appropriate to interpolate. The dotted lines near the top of the chart are representative of the fact that the impact of compaction is slightly larger for cohesive soils near the surface. The table in the bottom portion of Figure 2-13 gives multiplication factors for corrections that account for varying lift thickness, distance of compactor from the wall, roller width, and friction angle of the compacted soil. As with the surcharge load calculations, this method is based upon the assumption of a rigid wall and is therefore conservative (FHWA, 1999).

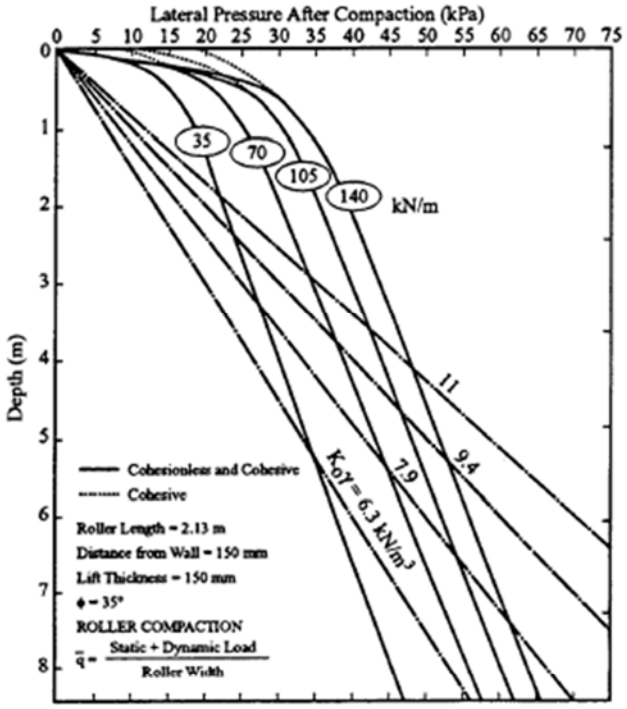


**ADJUSTMENT (MULTIPLICATION) FACTORS**

| Variables | | | Multiplier Factors for z = 0.6 m | 1.2 m | 2.4 m | 4.8 m |
|---|---|---|---|---|---|---|
| Lift thickness (t) and distance from wall (x) (Adjustments for these two factors are combined) | t=150 mm lifts | x = 0 | 1.00 | 1.00 | 1.00 | 1.00 |
| | | x = 60 mm | 1.00 | 1.00 | 1.00 | 1.00 |
| | | x = 150 mm | 1.00 | 1.00 | 1.00 | 1.00 |
| | | x = 300 mm | 0.87 | 0.88 | 0.89 | 0.90 |
| | t=300 mm lifts | x = 0 | 0.94 | 0.95 | 0.95 | 0.96 |
| | | x = 60 mm | 0.94 | 0.95 | 0.95 | 0.96 |
| | | x = 150 mm | 0.94 | 0.95 | 0.95 | 0.96 |
| | | x = 300 mm | 0.83 | 0.84 | 0.86 | 0.88 |
| Roller width (w) | | w = 0.38 m | 0.80 | 0.80 | 0.80 | 0.88 |
| | | w = 1.07 m | 0.96 | 0.94 | 0.94 | 0.97 |
| | | w = 2.13 m | 1.00 | 1.00 | 1.00 | 1.00 |
| | | w = 3.05 m | 1.00 | 1.01 | 1.02 | 1.04 |
| Friction angle (ϕ) | | ϕ = 25° | 0.59 | 0.70 | 0.81 | 0.96 |
| | | ϕ = 30° | 0.75 | 0.83 | 0.89 | 0.98 |
| | | ϕ = 35° | 1.00 | 1.00 | 1.00 | 1.00 |
| | | ϕ = 40° | 1.23 | 1.16 | 1.10 | 1.03 |

**Figure 2-13: Earth Pressures due to Compaction with Rollers (FHWA, 1999)**

### 2.4.2 Full Scale Culvert Load Tests

A field investigation performed by the University of Nebraska observed the structural behavior of a full-scale double barrel cast-in-place box culvert. Using 28 vibrating wire soil pressure cells placed around the perimeter of the culvert, as well as 40 vibrating wire strain gauges placed on reinforcement prior to installation, the researchers were able to measure the soil pressure, moment, and deflection of the structure. Measurements were recorded from each instrument following the placement of 2 feet of fill up to a fill height of 12 feet above the top slab. Furthermore, live load measurements were recorded in two manners. Wheel load tests were recorded by placing the rear axle of a test truck with a 22.8 kip load at 8 locations following each 2 feet of fill. After each 4 feet of fill, concentrated load tests were performed using a hydraulic press. This was done to observe the distribution of live load through soil layers of increasing depth. The live load measurements were then reduced by the corresponding soil load recorded at each fill level so that the effect of the live load could be isolated (Abdel-Karim, Tadros, & Benak, 1993).

Figures depicting the moments measured in this investigation are reproduced below.

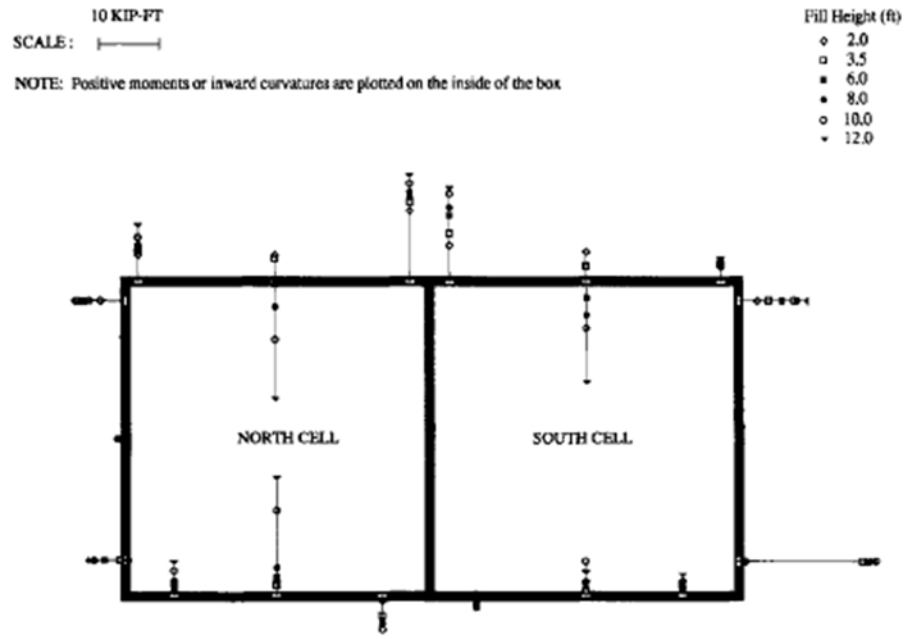


**Figure 2-14: Measured Moments due Only to Soil (Abdel-Karim, Tadros, & Benak, 1993)**

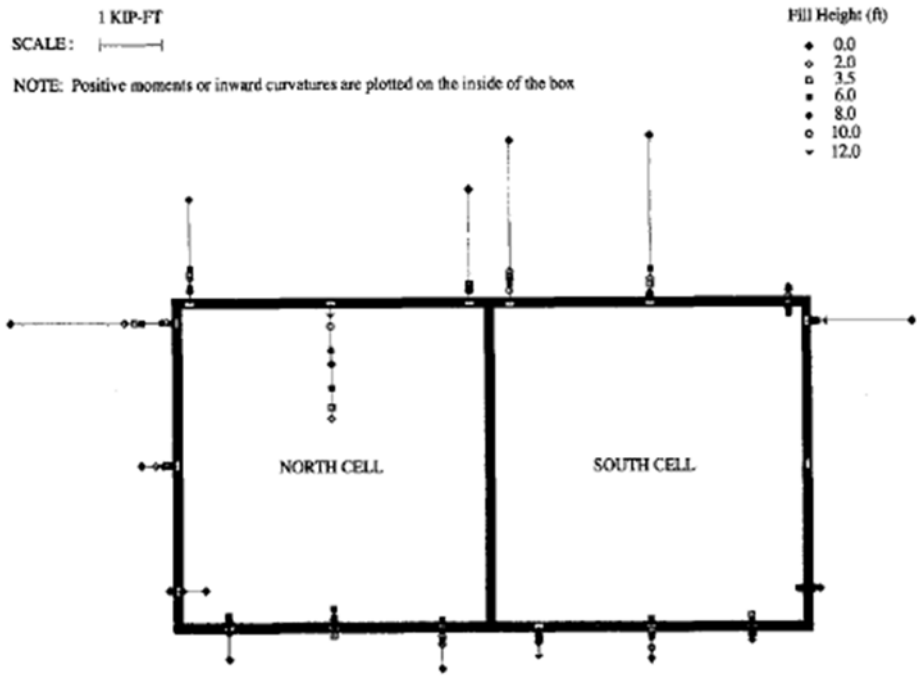


**Figure 2-15: Measured Moments due Only to Wheel Loads (Abdel-Karim, Tadros, & Benak, 1993)**

While the culvert investigated by the University of Nebraska had wing walls, these were not instrumented. Few full-scale load tests have been published, however, and several items of pertinence to this current thesis were gleaned from this investigation. As is seen in Figure 2-14 and Figure 2-15, significant moments were induced at the corners where the wing walls frame into the culvert. Also of note is the fact that the smaller the amount of fill above the top slab, the larger the effect of live load on this location. As the culverts constructed for the purpose of this current thesis had less than 2 feet of fill above the top slab, it follows that repeated wheel loads over the service life of these structures would induce moments at these corners which, when coupled with the already complex loading state that results from the lateral earth pressure upon the wing walls, could lead to cracking of traditionally built integral wing walls.

## 2.5 Corbel Design

A corbel is a "short (haunched) cantilever that projects from the face of a column or wall to support a concentrated load or beam reaction" (Caltrans, 2003). An example of a corbel with typical reinforcement is given below in Figure 2-16 which is a reproduction of Figure 8.15.5.8 from the Caltrans Bridge Design Specifications.

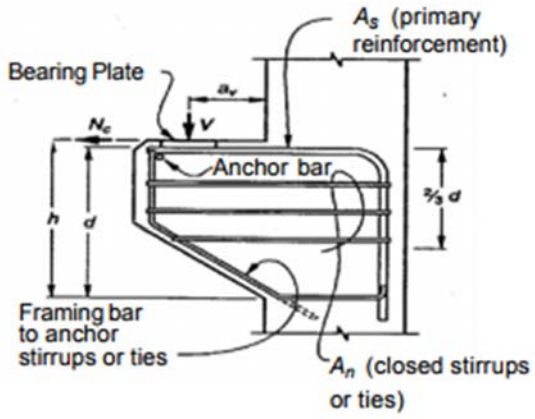


**Figure 2-16: Corbel with Typical Reinforcement (Caltrans, 2003)**

The variables shown in Figure 2-16 are defined as follows:

$A_n$ = area or reinforcement in corbel resisting tensile force, $N_c$

$a_v$ = shear span, distance between concentrated load and face of support

$A_s$ = area of flexural tension reinforcement

d = distance from extreme compression fiber to centroid of tension reinforcement

h = overall thickness of member

$N_c$ = design tensile force applied at top of corbel acting simultaneously with V

V = design shear force at section

(Caltrans, 2003).

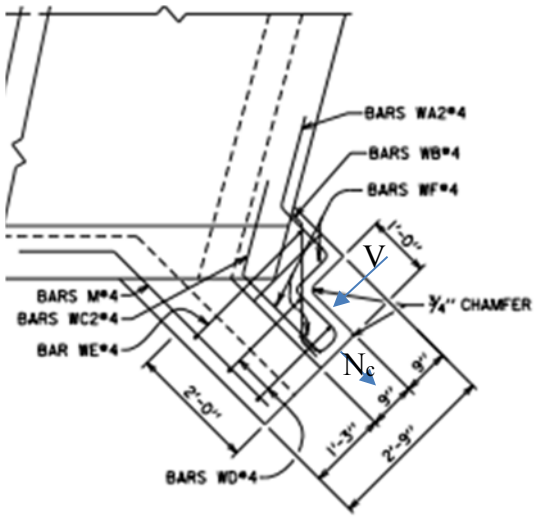


**Figure 2-17: Proposed Tab Detail**

Comparing Figure 2-16 with the proposed tab reinforcement, shown again above in Figure 2-17, it can be seen that the proposed tab design differs from a typical culvert in two key ways:

1. The lack of a tapering of the member at the face of the support
2. The lack of closed stirrups or ties

Beyond these two items, the proposed tab detail is sufficiently similar to a corbel to analyze it as such; however, these items are of concern when considering the provisions that must be met in order to use the corbel guidelines provided by Caltrans. First, the lack of a tapering does not constitute an inherent inability of the structure to resist the expected loads. If the tab itself is sufficiently thick to meet the shear demand, this difference can be overlooked. Second, the stirrups need not be closed if they have sufficient room to be developed fully, as is the case in the proposed culvert tab design.

The guidelines laid out by Caltrans were compared to and found to be consistent with the guidelines laid out by AASHTO (AASHTO, 2012). As Caltrans presents this information more succinctly, the guidance of Caltrans is thus used moving forward. The provisions, taken nearly verbatim from Section 8.15.5.8 of the Caltrans Bridge Design Specifications but with slight alterations for clarity, are as follows:

1. The ratio of $a_v/d$ must not exceed 1. The magnitude of $N_c$ must not exceed the magnitude of V. Distance d shall be measured at support.
2. Depth at outside edge of bearing area shall not be less than 0.5d.
3. Section at face of support shall be designed to resist simultaneously a shear $V_u$, a moment $M_u$, calculated as $[Va_v + N_c(h-d)]$, and a horizontal tensile force $N_u$. These forces are shown in a Free Body Diagram below in Figure 2-18. As shown, distance h shall be measured at the face of support. Figure 2-19 gives a diagram of typical corbel reinforcement to resist these loads.

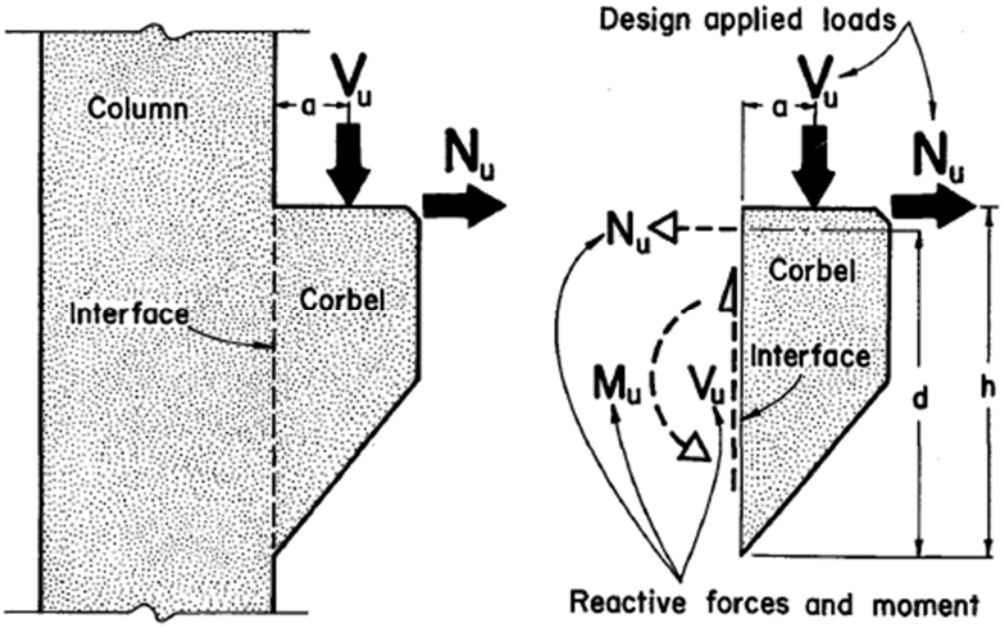


**Figure 2-18: Corbel as a free body diagram (Mattock, 1976)**

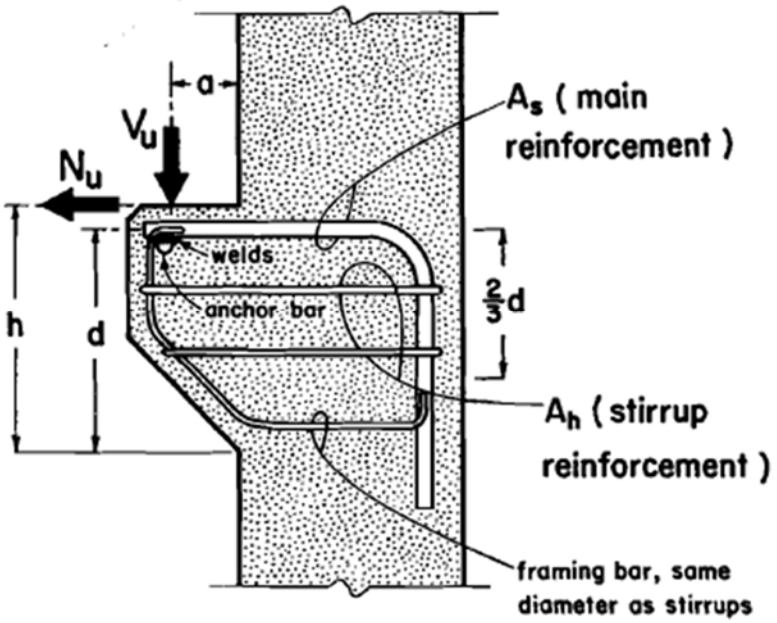


**Figure 2-19: Typical corbel reinforcement (Mattock, 1976)**

4. Closed stirrups or ties parallel to the primary flexural reinforcement ($A_s$), with a total area $A_h$ not less than $0.5(A_s-A_n)$, shall be uniformly distributed within two-thirds of the effective depth adjacent to $A_s$.
5. Ratio $\rho = A_s/bd$ shall not be taken less than $0.04(f'_c/f_y)$.

   Where

   b = width of the tab.

   For the purposes of this research, b is actually taken to be the width of a discrete design strip of the tab, as shown below in Figure 2-20 with the thick black lines and double-headed arrow.

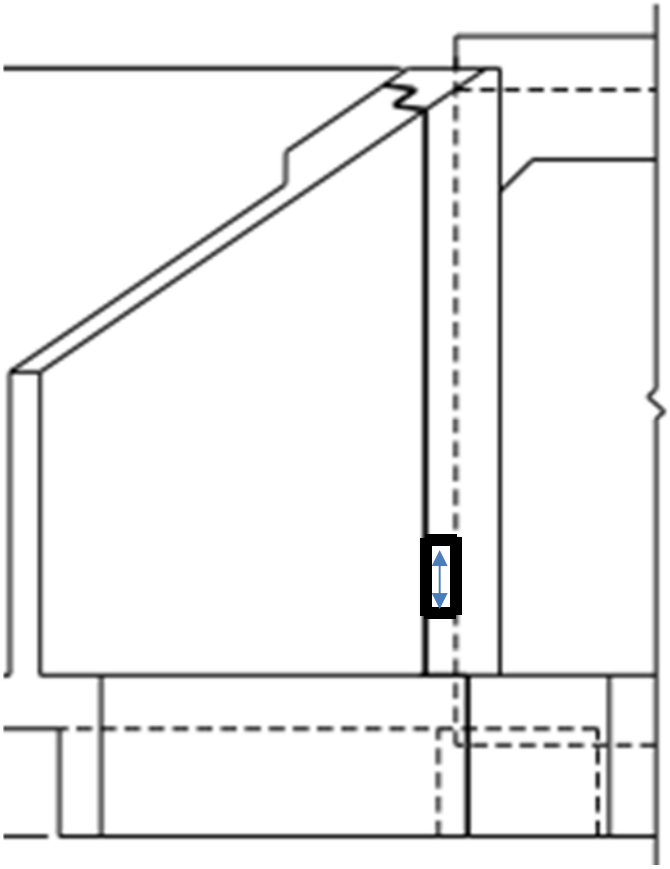

**Figure 2-20: Design strip of a tab**

6. At front face of corbel, primary tension reinforcement $A_s$ shall be anchored by some form of positive anchorage.
7. Bearing area of load on bracket or corbel shall not project beyond straight portion of primary flexural tension bars $A_s$, nor project beyond interior face of transverse anchor bar (if one is provided) (Caltrans, 2003).

### 2.5.1 Corbel Section Capacities

Per Caltrans, the section capacities of the corbel are as follows:

1. Shear strength, $V_n$, shall not exceed $0.2f'_c b_w d$ nor $800 b_w d$ in pounds. For shear-friction reinforcement perpendicular to shear plane, shear strength is computed as shown in Equation 2-11:

$$V_n = A_{vf} f_y m \qquad \textbf{Equation 2-11}$$

Where

$A_{vf}$ = Area of shear-friction reinforcement across the shear plane

$f_y$ = yield stress of reinforcement

m = coefficient of friction, taken as 1.4 for concrete placed monolithically

- AASHTO also requires that $V_n$ not exceed the following:
    i. $K_1 f'_c A_{cv}$
    ii. $K_2 A_{cv}$

    Where

    $K_1$ = fraction of concrete strength available to resist interface shear, taken as 0.3 for concrete placed monolithically

$K_2$ = limiting interface shear resistance, taken as 1.8 for concrete placed monolithically

$A_{cv}$ = area of concrete considered to be engaged in interface shear transfer, taken to be b*d ($in^2$)

(AASHTO, 2012)

2. Moment capacity, $M_n$, is calculated using Equation 2-12:

$$M_n = A_s f_y \left(d - {}^{a}/_{2}\right) \qquad \textbf{Equation 2-12}$$

Where "a" is calculated using Equation 2-13:

$$a = \frac{A_s f_y}{0.85 f_c' b} \qquad \textbf{Equation 2-13}$$

3. Tensile capacity, $P_{nt}$, is calculated using Equation 2-14:

$$P_{nt} = A_n f_y \qquad \textbf{Equation 2-14}$$

Where

$A_n$ = Area of closed stirrups

Ultimate tensile load, $N_{uc}$, shall always be regarded as a live load and shall not be taken as less than $0.2V_u$ unless special provisions are made to avoid tensile forces.

- Per ACI 318 – 14, the treatment of this tensile load as a live load is due to the large uncertainty involved in determining its magnitude, thus the use of the higher load factor given for live loads (ACI Committee 318, 2014).

4. $A_s$ shall be at least the greater of the following:

- $A_f + A_n$
- $2A_{vf}/3 + A_n$

Where $A_f$ is the area of steel resisting moment, which in this instance is equivalent to $A_s$.

(Caltrans, 2003)

### 2.5.2 LRFD Factors and Load Combinations

While the analysis and section capacities laid out by Caltrans coincided with AASHTO LRFD, there were differences between the two in regards to load factors, resistance factors, and load combinations. For the purposes of this research, the decision was made to defer to AASHTO.

For the purposes of this project, the tab of the culvert should be designed according to the Strength I Limit State, as outlined in the AASHTO LRFD Bridge Design specifications. The corresponding load combinations and load factors for these limit states is given in Table 3.4.1-1 of the AASHTO LRFD Bridge Design Code, which is reproduced below in Table 2-3: Load Combinations and Load Factors Table 2-3. A thick black box has been added around the Strength I Limit State to clearly indicate the relevant information. In instances where the expected dead load is more than 7 times larger than the expected live load, the Strength IV Limit State is appropriate; however, the only live load used in this analysis is the tension force, which is taken to be 20% of the dead load, and thus this limit state will never apply.

**Table 2-3: Load Combinations and Load Factors (AASHTO, 2012)**

| Load Combination Limit State | *DC DD DW EH EV ES EL PS CR SH* | *LL IM CE BR PL LS* | *WA* | *WS* | *WL* | *FR* | *TU* | *TG* | *SE* | Use One of These at a Time | | | | |
|---|---|---|---|---|---|---|---|---|---|---|---|---|---|---|
| | | | | | | | | | | *EQ* | *BL* | *IC* | *CT* | *CV* |
| Strength I (unless noted) | $\gamma_p$ | 1.75 | 1.00 | — | — | 1.00 | 0.50/1.20 | $\gamma_{TG}$ | $\gamma_{SE}$ | — | — | — | — | — |
| Strength II | $\gamma_p$ | 1.35 | 1.00 | — | — | 1.00 | 0.50/1.20 | $\gamma_{TG}$ | $\gamma_{SE}$ | — | — | — | — | — |
| Strength III | $\gamma_p$ | — | 1.00 | 1.40 | — | 1.00 | 0.50/1.20 | $\gamma_{TG}$ | $\gamma_{SE}$ | — | — | — | — | — |
| Strength IV | $\gamma_p$ | — | 1.00 | — | — | 1.00 | 0.50/1.20 | — | — | — | — | — | — | — |
| Strength V | $\gamma_p$ | 1.35 | 1.00 | 0.40 | 1.0 | 1.00 | 0.50/1.20 | $\gamma_{TG}$ | $\gamma_{SE}$ | — | — | — | — | — |
| Extreme Event I | $\gamma_p$ | γEQ | 1.00 | — | — | 1.00 | — | — | — | 1.00 | — | — | — | — |
| Extreme Event II | $\gamma_p$ | 0.50 | 1.00 | — | — | 1.00 | — | — | — | — | 1.00 | 1.00 | 1.00 | 1.00 |
| Service I | 1.00 | 1.00 | 1.00 | 0.30 | 1.0 | 1.00 | 1.00/1.20 | $\gamma_{TG}$ | $\gamma_{SE}$ | — | — | — | — | — |
| Service II | 1.00 | 1.30 | 1.00 | — | — | 1.00 | 1.00/1.20 | — | — | — | — | — | — | — |
| Service III | 1.00 | 0.80 | 1.00 | — | — | 1.00 | 1.00/1.20 | $\gamma_{TG}$ | $\gamma_{SE}$ | — | — | — | — | — |
| Service IV | 1.00 | — | 1.00 | 0.70 | — | 1.00 | 1.00/1.20 | — | 1.0 | — | — | — | — | — |
| Fatigue I— *LL, IM & CE* only | — | 1.50 | — | — | — | — | — | — | — | — | — | — | — | — |
| Fatigue II— *LL, IM & CE* only | — | 0.75 | — | — | — | — | — | — | — | — | — | — | — | — |

As seen in Table 2-3, except for live load, all of the relevant loads are multiplied by the load factor for permanent loads, $\gamma_p$. The appropriate value of this load factor is determined through use of Table 3.4.1-2 from the AASHTO LRFD Bridge Design Code, which is reproduced below in Table 2-4. Live load is multiplied by a factor of 1.75.

**Table 2-4: Load Factors for Permanent Loads, $\Upsilon_p$**

| Type of Load, Foundation Type, and Method Used to Calculate Downdrag | | Load Factor | |
|---|---|---|---|
| | | Maximum | Minimum |
| *DC*: Component and Attachments | | 1.25 | 0.90 |
| *DC*: Strength IV only | | 1.50 | 0.90 |
| *DD*: Downdrag | Piles, α Tomlinson Method | 1.4 | 0.25 |
| | Piles, λ Method | 1.05 | 0.30 |
| | Drilled shafts, O'Neill and Reese (1999) Method | 1.25 | 0.35 |
| *DW*: Wearing Surfaces and Utilities | | 1.50 | 0.65 |
| *EH*: Horizontal Earth Pressure | | | |
| • Active | | 1.50 | 0.90 |
| • At-Rest | | 1.35 | 0.90 |
| • *AEP* for anchored walls | | 1.35 | N/A |
| *EL*: Locked-in Construction Stresses | | 1.00 | 1.00 |
| *EV*: Vertical Earth Pressure | | | |
| • Overall Stability | | 1.00 | N/A |
| • Retaining Walls and Abutments | | 1.35 | 1.00 |
| • Rigid Buried Structure | | 1.30 | 0.90 |
| • Rigid Frames | | 1.35 | 0.90 |
| • Flexible Buried Structures | | | |
| ○ Metal Box Culverts and Structural Plate Culverts with Deep Corrugations | | 1.5 | 0.9 |
| ○ Thermoplastic culverts | | 1.3 | 0.9 |
| ○ All others | | 1.95 | 0.9 |
| *ES*: Earth Surcharge | | 1.50 | 0.75 |

As seen in Table 2-4, both a maximum and minimum load factor is given for each load type. It is appropriate to use the maximum load factor except in instances where the force effect of the load in question decreases the effect of another load.

For the purposes of this research, At-Rest earth pressure was used in the analysis and thus, the relevant load factor for Horizontal Earth Pressure would be 1.35. When Vertical Earth Pressure factors into the analysis, the appropriate factor would be 1.00, as its impact would serve to reduce the load on the tab being designed and this pressure is acting upon a retaining wall.

AASHTO gives a resistance factor of $\Phi = 0.70$ for compressive capacities when designing using a strut-and-tie model. Both the ACI and Caltrans guidance on the designing of corbels dictate one resistance factor to be used for all capacities because failure of brackets and corbels is

predominantly controlled by shear (ACI Committee 318, 2014). Because the factor of 0.70 is conservative in comparison to all other resistance factors that could arguably be applied, it was decided to follow this convention in the analysis performed on this project.

# CHAPTER 3: Constructed Culverts

This section provides information on the three culverts constructed for the purpose of this research project. All three used a novel approach previously mentioned in this thesis wherein the wing walls were constructed separately from the culvert as opposed to the typical practice of being cast integrally with the barrels. This approach alleviated the distresses associated with differential settlement. To allow for the now separated wing walls to take advantage of the stiffness of the culvert in resisting the lateral earth pressures associated with the backfill, tabs were added to the corners of the culvert which provided bearing support for the wing walls.

## 3.1 Chambers County Culvert

The culvert constructed in Chambers County crosses Whatley Creek on Chambers County Road 258.

### 3.1.1 Important Dates and Construction Photos

**Figure 3-1: Replaced Bridge in Chambers County**

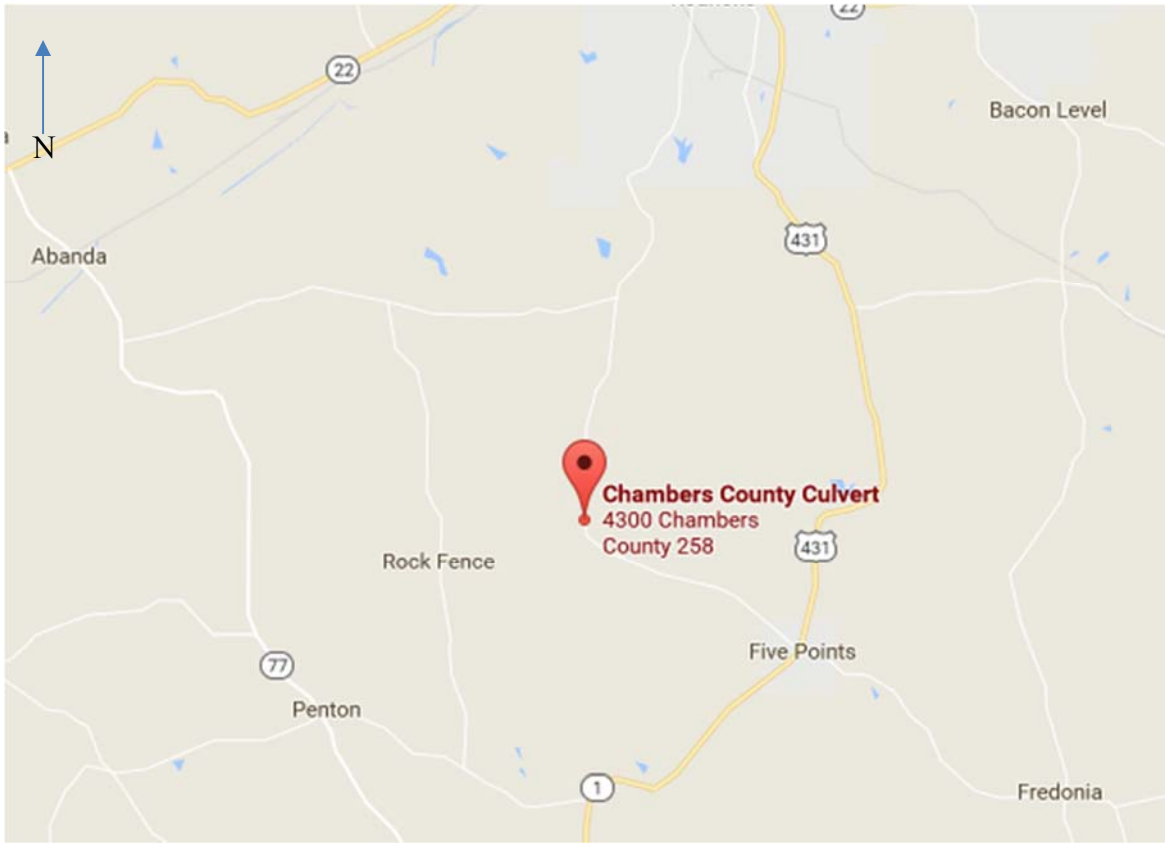


**Figure 3-2: Location of Chambers County Culvert (Google Maps, 2017)**

Below is a list of significant dates during the construction and analysis of the culvert in Chambers County, followed by a selection of photos showing the construction process.

- June 29, 2015: The southern wall of the culvert was placed with the pressure cells installed integrally in western tab.
- July 6, 2015: The pressure cells were installed in the eastern tab of the southern wall and the southern wing walls were placed.
- July 21, 2015: The southern half of the elevated mat was placed.
- August 24, 2015: The northern wall of the culvert was placed.

- August 27, 2015: Pressure cells were installed in both northern tabs and the northern wing walls were placed.
- September 9, 2015: The northern half of the elevated mat was placed.
- January 12, 2016: Significant backfill had been placed but no pavement.
- March 31, 2016: The pressure cell wires at Tab 3 were cut but still readable and a measurement recorded during significant rainfall.
- April 19, 2016: The first measurements after paving were recorded.
- September 13, 2016: A 24-hr cycle of measurements was recorded.
- November 17, 2016: All DEMEC studs and tell-tales were installed.

**Figure 3-3: Workers construct formwork for southern end of culvert**

**Figure 3-4: Formwork for embedded pressure cells**

**Figure 3-5: Southern wing wall formwork removed**

**Figure 3-6: Formwork for northern half of elevated mat**

**Figure 3-7: All formwork removed**

**Figure 3-8: Backfill completed**

**Figure 3-9: Paving completed**

## 3.2 Lee County Culvert

The culvert constructed in Lee County crosses a tributary to Halawakee Creek on Lee County Road 156.

### 3.2.1 Important Dates and Construction Photos

**Figure 3-10: Replaced Bridge in Lee County**

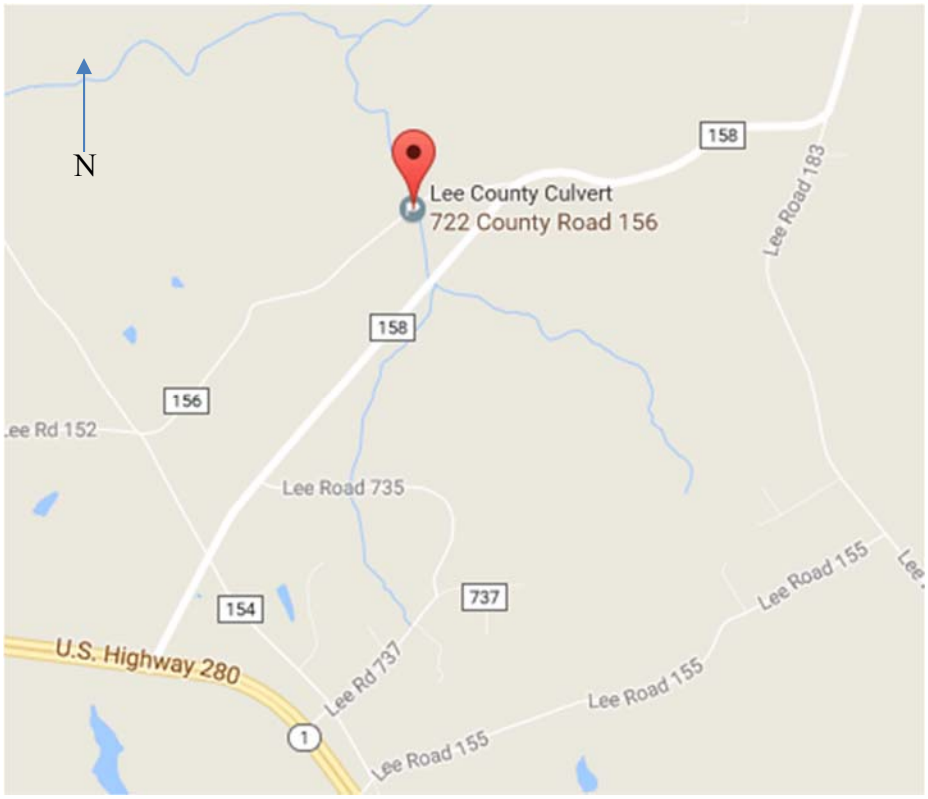


**Figure 3-11: Lee County Culvert Location (Google Maps, 2017)**

Below is a list of significant dates during the construction and analysis of the culvert in Lee County, followed by a selection of photos showing the construction process.

- January 14, 2016: The first visit to the site was made. Demolition of existing structure had not yet been completed.
- February 26, 2016: The culvert barrels were placed.
- March 8, 2016: Pressure cells were installed in the eastern tabs of the culvert and both eastern wing walls were placed.
- March 22, 2016: Pressure cells were installed in the western tabs of the culvert and both western walls were placed.

- August 29, 2016: Researchers were alerted that backfill was underway. Measurements were recorded periodically, as well as with an approximately 40 ton truck located near each tab location.
- September 28, 2016: Backfill had been completed and a tack coat was placed in preparation for the placement of a bearing surface.
- September 29, 2016: Measurements were recorded after each lane of the bearing surface was placed.
- October 13, 2016: Initial DEMEC studs were installed.
- November 4, 2016: Improved DEMEC studs were installed along with all 4 tell-tales.

**Figure 3-12: Water flow redirected**

**Figure 3-13: On-site water retention**

**Figure 3-14: Water flow redirected to construct western wing walls**

**Figure 3-15: Completed culvert**


**Figure 3-16: 40 ton truck placed near tab**

**Figure 3-17: Culvert in process of being paved**

**Figure 3-18: Paving competed**

## 3.3 Coosa County Culvert

The culvert constructed in Coosa County crosses Shelton Creek on Coosa County Road 68.

### 3.3.1 Important Dates and Construction Photos

**Figure 3-19: Replaced Bridge in Coosa County**

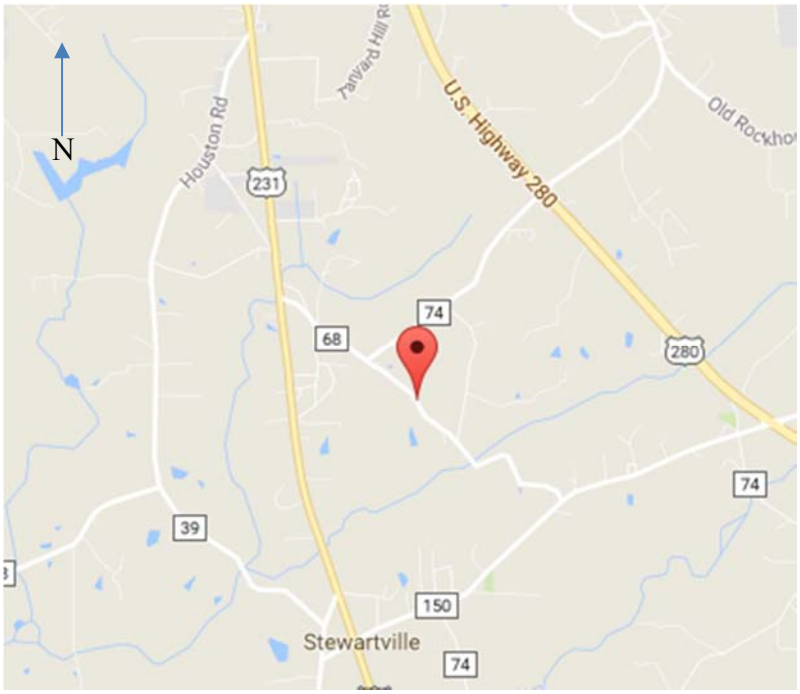


**Figure 3-20: Location of Culvert in Coosa County (Google Maps, 2017)**

Below is a list of significant dates during the construction and analysis of the culvert in Coosa County, followed by a selection of photos showing the construction process.

- March 29, 2016: The first visit to the site was made. Formwork for both culvert walls was already being erected and the necessary block out locations were explained.
- April 7, 2016: The western wall of the culvert was placed.
- April 14, 2016: The elevated mat of the culvert was placed.
- May 4, 2016: The northern wing walls were placed without pressure cells placed due to an error by the contractor regarding the placement of block-outs. The southern tabs were chiseled away to make space for the pressure cells to be placed appropriately.
- May 5, 2016: Pressure cells were installed in both of the southern tabs.
- May 9, 2016: The southern wing walls were placed.
- October 8, 2016: The first measurements post paving were recorded.

**Figure 3-21: Workers construct formwork for barrels**

**Figure 3-22: Workers install pressure cells in corrected block outs**

**Figure 3-23: Completed culvert**

# CHAPTER 4: CULVERT INSTRUMENTATION

## 4.1 Tab Pressure

### 4.1.1 Field Measurement of Lateral Earth Pressure

The primary load concern for the purposes of this project was that associated with lateral earth pressure. The magnitude of this pressure acting upon the tabs of the culverts was measured using Model 4810 Vibrating Wire Pressure Cells manufactured by Geokon, Inc, shown in Figure 4-1. This model was chosen because its intended use is the measuring of soil pressure on structures and because the expected values of pressures predicted by the finite element models fell within the applicable range and granularity of the sensors. Furthermore, the thin profile and 9 inch diameter of the pressure cells fit well within the necessary area of the tab and did not add much complexity to the construction process.

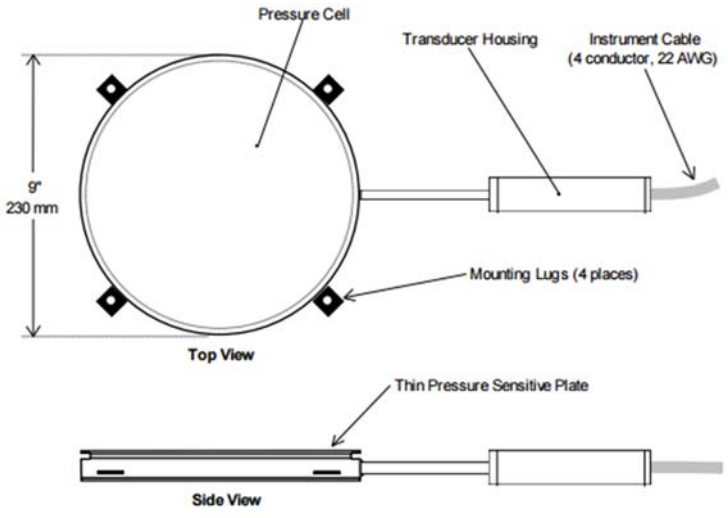


**Figure 4-1: Model 4810 Contact Pressure Cell (Geokon, Inc., 2011)**

These pressure cells operate based on hydraulic principles. Two thin, round, flat plates were welded together along their circumference and the gap between them was filled with hydraulic fluid. The specific cell used for this research was made with one rigid plate for bearing against the structure and on flexible plate which deforms according to the applied pressure. The flexibility of the plate exposed to the pressure functions such that the external soil pressure is in equilibrium with the hydraulic fluid between the plates. This fluid is connected hydraulically to a vibrating wire pressure transducer which converts the pressure into an electrical signal through the use of a plectrum that induces a corresponding vibration. This value is then transmitted through the connected wires. Also, a thermistor located within the transducer which provides a value for the temperature at the location of the cell. A depiction of this pressure cell is given in Figure 4-1 (Geokon, Inc., 2011).

Although it is typical to install these cells with the deformable face directly exposed to soil, the aim of this project was not to measure soil pressure, but rather the pressure experienced by the tab of the culvert. The cells were installed in the gap between the tab and wing wall and therefore measured the magnitude of the pressure transferred into the tab through contact with the wing wall. Review of literature did not uncover any previous attempts at using these pressure cells in a similar manner; however, the use of a bituminous material to cover the deformable face of the pressure cells ensured that the pressure applied to the cells was distributed appropriately and therefore it was believed that this application of these cells was valid.

The measurements recorded from the pressure cells were given in digits which were then converted to pressure values in both kPa and psf using the Equation 4-1 and Equation 4-2 (Geokon, Inc., 2011):

$$P_{Linear} = G(R_1 - R_0) + K(T_1 - T_0) - (S_1 - S_0) \qquad \textbf{Equation 4-1}$$

Where:

$P_{Linear}$ = Linear calculation of pressure (kPa or psf)

G = Linear gage factor (kPa/digit or psf/digit)

$R_1$ = Gage reading (digits)

$R_0$ = Initial gage reading (digits)

K = Thermal factor (kPa/°C or psf/°C)

$T_1$ = Temperature measurement from internal thermistor (°C)

$T_0$ = Initial temperature measurement from internal thermistor (°C)

$S_1$ = Barometric pressure at time of measurement (kPa or psf)

$S_0$ = Initial barometric pressure (kPa or psf)

$$P_{Poly} = AR_1^2 + BR_1 + C + K(T_1 - T_0) - (S_1 - S_0) \qquad \textbf{Equation 4-2}$$

Where:

$P_{Poly}$ = Polynomial calculation of pressure (kPa or psf)

A, B, and C = Constants provided for each individual cell based on laboratory testing

Because there was no reliable method to accurately determine the barometric pressure at the locations of the culverts and because the pressure cells were embedded within the culverts, the barometric pressure was assumed to be constant for the purpose of this research. The spreadsheets used to calculate pressure for this project were used to determine that this assumption had minimal effect on the magnitudes calculated.

Each instrumented tab contained three pressure cells distributed through its height, as shown below in Figure 4-2, with one placed 1 inch above the location of the cold joint at the bottom of the tab, one placed 2 inches below the lowest point of the slope of the top of the tab, and another placed directly in between the other two cells.

**Figure 4-2: Post installed pressure cells**

In order to take measurements from the pressure cells, a handheld reader was connected via alligator clamp to the five exposed wires of the pressure cells. The readout gave a temperature and a digit value which was then used to calculate pressure.

Prior to the construction of the first culvert, two methods of cell installation were proposed: embedded installation and post-construction installation. Each was utilized in the field in order to determine the best method with which to proceed.

### 4.1.2 Embedded Installation

The embedded method of installation required that the pressure cells be attached to the formwork, as shown below in Figure 4-3, so that they could be completely embedded in to the concrete of the tab, as shown be below Figure 4-4. The cells were attached using steel wire so that the wire could be cut when it came time to remove the formwork. Plastic cable ties were used to ensure the cables would follow an appropriate path to the top of the tab.

**Figure 4-3: Formwork prepared for embedded installation of pressure cells**

**Figure 4-4: Pressure cells embedded in culvert tab**

This method proved to be labor intensive due largely to the difficulty associated with the added care necessary to place the formwork with attached pressure cells while navigating through already placed reinforcing steel. There was also an increase in the difficulty of removing said formwork.

### 4.1.3 Post-Construction Installation

The post-construction method of pressure cell installation, shown above in Figure 4-2, involved using block-outs on the formwork, shown below in Figure 4-5, in order to create recesses in the hardened concrete of the tab, shown below in Figure 4-6, into which the cells could be installed using concrete screws. The cables were attached to the perimeter of the cells using zip ties to ensure that the cables would not pass in front of the cells and affect pressure measurements.

**Figure 4-5: Formwork with block-outs for post installation**

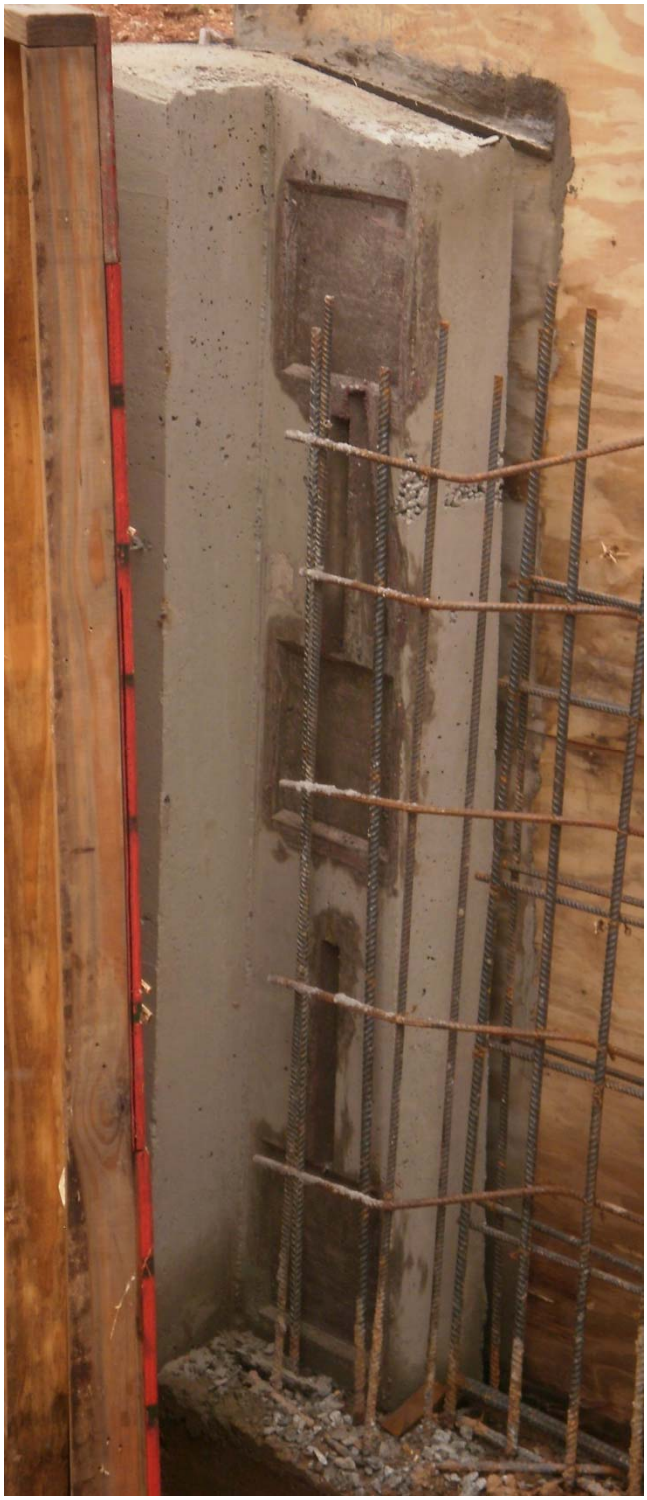

**Figure 4-6: Recesses in tab for post installation**

The method of post-construction installation allowed for reusability of formwork and resulted in an easier construction process overall in comparison to the embedded method of installation. An added benefit of this method was that, unlike the embedded cells, the post installed cells protruded a slight amount beyond the face of the tab which increased the likelihood of contact with the wing wall registering as pressure on the cells. For these reasons, it was decided that the post-construction installation method was the better choice; thus, it was utilized for all subsequent installations on this project.

## 4.2 Gap Movement Measurement across Horizontal Face

The movement of the gap between the wing wall and tab on the horizontal face of each was measured using a 200 mm Mayes demountable mechanical concrete strain gauge (DEMEC), shown below in Figure 4-7. The DEMEC gauge has one fixed point and one movable point that are set apart at a fixed distance by a rigid bar. The movable point allows for variability in the distance between the two points and their separation is measured by the attached dial gauge.


**Figure 4-7: DEMEC Concrete Strain Gauge**

To use the DEMEC, metal studs, with dimples that serve as receptacles for the two points on the DEMEC, were installed a set distance apart into the concrete, as seen in Figure 4-8. The x-marks on Figure 4-9 indicate the approximate location of the studs on the culvert.

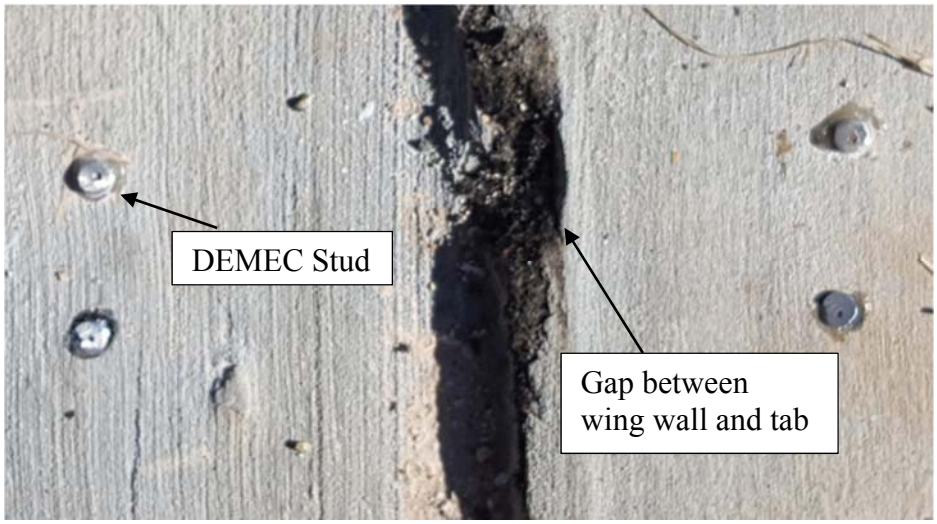


**Figure 4-8: DEMEC Studs**

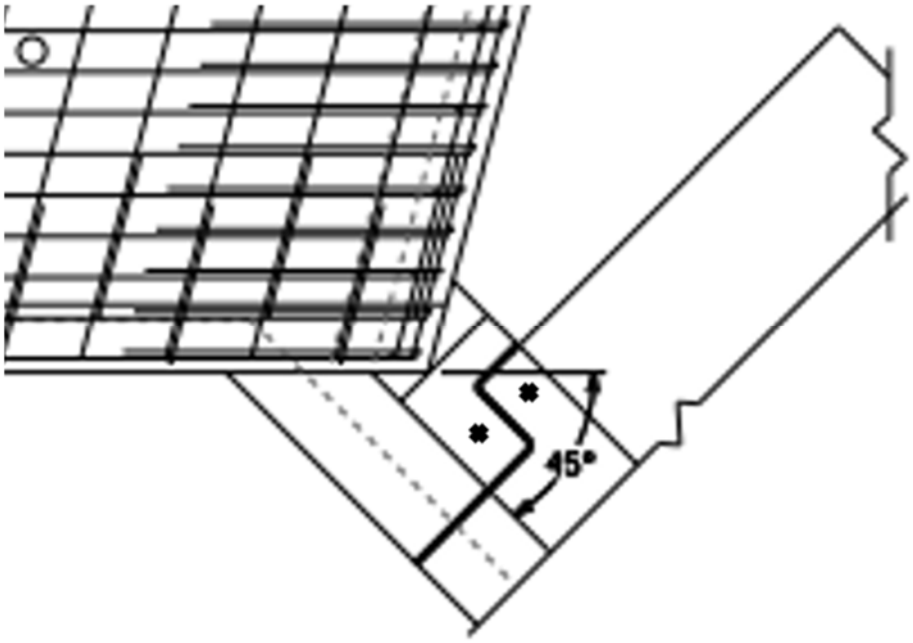


**Figure 4-9: Location of DEMEC Studs**

These metal studs were fabricated by sawing off small lengths of 3/8 inch threaded rod. Dimples in these lengths were created using a drill press. The studs were installed by first drilling two holes into the concrete using a template to ensure the proper separation, then filling the hole with a quick setting epoxy, and finally placing the studs into the holes. Originally, the dimples were created using a 3/32 inch drill bit, with this diameter allowing for the use of a setting tool to create small indentations within the dimples for the placement of the DEMEC points when taking readings. These studs, however, quickly showed signs of rust when installed and thus, it was decided to fabricate new studs using a 1/16 inch drill bit and going deeper into the stud than was previously done with the wider diameter. This allowed for the points of the DEMEC to seat upon the perimeter of the dimple which decreased accuracy, but increased the repeatability of the process while mitigating the effects of rust. A picture of the two types of installed studs is shown below in Figure 4-8, with the top two being those with the larger diameters which show faint signs of rust. This picture was taken at the culvert in Lee County as it was the only culvert where the larger diameter studs were installed.

To take measurements with the DEMEC gauge, first a measurement was recorded from a reference bar which allowed for the effects of temperature to be taken into account. Then, the DEMEC gauge was placed into the metal studs and another measurement was recorded. The gauge is read such that the smaller circle provides the first two digits of the measurement and the outer circle provides the values of the last two digits. To get a value for the movement of the gap, the Equation 4-3 was used:

$$\Delta = [(R_i - R_{ref_i}) - (R_0 - R_{ref_0})]k * l \qquad \textbf{Equation 4-3}$$

Where:

$\Delta$ = change in gap opening with respect to initial gap width (mm)

R = measurement recorded from the studs installed into the concrete

$R_{ref}$ = measurement recorded from the reference bar

k = constant representing the strain value of division on the dial (shown in Figure 4-7)

l = gauge length of the DEMEC used (200 mm)

$d_0$ = initial gap width (mm)

This method assumes that all movement between the studs is concentrated within the gap; however, this is not necessarily the case. The movement of the concrete caused by temperature change could change the distance between the studs without an impact on the width of the gap by a magnitude large enough to be registered by the gauge used.

### 4.3 Gap Movement Measurement across Vertical Face

The movement of the gap between the wing wall and tab on the vertical face was measured using tell-tales, as shown below in Figure 4-10. These were used in place of the DEMEC due to the potential for larger displacements that fall outside of the range of the DEMEC. The tell-tales provided a visual depiction of gap movement by attaching one half of the tell-tale to either side of the gap, with the graduated half of the tell-tale overlapped by an indicator for the original location of the center. Over time, the magnitude of the movement of the gap was quantified by reading where the indicator aligned with the scale.

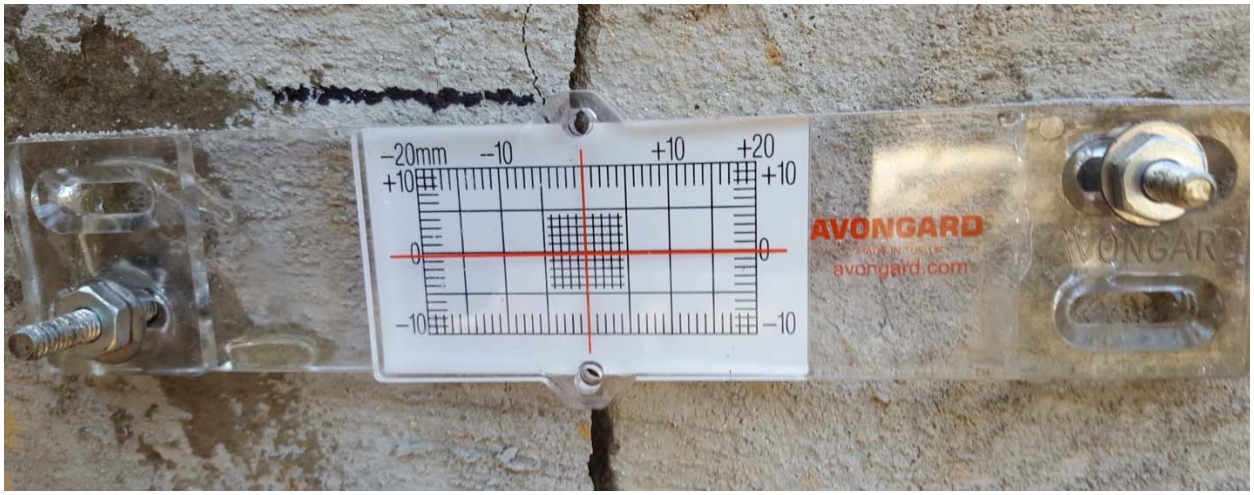


**Figure 4-10: Tell-tale**

The tell-tales were installed by first marking the location of the tell-tale holes on the concrete with a marker, such that the center of the tell-tale aligned with the gap. As shown above in Figure 4-10, only two screws were used to install the tell-tales due to the holes in the tell-tale being too close for two holes to be drilled on one side without compromising the integrity of the concrete between the two holes. A caulk gun was then used to fill the holes with silicone adhesive and a screw was placed head first into each hole. Once the adhesive had set, the parts of the tell-tale that would make contact with the concrete were also coated in adhesive and the tell-tale was placed onto the screws and pushed flush with the concrete. Finally, a washer and nut were fixed onto the exposed threads of the screws and hand tightened.

In order to track the movement of the gap, a photo of each tell-tale was taken during all site visits that followed their installation.

# CHAPTER 5: RESULTS AND DISCUSSION

## 5.1 Overview

This section contains the charts created using the data collected from the pressure cells and the DEMEC strain gauge. Also included is the procedure used for and results obtained from the tests run on the concrete used during this research project. The raw data used in the generation of these charts and tables is provided in Appendix A.

Note that only two tabs of the culvert constructed in Coosa County were instrumented due to an error with formwork and a need to maintain the construction schedule.

## 5.2 Pressure versus Time

The charts in this section show the pressure measurements recorded at each pressure cell over the course of data collection. The vertical scale of each chart is scaled to the maximum pressure measured over the course of the entire project. The dataset displayed for each cell begins from the measurement that was recorded when the cell was installed with the face open to air.

The legend in the top left corner uses a two character abbreviation to explain the significance of each data set. The first character is either a ‘B’ to signify the bottom cell, ‘M’ to signify the middle cell, or ‘T’ to signify the top cell. The second character gives the number of the tab that contains the cell. The schematic of the culvert in the top right corner gives a reference arrow to orient the culvert to cardinal directions, uses ‘≈’ to show the orientation of water flow beneath the culvert, and the circle indicates the tab that is represented in the given chart. Finally, vertical lines and text callouts are used to highlight key events that occurred over the course of observation.

### 5.2.1 Chambers County

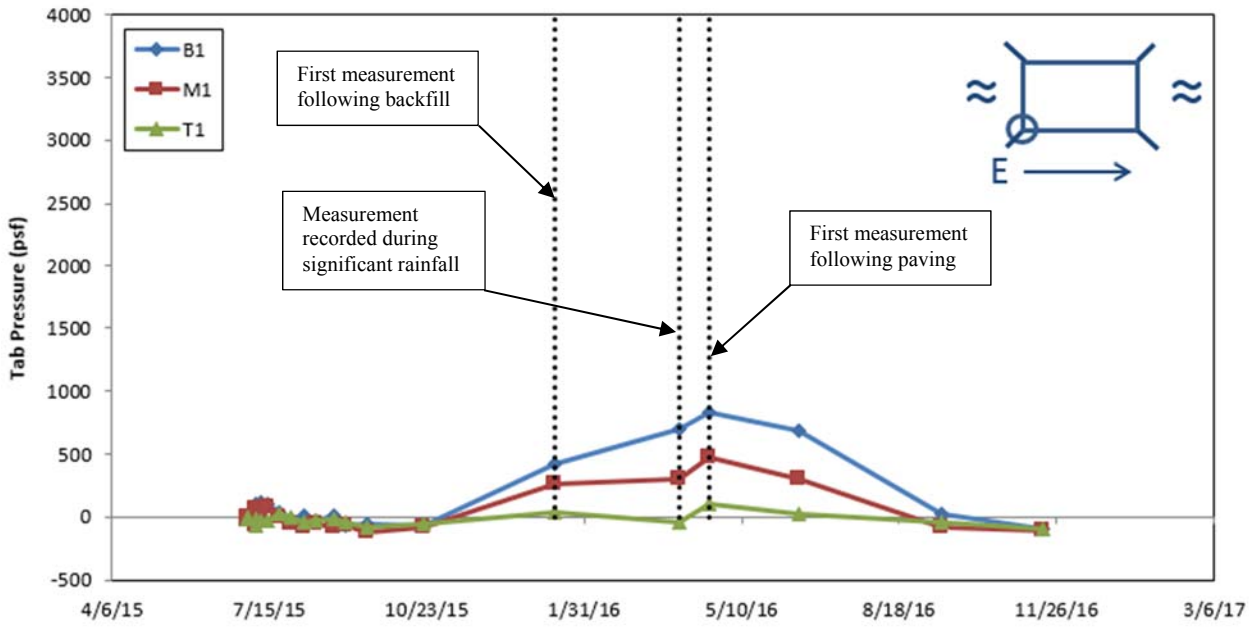


**Figure 5-1: Chambers County Tab 1, Pressure versus Time**

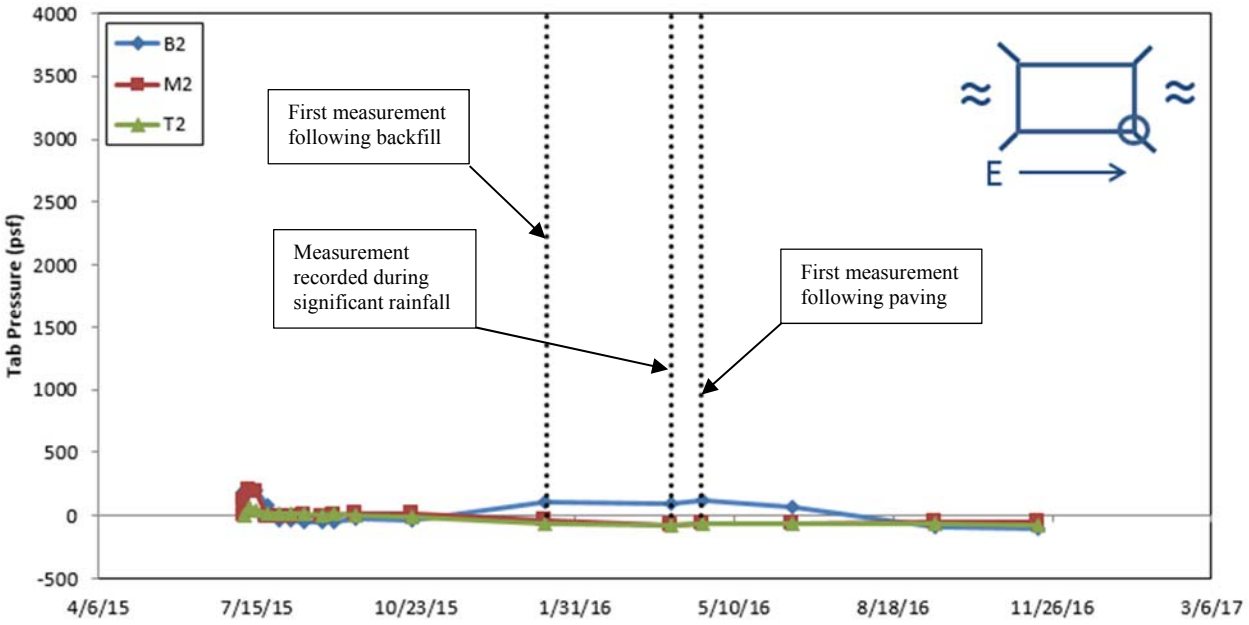


**Figure 5-2: Chambers County Tab 2, Pressure versus Time**

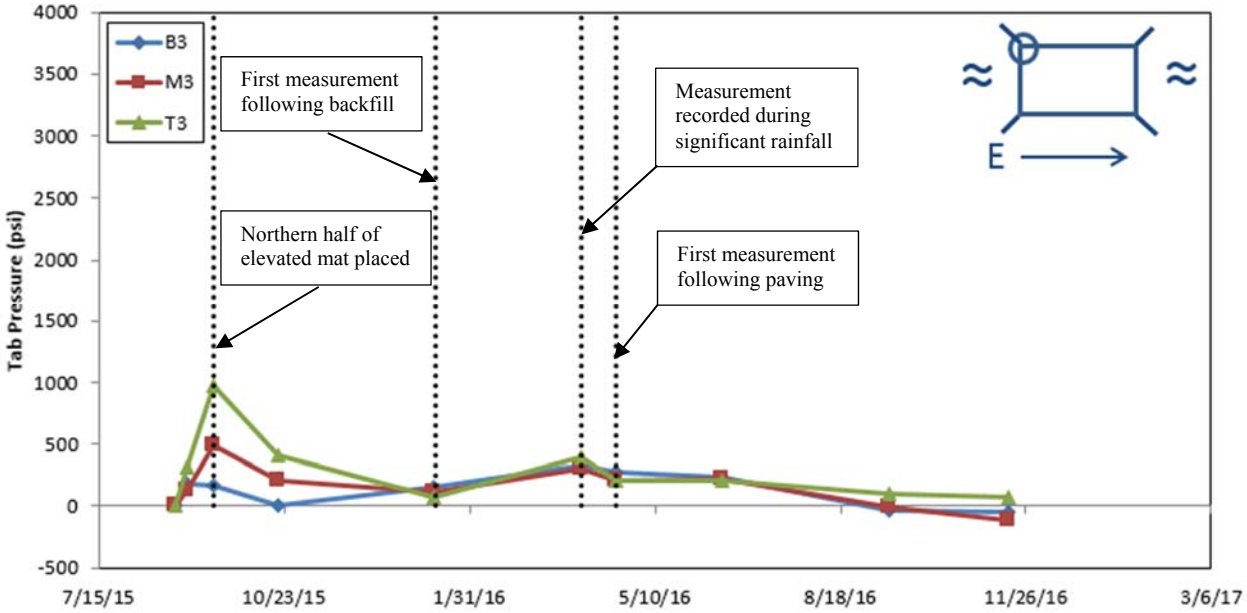


**Figure 5-3: Chambers County Tab 3, Pressure versus Time**

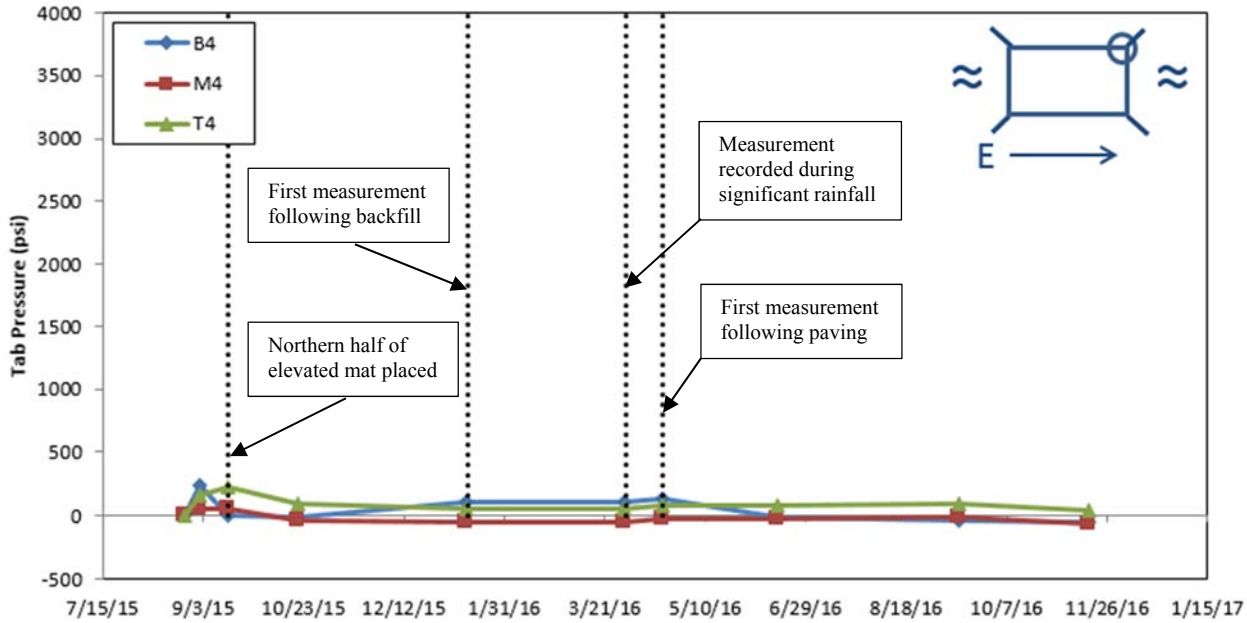


**Figure 5-4: Chambers County Tab 4, Pressure versus Time**

### 5.2.2 Lee County

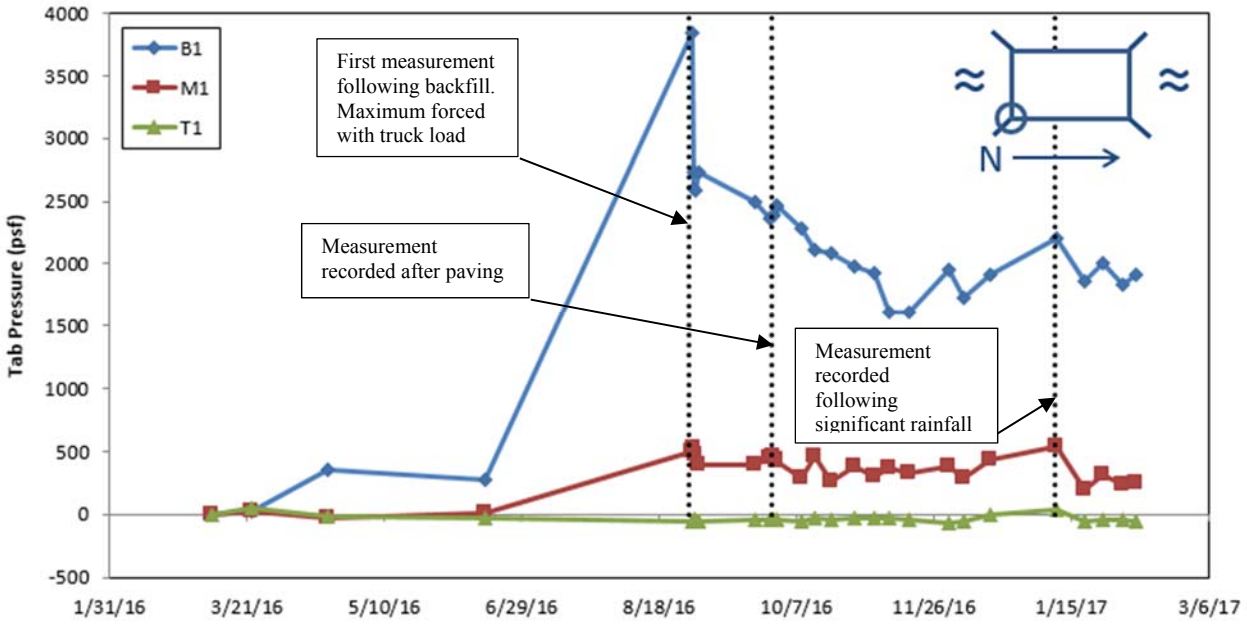


**Figure 5-5: Lee County Tab 1, Pressure versus Time**

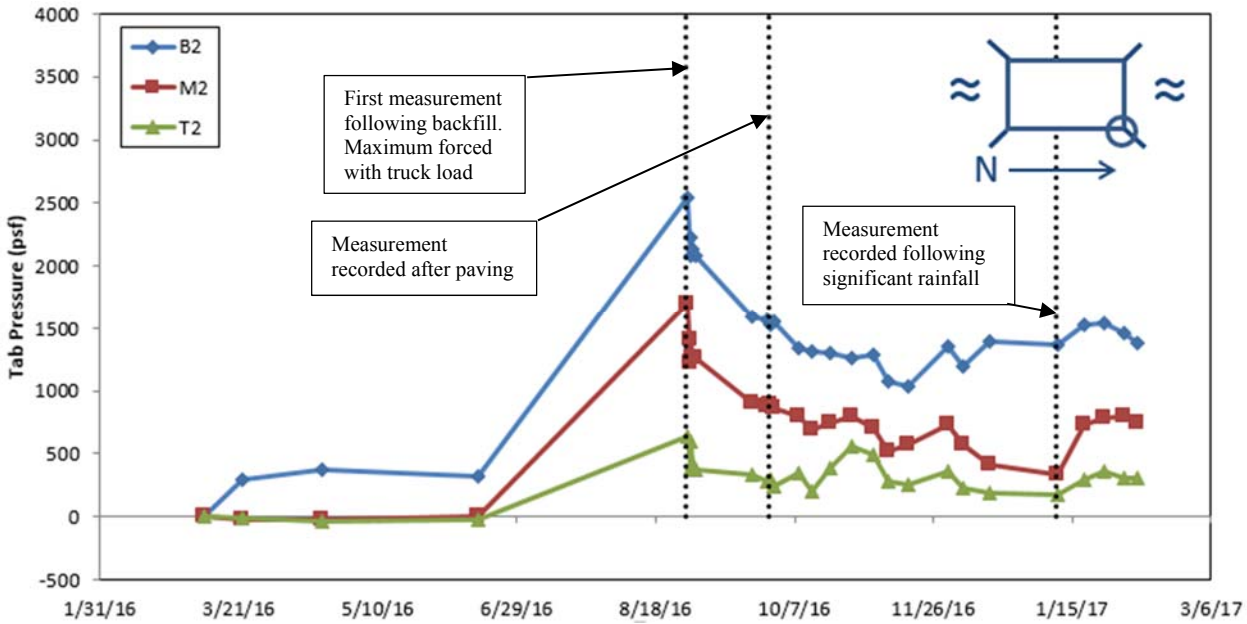


**Figure 5-6: Lee County Tab 2, Pressure versus Time**

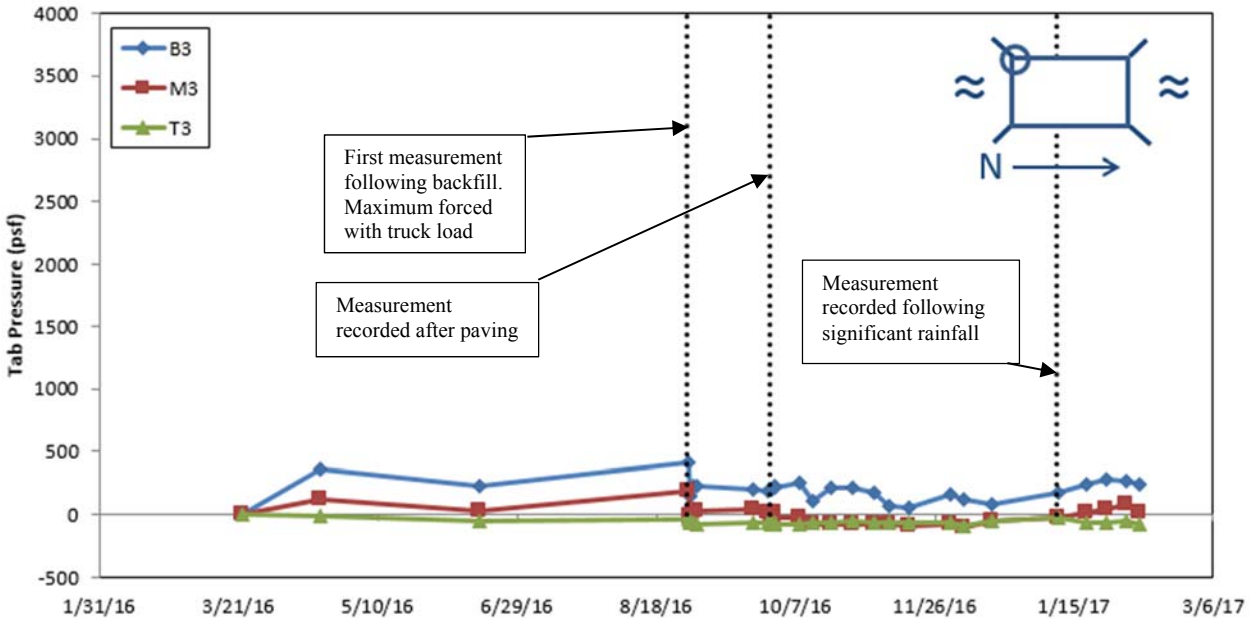


**Figure 5-7: Lee County Tab 3, Pressure versus Time**

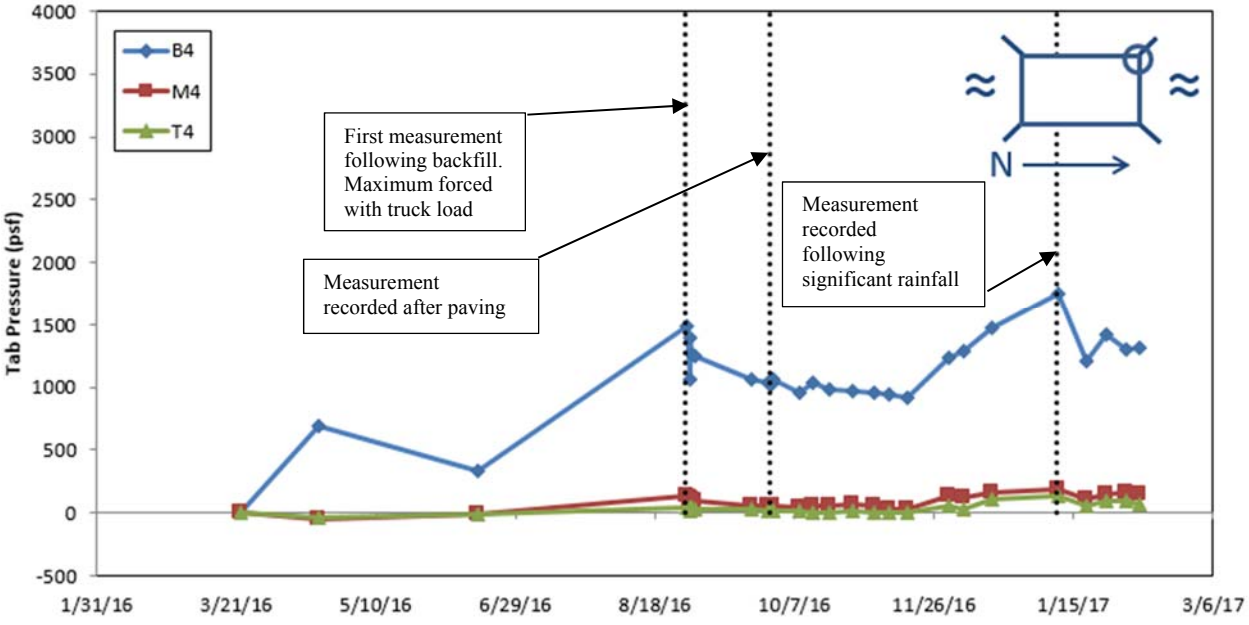


**Figure 5-8: Lee County Tab 4, Pressure versus Time**

### 5.2.3 Coosa County

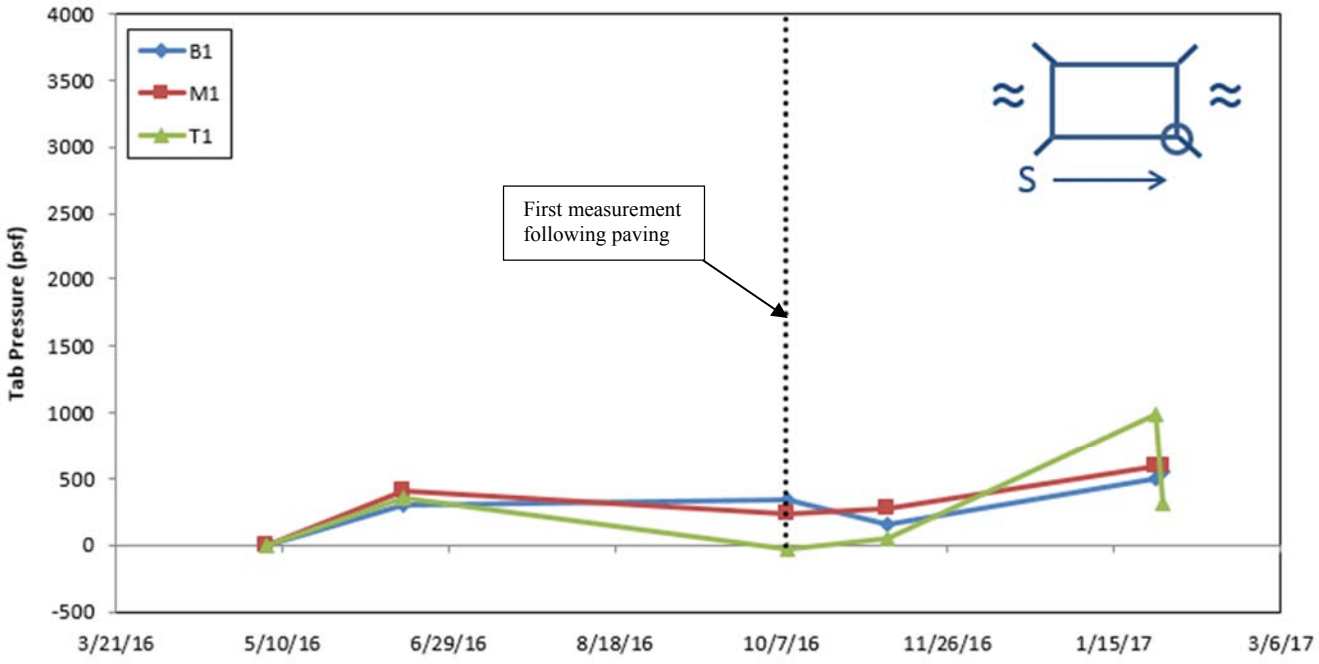


**Figure 5-9: Coosa County Tab 1, Pressure versus Time**

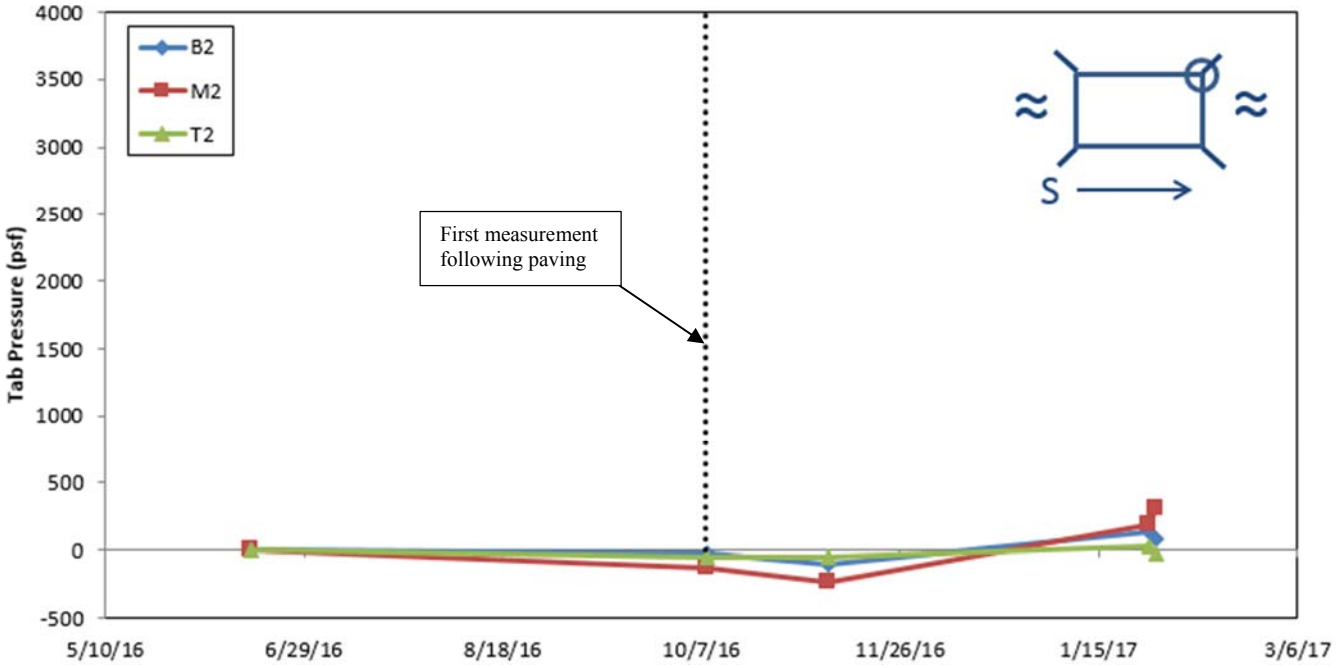


**Figure 5-10: Coosa County Tab 2, Pressure versus Time**

### 5.2.4 Pressure versus Time Discussion

Through visual inspection of the charts generated showing the change in tab pressure over time, several things were inferred about the pressure acting upon the tab.

First, it was evident that until backfill was placed, the tab experienced negligible pressure from the bearing force of the wing wall. Unfortunately, the culvert in Lee County was the only culvert for which the contractors gave notice to the researchers that back fill was underway. Because of this, it is likely that the largest magnitude of tab pressure at the culverts in Coosa County and Chambers County were not recorded. The largest magnitude of pressure recorded in Lee County, as well as in general for the project, occurred on August 29, 2016, when backfill reached the required height prior to pavement. In addition to backfill, this measurement was recorded with an approximately 40 ton truck load parked as close to each tab as possible. This was done to exaggerate the surcharge load that would be associated with trucks carrying backfill and associated with compactors. Measurements were also recorded during compaction; however, these did not reach the same magnitudes.

Second, it was observed that the general trend over time, following the placement of backfill, was a gradual reduction of pressure, trending toward zero. Certainly, fluctuations of load still occurred within this time frame due to environmental factors, chief among them being rain, but the culvert in Coosa County is the only culvert with an overall maximum pressure observed after the placement of pavement. This is almost certainly because of the lack of communication with contractors and the travel distance to Coosa County, which resulted in crucial measurements not being recorded. It is likely that the maximum pressure in Coosa County went unrecorded. Aside from the culvert in Coosa County, only Tab 4 of the culvert in Lee County (Figure 5-8) experienced

a local maximum pressure after the placement of pavement. On January 9, 2017 during an extended period of heavy rain, this tab experienced a pressure 17% higher than its previous maximum pressure which was observed during backfill; however, this local maximum pressure was only 46% of the maximum pressure recorded for that culvert during backfill.

Finally, it was observed that the maximum pressure occurred most often at the bottom of the tab. This observation is more clearly demonstrated in the following section.

### 5.3 Pressure versus Height

The charts in this section were generated using the same data given in the previous section; however, on these charts, the data is presented in a way that allows for a visual representation of the vertical distribution of the load acting on the tab and has been pared down by eliminating data sets that were redundant. Each data line on the chart represents one set of measurements recorded from each cell within the tab. Each data point on a line represents the height of a pressure cell. As with the previous section, these charts are scaled to accommodate the maximum pressure recorded over the course of the entire project.

The schematic of the culvert in the top right corner gives a reference arrow to orient the culvert to cardinal directions, uses '≈' to show the orientation of water flow beneath the culvert, and the circle indicates the tab that is represented in the given chart. The legend beneath this schematic indicates the importance of the date represented by each of the data sets. Each chart includes the initial measurement, the key measurements indicated with vertical lines on the charts in Section 5.2, and the latest measurement recorded. The charts generated for Coosa County include all measurements due to the overall lack of them.

### 5.3.1 Chambers County

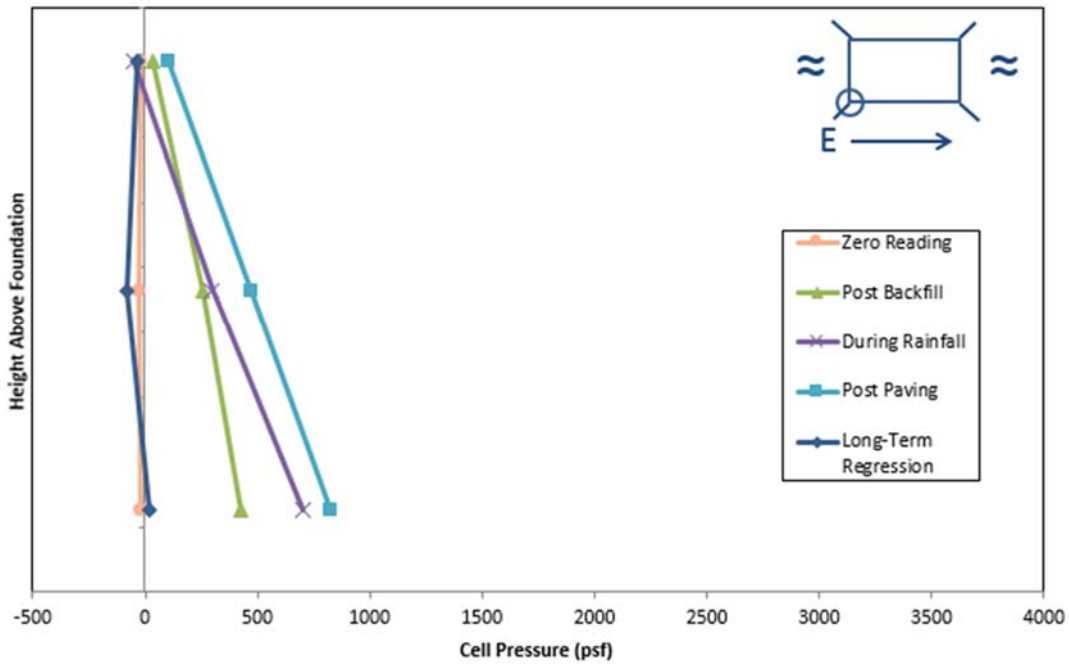


**Figure 5-11: Chambers County Tab 1, Pressure versus Height**

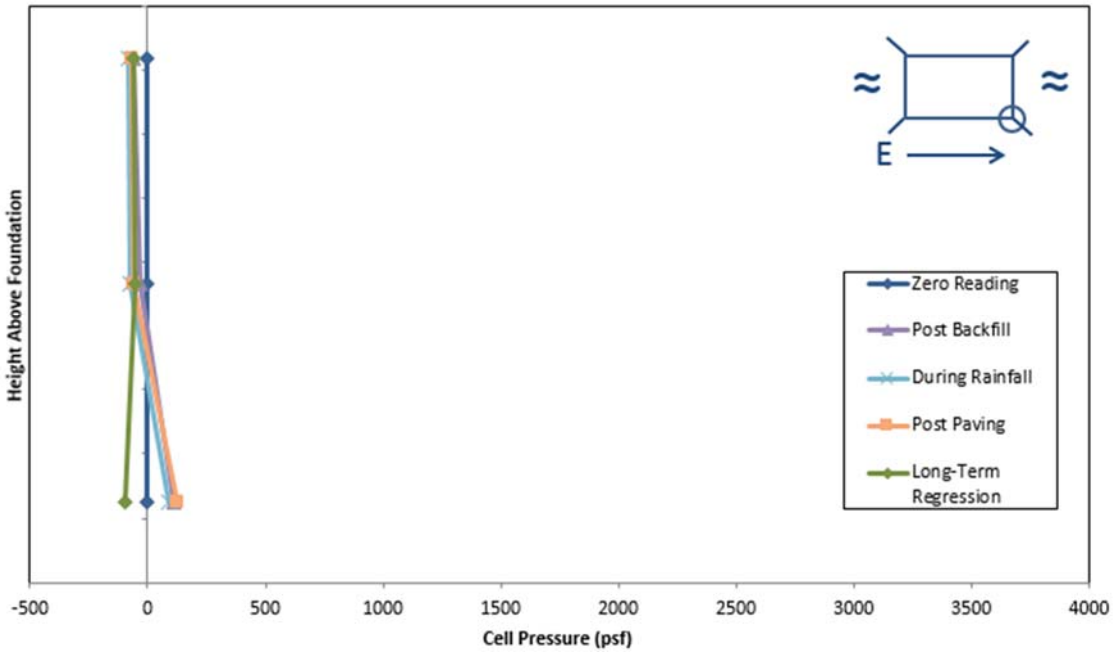


**Figure 5-12: Chambers County Tab 2, Pressure versus Height**

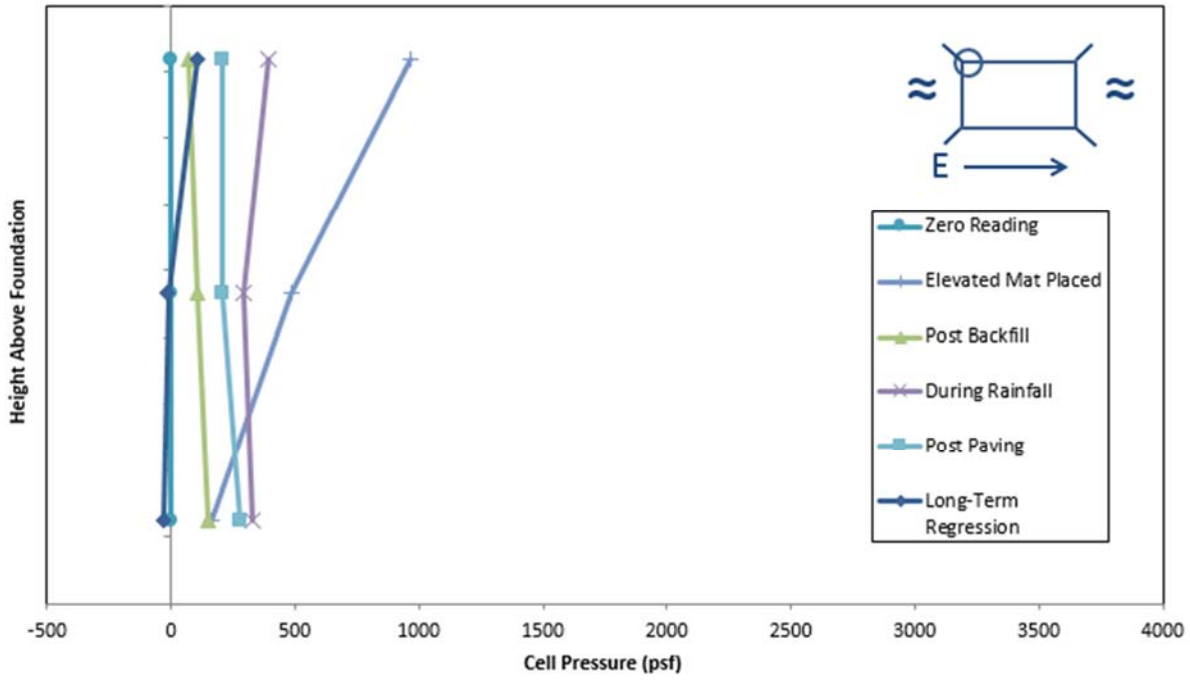


**Figure 5-13: Chambers County Tab 3, Pressure versus Height**

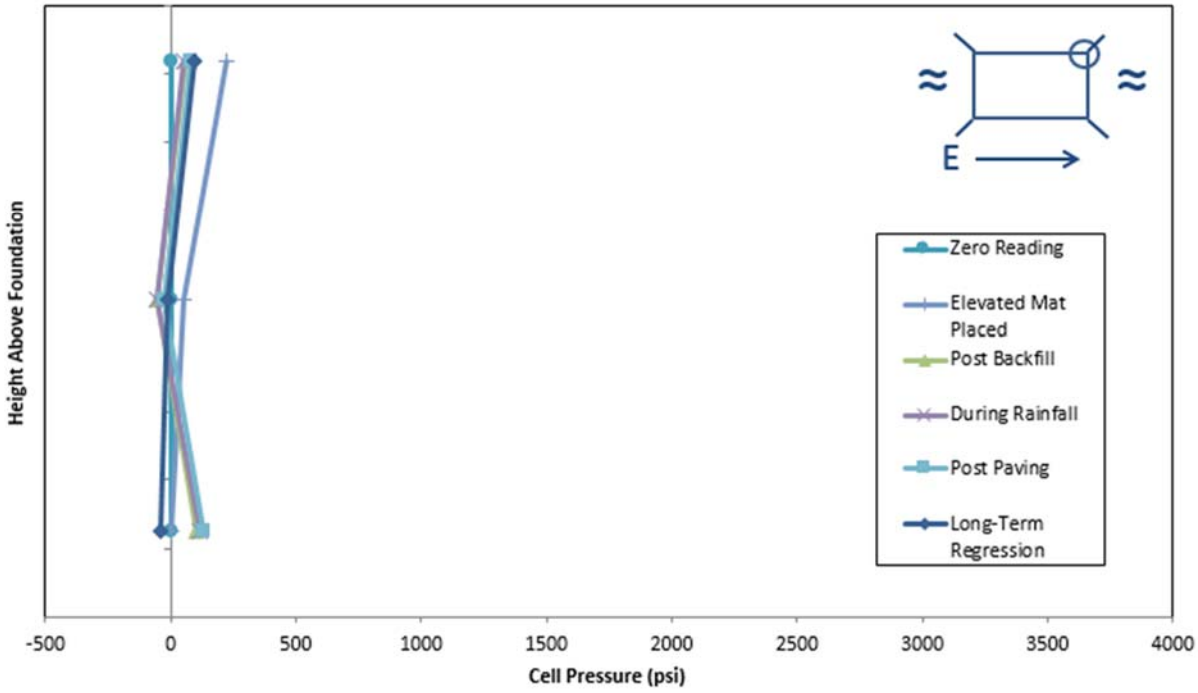


**Figure 5-14: Chambers County Tab 4, Pressure versus Height**

### 5.3.2 Lee County

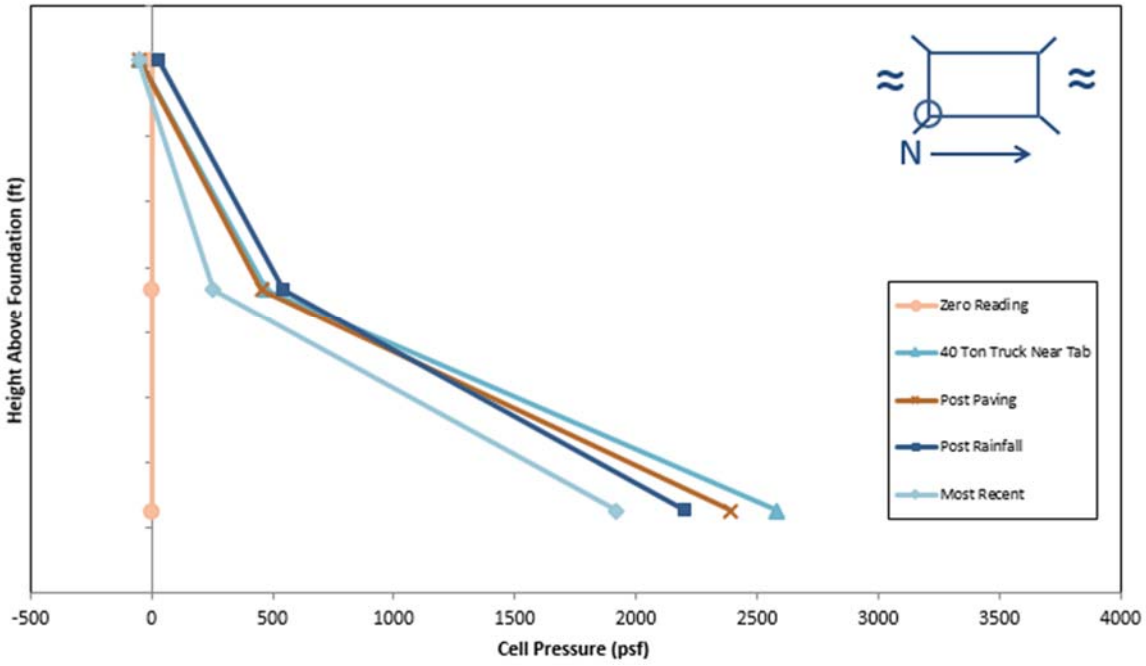


**Figure 5-15: Lee County Tab 1, Pressure versus Height**

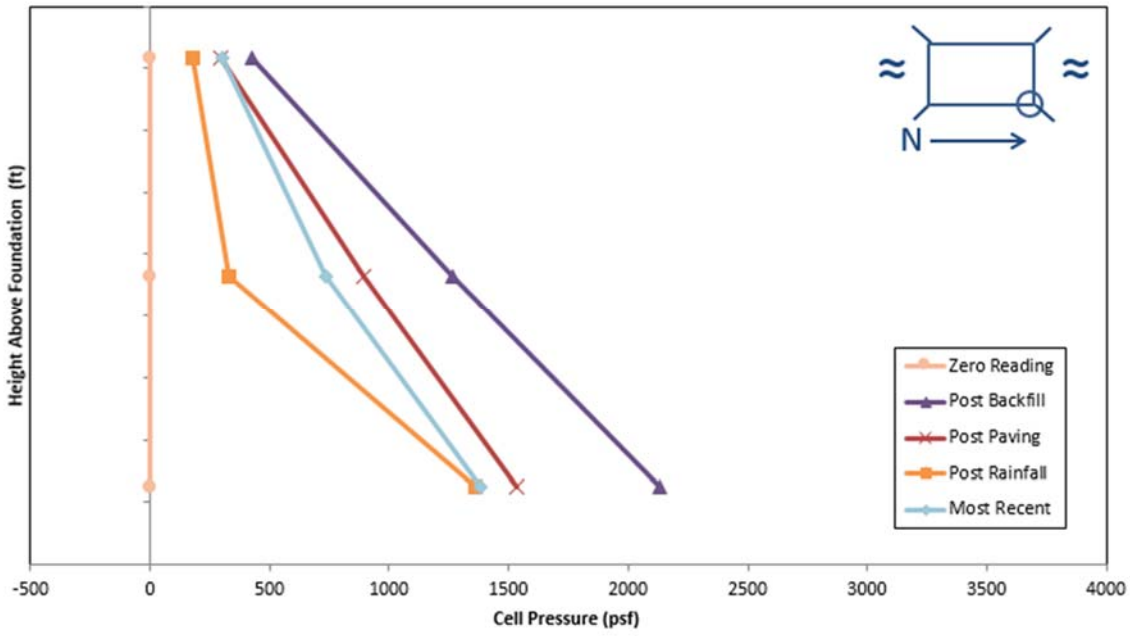


**Figure 5-16: Lee County Tab 2, Pressure versus Height**

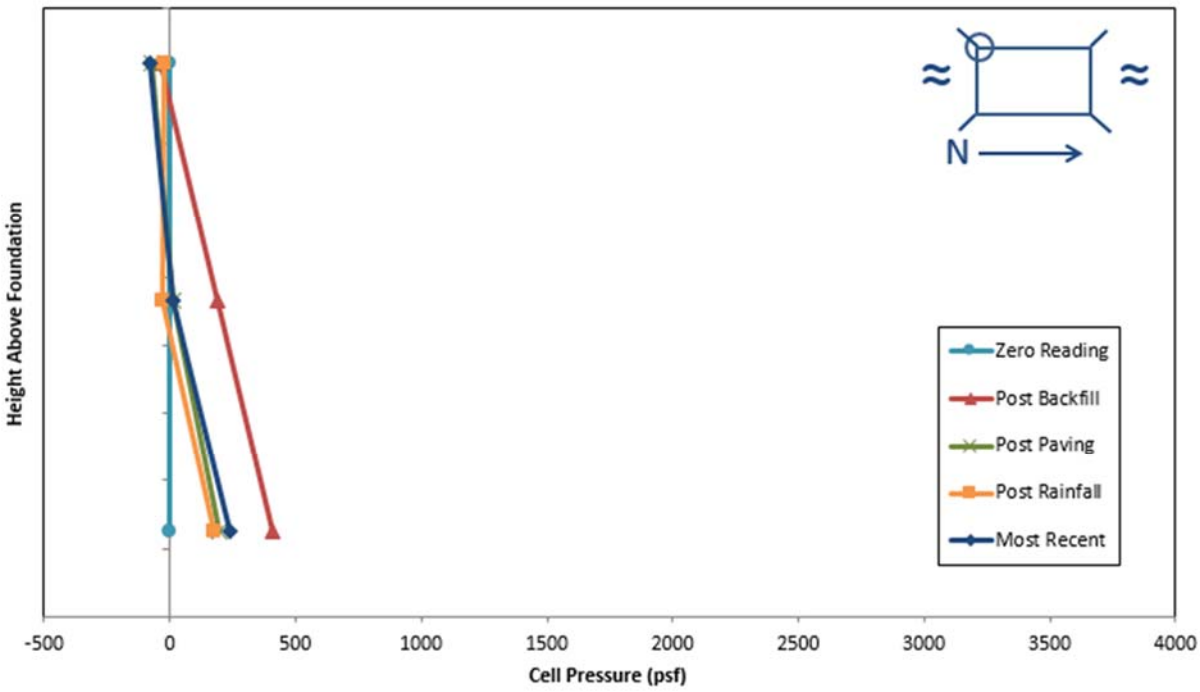


**Figure 5-17: Lee County Tab 3, Pressure versus Height**

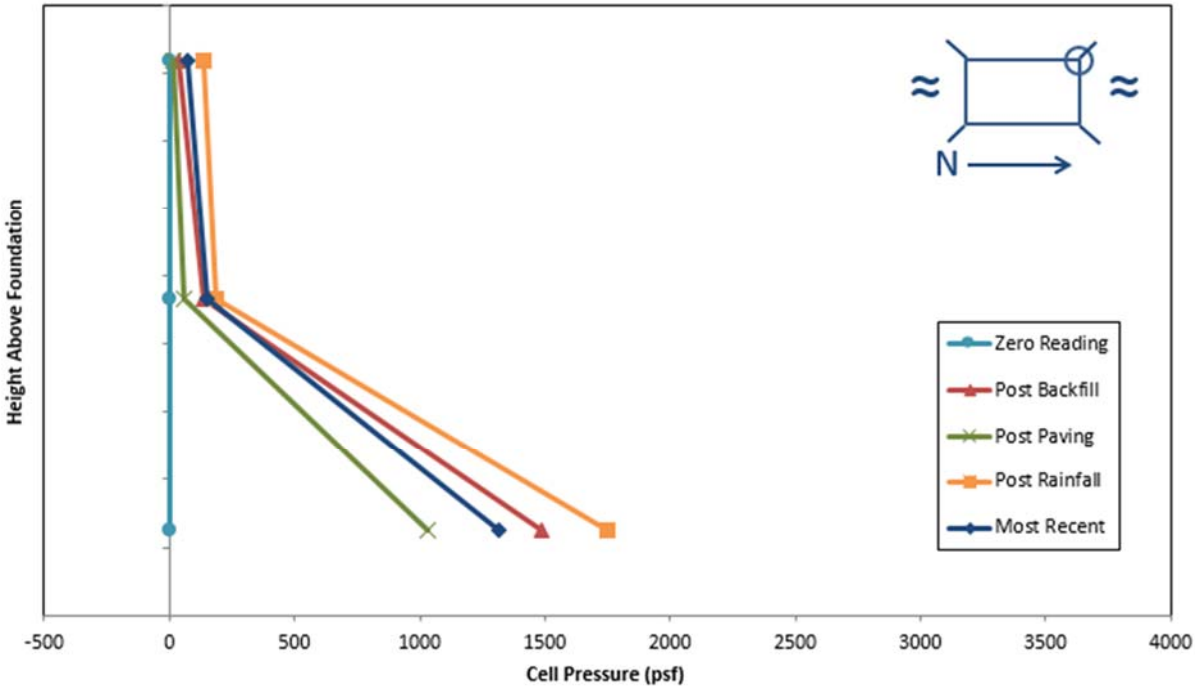


**Figure 5-18: Lee County Tab 4, Pressure versus Height**

### 5.3.3 Coosa County

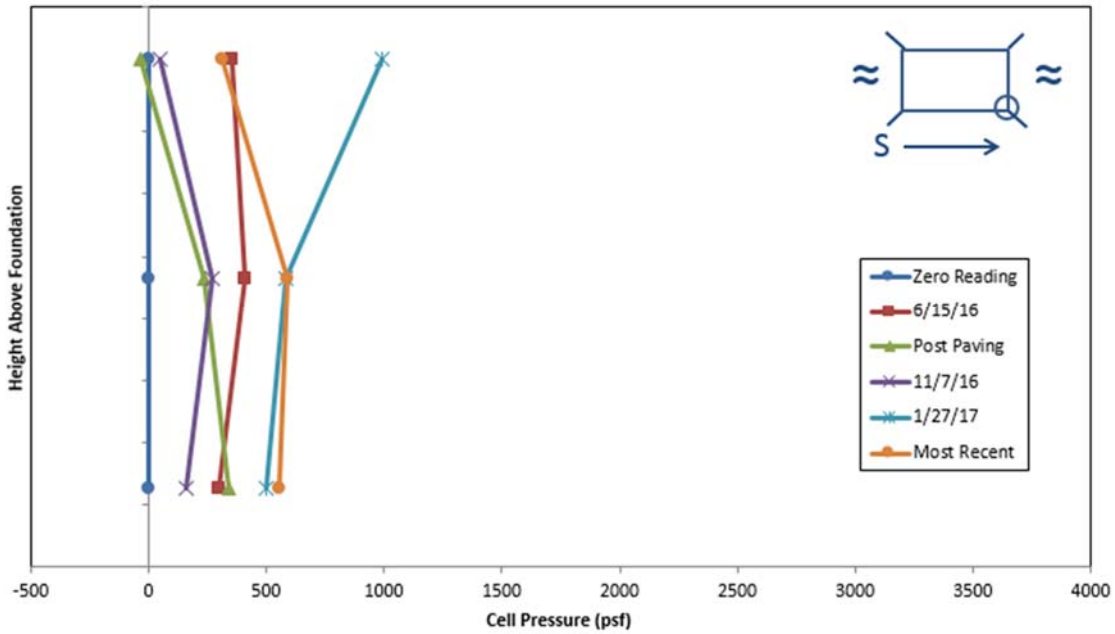


**Figure 5-19: Coosa County Tab 1, Pressure versus Height**

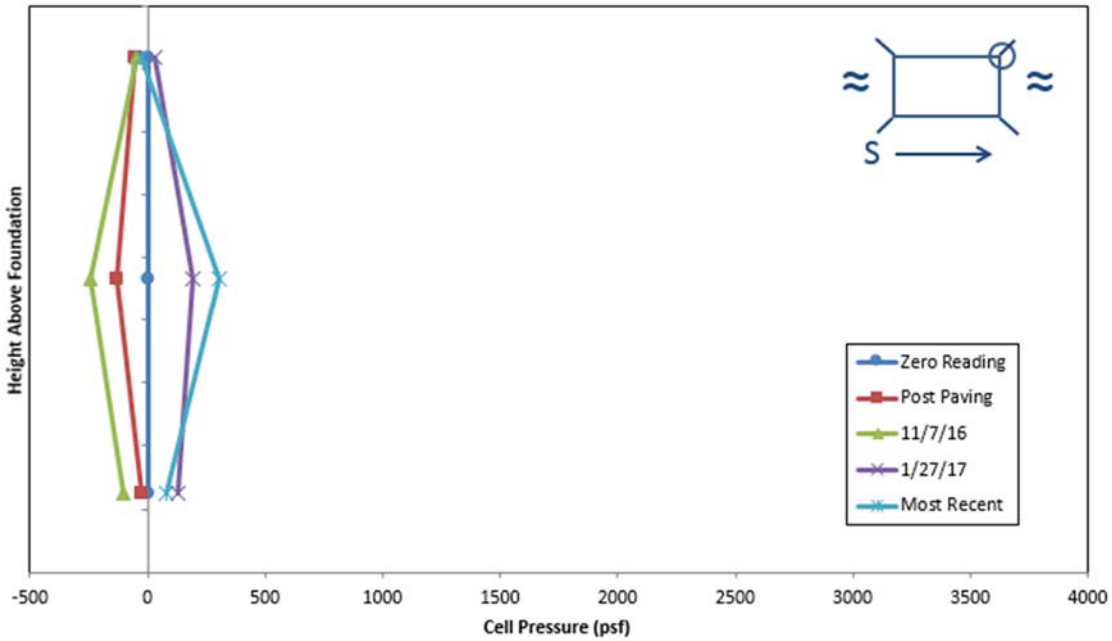


**Figure 5-20: Coosa County Tab 2, Pressure versus Height**

### 5.3.4 Pressure versus Height Discussion

The charts in Section 5.3 Pressure versus Height show the pressure distribution along the height of the tab at each discrete instance when a measurement was recorded. This provided some insight into the way the wing walls moved in relation to the tab. Three general types of wing wall movement were predicted as possibilities: uniform translation resulting in equal pressure at all cell locations, rotation or flexure resulting in greater pressure at the bottom cell locations, and rotation or flexure resulting in greater pressure at the top cell location.

The culvert in Chambers County displayed evidence in support of each of the three types of wing wall movements. Tab 1 (Figure 5-11) showed a strong linear correlation in support of the rotation which would place greater pressure on the bottom of the tab. Tab 2 (Figure 5-12) showed evidence which predominantly supported this same rotation; however, on two instances, early during construction and prior to the placement of backfill, the bottommost cell experienced a pressure roughly equivalent to the cell placed in the middle of the tab. In both instances, the topmost cell experienced significantly less pressure. If this was indicative of uniform translation, it is possible that the unrestrained nature of the top of the tab, in relation to the heel and embedded toe restrained bottom of the tab, allowed for more flexibility and thus a reduction in the induced pressure. Tab 3 (Figure 5-13) showed evidence of rotation of the wing wall which resulted in a linear distribution in which the greatest pressure occurred at the top of the tab. Comparing this with the Pressure versus Time graph for the same tab (Figure 5-3) showed that this pressure distribution occurred on September 15, 2015, which was during the construction of the culvert and prior to backfill. Most of the discrete measurements recorded on this tab, however, support a uniform translation, with the magnitudes at each cell location being roughly the same, albeit

comparatively small. As with Tab 3, Tab 4 (Figure 5-14), showed evidence of translation; however, it is noteworthy that Tab 4 experienced very little pressure in general.

The culvert in Coosa County displayed evidence of wing wall rotation about the horizontal axis at all tab locations; for every measurement recorded, the bottom cell experienced the greatest pressure and the pressure decreased with height. Tabs 2 and 3 (Figure 5-16 and Figure 5-17) showed strong linear correlations which supported the assumed linear distribution used when modeling lateral soil pressure. Tab 1 and 4 (Figure 5-15 and Figure 5-18) showed evidence of a nonlinear distribution of pressure; however, the concavity was such that a linear approximation was appropriate and conservative for design.

The culvert in Coosa County presented evidence of uniform translation as well as rotation resulting in greater pressure at the top of the tab on Tab 1 (Figure 5-19); however, Tab 2 (Figure 5-20) showed a potentially unforeseen type of behavior for the wing wall wherein the center portion of the wing wall bulged, resulting in a distribution where the pressure was greatest at the central cell and nearly zero at both other locations. It is important to note the magnitudes of all pressures in Tab 2 of the culvert in Coosa County were quite small and thus the effect of this nonlinearity was minimal.

Although evidence for all proposed types of movements were observed, seven of ten instrumented tabs predominantly exhibited evidence of wing wall rotation about the horizontal axis which resulted in the greatest pressure being recorded at the bottom cell. Furthermore, both of the tabs in Coosa County were among the three other cases and these both experienced comparatively small pressures. These results, taken in total, suggest that the greatest pressure will

occur at the bottom of the tab, but it is still important to provide reinforcement for potential maximum pressures throughout.

## 5.4 Pressure Comparisons between Tabs by Location

The charts in this section again present the same data; however, rather than showing the pressures occurring at a single tab, each chart represents a cell location and shows the data from that location at each of the instrumented tabs at a given culvert. Unlike the previous charts, these charts are scaled to accommodate the local maximum pressure in order to magnify the pressure trends and more easily allow for the comparison of the trends observed at each cell height.

The legend in the top left corner uses a two character abbreviation to explain the significance of each data set. The first character is either a ‘B’ to signify the bottom cell, ‘M’ to signify the middle cell, or ‘T’ to signify the top cell. The second character gives the number of the tab that contains the cell. The schematic of the culvert, typically located in the top right corner, gives a reference arrow to orient the culvert to cardinal directions, uses ‘≈’ to show the orientation of water flow beneath the culvert, and each tab is marked with a number to indicate how that tab was labeled for this research.

### 5.4.1 Chambers County

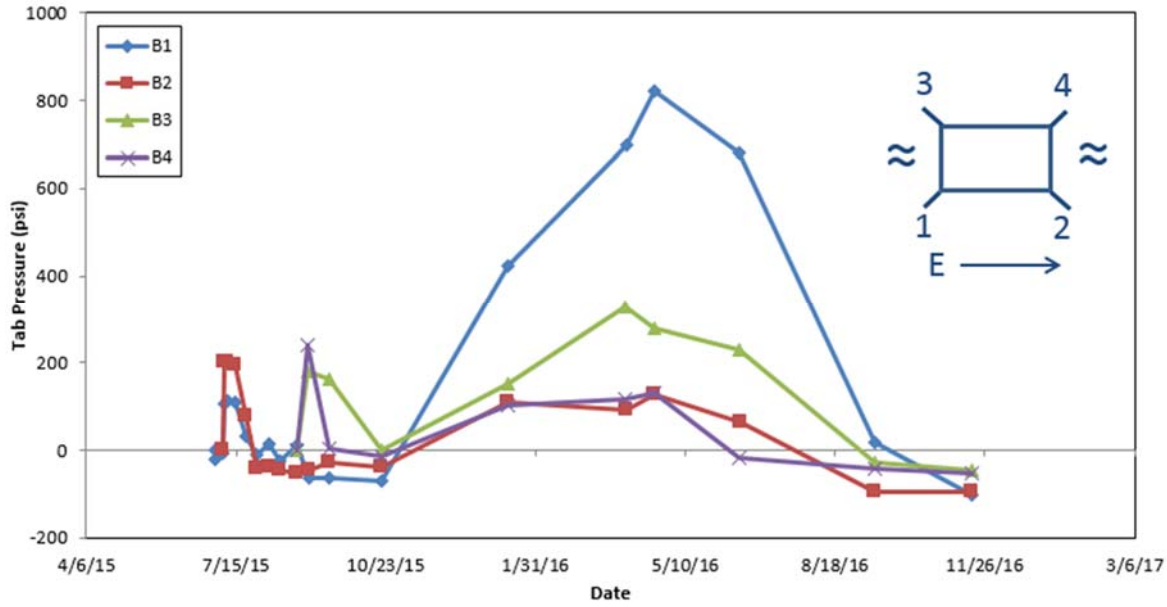


**Figure 5-21: Chambers County Bottom Cells**

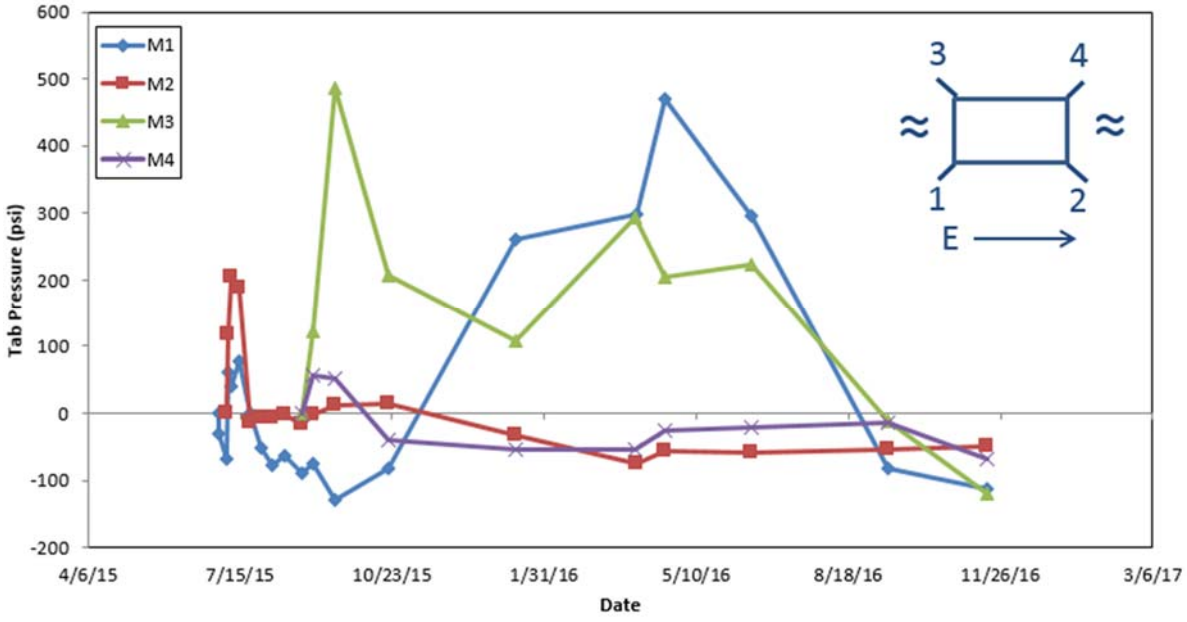


**Figure 5-22: Chambers County Middle Cells**

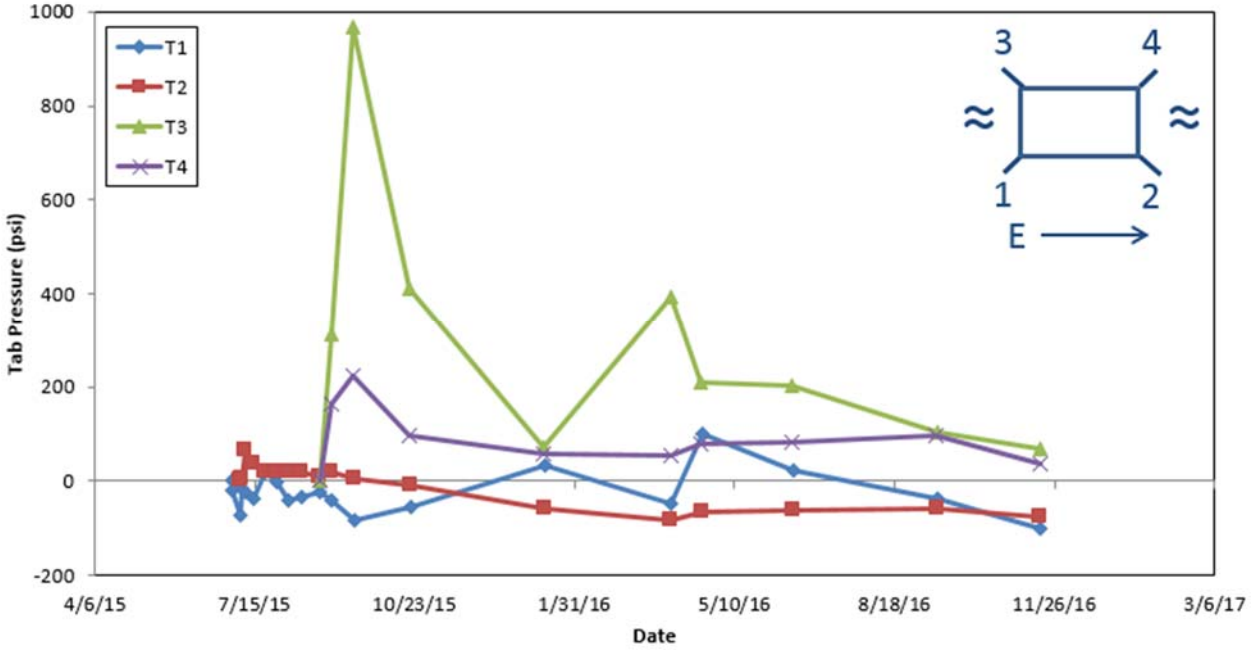


**Figure 5-23: Chambers County Top Cells**

### 5.4.2 Lee County

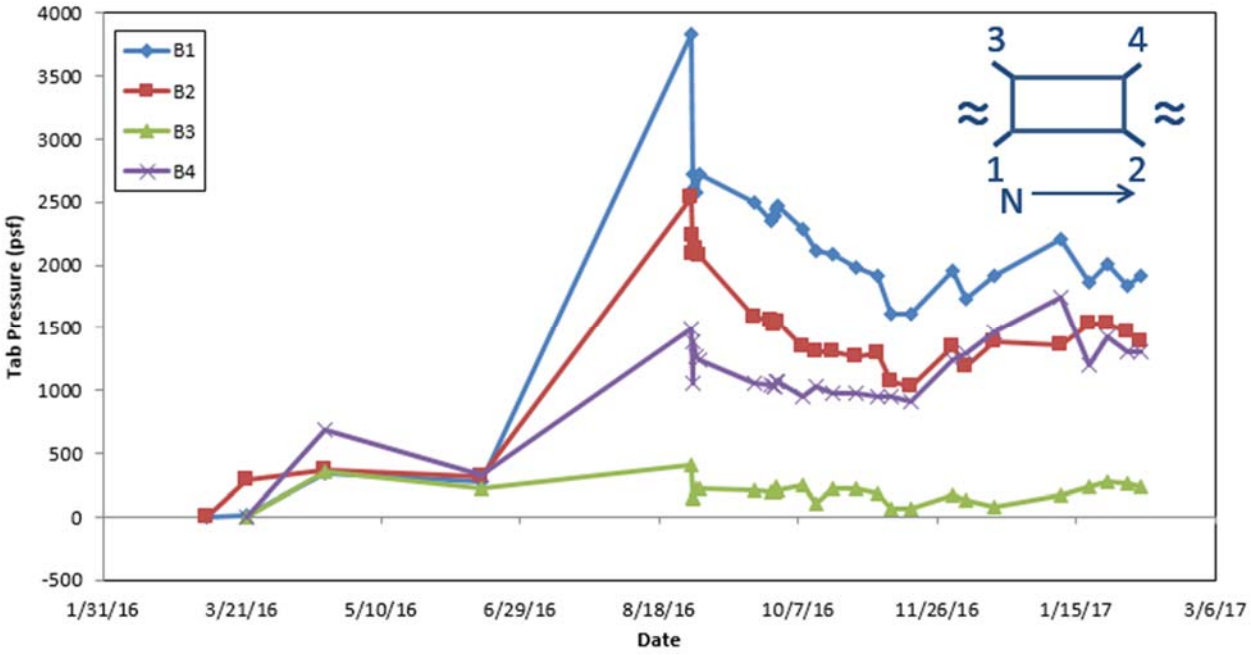


**Figure 5-24: Lee County Bottom Cells**

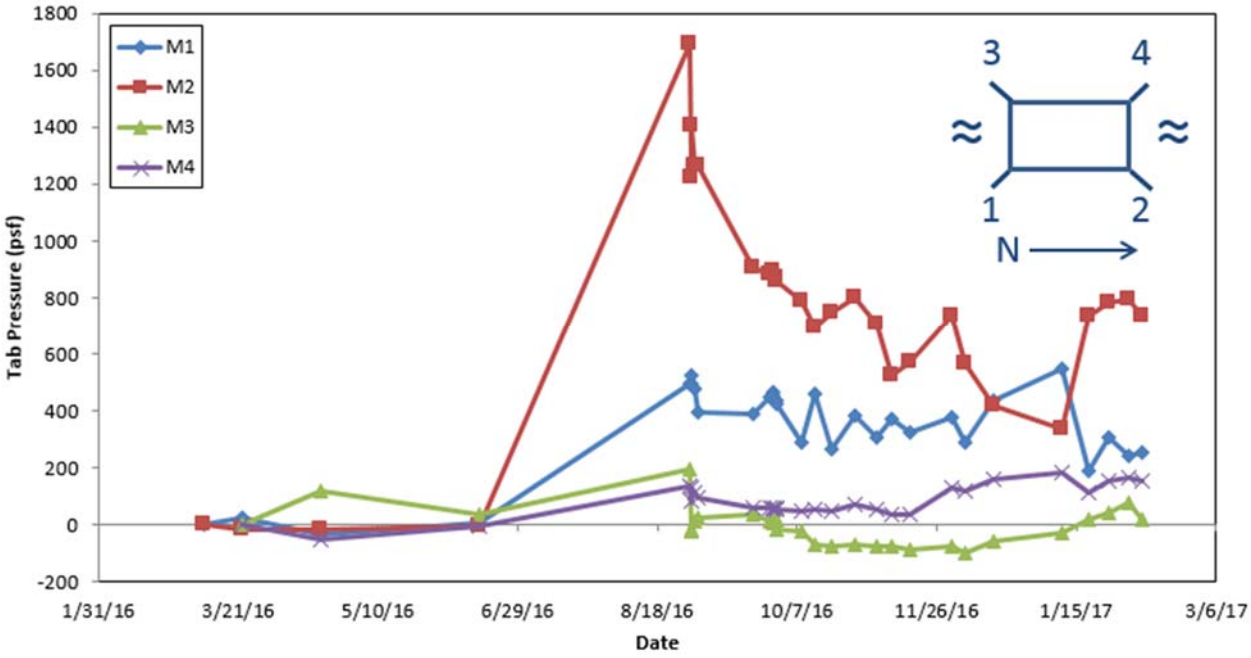


**Figure 5-25: Lee County Middle Cells**

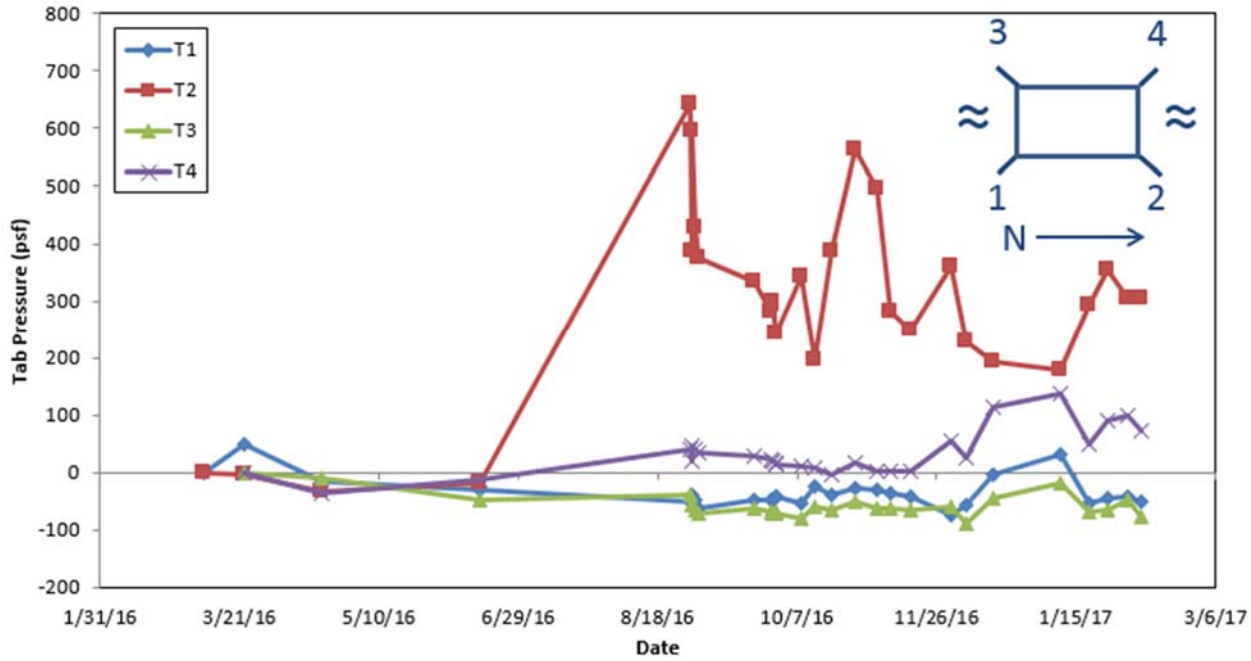


**Figure 5-26: Lee County Top Cells**

### 5.4.3 Coosa County

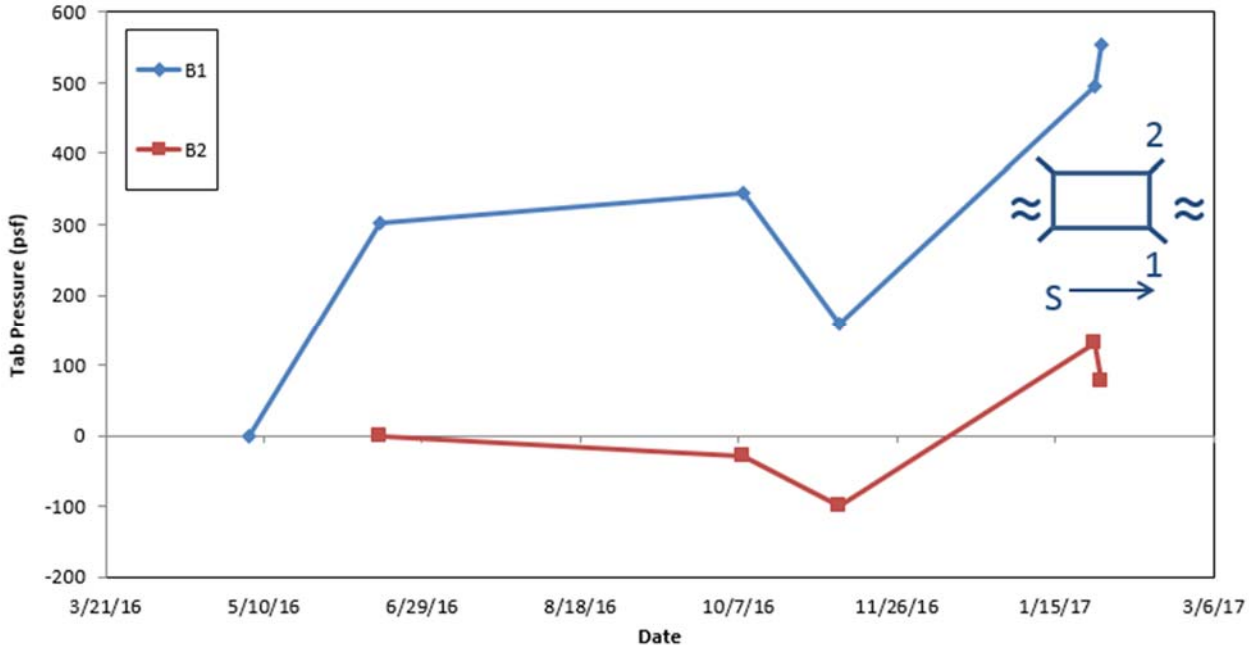


**Figure 5-27: Coosa County Bottom Cells**

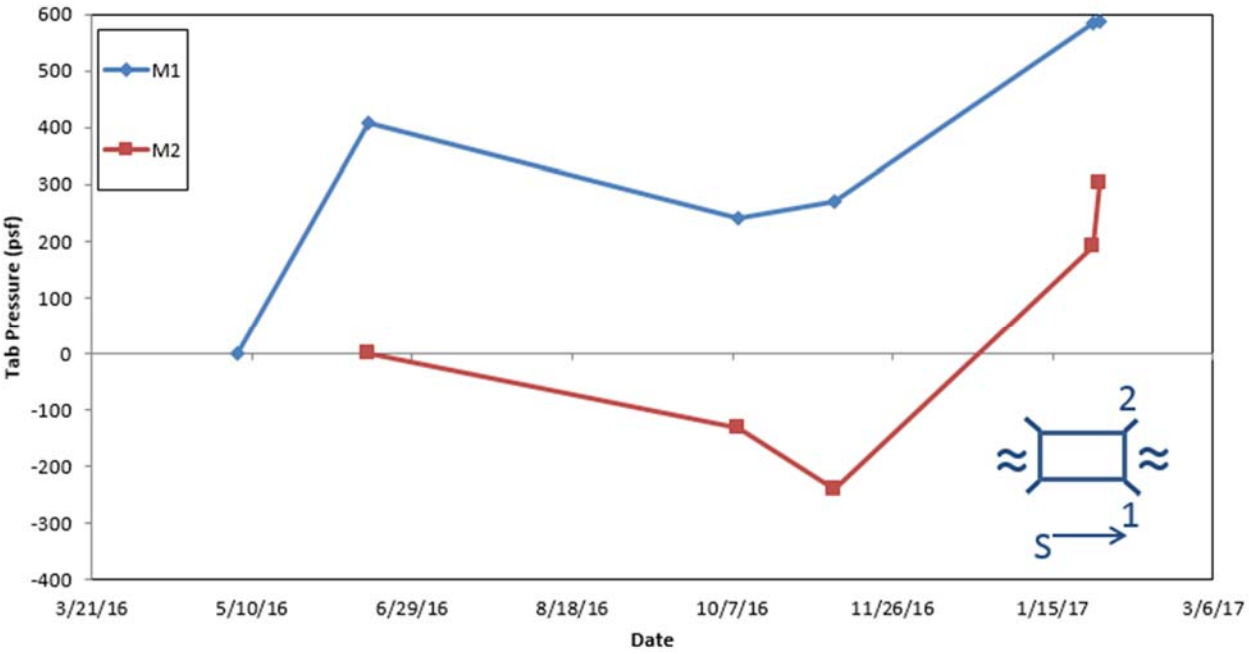


**Figure 5-28: Coosa County Middle Cells**

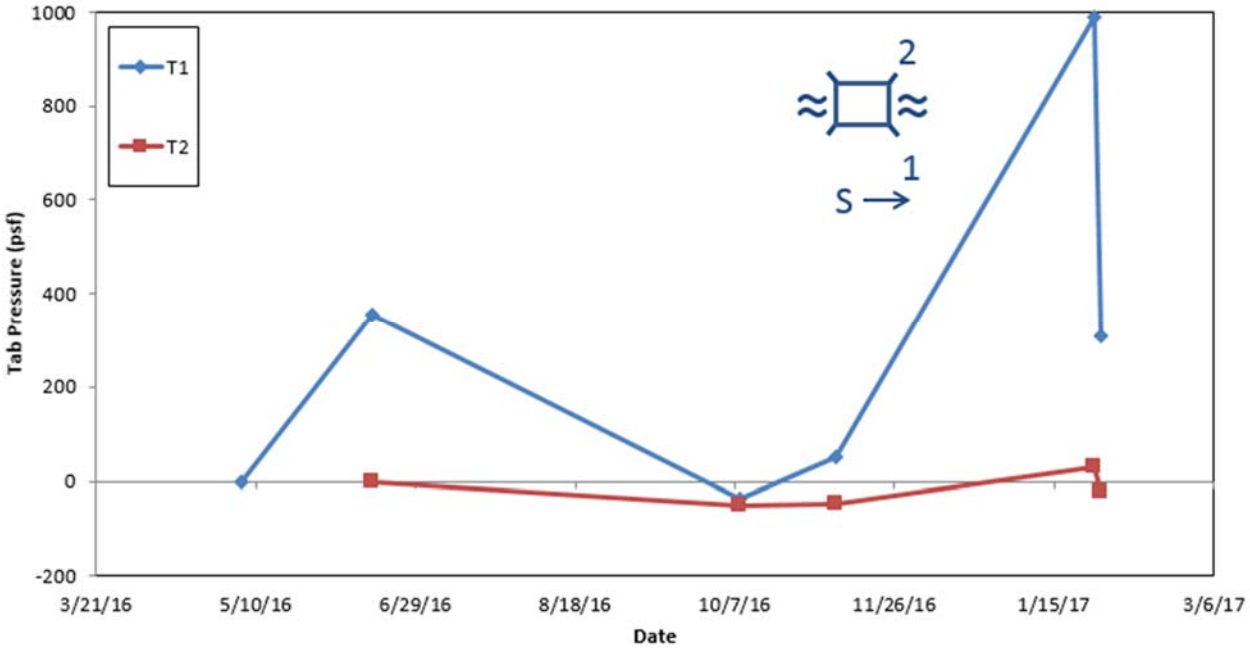


**Figure 5-29: Coosa County Top Cells**

### 5.4.4 Discussion

The charts given in Section 5.4 illustrate that, although the magnitude of the pressure may vary wildly, the trends in pressure follow roughly the same trajectory over time for each comparable cell location in each tab at a given culvert location. These charts were magnified such that the trends were more readily apparent on the culverts that experienced minimal load.

## 5.5 24-Hour Cycle Pressure Measurements

The charts in this section depict the pressure measurements recorded hourly over the course of a 24-Hour period at Chambers County. Rather than depict the actual magnitude of the pressure observed, these charts display the variation in the pressure in relation to the initial measurement. The charts are scaled to accommodate the largest variation observed at a location and the data is presented both in tab groupings and in cell location groupings.

The legend in the top left corner uses a two character abbreviation to explain the significance of each data set. The first character is either a 'B' to signify the bottom cell, 'M' to signify the middle cell, or 'T' to signify the top cell. The second character gives the number of the tab that contains the cell. The schematic of the culvert in the top right corner gives a reference arrow to orient the culvert to cardinal directions and uses '≈' to show the orientation of water flow beneath the culvert. The graphs that depict the results in tab groupings use a circle to indicate the tab that is represented in the given chart and those that depict the results in cell location groupings label each tab with the number was assigned to each tab for this project.

### 5.5.1 Chambers County

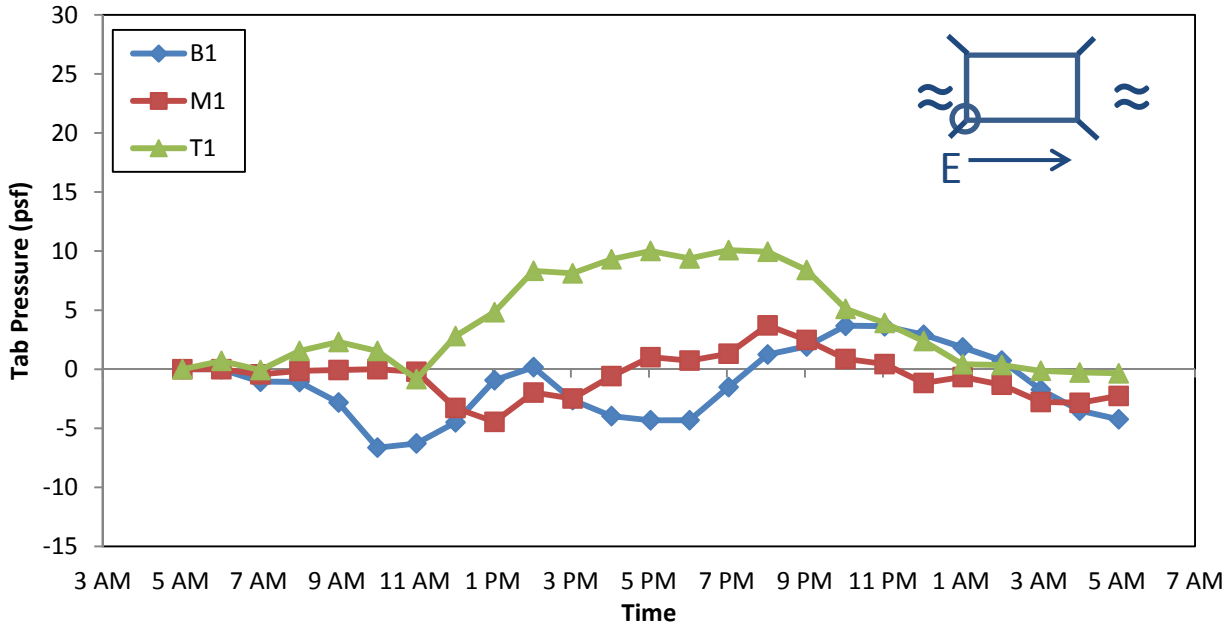


**Figure 5-30: Chambers County Tab 1, 24-Hour Cycle**

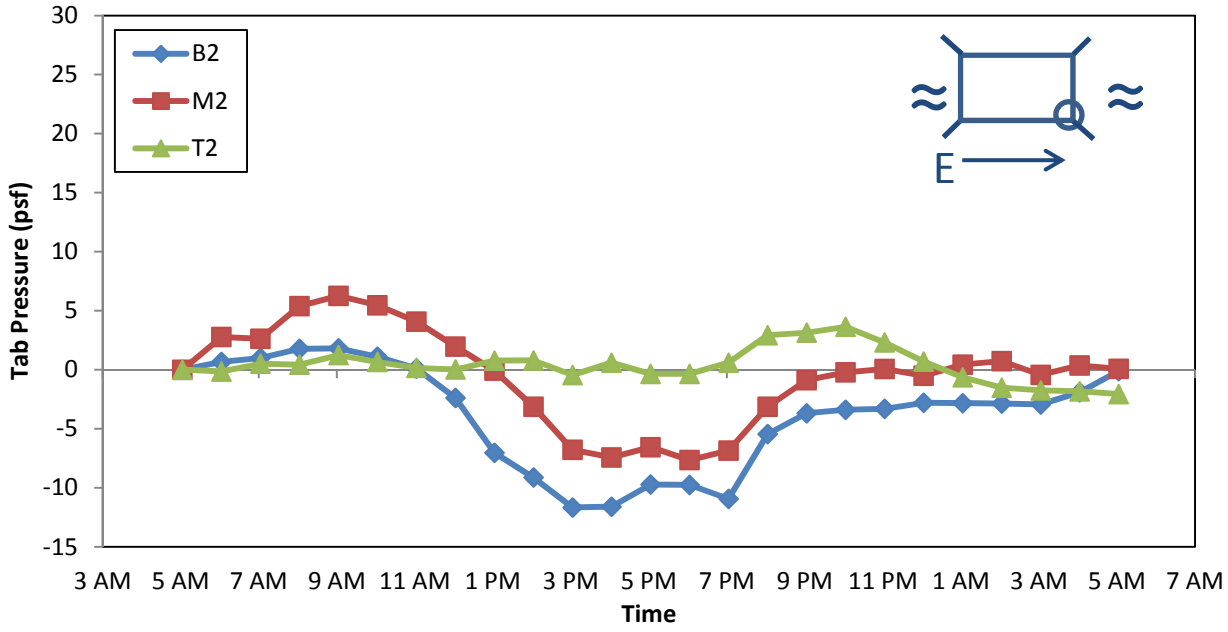


**Figure 5-31: Chambers County Tab 2, 24-Hour Cycle**

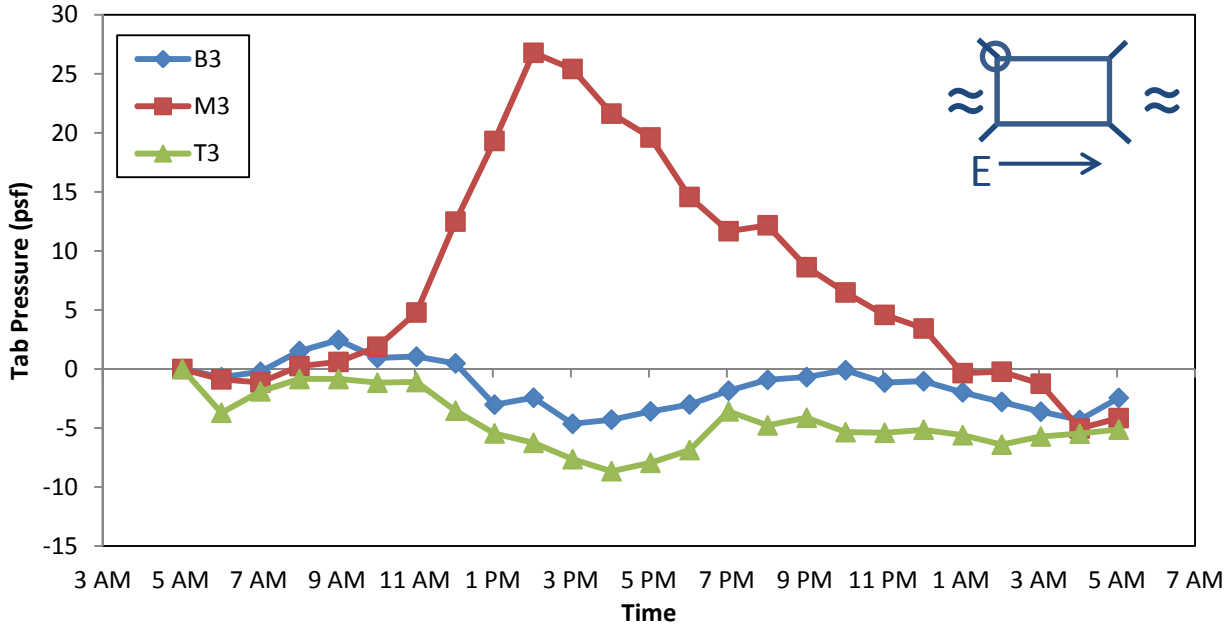


**Figure 5-32: Chambers County Tab 3, 24-Hour Cycle**

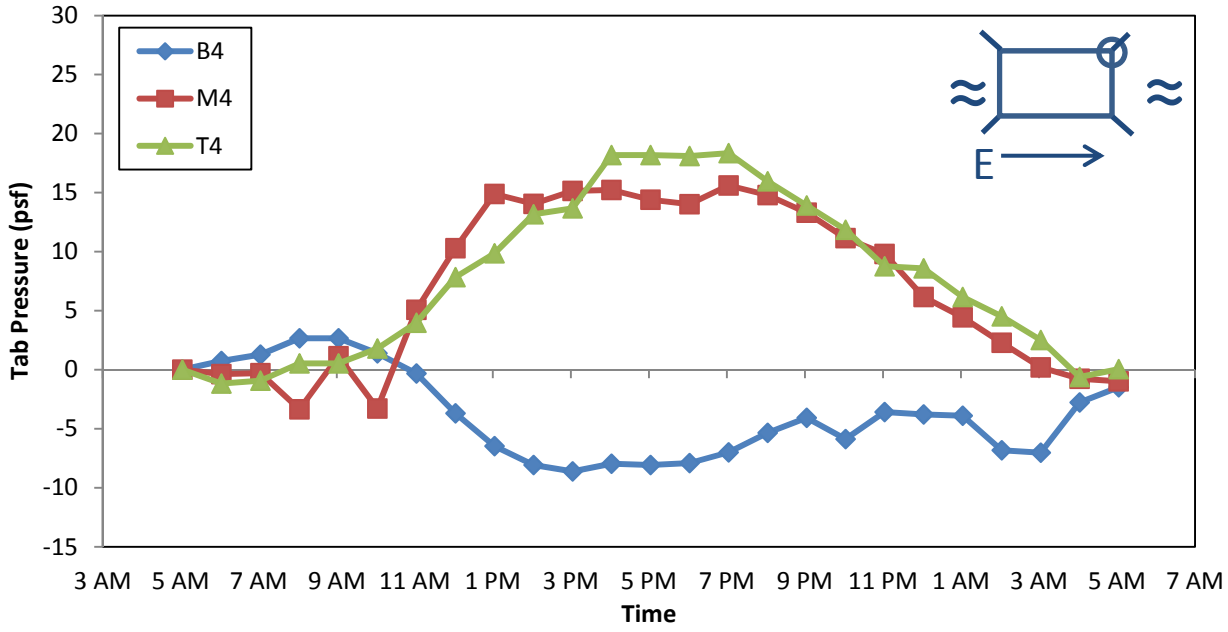


**Figure 5-33: Chambers County Tab 4, 24-Hour Cycle**

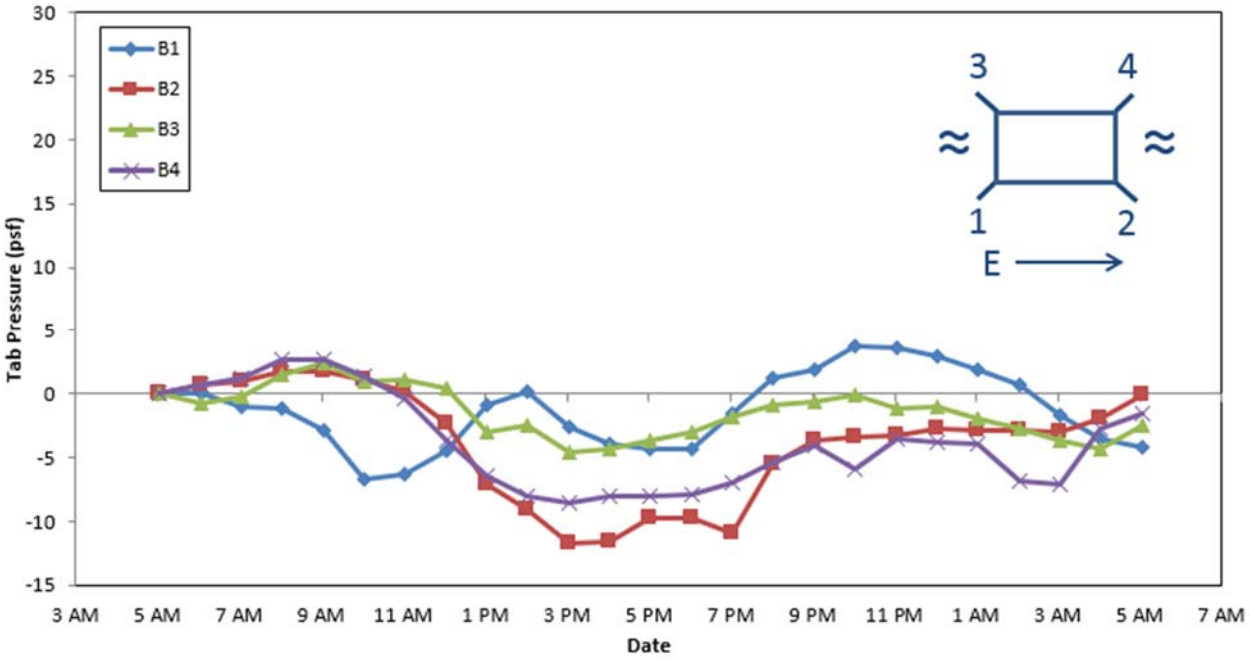


**Figure 5-34: Chambers County Bottom Cells, 24-Hour Cycle**

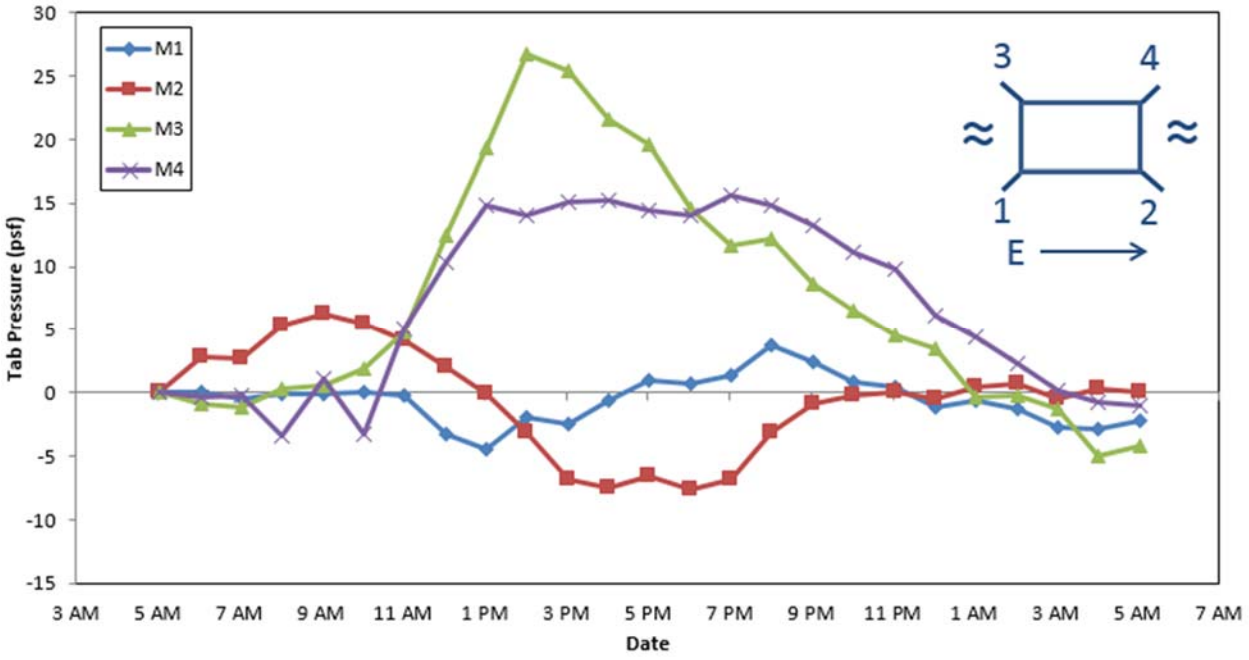


**Figure 5-35: Chambers County Middle Cells, 24-Hour Cycle**

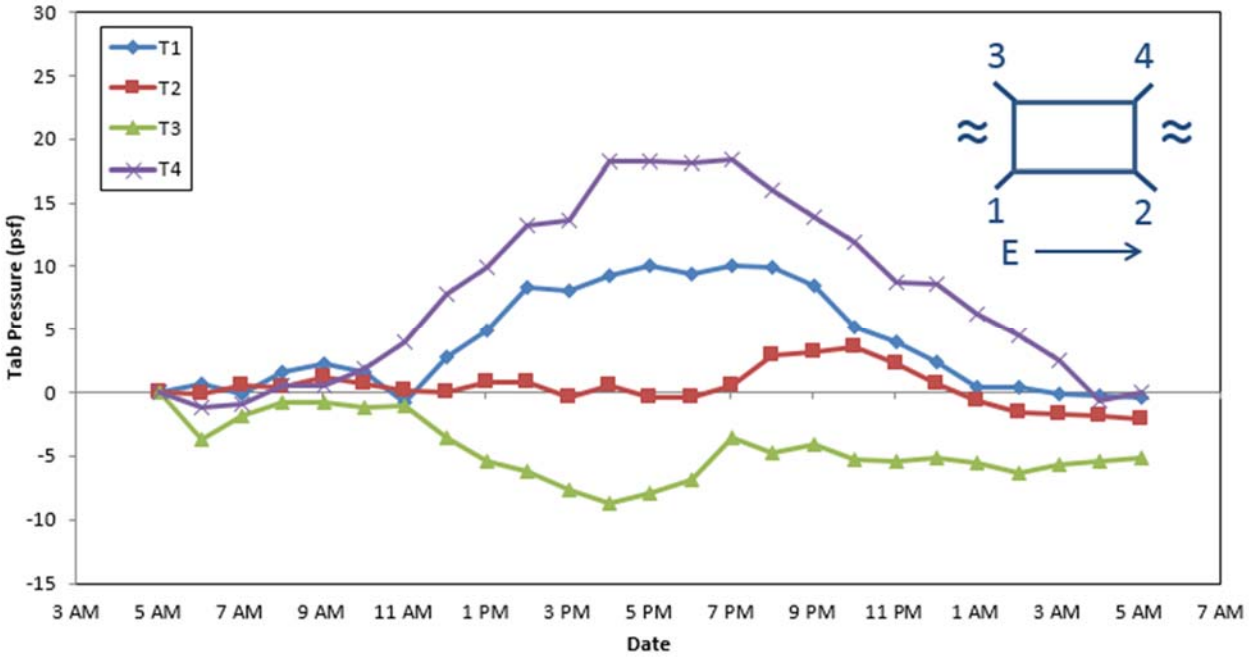


**Figure 5-36: Chambers County Top Cells, 24-Hour Cycle**

### 5.5.2 Pressure Comparisons between Tabs by Location Discussion

These results illustrate that throughout the course of an entire day, barring rain, the variation in tab pressure was comparatively minimal. These charts were generated using data collected from the culvert in Chambers County over a 24-hour period starting at 5:00 AM on September 13, 2016. The points plotted on the charts represent the change in pressure relative to the 5:00 AM value.

The top pressure cell in Tab 1 (Figure 5-30) experienced the greatest magnitude of variation at that location, with the maximum change being an increase of 10 psf observed at 8:00 PM. While this was a 25% change from the starting pressure, it is important to note that the top cell at this location generally experiences very little pressure in general, as can be seen in Figure 5-1. For further context, this change was equal in magnitude to 1.0% of the maximum pressure observed at this culvert. Because the top cell is nearest to the surface, it follows that the concrete surrounding it would be more impacted by the heat of the sun. This could, in turn, lead to a higher pressure measurement by the cell if the concrete expands such that the joint between the wing wall and culvert tab narrows. The increase in pressure held relatively stable from 2 PM until 8 PM, suggesting there is a lag between the increase in environmental temperature and the increase in pressure at the cell level.

The bottom pressure cell in Tab 2 (Figure 5-31) experienced the greatest magnitude of variation at that location, with the maximum change being a decrease of 12 psf observed at 4:00 PM. This represented at 13% change from the starting pressure; however, as with Tab 1, it is important to note that Tab 2 typically experienced very little pressure in general. This change was equal in magnitude to 1.2% of the maximum pressure observed at this culvert. The pressure at the top cell held relatively steady while the pressure at the other locations dropped starting at 9:00

AM, following a brief period of increase for the pressure at the middle cell. That the top cell did not experience a similar drop in pressure is partially explained by its proximity to the surface and, therefore, increased susceptibility of the surrounding concrete to the heat of the sun.

The middle pressure cell in Tab 3 (Figure 5-32) experienced the greatest magnitude of variation at that location with the maximum change being an increase of 27 psf recorded at 3:00 PM. This was also the largest magnitude recorded in general and represented an increase of 140% from the starting pressure, which included a transition from negative pressure values to positive pressure values, taken relative to the 5:00 AM measurement. Again, it is noteworthy that, as seen in Figure 5-3, Tab 3 typically experienced very little pressure and that this pressure change was equal in magnitude to 2.8% of the maximum pressure recorded at this culvert. A potential explanation for this increase is that Tab 3 is the less shaded of the two eastward facing tabs and thus, its face was the most exposed to the rising sun. The pressure began increasingly rapidly at 9:00 AM and continued at a near constant rate until 3:00 PM, at which point it decreased at a similar rate. This was indicative of the same lag between external temperature and cell pressure discussed for Tab 1. It was strange, however, that this large increase at the middle cell location coincided with decreases at both other cell locations. Perhaps the expansion of the middle cell due to heat created a bridging effect between the tab and wing wall and relieved the other two cells of pressure throughout the course of the day.

The top pressure cell in Tab 4 (Figure 5-33) experienced the greatest magnitude of variation at the location with the maximum change being an increase of 18 psf observed at 8:00 PM. This pressure held relatively constant from 5:00 PM until 8:00 PM at which point it decreased at a similar rate to that at which it had grown. This represented a 21% change from the initial pressure

and a magnitude of change equal to 1.9% of the maximum pressure observed at this culvert. Like all previous tabs discussed, it is important to point out that the pressures observed at Tab 4 were minimal, which can be seen in Figure 5-4. Another noteworthy item about this chart was that the middle cell experienced a similar trend in pressure to the top cell, while the bottom cell experienced a decrease. A potential explanation was that the temperature increased similarly for the concrete surrounding the two upper locations while the concrete surrounding the bottom cell was kept cool by running water.

Figure 5-34, Figure 5-35, and Figure 5-36 showed that the trends of the pressure variation were most similar across the bottom cells while the other two locations varied significantly. With the variations being so comparatively small throughout the day, it was likely that this is due to environmental factors, such as the degree of exposure to direct sunlight and atmospheric pressure, which was neglected in this research. Atmospheric pressure typically varies by around 0.0435psi daily (Mentzer, 2017). This range of atmospheric pressure corresponds to roughly 12 psf difference in a given cell with all other things held equal, meaning the daily change in atmospheric pressure could potentially explain the majority of this pressure variation. The similarity between the bottom cells was perhaps explained by their proximity to running water which could serve as an agent of cooling for the concrete surrounding these cells.

## 5.6 Gap Width

This chart depicts the change in the width of the gap between the wing wall and the culvert tab at the top face of each. Each data point represents a change from the base measurement which has been set to zero based on the date of installation. A positive value on this chart indicates a widening of the gap while a negative value represents a narrowing of the gap. This assumes that

all movement between reference points was concentrated within the gap, although this is not necessarily true, as the expansion of concrete due to temperature could result in the reference points being further away from each other while the gap has actually narrowed.

The legend in the top right corner indicates which data set represent the trend for each tab. The schematic of the culvert, typically located in the top right corner, gives a reference arrow to orient the culvert to cardinal directions, uses '≈' to show the orientation of water flow beneath the culvert, and each tab is marked with a number to indicate how that tab was labeled for this research.

### 5.6.1 Lee County

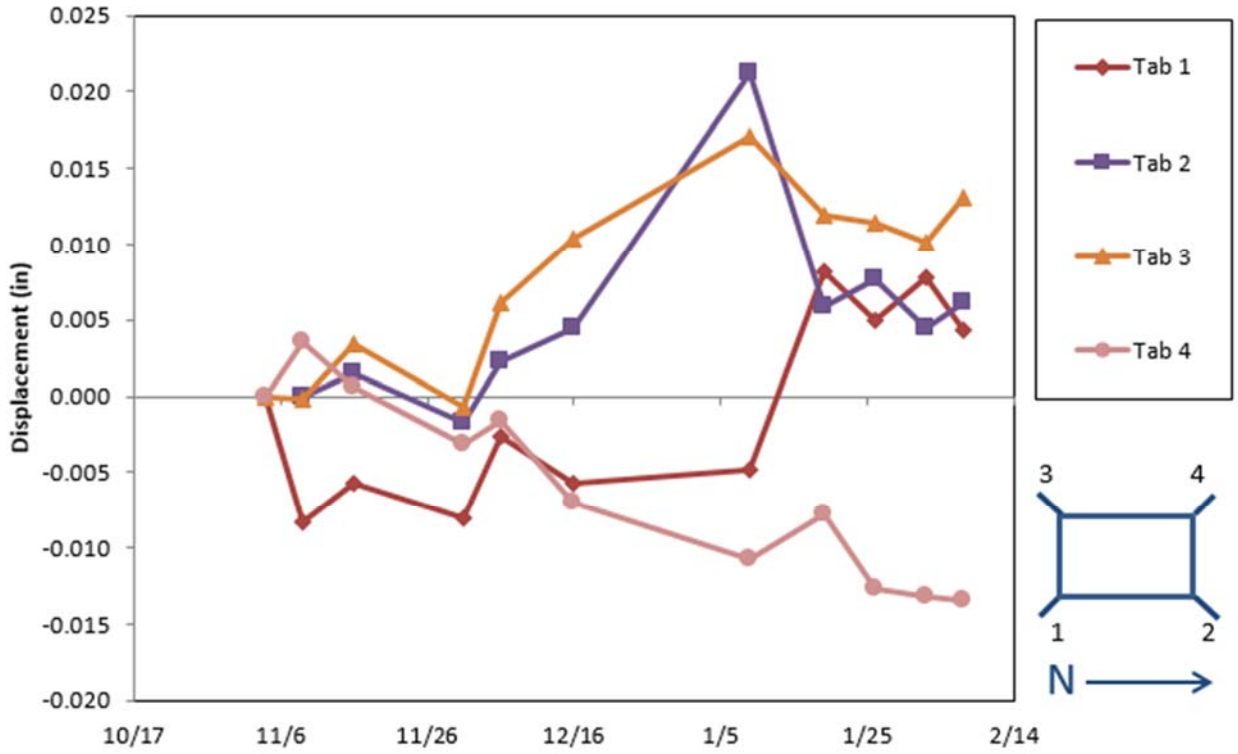


**Figure 5-37: Lee County Gap Width**

### 5.6.2 Discussion

Figure 5-37 shows the change in the width of the gap between the wing wall and culvert tab starting from the reference width that existed on November 4, 2016. Negative values indicate a closing of the gap while positive values indicate an opening of the gap. It was theorized that the gap movement would correspond to pressure changes experienced by the topmost cell, due to the location of the gap measurements; however, attempts to find correlations were not fruitful. This was likely due to the changes being on the order of hundredths of an inch while the studs were fabricated in a way that does not allow for this level of accuracy.

## 5.7 Concrete Testing

### 5.7.1 Modulus of Elasticity Testing

As part of the overall project, a separate researcher, Pavel Voitenko, created finite element computer models of each culvert to predict the loads experienced by the wing walls. In order to refine these models, concrete samples were taken from each project placement and tested to determine representative value of compressive strength ($f'_c$) and modulus of elasticity ($E_c$) for each of the culverts per ASTM Specification C469. The average values for each culvert can be found in this section with the raw data provided in Appendix A.

#### 5.7.1.1 Specimen Creation Procedure

During each concrete placement, three representative cylinders were created per ASTM Specification C31, using a standard 12 in. tall cylinder mold with a 6 in. diameter. Each cylinder was created using three lifts of roughly equal depth and each lift was tamped 25 times using a steel rod prior to the next lift being added. Once all lifts had been completed, the perimeter of each cylinder was knocked with a rubber mallet to work out any excess air bubbles and water. Next, the

surface of the cylinder was screeded to ensure a smooth surface. The cylinder mold was then capped and placed in a water filled box on site where it was left to cure for two days. After this period had passed from the creation of a cylinder, it was then transferred to Auburn University where the mold was stripped, the cylinder was marked with its date of casting and the location of the project, and the cylinder was placed in the Auburn University moist curing room until 28 days had elapsed from the date of casting.

#### 5.7.1.2 Testing Procedure

Once a group of cylinders had aged to 28 days, they were removed from the moist curing room, their surface was wiped dry, and they were tested per the standards set forth in ASTM C649. A picture of the test set up with a cylinder and compressometer is shown below in Figure 5-38.


**Figure 5-38: Modulus of Elasticity testing**

Once all of these runs were completed, the collected data was used to calculate a representative value of the modulus of elasticity using Equation 5-1 (ASTM C469/C469M, 2014):

$$E_c = \frac{\left(P_{40\%} - P_{50\mu\epsilon}\right)/A}{\left(\epsilon_{40\%}/2l_g\right) - 0.00005}$$ **Equation 5-1**

Where:

$E_c$ = Modulus of Elasticity (psi)

$P_{40\%}$ = Target Load for each run (lbs)

$P_{50\mu\varepsilon}$ = Average of recorded loads at 50 microstrains (lbs)

A = Cross-sectional area of cylinder ($in^2$)

$\varepsilon_{40\%}$ = Average of recorded strains at target load (in/in)

$l_g$ = gauge length of compressometer (in)

### 5.7.2 Concrete Test Results

**Table 5-1: Culvert Concrete Averages**

| | 28 Day Averages | |
|---|---|---|
| | $E_c$ (ksi) | $f'_c$ (psi) |
| Chambers County | 3400 | 4280 |
| Lee County | 5900 | 5260 |
| Coosa County | 4950 | 5290 |

## 5.8 Summary

The broad lessons that can be learned from the information provided in the above charts are as follows:

- The greatest pressure in the culvert tab is likely to occur at the bottom of the tab
- The greatest pressure in the culvert tab is likely to occur during the process of backfill
- Over time, the pressure on the culvert tab trends toward zero
- Daily variations in tab pressure are minimal but occur most predominantly in the upper portions of the tab

# CHAPTER 6: RECOMMENDED DESIGN PROCEDURE

## 6.1 Overview

Considering that soil is the primary load source involved in the interaction between the wing wall and culvert tab, a design procedure was developed which determined design loads for the culvert tab based upon the dimensions of the wing wall and soil properties of the backfill while considering two possible critical loading conditions. Following the determination of a design load, the controlling load was used to design 1 foot tall horizontal strips of the culvert tabs as corbels per the guidelines discussed in Section 2.5: Corbel Design.

## 6.2 Analytical Justification

Prior to developing a design approach, it was necessary to determine an analytical procedure to estimate design loads that were theoretically possible and reasonably conservative in comparison to the experimental values observed in the field.

### 6.2.1 Assumptions

To perform this analysis, at-rest lateral earth pressure was used as (a) it provides an intermediate value of earth pressure and (b) the wall rotation magnitudes required to develop active or passive pressure was not likely to occur.

The unit weight of concrete was conservatively assumed to be the following:

- $w_c$ = 150pcf

Soil properties were assumed in keeping with guidelines laid out in AASHTO. The Iowa DOT explicitly states conservative estimates for soil properties that align with these AASHTO guidelines and with typical assumptions made in practice. These are as follows:

- $\Phi'_f = 30°$, angle of internal friction of soil
- $\beta = 10°$, slope angle of backfill surface behind retaining wall
- $\gamma = 120$ pcf, unit weight of soil

(IOWA DOT, 2013)

The friction factor for soil acting upon the concrete was taken from the FHWA Retaining Wall Manual and is as follows:

- $\tan(\delta) = 45°$

(FHWA, 1999)

### 6.2.2 Soil Load Determination

To estimate the loads acting upon the tab, it was necessary to first estimate the resultant forces caused by the lateral earth pressure acting upon the wing wall. These were determined using the following procedure, referencing the free-body diagram given in Figure 6-1:

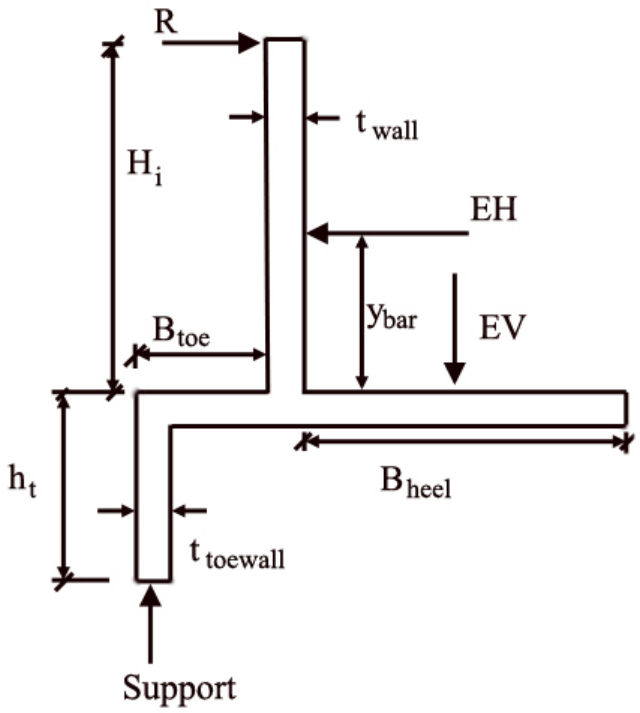


**Figure 6-1: Wing Wall Free-Body Diagram**

1. Height of wing wall, h, was expressed as function of its length, as shown in Equation 6-1:

$$h(x) = h_i + m_{wall}x \qquad \textbf{Equation 6-1}$$

Where

$m_{wall}$ = slope of wing wall height, $\frac{(h_f - h_i)}{l_w}$

$h_i$ = initial height of wing wall taken at culvert support, ft

$h_f$ = height of wing wall at furthest point from culvert, ft

$l_w$ = length of wing wall, ft

x = distance along wing wall taken from culvert, ft

2. Height of soil exerting pressure, $H_{soil}$, was expressed as a function of the height of the wing wall and assumed backfill slope, as shown in Equation 6-2:

$$H_{soil}(x) = d_{footing} + h(x) + B_{heel} \tan \beta \qquad \textbf{Equation 6-2}$$

Where

$d_{footing}$ = depth of the footing, ft

$B_{heel}$ = width of wing wall heel, ft

3. The resultant force of the lateral earth pressure, P(x), expressed as a force per unit length was determined as a function of the height of the soil and assumed soil properties using Equation 6-3:

$$P(x) = 0.5 k_0 \gamma [H_{soil}(x)]^2 \qquad \textbf{Equation 6-3}$$

Where

$k_0$ = coefficient of at-rest lateral earth pressure, $k_0 = 1 - sin\phi'_f$

The origin of these expressions given in steps 2 and 3 can be better understood by reviewing Figure 6-2 below.

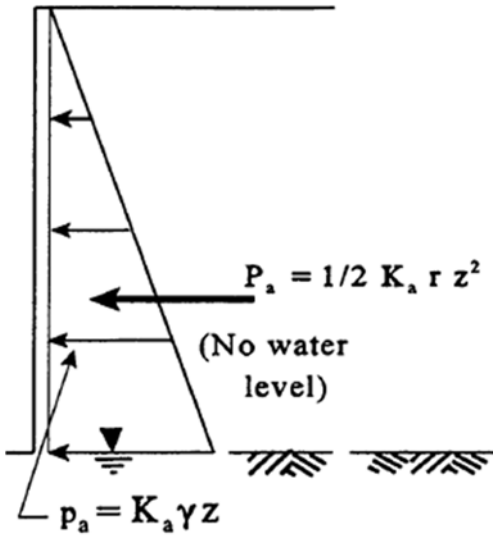


**Figure 6-2: Resultant forces from lateral earth pressure (FHWA, 1999)**

4. The horizontal resultant force of the total lateral earth pressure acting on the wing wall, $P_{hwall}$, was determined by integrating the p(x) over the length of the wing wall, as shown in Equation 6-4:

$$P_{hwall} = \int_0^{l_w} p(x) \cos(\beta)\, dx \qquad \textbf{Equation 6-4}$$

5. The vertical resultant force of all earth pressure, $P_{vwall}$, was determined by integrating the vertical component of the lateral earth pressure and the weight of the soil over the length of the wing wall, using assumed soil properties, as shown in Equation 6-5:

$$P_{vwall} = \int_0^{l_w} [p(x) \sin(\beta) + H_{soil}(x) \gamma B_{heel}]\, dx \qquad \textbf{Equation 6-5}$$

## 6.3 Critical Loading Conditions

### 6.3.1 Wing Wall Translation

The first critical loading condition considered was that of out-of-plane translation of the wing wall. For this scenario to occur, some sort of failure of the toe wall would be necessary; therefore, the impact of the toe wall was neglected. Without the effect of the toe wall, there is nothing to provide stability to the wing wall at the end furthest from the culvert in the event of a translation. For this reason, it is conservatively assumed that all of the lateral soil pressure on the wall would be transmitted to the culvert tab. If this scenario were to occur, the wing wall would likely have failed and require rehabilitation; however, with the culvert tab being designed to withstand a maximum loading of this nature, the damage to the body of the culvert itself would be mitigated, unlike with integrally constructed wing walls.

To determine this maximum tab loading, the horizontal resultant force of lateral earth pressure, $P_{hwall}$, was converted to an equivalent linear distribution along the height of the tab, similar to the distribution shown in Figure 6-3, as if the magnitude were the resultant force of an earth load acting solely upon the tab, rather than the entire surface of the wall. The magnitude of the base of this distribution was then used as the design force for each horizontal design strip of the tab. This magnitude, $p_{tab}$, was calculated using Equation 6-6:

$$p_{tab} = \frac{2 * P_{hwall}}{h_i} \qquad \textbf{Equation 6-6}$$

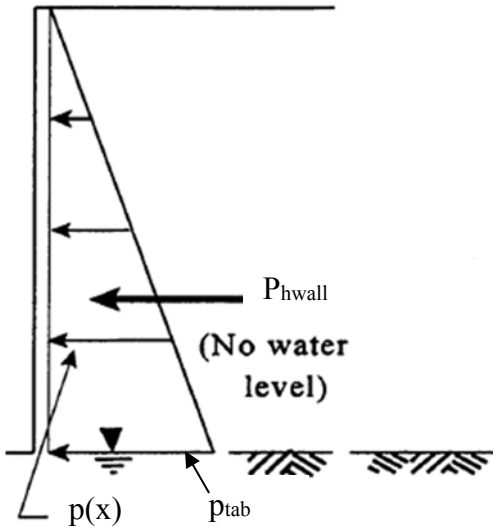


**Figure 6-3: Wing Wall Translation Tab Loading**

This technically produces a force per unit length, as with p(x), and thus must be multiplied by the width of the tab. This width was 1ft at all locations. Table 6-1 below compares the unfactored results of this analysis to the maximum forces observed in the field. Field observations were recorded in psf, but considering the area of the pressure cell was less than $1ft^2$, these values were conservatively assumed to be constant over an entire 1ftx1ft design strip of the tab, and thus were converted to kips.

**Table 6-1: Wing Wall Translation Analytical versus Experimental**

| | Chambers County | Lee County | Coosa County |
|---|---|---|---|
| $P_{analytical}$ (kips) | 6.4 | 4.7 | 6.6 |
| $P_{experimental}$ (kips) | 0.97 | 2.6 (3.8) | 0.99 |

Of note, only the culvert constructed in Lee County was observed during the process of backfill and this was when the maximum pressure within the parentheses and marked with an

asterisk was recorded. When this pressure was recorded, a fully loaded dump truck, weighting approximately 40 tons, was placed as near to each tab as possible. The effect of the truck could be estimated by treating it as a surcharge, as outlined in Section 2.4.1.4.2, but as the observed pressure was less than the pressure calculated through analysis, these steps were not taken. The value outside of the parentheses was measures after backfill after the dump truck had been removed.

### 6.3.2 Wing Wall Rotation

The second scenario considered was rotation of the wing wall which would result in contact between the culvert tab and wing wall at the top of the tab. Static analysis was performed referencing the free-body diagram shown in Figure 6-4. For this scenario, the horizontal resultant force of the lateral earth pressure was placed at the vertical coordinate of the centroid of the soil load. The toe wall was taken as the fulcrum of rotation, but the soil loads upon the toe wall were neglected. The vertical coordinate of the centroid of the soil load, $\bar{y}$, was calculated using Equation 6-7:

$$\bar{y} = \frac{1}{3}\frac{\int_0^{l_w} h(x)^3 dx}{\int_0^{l_w} h(x)^2 dx}$$ **Equation 6-7**

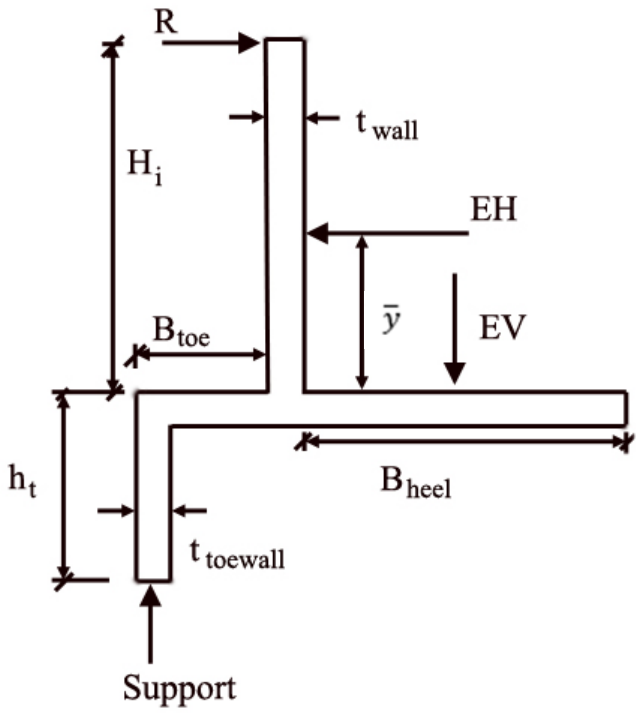


**Figure 6-4: Wing Wall Free-Body Diagram**

The variables shown in Figure 6-4 are defined as follows:

R = the force transmitted from the wall to the tab

$t_{wall}$ = thickness of the wing wall

$t_{toewall}$ = thickness of toe wall

$B_{toe}$ = width of toe

$B_{heel}$ = width of heel

$H_i$ = maximum height of wing wall

$h_t$ = height of toe wall

EV = vertical earth pressure, $P_v$

EH = horizontal earth pressure, $P_h$

The magnitude of R was calculated using Equation 6-8:

$$R = \frac{P_h(h_t + y_{bar}) - P_v(0.5B_{heel} + t_{wall} + B_{toe} - 0.5t_{toewall})}{h_t + H_i}$$ **Equation 6-8**

Table 6-2 below compares the unfactored results of this analysis to the maximum pressures observed in the field. Of note, only the culvert constructed in Lee County was observed during the process of backfill and this was when the maximum pressure within the parentheses and marked with an asterisk was recorded. When this pressure was recorded, a fully loaded dump truck, weighting approximately 40 tons, was placed as near to each tab as possible. The effect of the truck could be estimated by treating it as a surcharge, as outlined in Section 2.4.1.4.2, but as the observed pressure was less than the pressure calculated through analysis, these steps were not taken. The value outside of the parentheses was measures after backfill after the dump truck had been removed.

**Table 6-2: Wing Wall Rotation Analytical versus Experimental**

| | Chambers County | Lee County | Coosa County |
|---|---|---|---|
| $R_{analytical}$ (kips) | -16 | -17 | -11 |
| $R_{experimental}$ (kips) | 0.97 | 2.6 (3.8) | 0.99 |

The negative values calculated in this process represent a reaction that acts opposite the direction shown in the free-body, meaning there would be a tensile force on the tab. No such load could be imparted upon the tab as the tab is completely separated from the wing wall and as such, this load will not be used in design. This negative value is due to the large width of the heel which bears a significant amount of soil weight to counteract the overturning that would be required for this loading mechanism. It is still important to perform this check in design for cases where a smaller heel is used. The larger magnitude of these loads also highlights the amount of force that

occurs at this joint for traditionally built culverts with integral wing walls. Because the values returned from the wing wall translation case controlled, these values were taken to be the shear demand, V.

## 6.4 Design Procedure Results

Using the provisions outlined in Section 2.5.1, capacities for each of the three constructed culverts were calculated using the sectional properties given below in Table 6-3.

**Table 6-3: Culvert Tab Sectional Properties**

| | Chambers County | Lee County | Coosa County |
|---|---|---|---|
| $A_{vf}$ ($in^2$)/ft | 0.8 | 0.8 | 0.8 |
| $A_n$ ($in^2$)/ft | 0.4 | 0.4 | 0.4 |
| $A_s$ ($in^2$)/ft | 0.4 | 0.4 | 0.4 |
| $A_{st}$ ($in^2$)/ft | 0.9 | 0.9 | 0.9 |
| $f'_c$ (psi) | 4000 | 4000 | 4000 |
| $f_y$ (ksi) | 60 | 60 | 60 |
| b (in) | 12 | 12 | 12 |
| d (in) | 5.75 | 6.75 | 7.75 |
| a (in) | 0.60 | 0.60 | 0.60 |

These properties were taken from the design drawings, as explained below using Figure 6-5 and Figure 6-6.

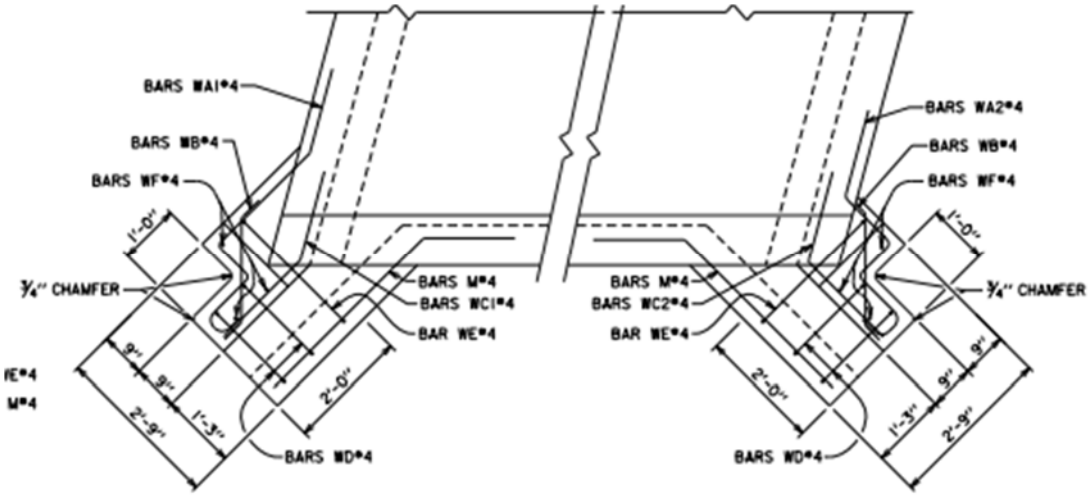


**Figure 6-5: Wall Tab Detail Plan View**

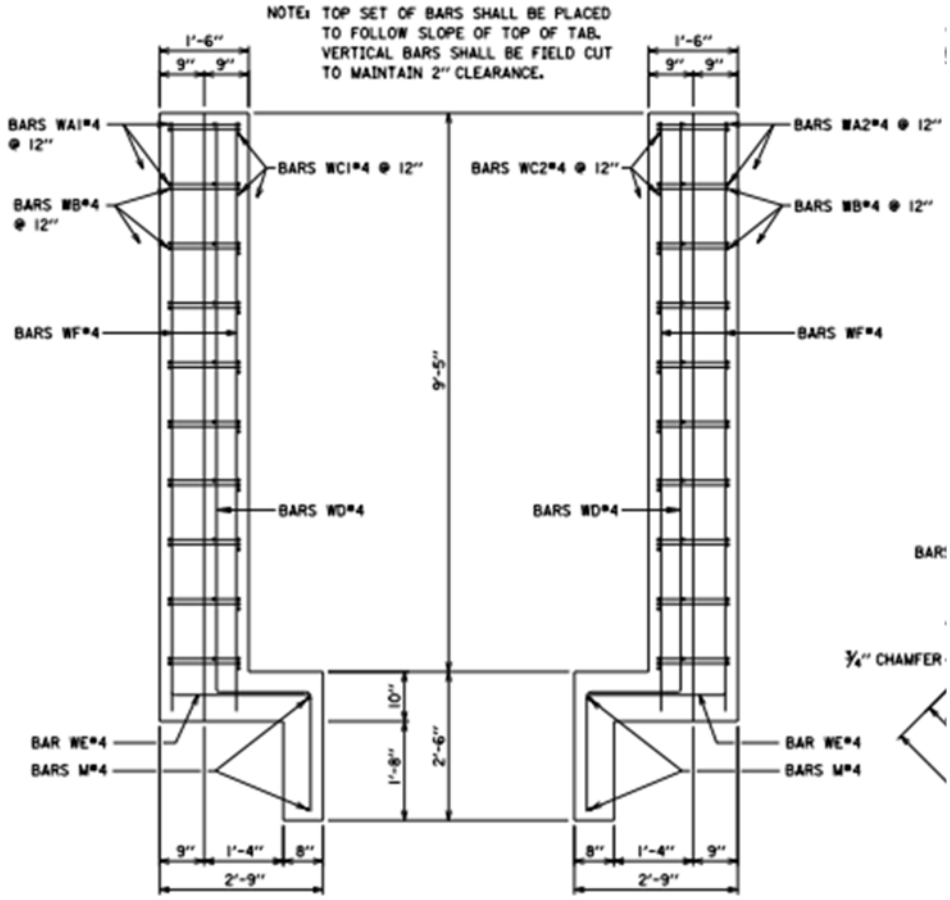


**Figure 6-6: Wall Tab Detail End View**

As can be seen in Figure 6-5 and Figure 6-6, the area of shear resisting reinforcement, $A_{vf}$, comprised four legs of a #4 bar, which amounted to 0.8 $in^2$. No stirrups were used, which is reasonable considering the narrowness of the member, but a value for $A_n$ of 0.4 $in^2$, or half of the bars active in shear, was used in order to determine the amount of steel that was active in resisting tension, $A_{st}$, per the provisions given in Section 2.5.1. Moment-resisting reinforcement comprised two legs of a #4 bar, thus $A_s$ was taken 0.4 $in^2$.

While test values of concrete compressive strength were determined for each culvert during the course of this research, the $f'_c$ value of 4000 psi was specified on the design drawings and was thus used in this analysis. The 60 ksi value of $f_y$ was also specified on the design drawings. The value of b was taken to be 12 in./ft as this was the design width used for analysis. The only dimension in which the three culverts differed was that of effective depth of reinforcement, d, due to the difference in tab thickness at each culvert. This value was determined by subtracting the typical 2 in. of cover from each of the tab thicknesses and half of a bar diameter. The value of "a" was calculated using the equations provided in Section 2.5.1. Using this information, section capacities were calculated using the equations provided in Section 2.5.1. As stated in Section 2.5.2, all section capacities were reduced by applying a factor of 0.70.

Ultimate tensile load, $N_{uc}$, was taken to be 20% of the shear load, $V_u$. Ultimate moment, $M_u$, was calculated as laid out in Section 2.5. Shear span, $a_v$, of each of the culvert tabs was conservatively taken to be 10 in., determined by subtracting the 2 in. of cover from the 12 in. length of the tab. The shear load, V, was multiplied by a load factor of 1.35 per Table 2-3, to determine $V_u$.

Table 6-4, below, gives the results of these calculations for each culvert tab. As can be seen, flexural demand controlled for each tab, but no tab failed under any of the design considerations.

**Table 6-4: Section Demands and Capacities**

| | $V_u$ (kips/ft) | $\Phi V_n$ (kips/ft) | $N_{uc}$ (kips/ft) | $\Phi P_{nt}$ (kips/ft) | $M_u$ (kip*ft/ft) | $\Phi M_n$ (kip*ft/ft) |
|---|---|---|---|---|---|---|
| Chambers County | 8.6 | 38.6 | 1.7 | 39.2 | 7.6 | 7.6 |
| Lee County | 6.3 | 45.4 | 1.3 | 39.2 | 5.6 | 9.0 |
| Coosa County | 8.9 | 47.0 | 1.8 | 39.2 | 7.8 | 10.4 |

# CHAPTER 7: SUMMARY, CONCLUSIONS, AND RECOMMENDATIONS

## 7.1 Summary

Three culverts were constructed utilizing a design wherein the wing wall was separated from the culvert and laterally supported by a tab protruding from the body of the culvert. This was done to mitigate issues that frequently arise in culverts constructed with integral wing walls due to differential settlement and localized accumulation of stress at the joint where wing walls frame into the body of a culvert. Earth pressure cells were installed in the tabs of these culverts to measure the stresses that were induced within these tabs. Periodic data collection was performed and showed that the tabs likely experienced the greatest pressure condition during the backfill and paving portions of construction and that this initial spike gradually reduced over time, except when environmental conditions, such as rain, lead to temporary spikes.

During construction of each culvert, concrete samples were taken and tested to provide more accurate concrete data for the analytical computer models being built in tandem to perform more rigorous analysis on the proposed culvert design.

Following the construction and monitoring of these culverts, an LRFD design procedure was formulated which took into account the lateral earth pressure acting upon the wing walls and considered two possible mechanisms of load transfer to the tabs. The values of structural demand arrived at through this procedure were compared with the pressure values observed in the field to gauge the validity of this approach.

Finally, the culvert tabs were analyzed using the approach outlined for corbels in the Caltrans Bridge Design Specifications to determine if the loads dictated by the aforementioned approach resulted in a reasonable reinforcing demand.

## 7.2 Conclusions

The design analyzed in this research proved to adequately address the issues it was intended to address. Removing the mechanical connection between the wing wall and culvert body eliminated the cracking that is frequently seen at this joint. Furthermore, designing the wing walls as independent retaining walls resulted in a design that minimally loaded the culvert tabs. While the slightly more labor intensive construction necessitated by the increased intricacy of this design may have caused a slight increase in construction costs, the mitigation of the issues faced by integral wing walls presents an opportunity for cost savings in maintenance over the service life of the culvert.

The design procedure recommended in this thesis yielded a reasonably conservative design load and the practice of designing the culvert tab as a corbel resulted in a design that resisted these prescribed loads with a reasonable amount of reinforcing steel. As such, it is the conclusion of this thesis that the proposed design is efficient and worthy of continued use.

## 7.3 Recommendations

The conclusions of this thesis were based upon a relatively short period of observation and thus it is recommended that the culverts continue to be monitored for any possible signs of distress which may not yet be evident.

It is recommended that the suggested design procedure be implemented in the design of all future culverts of this type. The design of the culvert tabs as corbels necessitates a slight shift in

the configuration of reinforcing from that seen in the culverts constructed for this research; however, the volume of steel necessary is not increased.

If future culverts of this kind are instrumented in a similar manner, it is recommended that the importance of notifying the researchers prior to backfill be stressed even more emphatically. This notification requirement was stipulated on the construction documents and was repeated to the contractors often; however, two of three culverts were backfilled with no notification given to the research team and the third culvert was roughly 75% backfilled when notification was given. As seen in this thesis, this period of time produced the greatest pressure measurement and thus monitoring of this period of time on future culverts could potentially change the findings of this research.

It is also recommended that measures be taken to monitor the moment that is induced in the reinforcing steel in both the culvert tab and the reinforcing wall near the culvert. This could perhaps be done through the use of strain gauges attached to the reinforcing steel prior to installation. This would allow for further refining of the design procedure of the culvert tabs and could give insight into the bending condition of the wing wall. The bending of the wing wall becomes more of a concern if the size of the wing wall heel is reduced and the likelihood of a rotation condition is increased.

## References


AASHTO. (2012). AASHTO LRFD Bridge Design Specifications.

Abdel-Karim, A. M., Tadros, M. K., & Benak, J. V. (1993). Structural Response of Full-Scale Concrete Box Culvert. *Journal of Structural Engineering*, 38-54.

ACI Committee 318. (2014). *Building Code Requirements for Structural Concrete (ACI 318-14); and Commentary (ACI 318R-14).* Farmington Hills, MI: American Concrete Institute.

Ahmed, B., Amanat, K. M., Safiullah, A. M., & Choudhury, J. R. (2002). Causes of Cracking of Culverts on Filled Soil and Their Performance After Repair. *Journal of Civil Engineering*.

ALDOT. (2005, June 29). *ALDOT-249 Procedure for Acceptance of Fine and Coarse Aggregates.* Retrieved from Alabama Department of Transportation: http://www.dot.state.al.us/mtweb/Testing/testing_manual/pdf/Pro/ALDOT249.pdf

ALDOT. (2012, January 9). *Special Provision No.12-0152.* Retrieved from Alabama Department of Transportation: https://www.dot.state.al.us/conweb/pdf/Specifications/2012%20GASP%20Summary/12-0152.pdf

ASTM C469/C469M. (2014). Standard Test Method for Static Modulus of Elasticity and Poisson's Ratio of Concrete in Compression. *ASTM Standard C469/C469M*. West Conshohocken, PA: ASTM International.

ASTM International. (2003). Standard Practice for Making and Curing Concrete Test Specimens in the Field. *C 31/C 31M - 00*. West Conshohocken, PA: ASTM International.

Burland, J. B., & Wroth, C. P. (1974). Settlement of Buildings and Associated Damage. *Conference on the Settlement of Structures Proceedings* (pp. 611-654). Cambridge: British Geotechnical Society.

Caltrans. (2003). Section 8: Reinforced Concrete. *Bridge Design Specifications*. Sacremento, CA, USA: California Department of Transportation.

Caltrans. (2004). Bridge Design Specifications. Sacramento, CA, USA: California Department of Tranportation.

Center for Dirt and Gravel Road Studies. (2004, June 1). *Headwalls & Endwalls.* Retrieved from Penn State Center for Dirt and Gravel Road Studies: https://www.dirtandgravel.psu.edu/sites/default/files/General%20Resources/Technical%20Bulletins/IB_Headwalls_and_Endwalls.pdf

Cook, R. A., & Bloomquist, D. (2002). *Evaluation of Precast Box Culvert Systems.* Gainesville, Florida: University of Florida.

Coulomb, C. A. (1776). *Essai sur une application des règles de maximis & minimis à quelques problèmes de statique, relatifs à l'architecture.* Paris: De l'Imprimerie Royale.

Emmons, P. H. (1993). *Concrete Repair and Maintenance Illustrated: Problem Analysis, Repair Strategy, Techniques.* Kingston, MA: R.S. Means.

FHWA. (1999, April). Earth Retaining Structures. *Training Course In Geotechnical and Foundation Engineering, NHI Course No. 13236 - Module 6*. Springfield, VA: U.S. Department of Commerce Natinal Technical Information Service.

Geokon, Inc. (2011). *Models 4800, 4810, 4815, 4820 and 4830 VW Earth Pressure Cells.* Lebanon, NH: Geokon, Inc.

Google Maps. (2017). 4300 County Road 258. La Fayette, Alabama.

Google Maps. (2017). 722 Lee Rd 156. Opelika , Alabama.

Google Maps. (2017). County Road 68. Sylacuaga, Alabama.

IOWA DOT. (2013). *LRFD Bridge Design Manual.* Des Moines, Iowa.

Kerenyi, K., Jones, J. S., Goeden, K., & Oien, P. (2005, September). *A Better Design for Box Culverts?* Retrieved January 16, 2017, from https://www.fhwa.dot.gov/publications/publicroads/05sep/07.cfm

Mattock, A. H. (1976). Design proposals for reinforced concrete corbels. *PCI Journal*, 18-42.

McCormac, J. C., & Brown, R. H. (2014). *Design of Reinforced Concrete* (9 ed.). Hoboken, NJ, United States of America: Wiley.

Mentzer, A. P. (2017, April 24). *What Is the Range of Barometric Pressure?* Retrieved from Sciencing: https://sciencing.com/range-barometric-pressure-5505227.html

Merriam-Webster. (2016). *Concrete*. Retrieved December 12, 2016, from https://www.merriam-webster.com/dictionary/concrete

Minton, L. W. (2012). *Mitigation of Cracking in Cast-In-Place Reinforced Concrete Box Culverts in Alabama.* Auburn, Alabama: Auburn University.

Portland Cement Association. (2014). *Corrosion of Embedded Metals*. Retrieved February 5, 2015, from http://www.cement.org/for-concrete-books-learning/concrete-technology/durability/corrosion-of-embedded-materials

Rankine, W. J. (1857). *On the Stability of Loose Earth.* Royal Society of London.

Schall, J. D., Thompson, P. L., Zerges, S. M., Kilgore, R. T., & Morris, J. L. (2012). *Hydraulic Design of Highway Culverts, Third Edition.* Washington, D.C.: U.S. Department of Transportation.

Tullmin, M. (2001). *Reinforcing Steel Corrosion in Concrete*. Retrieved February 5, 2015, from http://www.corrosion-club.com/concretecorrosion.htm

## Appendix A: Raw Data

### Constructed Culvert Design Drawings and Boring Logs

#### Chambers County

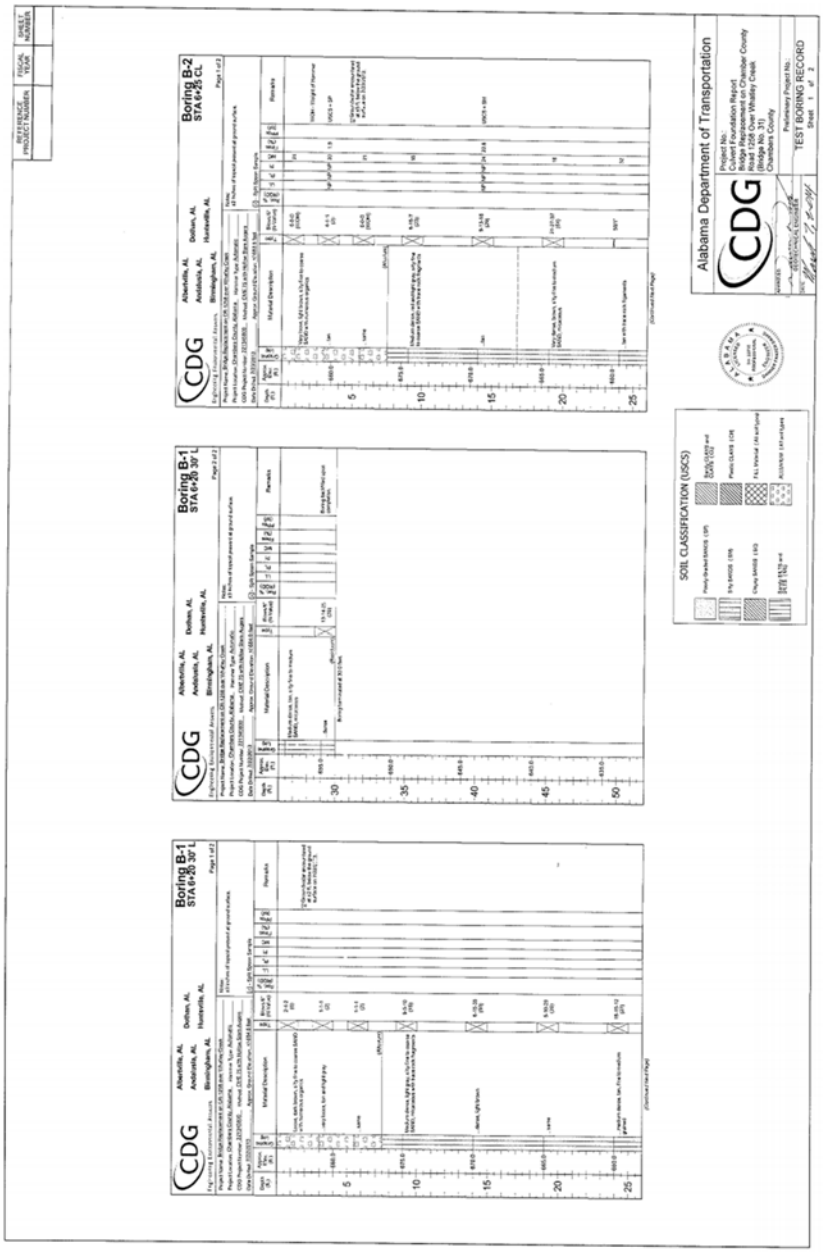


**Figure A-1: Chambers County Boring Logs**

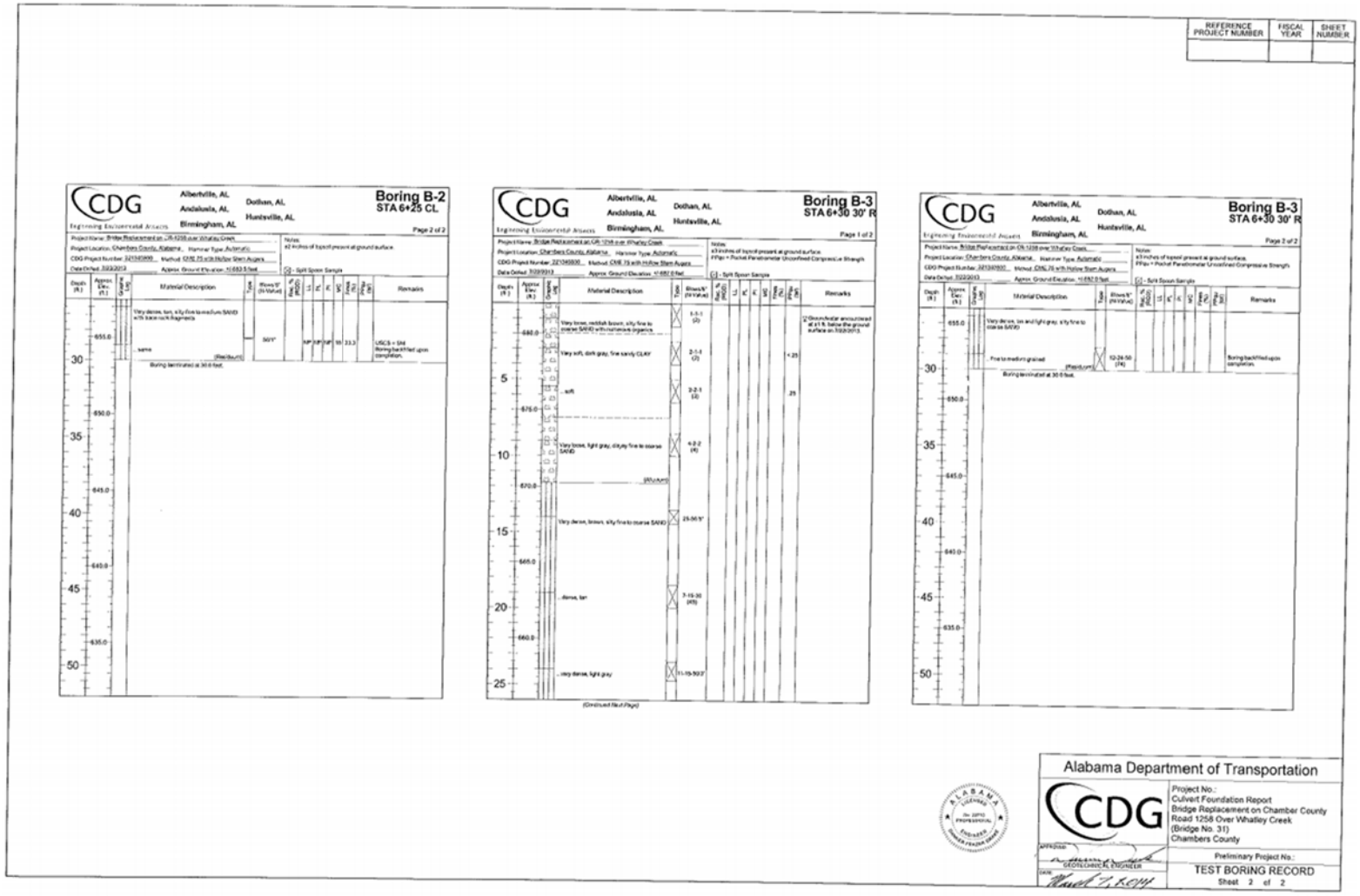


**Figure A-2: Chambers County Boring Logs**

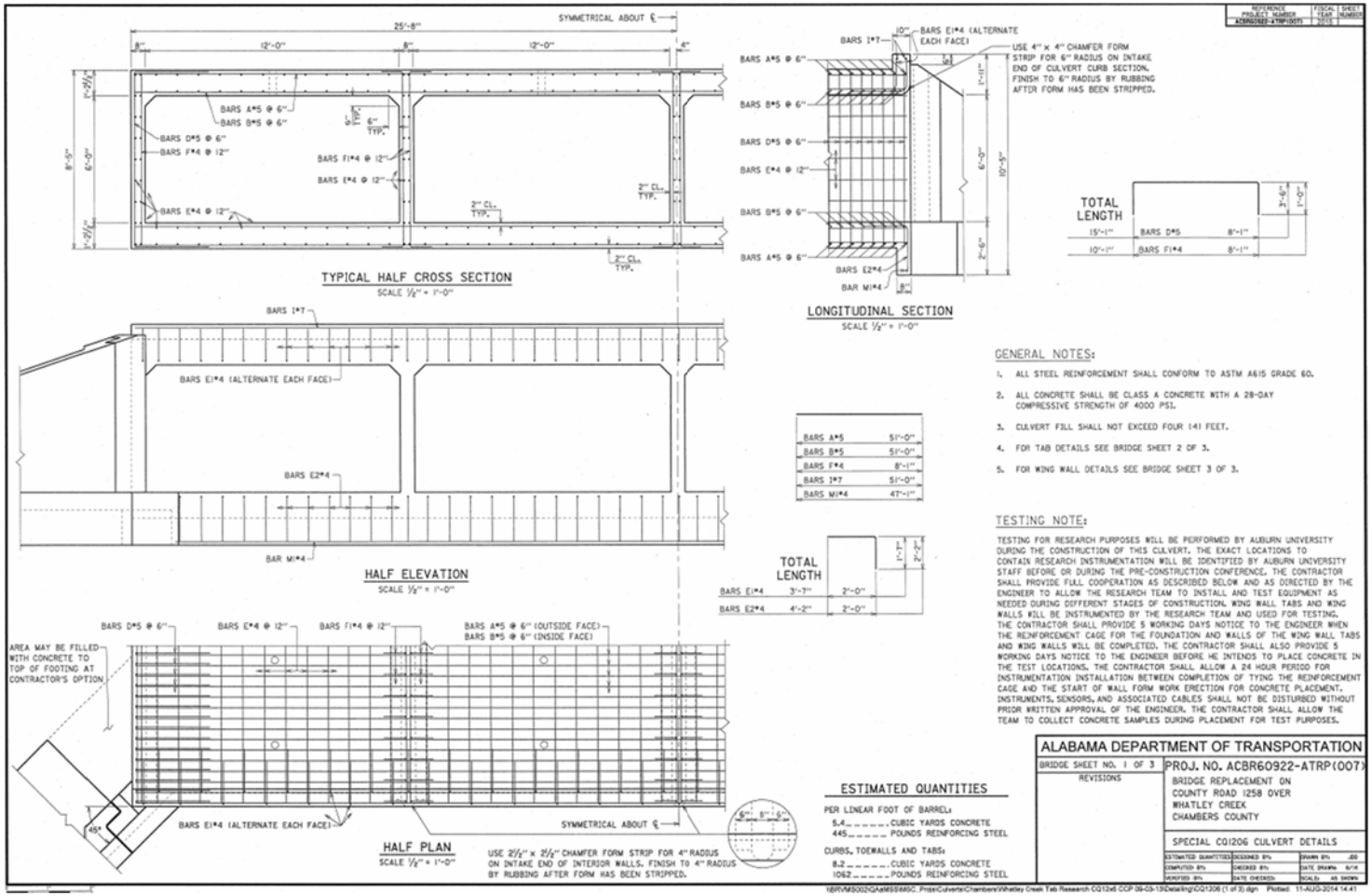


**Figure A-3: Chambers County Design Drawings**

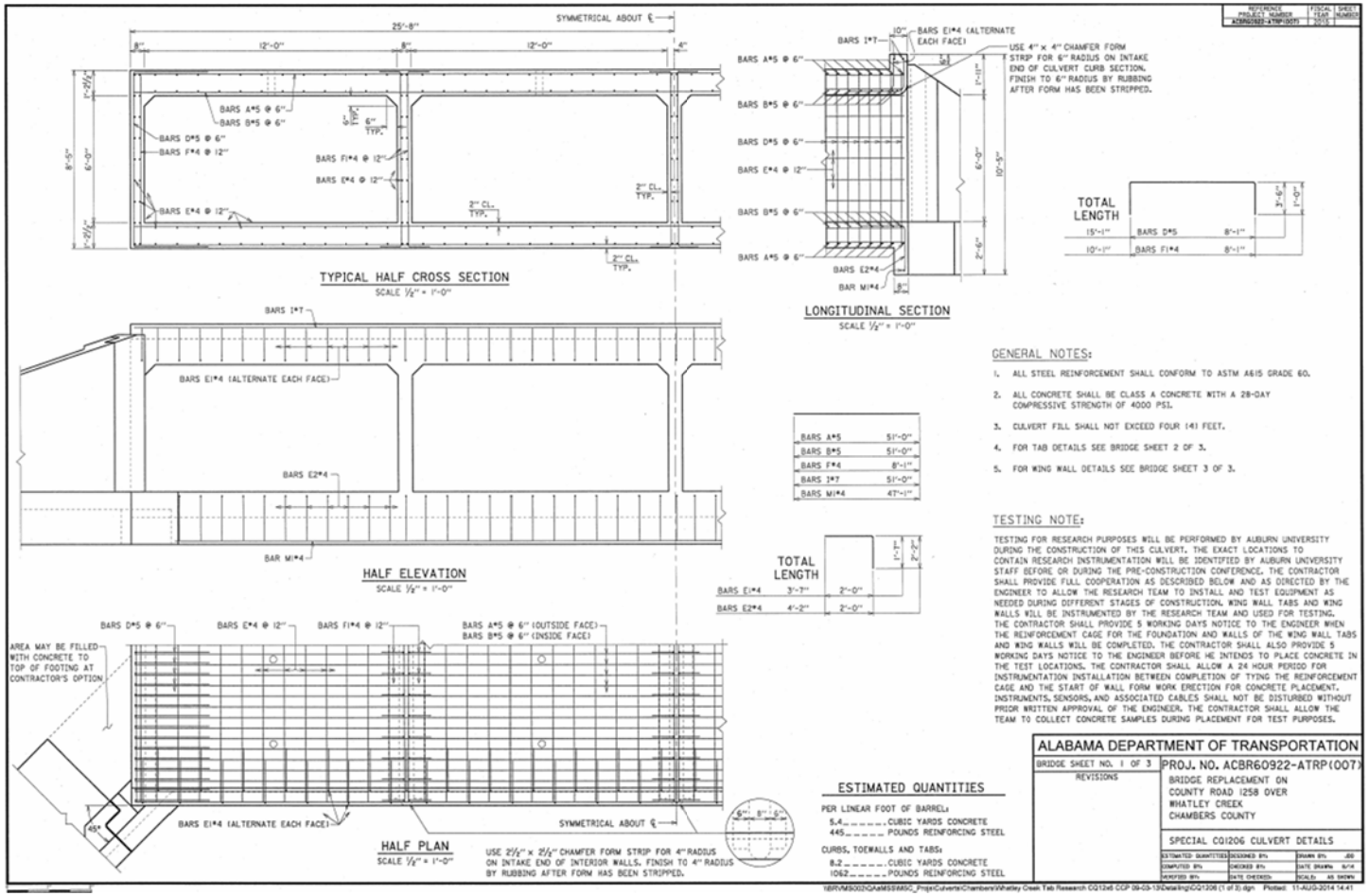


**Figure A-4: Chambers County Design Drawings**

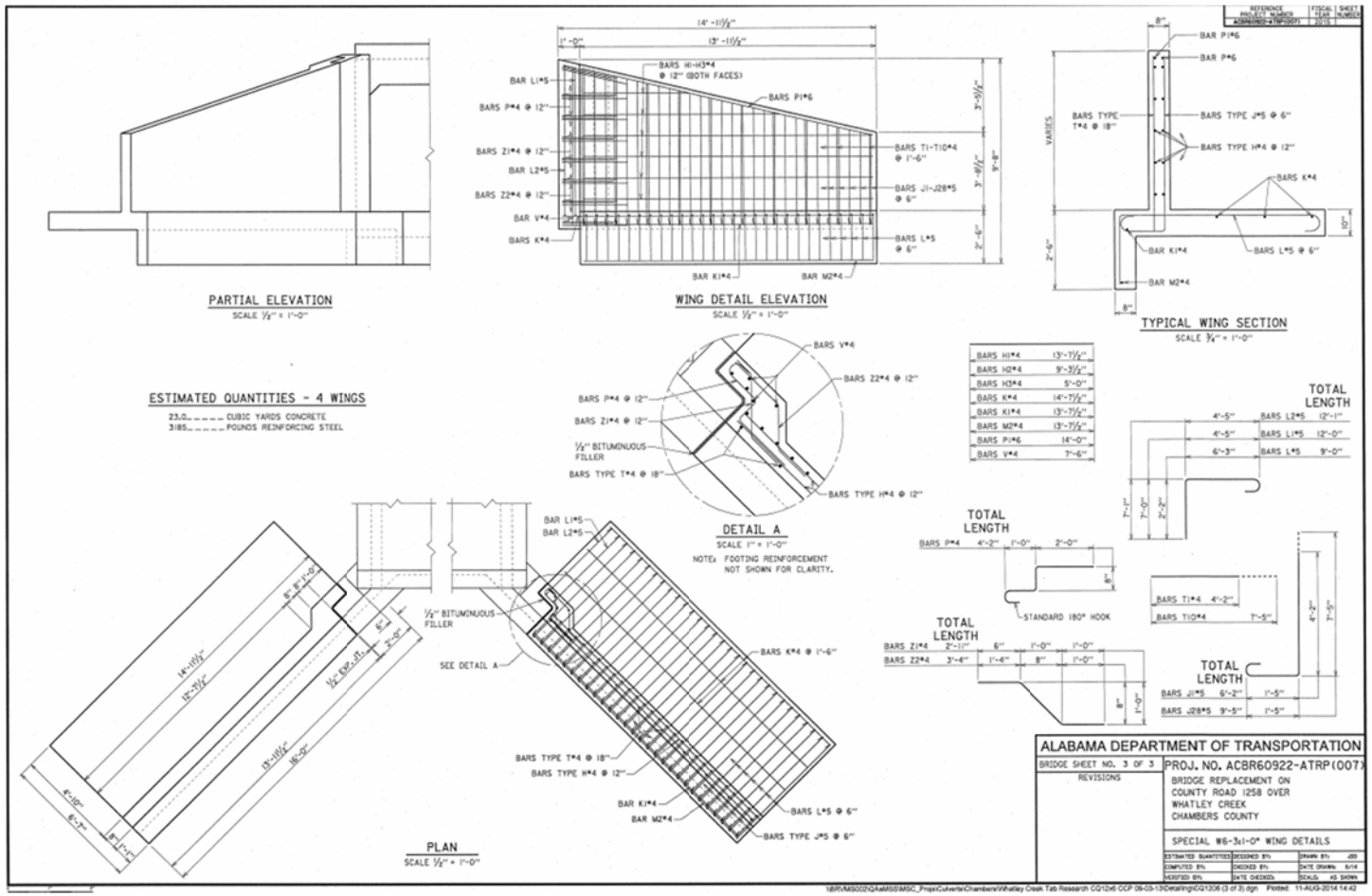


**Figure A-5: Chambers County Design Drawings**

## Lee County

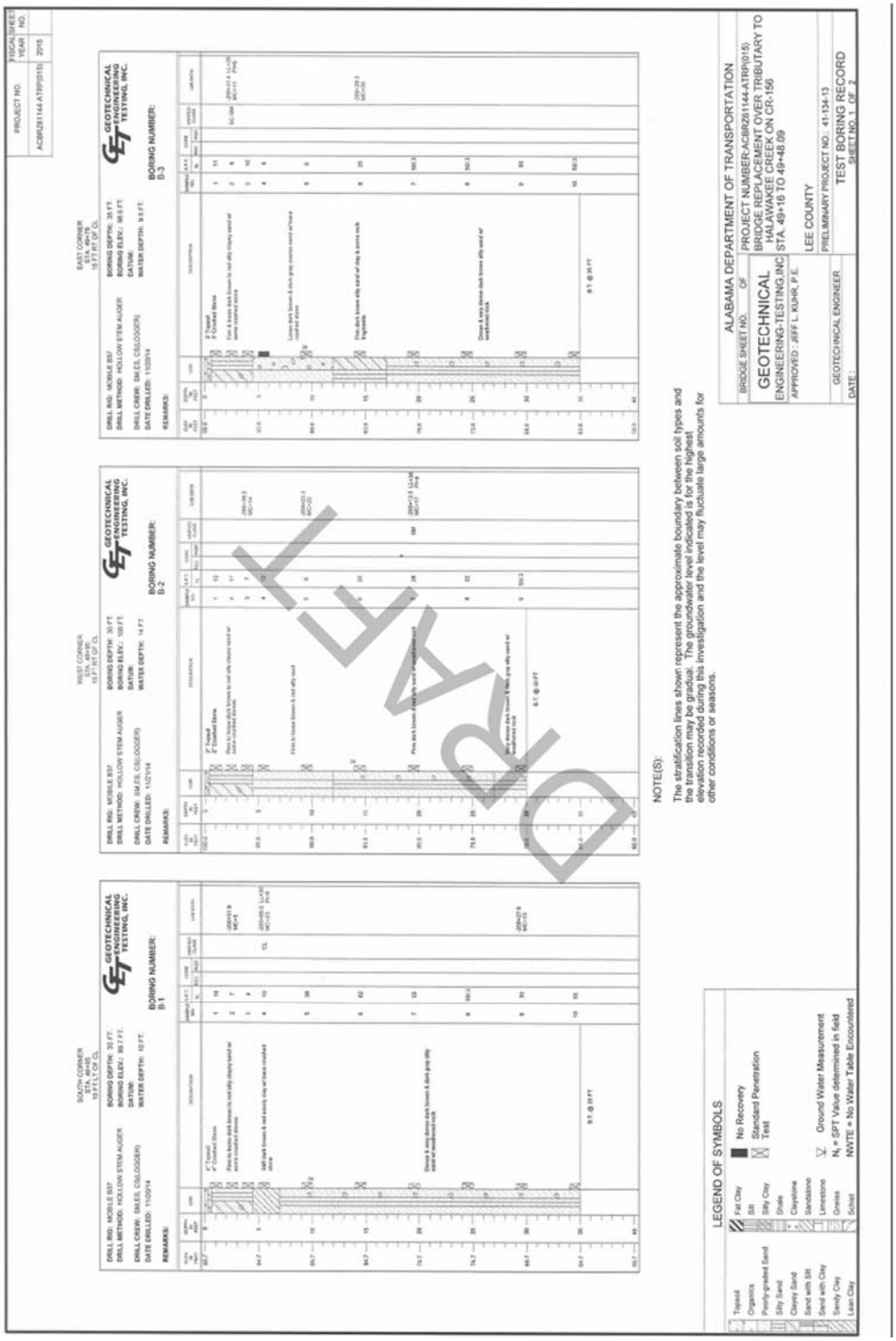


**Figure A-6: Lee County Boring Logs**

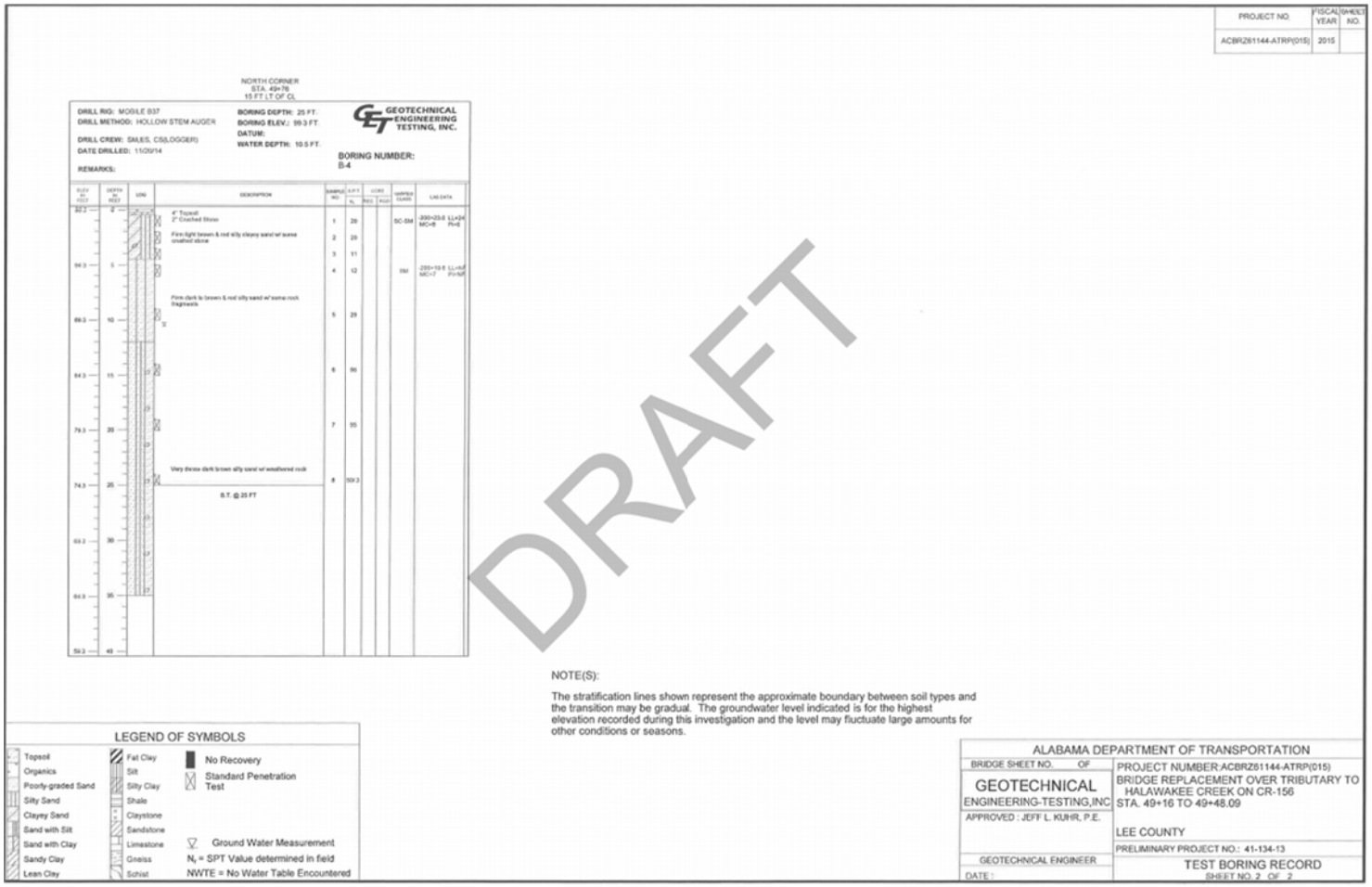



**Figure A-7: Lee County Boring Logs**

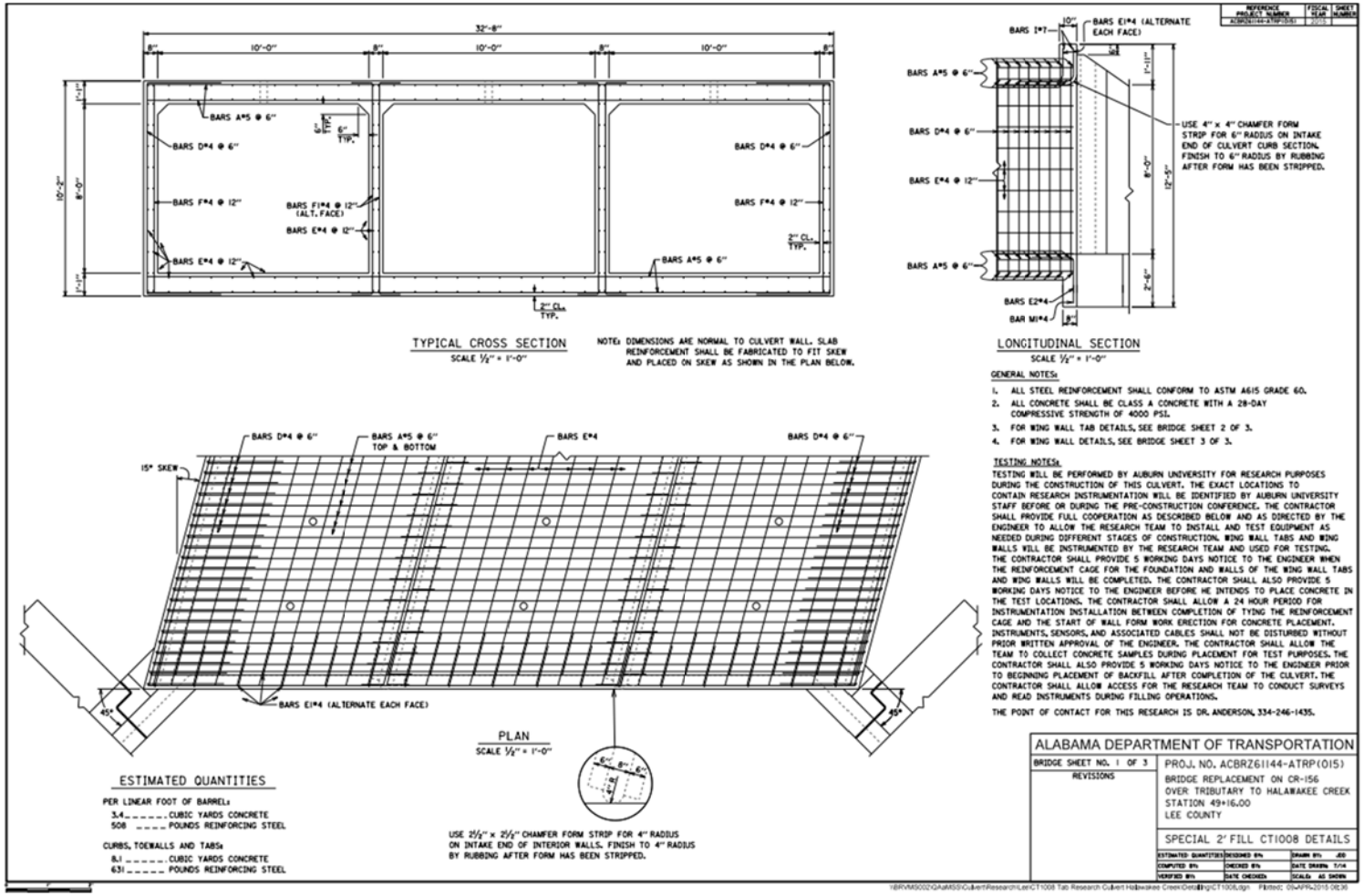


**Figure A-8: Lee County Design Drawings**

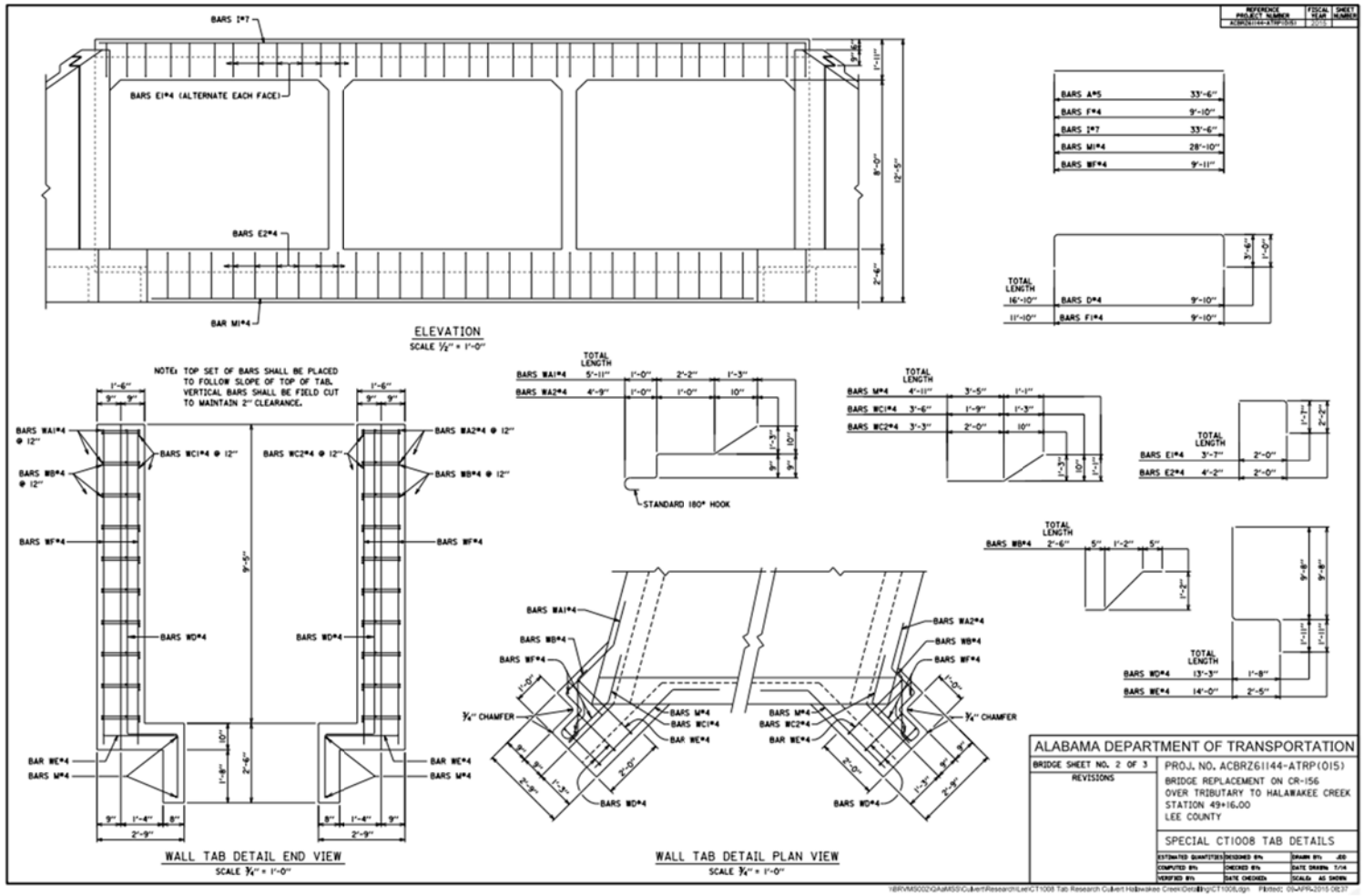


**Figure A-9: Lee County Design Drawings**

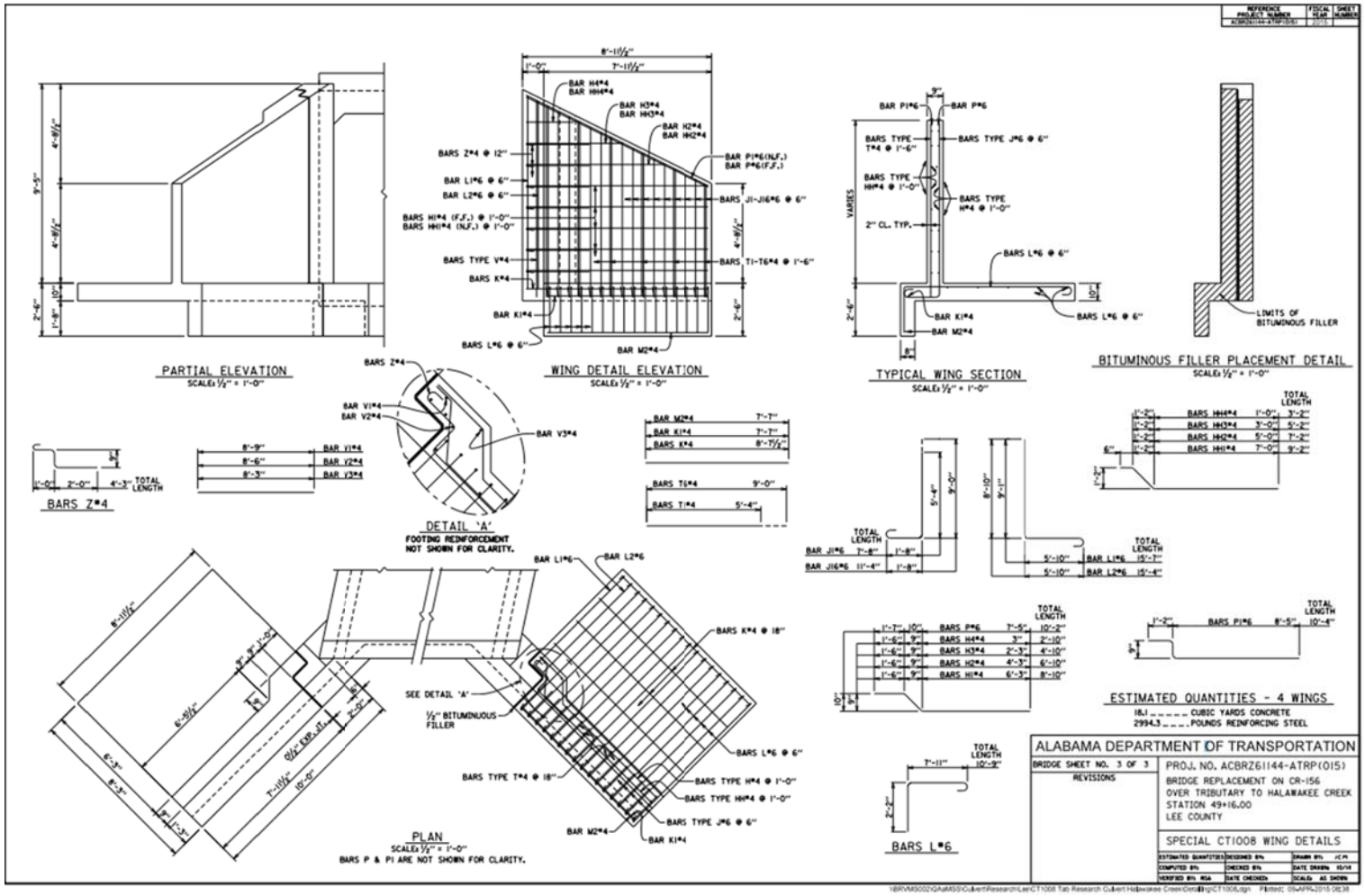


**Figure A-10: Lee County Design Drawings**

**Coosa County**

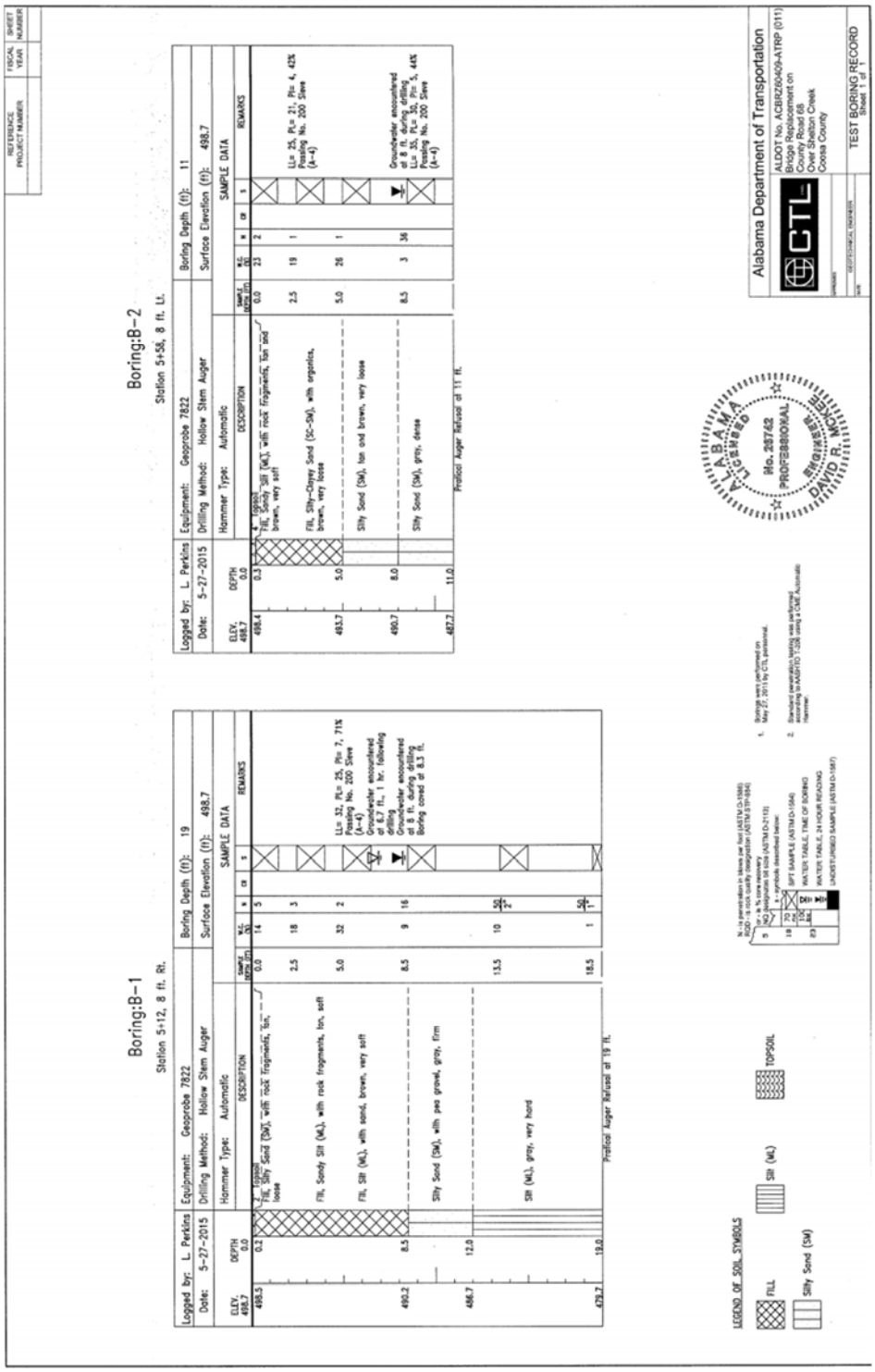


**Figure A-11: Coosa County Boring Logs**

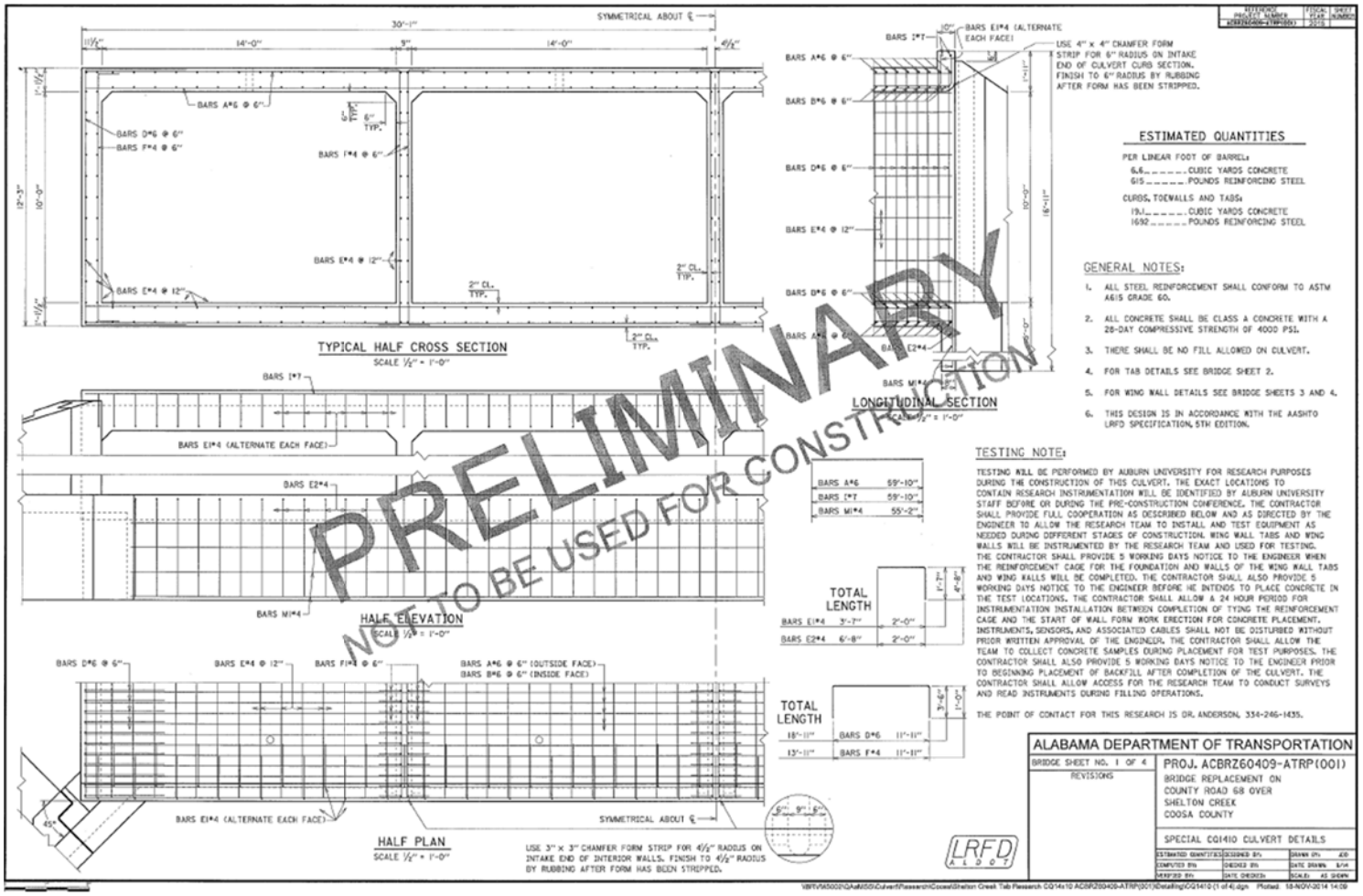


**FigureA-12: Coosa County Design Drawings**

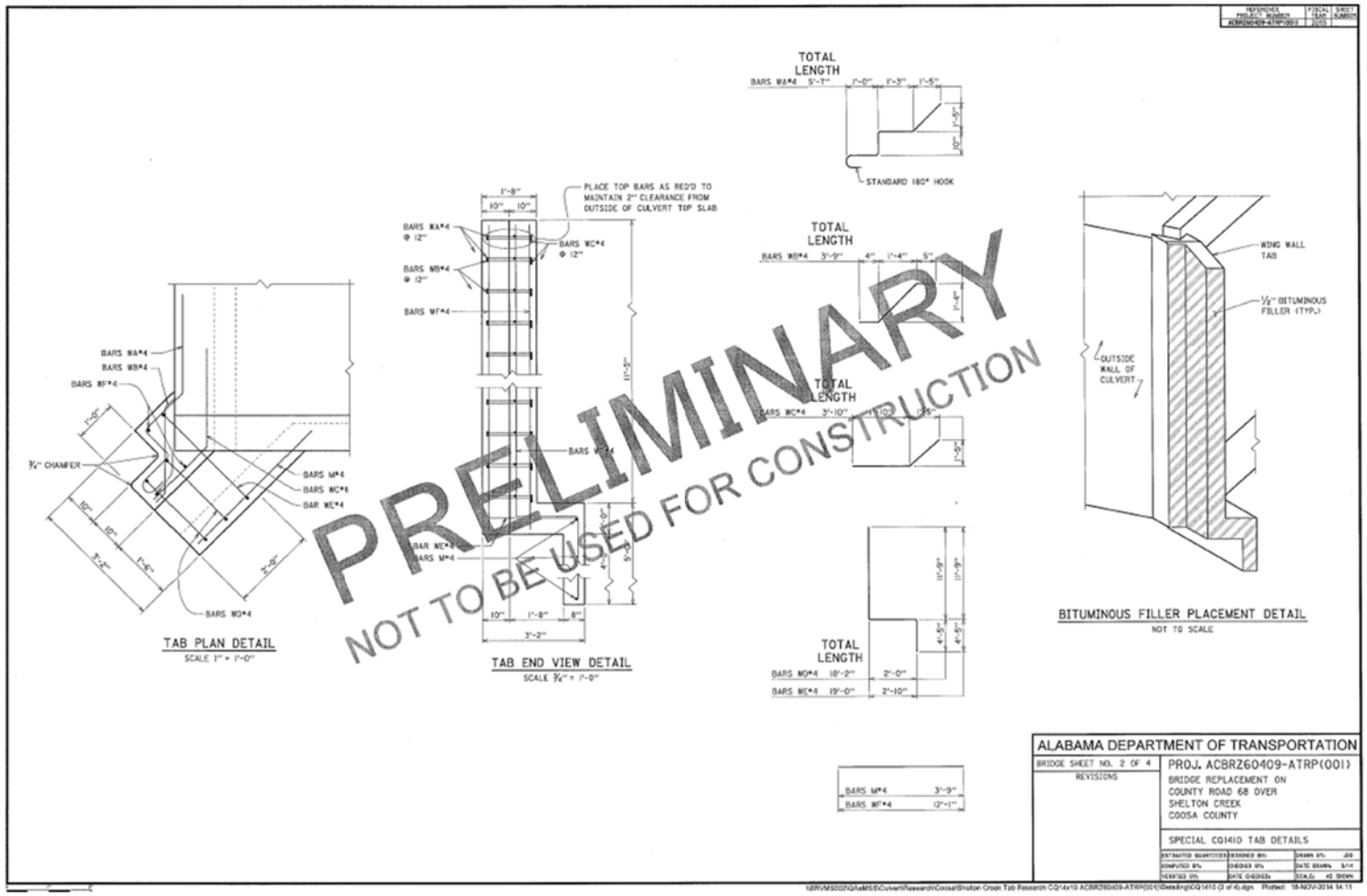


**Figure A-13: Coosa County Design Drawings**

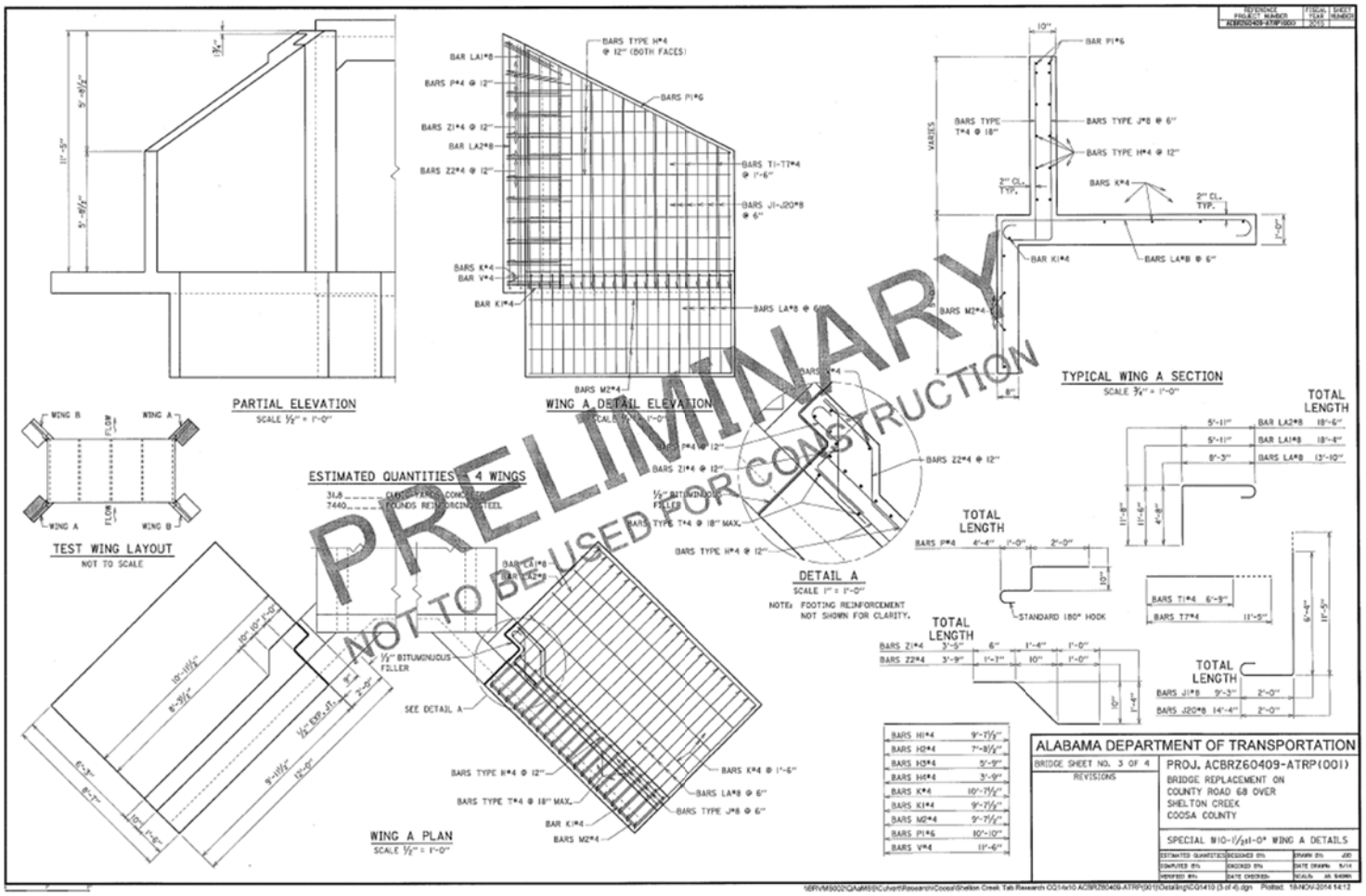


**Figure A-14: Coosa County Design Drawings**

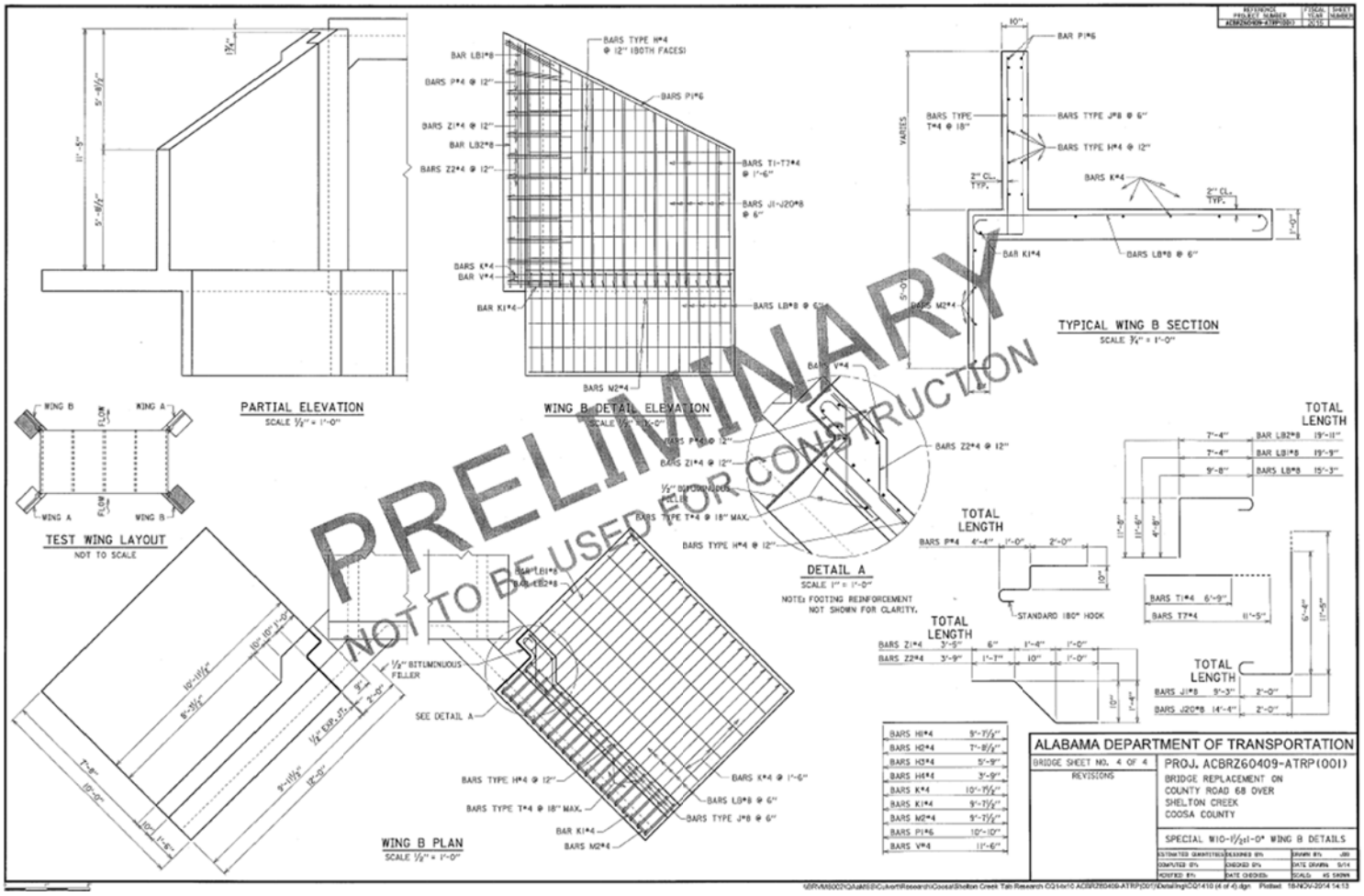


**Figure A-15: Coosa County Design Drawings**

**Pressure Cell Calibration Data**

**Chambers County:**

**Table A-1: Chambers County Cell B1 - Serial Number 1504285**

| Pressure | | | | Pressure | | | |
|---|---|---|---|---|---|---|---|
| Initial Reading | $R_0$ | 8896.5 | digits | Initial Reading | $R_0$ | 8896.5 | digits |
| Current Reading | $R_1$ | 8896.5 | digits | Current Reading | $R_1$ | 8896.5 | digits |
| Barometric Pressures | $S_0$ | 14.6117 | psi | Barometric Pressures | $S_0$ | 100.77 | kPa |
| | $S_1$ | 14.6117 | psi | | $S_1$ | 100.77 | kPa |
| Temperatures | $T_0$ | 37.6 | °C | Temperatures | $T_0$ | 37.6 | °C |
| | $T_1$ | 37.6 | °C | | $T_1$ | 37.6 | °C |
| Calibration Factc | G | -0.02433 | psi/digit | Calibration Factc | G | -0.1678 | kPa/digit |
| Polynomial Gage Factors | A | -5.8E-08 | | Polynomial Gage Factors | A | -4E-07 | |
| | B | -0.02354 | | | B | -0.1623 | |
| | C | 214.0 | | | C | 1475.7 | |
| Thermal Factor | K | 0.001335 | psi/°C | Thermal Factor | K | 0.009204 | kPa/°C |
| | | | | | | | |
| Calculated Pressure | | | | Calculated Pressure | | | |
| Linear | 0.0 | psf | | Linear | 0.0 | kPa | |
| Polynomial | 0.0 | psf | | Polynomial | 0.0 | kPa | |

**Table A-2: Chambers County M1 - Serial Number 1504284**

| Pressure | | | | Pressure | | | |
|---|---|---|---|---|---|---|---|
| Initial Reading | $R_0$ | 8882.1 | digits | Initial Reading | $R_0$ | 8882.1 | digits |
| Current Reading | $R_1$ | 8882.1 | digits | Current Reading | $R_1$ | 8882.1 | digits |
| Barometric Pressures | $S_0$ | 14.6117 | psi | Barometric Pressures | $S_0$ | 100.77 | kPa |
| | $S_1$ | 14.6117 | psi | | $S_1$ | 100.77 | kPa |
| Temperatures | $T_0$ | 38.6 | °C | Temperatures | $T_0$ | 38.6 | °C |
| | $T_1$ | 38.6 | °C | | $T_1$ | 38.6 | °C |
| Calibration Factc | G | -0.02533 | psi/digit | Calibration Factc | G | -0.1746 | kPa/digit |
| Polynomial Gage Factors | A | -8.15E-08 | | Polynomial Gage Factors | A | -5.62E-07 | |
| | B | -0.0242 | | | B | -0.1668 | |
| | C | 221.4 | | | C | 1525.9 | |
| Thermal Factor | K | 0.005057 | psi/°C | Thermal Factor | K | 0.03486 | kPa/°C |
| | | | | | | | |
| Calculated Pressure | | | | Calculated Pressure | | | |
| Linear | 0.0 | psf | | Linear | 0.0 | kPa | |
| Polynomial | 0.0 | psf | | Polynomial | 0.0 | kPa | |

**Table A-3: Chambers County T1 - Serial Number 1504286**

| Pressure | | | |
|---|---|---|---|
| Initial Reading | $R_0$ | 8739.2 | digits |
| Current Reading | $R_1$ | 8739.2 | digits |
| Barometric Pressures | $S_0$ | 14.6117 | psi |
| | $S_1$ | 14.6117 | psi |
| Temperatures | $T_0$ | 36.9 | °C |
| | $T_1$ | 36.9 | °C |
| Calibration Factc | G | -0.0243 | psi/digit |
| Polynomial Gage Factors | A | -9E-08 | |
| | B | -0.02309 | |
| | C | 208.7 | |
| Thermal Factor | K | 0.004862 | psi/°C |
| | | | |
| Calculated Pressure | | | |
| Linear | 0.0 | psf | |
| Polynomial | 0.0 | psf | |

| Pressure | | | |
|---|---|---|---|
| Initial Reading | $R_0$ | 8739.2 | digits |
| Current Reading | $R_1$ | 8739.2 | digits |
| Barometric Pressures | $S_0$ | 100.77 | kPa |
| | $S_1$ | 100.77 | kPa |
| Temperatures | $T_0$ | 36.9 | °C |
| | $T_1$ | 36.9 | °C |
| Calibration Factc | G | -0.1676 | kPa/digit |
| Polynomial Gage Factors | A | -6.21E-07 | |
| | B | -0.1592 | |
| | C | 1438.7 | |
| Thermal Factor | K | 0.03353 | kPa/°C |
| | | | |
| Calculated Pressure | | | |
| Linear | 0.0 | kPa | |
| Polynomial | 0.0 | kPa | |

**Table A-4: Chambers County B2 - Serial Number 1517360**

| Pressure | | | |
|---|---|---|---|
| Initial Reading | $R_0$ | 8820 | digits |
| Current Reading | $R_1$ | 8820 | digits |
| Barometric Pressures | $S_0$ | 14.3920 | psi |
| | $S_1$ | 14.3920 | psi |
| Temperatures | $T_0$ | 25.3 | °C |
| | $T_1$ | 25.3 | °C |
| Calibration Factc | G | -0.02555 | psi/digit |
| Polynomial Gage Factors | A | -8.195E-08 | |
| | B | -0.02442 | |
| | C | 221.8 | |
| Thermal Factor | K | 0.0025 | psi/°C |
| | | | |
| Calculated Pressure | | | |
| Linear | 0.0 | psf | |
| Polynomial | 0.0 | psf | |

| Pressure | | | |
|---|---|---|---|
| Initial Reading | $R_0$ | 8820 | digits |
| Current Reading | $R_1$ | 8820 | digits |
| Barometric Pressures | $S_0$ | 99.23 | kPa |
| | $S_1$ | 99.23 | kPa |
| Temperatures | $T_0$ | 25.3 | °C |
| | $T_1$ | 25.3 | °C |
| Calibration Factc | G | -0.1761 | kPa/digit |
| Polynomial Gage Factors | A | -5.65E-07 | |
| | B | -0.1684 | |
| | C | 1529.2 | |
| Thermal Factor | K | 0.01723 | kPa/°C |
| | | | |
| Calculated Pressure | | | |
| Linear | 0.0 | kPa | |
| Polynomial | 0.0 | kPa | |

**Table A-5: Chambers County M2 - Serial Number 1517358**

| Pressure | | | |
|---|---|---|---|
| Initial Reading | $R_0$ | 8845.2 | digits |
| Current Reading | $R_1$ | 8845.2 | digits |
| Barometric Pressures | $S_0$ | 14.3920 | psi |
| | $S_1$ | 14.3920 | psi |
| Temperatures | $T_0$ | 26 | °C |
| | $T_1$ | 26 | °C |
| Calibration Factc | G | -0.02527 | psi/digit |
| Polynomial Gage Factors | A | -1.066E-07 | |
| | B | -0.02442 | |
| | C | 224.3 | |
| Thermal Factor | K | 0.01008 | psi/°C |
| | | | |
| Calculated Pressure | | | |
| Linear | 0.0 | psf | |
| Polynomial | 0.0 | psf | |

| Pressure | | | |
|---|---|---|---|
| Initial Reading | $R_0$ | 8845.2 | digits |
| Current Reading | $R_1$ | 8845.2 | digits |
| Barometric Pressures | $S_0$ | 99.23 | kPa |
| | $S_1$ | 99.23 | kPa |
| Temperatures | $T_0$ | 26 | °C |
| | $T_1$ | 26 | °C |
| Calibration Factc | G | -0.1742 | kPa/digit |
| Polynomial Gage Factors | A | -7.348E-07 | |
| | B | -0.1684 | |
| | C | 1547.0 | |
| Thermal Factor | K | 0.06948 | kPa/°C |
| | | | |
| Calculated Pressure | | | |
| Linear | 0.0 | kPa | |
| Polynomial | 0.0 | kPa | |

**Table A-6: Chambers County T2 - Serial Number 1517359**

| Pressure | | | |
|---|---|---|---|
| Initial Reading | $R_0$ | 8768.2 | digits |
| Current Reading | $R_1$ | 8768.2 | digits |
| Barometric Pressures | $S_0$ | 14.3920 | psi |
| | $S_1$ | 14.3920 | psi |
| Temperatures | $T_0$ | 27 | °C |
| | $T_1$ | 27 | °C |
| Calibration Factc | G | -0.02543 | psi/digit |
| Polynomial Gage Factors | A | -1.186E-07 | |
| | B | -0.02381 | |
| | C | 217.9 | |
| Thermal Factor | K | 0.005331 | psi/°C |
| | | | |
| Calculated Pressure | | | |
| Linear | 0.0 | psf | |
| Polynomial | 0.0 | psf | |

| Pressure | | | |
|---|---|---|---|
| Initial Reading | $R_0$ | 8768.2 | digits |
| Current Reading | $R_1$ | 8768.2 | digits |
| Barometric Pressures | $S_0$ | 99.23 | kPa |
| | $S_1$ | 99.23 | kPa |
| Temperatures | $T_0$ | 27 | °C |
| | $T_1$ | 27 | °C |
| Calibration Factc | G | -0.1753 | kPa/digit |
| Polynomial Gage Factors | A | -8.176E-07 | |
| | B | -0.1642 | |
| | C | 1502.6 | |
| Thermal Factor | K | 0.03676 | kPa/°C |
| | | | |
| Calculated Pressure | | | |
| Linear | 0.0 | kPa | |
| Polynomial | 0.0 | kPa | |

**Table A-7: Chambers County B3 - Serial Number 1518127**

| Pressure | | | |
|---|---|---|---|
| Initial Reading | $R_0$ | 8815 | digits |
| Current Reading | $R_1$ | 8815 | digits |
| Barometric Pressures | $S_0$ | 14.2950 | psi |
| | $S_1$ | 14.2950 | psi |
| Temperatures | $T_0$ | 25.2 | °C |
| | $T_1$ | 25.2 | °C |
| Calibration Factc | G | -0.02432 | psi/digit |
| Polynomial Gage Factors | A | -9.129E-08 | |
| | B | -0.02309 | |
| | C | 210.6 | |
| Thermal Factor | K | 0.008176 | psi/°C |
| | | | |
| Calculated Pressure | | | |
| Linear | 0.0 | psf | |
| Polynomial | 0.0 | psf | |

| Pressure | | | |
|---|---|---|---|
| Initial Reading | $R_0$ | 8815 | digits |
| Current Reading | $R_1$ | 8815 | digits |
| Barometric Pressures | $S_0$ | 98.56 | kPa |
| | $S_1$ | 98.56 | kPa |
| Temperatures | $T_0$ | 25.2 | °C |
| | $T_1$ | 25.2 | °C |
| Calibration Factc | G | -0.1677 | kPa/digit |
| Polynomial Gage Factors | A | -6.294E-07 | |
| | B | -0.1592 | |
| | C | 1452.3 | |
| Thermal Factor | K | 0.05637 | kPa/°C |
| | | | |
| Calculated Pressure | | | |
| Linear | 0.0 | kPa | |
| Polynomial | 0.0 | kPa | |

**Table A-8: Chambers County M3 - Serial Number 1518125**

| Pressure | | | |
|---|---|---|---|
| Initial Reading | $R_0$ | 8722 | digits |
| Current Reading | $R_1$ | 8722 | digits |
| Barometric Pressures | $S_0$ | 14.2950 | psi |
| | $S_1$ | 14.2950 | psi |
| Temperatures | $T_0$ | 24.2 | °C |
| | $T_1$ | 24.2 | °C |
| Calibration Factc | G | -0.02626 | psi/digit |
| Polynomial Gage Factors | A | -9.08E-08 | |
| | B | -0.02502 | |
| | C | 225.1 | |
| Thermal Factor | K | 0.008949 | psi/°C |
| | | | |
| Calculated Pressure | | | |
| Linear | 0.0 | psf | |
| Polynomial | 0.0 | psf | |

| Pressure | | | |
|---|---|---|---|
| Initial Reading | $R_0$ | 8722 | digits |
| Current Reading | $R_1$ | 8722 | digits |
| Barometric Pressures | $S_0$ | 98.56 | kPa |
| | $S_1$ | 98.56 | kPa |
| Temperatures | $T_0$ | 24.2 | °C |
| | $T_1$ | 24.2 | °C |
| Calibration Factc | G | -0.181 | kPa/digit |
| Polynomial Gage Factors | A | -6.26E-07 | |
| | B | -0.1725 | |
| | C | 1552.2 | |
| Thermal Factor | K | 0.0617 | kPa/°C |
| | | | |
| Calculated Pressure | | | |
| Linear | 0.0 | kPa | |
| Polynomial | 0.0 | kPa | |

**Table A-9: Chambers County T3 - Serial Number 1518126**

| Pressure | | | |
|---|---|---|---|
| Initial Reading | $R_0$ | 8757.4 | digits |
| Current Reading | $R_1$ | 8757.4 | digits |
| Barometric Pressures | $S_0$ | 14.2950 | psi |
| | $S_1$ | 14.2950 | psi |
| Temperatures | $T_0$ | 24.7 | °C |
| | $T_1$ | 24.7 | °C |
| Calibration Factc | G | -0.02559 | psi/digit |
| Polynomial Gage Factors | A | -1.11E-07 | |
| | B | -0.02408 | |
| | C | 219.4 | |
| Thermal Factor | K | 0.001997 | psi/°C |
| | | | |
| Calculated Pressure | | | |
| Linear | 0.0 | psf | |
| Polynomial | 0.0 | psf | |

| Pressure | | | |
|---|---|---|---|
| Initial Reading | $R_0$ | 8757.4 | digits |
| Current Reading | $R_1$ | 8757.4 | digits |
| Barometric Pressures | $S_0$ | 98.56 | kPa |
| | $S_1$ | 98.56 | kPa |
| Temperatures | $T_0$ | 24.7 | °C |
| | $T_1$ | 24.7 | °C |
| Calibration Factc | G | -0.1764 | kPa/digit |
| Polynomial Gage Factors | A | -7.65E-07 | |
| | B | -0.166 | |
| | C | 1512.4 | |
| Thermal Factor | K | 0.01377 | kPa/°C |
| | | | |
| Calculated Pressure | | | |
| Linear | 0.0 | kPa | |
| Polynomial | 0.0 | kPa | |

**Table A-10: Chambers County B4 - Serial Number 1518128**

| Pressure | | | |
|---|---|---|---|
| Initial Reading | $R_0$ | 8737.5 | digits |
| Current Reading | $R_1$ | 8737.5 | digits |
| Barometric Pressures | $S_0$ | 14.2950 | psi |
| | $S_1$ | 14.2950 | psi |
| Temperatures | $T_0$ | 28.3 | °C |
| | $T_1$ | 28.3 | °C |
| Calibration Factc | G | -0.02588 | psi/digit |
| Polynomial Gage Factors | A | -5.885E-08 | |
| | B | -0.02508 | |
| | C | 223.6 | |
| Thermal Factor | K | 0.007305 | psi/°C |
| | | | |
| Calculated Pressure | | | |
| Linear | 0.0 | psf | |
| Polynomial | 0.0 | psf | |

| Pressure | | | |
|---|---|---|---|
| Initial Reading | $R_0$ | 8737.5 | digits |
| Current Reading | $R_1$ | 8737.5 | digits |
| Barometric Pressures | $S_0$ | 98.56 | kPa |
| | $S_1$ | 98.56 | kPa |
| Temperatures | $T_0$ | 28.3 | °C |
| | $T_1$ | 28.3 | °C |
| Calibration Factc | G | -0.1785 | kPa/digit |
| Polynomial Gage Factors | A | -4.057E-07 | |
| | B | -0.1729 | |
| | C | 1541.7 | |
| Thermal Factor | K | 0.05037 | kPa/°C |
| | | | |
| Calculated Pressure | | | |
| Linear | 0.0 | kPa | |
| Polynomial | 0.0 | kPa | |

**Table A-11: Chambers County M4 - Serial Number 1518129**

| Pressure | | | |
|---|---|---|---|
| Initial Reading | $R_0$ | 8814.2 | digits |
| Current Reading | $R_1$ | 8814.2 | digits |
| Barometric Pressures | $S_0$ | 14.2950 | psi |
| | $S_1$ | 14.2950 | psi |
| Temperatures | $T_0$ | 27.6 | °C |
| | $T_1$ | 27.6 | °C |
| Calibration Factc | G | -0.02599 | psi/digit |
| Polynomial Gage Factors | A | -6.563E-08 | |
| | B | -0.02508 | |
| | C | 226.2 | |
| Thermal Factor | K | 0.004983 | psi/°C |
| | | | |
| Calculated Pressure | | | |
| Linear | 0.0 | psf | |
| Polynomial | 0.0 | psf | |

| Pressure | | | |
|---|---|---|---|
| Initial Reading | $R_0$ | 8814.2 | digits |
| Current Reading | $R_1$ | 8814.2 | digits |
| Barometric Pressures | $S_0$ | 98.56 | kPa |
| | $S_1$ | 98.56 | kPa |
| Temperatures | $T_0$ | 27.6 | °C |
| | $T_1$ | 27.6 | °C |
| Calibration Factc | G | -0.1792 | kPa/digit |
| Polynomial Gage Factors | A | -4.525E-07 | |
| | B | -0.1729 | |
| | C | 1559.1 | |
| Thermal Factor | K | 0.03435 | kPa/°C |
| | | | |
| Calculated Pressure | | | |
| Linear | 0.0 | kPa | |
| Polynomial | 0.0 | kPa | |

**Table A-12: Chambers County T4 - Serial Number 1518130**

| Pressure | | | |
|---|---|---|---|
| Initial Reading | $R_0$ | 8784 | digits |
| Current Reading | $R_1$ | 8784 | digits |
| Barometric Pressures | $S_0$ | 14.2950 | psi |
| | $S_1$ | 14.2950 | psi |
| Temperatures | $T_0$ | 27.2 | °C |
| | $T_1$ | 27.2 | °C |
| Calibration Factc | G | -0.02613 | psi/digit |
| Polynomial Gage Factors | A | -6.905E-08 | |
| | B | -0.02518 | |
| | C | 226.5 | |
| Thermal Factor | K | 0.002983 | psi/°C |
| | | | |
| Calculated Pressure | | | |
| Linear | 0.0 | psf | |
| Polynomial | 0.0 | psf | |

| Pressure | | | |
|---|---|---|---|
| Initial Reading | $R_0$ | 8784 | digits |
| Current Reading | $R_1$ | 8784 | digits |
| Barometric Pressures | $S_0$ | 98.56 | kPa |
| | $S_1$ | 98.56 | kPa |
| Temperatures | $T_0$ | 27.2 | °C |
| | $T_1$ | 27.2 | °C |
| Calibration Factc | G | -0.1802 | kPa/digit |
| Polynomial Gage Factors | A | -4.761E-07 | |
| | B | -0.1736 | |
| | C | 1561.6 | |
| Thermal Factor | K | 0.02056 | kPa/°C |
| | | | |
| Calculated Pressure | | | |
| Linear | 0.0 | kPa | |
| Polynomial | 0.0 | kPa | |

**Lee County:**

**Table A-13: Lee County B1 - Serial Number 1606017**

| Pressure | | | |
|---|---|---|---|
| Initial Reading | $R_0$ | 8832.7 | digits |
| Current Reading | $R_1$ | 8832.7 | digits |
| Barometric Pressures | $S_0$ | 14.6488 | psi |
| | $S_1$ | 14.6488 | psi |
| Temperatures | $T_0$ | 19.4 | °C |
| | $T_1$ | 19.4 | °C |
| Calibration Factc | G | -0.0243 | psi/digit |
| Polynomial Gage Factors | A | -9.2E-08 | |
| | B | -0.02306 | |
| | C | 210.8 | |
| Thermal Factor | K | 0.006612 | psi/°C |
| | | | |
| Calculated Pressure | | | |
| Linear | 0.0 | psf | |
| Polynomial | 0.0 | psf | |

| Pressure | | | |
|---|---|---|---|
| Initial Reading | $R_0$ | 8832.7 | digits |
| Current Reading | $R_1$ | 8832.7 | digits |
| Barometric Pressures | $S_0$ | 101 | kPa |
| | $S_1$ | 101 | kPa |
| Temperatures | $T_0$ | 19.4 | °C |
| | $T_1$ | 19.4 | °C |
| Calibration Factc | G | -0.1675 | kPa/digit |
| Polynomial Gage Factors | A | -6.3E-07 | |
| | B | -0.159 | |
| | C | 1453.7 | |
| Thermal Factor | K | 0.04559 | kPa/°C |
| | | | |
| Calculated Pressure | | | |
| Linear | 0.0 | kPa | |
| Polynomial | 0.0 | kPa | |

**Table A-14: Lee County M1 - Serial Number 1606020**

| Pressure | | | |
|---|---|---|---|
| Initial Reading | $R_0$ | 8915.3 | digits |
| Current Reading | $R_1$ | 8915.3 | digits |
| Barometric Pressures | $S_0$ | 14.6488 | psi |
| | $S_1$ | 14.6488 | psi |
| Temperatures | $T_0$ | 22.9 | °C |
| | $T_1$ | 22.9 | °C |
| Calibration Factc | G | -0.02498 | psi/digit |
| Polynomial Gage Factors | A | -7.83E-08 | |
| | B | -0.02389 | |
| | C | 219.2 | |
| Thermal Factor | K | 0.004579 | psi/°C |
| | | | |
| Calculated Pressure | | | |
| Linear | 0.0 | psf | |
| Polynomial | 0.0 | psf | |

| Pressure | | | |
|---|---|---|---|
| Initial Reading | $R_0$ | 8915.3 | digits |
| Current Reading | $R_1$ | 8915.3 | digits |
| Barometric Pressures | $S_0$ | 101 | kPa |
| | $S_1$ | 101 | kPa |
| Temperatures | $T_0$ | 22.9 | °C |
| | $T_1$ | 22.9 | °C |
| Calibration Factc | G | -0.1722 | kPa/digit |
| Polynomial Gage Factors | A | -5.4E-07 | |
| | B | -0.1647 | |
| | C | 1511.3 | |
| Thermal Factor | K | 0.03157 | kPa/°C |
| | | | |
| Calculated Pressure | | | |
| Linear | 0.0 | kPa | |
| Polynomial | 0.0 | kPa | |

**Table A-15: Lee County T1 - Serial Number 1606015**

| Pressure | | | |
|---|---|---|---|
| Initial Reading | $R_0$ | 8786.4 | digits |
| Current Reading | $R_1$ | 8786.4 | digits |
| Barometric Pressures | $S_0$ | 14.6488 | psi |
| | $S_1$ | 14.6488 | psi |
| Temperatures | $T_0$ | 23.9 | °C |
| | $T_1$ | 23.9 | °C |
| Calibration Factc | G | -0.02406 | psi/digit |
| Polynomial Gage Factors | A | -8.78E-08 | |
| | B | -0.02288 | |
| | C | 207.8 | |
| Thermal Factor | K | -0.000325 | psi/°C |
| | | | |
| Calculated Pressure | | | |
| Linear | 0.0 | psf | |
| Polynomial | 0.0 | psf | |

| Pressure | | | |
|---|---|---|---|
| Initial Reading | $R_0$ | 8786.4 | digits |
| Current Reading | $R_1$ | 8786.4 | digits |
| Barometric Pressures | $S_0$ | 101 | kPa |
| | $S_1$ | 101 | kPa |
| Temperatures | $T_0$ | 23.9 | °C |
| | $T_1$ | 23.9 | °C |
| Calibration Factc | G | -0.1659 | kPa/digit |
| Polynomial Gage Factors | A | -6.05E-07 | |
| | B | -0.1577 | |
| | C | 1432.3 | |
| Thermal Factor | K | -0.002242 | kPa/°C |
| | | | |
| Calculated Pressure | | | |
| Linear | 0.0 | kPa | |
| Polynomial | 0.0 | kPa | |

**Table A-16: Lee County B2 - Serial Number 1606022**

| Pressure | | | |
|---|---|---|---|
| Initial Reading | $R_0$ | 8871 | digits |
| Current Reading | $R_1$ | 8871 | digits |
| Barometric Pressures | $S_0$ | 14.6488 | psi |
| | $S_1$ | 14.6488 | psi |
| Temperatures | $T_0$ | 21.6 | °C |
| | $T_1$ | 21.6 | °C |
| Calibration Factc | G | -0.02615 | psi/digit |
| Polynomial Gage Factors | A | -5.674E-08 | |
| | B | -0.02536 | |
| | C | 229.4 | |
| Thermal Factor | K | 0.004504 | psi/°C |
| | | | |
| Calculated Pressure | | | |
| Linear | 0.0 | psf | |
| Polynomial | 0.0 | psf | |

| Pressure | | | |
|---|---|---|---|
| Initial Reading | $R_0$ | 8871 | digits |
| Current Reading | $R_1$ | 8871 | digits |
| Barometric Pressures | $S_0$ | 101 | kPa |
| | $S_1$ | 101 | kPa |
| Temperatures | $T_0$ | 21.6 | °C |
| | $T_1$ | 21.6 | °C |
| Calibration Factc | G | -0.1803 | kPa/digit |
| Polynomial Gage Factors | A | -3.912E-07 | |
| | B | -0.1749 | |
| | C | 1582.3 | |
| Thermal Factor | K | 0.03105 | kPa/°C |
| | | | |
| Calculated Pressure | | | |
| Linear | 0.0 | kPa | |
| Polynomial | 0.0 | kPa | |

**Table A-17: Lee County M2 - Serial Number 1606023**

| Pressure | | | |
|---|---|---|---|
| Initial Reading | $R_0$ | 8830.5 | digits |
| Current Reading | $R_1$ | 8830.5 | digits |
| Barometric Pressures | $S_0$ | 14.6488 | psi |
| | $S_1$ | 14.6488 | psi |
| Temperatures | $T_0$ | 22.9 | °C |
| | $T_1$ | 22.9 | °C |
| Calibration Factc | G | -0.02484 | psi/digit |
| Polynomial Gage Factors | A | 7.902E-08 | |
| | B | -0.1638 | |
| | C | 1440.3 | |
| Thermal Factor | K | 0.008322 | psi/°C |
| | | | |
| Calculated Pressure | | | |
| Linear | 0.0 | psf | |
| Polynomial | 0.0 | psf | |

| Pressure | | | |
|---|---|---|---|
| Initial Reading | $R_0$ | 8830.5 | digits |
| Current Reading | $R_1$ | 8830.5 | digits |
| Barometric Pressures | $S_0$ | 101 | kPa |
| | $S_1$ | 101 | kPa |
| Temperatures | $T_0$ | 22.9 | °C |
| | $T_1$ | 22.9 | °C |
| Calibration Factc | G | -0.1713 | kPa/digit |
| Polynomial Gage Factors | A | -5.449E-07 | |
| | B | -0.1638 | |
| | C | 1488.9 | |
| Thermal Factor | K | 0.05738 | kPa/°C |
| | | | |
| Calculated Pressure | | | |
| Linear | 0.0 | kPa | |
| Polynomial | 0.0 | kPa | |

**Table A-18: Lee County T2 - Serial Number 1606024**

| Pressure | | | |
|---|---|---|---|
| Initial Reading | $R_0$ | 8748.3 | digits |
| Current Reading | $R_1$ | 8748.3 | digits |
| Barometric Pressures | $S_0$ | 14.6488 | psi |
| | $S_1$ | 14.6488 | psi |
| Temperatures | $T_0$ | 23.3 | °C |
| | $T_1$ | 23.3 | °C |
| Calibration Factc | G | -0.02383 | psi/digit |
| Polynomial Gage Factors | A | -5.648E-08 | |
| | B | -0.02308 | |
| | C | 206.2 | |
| Thermal Factor | K | 0.0009396 | psi/°C |
| | | | |
| Calculated Pressure | | | |
| Linear | 0.0 | psf | |
| Polynomial | 0.0 | psf | |

| Pressure | | | |
|---|---|---|---|
| Initial Reading | $R_0$ | 8748.3 | digits |
| Current Reading | $R_1$ | 8748.3 | digits |
| Barometric Pressures | $S_0$ | 101 | kPa |
| | $S_1$ | 101 | kPa |
| Temperatures | $T_0$ | 23.3 | °C |
| | $T_1$ | 23.3 | °C |
| Calibration Factc | G | -0.1643 | kPa/digit |
| Polynomial Gage Factors | A | -3.894E-07 | |
| | B | -0.1591 | |
| | C | 1421.7 | |
| Thermal Factor | K | 0.006479 | kPa/°C |
| | | | |
| Calculated Pressure | | | |
| Linear | 0.0 | kPa | |
| Polynomial | 0.0 | kPa | |

**Table A-19: Lee County B3 - Serial Number 1606016**

| Pressure | | | |
|---|---|---|---|
| Initial Reading | R0 | 8727.6 | digits |
| Current Reading | R1 | 8727.6 | digits |
| Barometric | S0 | 14.6488 | psi |
| Pressures | S1 | 14.6488 | psi |
| Temperatures | T0 | 8.6 | °C |
| | T1 | 8.6 | °C |
| Calibration Factc | G | -0.02548 | psi/digit |
| Polynomial Gage Factors | A | -9.248E-08 | |
| | B | -0.02422 | |
| | C | 218.4 | |
| Thermal Factor | K | 0.0116 | psi/°C |
| | | | |
| Calculated Pressure | | | |
| Linear | 0.0 | psf | |
| Polynomial | 0.0 | psf | |

| Pressure | | | |
|---|---|---|---|
| Initial Reading | R0 | 8727.6 | digits |
| Current Reading | R1 | 8727.6 | digits |
| Barometric | S0 | 101 | kPa |
| Pressures | S1 | 101 | kPa |
| Temperatures | T0 | 8.6 | °C |
| | T1 | 8.6 | °C |
| Calibration Factc | G | -0.1757 | kPa/digit |
| Polynomial Gage Factors | A | -6.376E-07 | |
| | B | -0.167 | |
| | C | 1506.1 | |
| Thermal Factor | K | 0.08001 | kPa/°C |
| | | | |
| Calculated Pressure | | | |
| Linear | 0.0 | kPa | |
| Polynomial | 0.0 | kPa | |

**Table A-20: Lee County M3 - Serial Number 1606021**

| Pressure | | | |
|---|---|---|---|
| Initial Reading | $R_0$ | 8743 | digits |
| Current Reading | $R_1$ | 8743 | digits |
| Barometric Pressures | $S_0$ | 14.6488 | psi |
| | $S_1$ | 14.6488 | psi |
| Temperatures | $T_0$ | 9.5 | °C |
| | $T_1$ | 9.5 | °C |
| Calibration Factc | G | -0.02425 | psi/digit |
| Polynomial Gage Factors | A | -7.316E-08 | |
| | B | -0.02327 | |
| | C | 209.0 | |
| Thermal Factor | K | 0.004511 | psi/°C |
| | | | |
| Calculated Pressure | | | |
| Linear | 0.0 | psf | |
| Polynomial | 0.0 | psf | |

| Pressure | | | |
|---|---|---|---|
| Initial Reading | $R_0$ | 8743 | digits |
| Current Reading | $R_1$ | 8743 | digits |
| Barometric Pressures | $S_0$ | 101 | kPa |
| | $S_1$ | 101 | kPa |
| Temperatures | $T_0$ | 9.5 | °C |
| | $T_1$ | 9.5 | °C |
| Calibration Factc | G | -0.1672 | kPa/digit |
| Polynomial Gage Factors | A | -5.044E-07 | |
| | B | -0.1604 | |
| | C | 1440.9 | |
| Thermal Factor | K | 0.0311 | kPa/°C |
| | | | |
| Calculated Pressure | | | |
| Linear | 0.0 | kPa | |
| Polynomial | 0.0 | kPa | |

**Table A-21: Lee County T3 - Serial Number 1606019**

| Pressure | | | |
|---|---|---|---|
| Initial Reading | $R_0$ | 9028.3 | digits |
| Current Reading | $R_1$ | 9028.3 | digits |
| Barometric Pressures | $S_0$ | 14.6488 | psi |
| | $S_1$ | 14.6488 | psi |
| Temperatures | $T_0$ | 10.8 | °C |
| | $T_1$ | 10.8 | °C |
| Calibration Factc | G | -0.02458 | psi/digit |
| Polynomial Gage Factors | A | -6.817E-08 | |
| | B | -0.02362 | |
| | C | 218.8 | |
| Thermal Factor | K | 0.002428 | psi/°C |
| | | | |
| Calculated Pressure | | | |
| Linear | 0.0 | psf | |
| Polynomial | 0.0 | psf | |

| Pressure | | | |
|---|---|---|---|
| Initial Reading | $R_0$ | 9028.3 | digits |
| Current Reading | $R_1$ | 9028.3 | digits |
| Barometric Pressures | $S_0$ | 101 | kPa |
| | $S_1$ | 101 | kPa |
| Temperatures | $T_0$ | 10.8 | °C |
| | $T_1$ | 10.8 | °C |
| Calibration Factc | G | -0.1695 | kPa/digit |
| Polynomial Gage Factors | A | -0.00000047 | |
| | B | -0.1629 | |
| | C | 1509.0 | |
| Thermal Factor | K | 0.01674 | kPa/°C |
| | | | |
| Calculated Pressure | | | |
| Linear | 0.0 | kPa | |
| Polynomial | 0.0 | kPa | |

**Table A-22: Lee County B4 - Serial Number 1606018**

| Pressure | | | |
|---|---|---|---|
| Initial Reading | $R_0$ | 8887 | digits |
| Current Reading | $R_1$ | 8887 | digits |
| Barometric Pressures | $S_0$ | 14.6488 | psi |
| | $S_1$ | 14.6488 | psi |
| Temperatures | $T_0$ | 9 | °C |
| | $T_1$ | 9 | °C |
| Calibration Factc | G | -0.02539 | psi/digit |
| Polynomial Gage Factors | A | -3.909E-08 | |
| | B | -0.02485 | |
| | C | 223.9 | |
| Thermal Factor | K | 0.00188 | psi/°C |
| | | | |
| Calculated Pressure | | | |
| Linear | 0.0 | psf | |
| Polynomial | 0.0 | psf | |

| Pressure | | | |
|---|---|---|---|
| Initial Reading | $R_0$ | 8887 | digits |
| Current Reading | $R_1$ | 8887 | digits |
| Barometric Pressures | $S_0$ | 101 | kPa |
| | $S_1$ | 101 | kPa |
| Temperatures | $T_0$ | 9 | °C |
| | $T_1$ | 9 | °C |
| Calibration Factc | G | -0.1751 | kPa/digit |
| Polynomial Gage Factors | A | -2.695E-07 | |
| | B | -0.1713 | |
| | C | 1543.6 | |
| Thermal Factor | K | 0.01296 | kPa/°C |
| | | | |
| Calculated Pressure | | | |
| Linear | 0.0 | kPa | |
| Polynomial | 0.0 | kPa | |

**Table A-23: Lee County M4 - Serial Number 1606026**

| Pressure | | | |
|---|---|---|---|
| Initial Reading | $R_0$ | 8825 | digits |
| Current Reading | $R_1$ | 8825 | digits |
| Barometric Pressures | $S_0$ | 14.6488 | psi |
| | $S_1$ | 14.6488 | psi |
| Temperatures | $T_0$ | 12.3 | °C |
| | $T_1$ | 12.3 | °C |
| Calibration Factc | G | -0.02511 | psi/digit |
| Polynomial Gage Factors | A | -4.358E-08 | |
| | B | -0.02451 | |
| | C | 219.7 | |
| Thermal Factor | K | 0.009275 | psi/°C |
| | | | |
| Calculated Pressure | | | |
| Linear | 0.0 | psf | |
| Polynomial | 0.0 | psf | |

| Pressure | | | |
|---|---|---|---|
| Initial Reading | $R_0$ | 8825 | digits |
| Current Reading | $R_1$ | 8825 | digits |
| Barometric Pressures | $S_0$ | 101 | kPa |
| | $S_1$ | 101 | kPa |
| Temperatures | $T_0$ | 12.3 | °C |
| | $T_1$ | 12.3 | °C |
| Calibration Factc | G | -0.1731 | kPa/digit |
| Polynomial Gage Factors | A | -3.005E-07 | |
| | B | -0.169 | |
| | C | 1514.8 | |
| Thermal Factor | K | 0.06395 | kPa/°C |
| | | | |
| Calculated Pressure | | | |
| Linear | 0.0 | kPa | |
| Polynomial | 0.0 | kPa | |

**Table A-24: Lee County T4 - Serial Number 1606025**

| Pressure | | | |
|---|---|---|---|
| Initial Reading | $R_0$ | 8801.3 | digits |
| Current Reading | $R_1$ | 8801.3 | digits |
| Barometric Pressures | $S_0$ | 14.6488 | psi |
| | $S_1$ | 14.6488 | psi |
| Temperatures | $T_0$ | 14.3 | °C |
| | $T_1$ | 14.3 | °C |
| Calibration Factc | G | -0.02455 | psi/digit |
| Polynomial Gage Factors | A | -8.718E-08 | |
| | B | -0.02336 | |
| | C | 212.4 | |
| Thermal Factor | K | 0.006904 | psi/°C |
| | | | |
| Calculated Pressure | | | |
| Linear | 0.0 | psf | |
| Polynomial | 0.0 | psf | |

| Pressure | | | |
|---|---|---|---|
| Initial Reading | $R_0$ | 8801.3 | digits |
| Current Reading | $R_1$ | 8801.3 | digits |
| Barometric Pressures | $S_0$ | 101 | kPa |
| | $S_1$ | 101 | kPa |
| Temperatures | $T_0$ | 14.3 | °C |
| | $T_1$ | 14.3 | °C |
| Calibration Factc | G | -0.1693 | kPa/digit |
| Polynomial Gage Factors | A | -6.011E-07 | |
| | B | -0.1611 | |
| | C | 1464.5 | |
| Thermal Factor | K | 0.0476 | kPa/°C |
| | | | |
| Calculated Pressure | | | |
| Linear | 0.0 | kPa | |
| Polynomial | 0.0 | kPa | |

**Coosa County:**

**Table A-25: Coosa County B1 - Serial Number 1606031**

| Pressure | | | |
|---|---|---|---|
| Initial Reading | $R_0$ | 8828.2 | digits |
| Current Reading | $R_1$ | 8828.2 | digits |
| Barometric Pressures | $S_0$ | 14.6488 | psi |
| | $S_1$ | 14.6488 | psi |
| Temperatures | $T_0$ | 23.3 | °C |
| | $T_1$ | 23.3 | °C |
| Calibration Factc | G | -0.02495 | psi/digit |
| Polynomial Gage Factors | A | -7.94E-08 | |
| | B | -0.02386 | |
| | C | 216.8 | |
| Thermal Factor | K | 0.007894 | psi/°C |
| | | | |
| Calculated Pressure | | | |
| Linear | 0.0 | psf | |
| Polynomial | 0.0 | psf | |

| Pressure | | | |
|---|---|---|---|
| Initial Reading | $R_0$ | 8828.2 | digits |
| Current Reading | $R_1$ | 8828.2 | digits |
| Barometric Pressures | $S_0$ | 101 | kPa |
| | $S_1$ | 101 | kPa |
| Temperatures | $T_0$ | 23.3 | °C |
| | $T_1$ | 23.3 | °C |
| Calibration Factc | G | -0.172 | kPa/digit |
| Polynomial Gage Factors | A | -5.48E-07 | |
| | B | -0.1645 | |
| | C | 1494.9 | |
| Thermal Factor | K | 0.05443 | kPa/°C |
| | | | |
| Calculated Pressure | | | |
| Linear | 0.0 | kPa | |
| Polynomial | 0.0 | kPa | |

**Table A-26: Coosa County M1 - Serial Number 1606032**

| Pressure | | | |
|---|---|---|---|
| Initial Reading | $R_0$ | 9012.9 | digits |
| Current Reading | $R_1$ | 9012.9 | digits |
| Barometric Pressures | $S_0$ | 14.6488 | psi |
| | $S_1$ | 14.6488 | psi |
| Temperatures | $T_0$ | 20 | °C |
| | $T_1$ | 20 | °C |
| Calibration Factc | G | -0.02547 | psi/digit |
| Polynomial Gage Factors | A | -8.24E-08 | |
| | B | -0.02431 | |
| | C | 225.8 | |
| Thermal Factor | K | 0.00363 | psi/°C |
| | | | |
| Calculated Pressure | | | |
| Linear | 0.0 | psf | |
| Polynomial | 0.0 | psf | |

| Pressure | | | |
|---|---|---|---|
| Initial Reading | $R_0$ | 9012.9 | digits |
| Current Reading | $R_1$ | 9012.9 | digits |
| Barometric Pressures | $S_0$ | 101 | kPa |
| | $S_1$ | 101 | kPa |
| Temperatures | $T_0$ | 20 | °C |
| | $T_1$ | 20 | °C |
| Calibration Factc | G | -0.1756 | kPa/digit |
| Polynomial Gage Factors | A | -5.68E-07 | |
| | B | -0.1676 | |
| | C | 1556.7 | |
| Thermal Factor | K | 0.02503 | kPa/°C |
| | | | |
| Calculated Pressure | | | |
| Linear | 0.0 | kPa | |
| Polynomial | 0.0 | kPa | |

**Table A-27: Coosa County T1 - Serial Number 1606036**

| Pressure | | | |
|---|---|---|---|
| Initial Reading | $R_0$ | 8817.6 | digits |
| Current Reading | $R_1$ | 8817.6 | digits |
| Barometric Pressures | $S_0$ | 14.6488 | psi |
| | $S_1$ | 14.6488 | psi |
| Temperatures | $T_0$ | 21 | °C |
| | $T_1$ | 21 | °C |
| Calibration Factc | G | -0.02581 | psi/digit |
| Polynomial Gage Factors | A | -1.03E-07 | |
| | B | -0.02439 | |
| | C | 223.0 | |
| Thermal Factor | K | 0.01494 | psi/°C |
| | | | |
| Calculated Pressure | | | |
| Linear | 0.0 | psf | |
| Polynomial | 0.0 | psf | |

| Pressure | | | |
|---|---|---|---|
| Initial Reading | $R_0$ | 8817.6 | digits |
| Current Reading | $R_1$ | 8817.6 | digits |
| Barometric Pressures | $S_0$ | 101 | kPa |
| | $S_1$ | 101 | kPa |
| Temperatures | $T_0$ | 21 | °C |
| | $T_1$ | 21 | °C |
| Calibration Factc | G | -0.1779 | kPa/digit |
| Polynomial Gage Factors | A | -7.07E-07 | |
| | B | -0.1682 | |
| | C | 1538.1 | |
| Thermal Factor | K | 0.103 | kPa/°C |
| | | | |
| Calculated Pressure | | | |
| Linear | 0.0 | kPa | |
| Polynomial | 0.0 | kPa | |

**Table A-28: Coosa County B2 - Serial Number 1607328**

| Pressure | | | |
|---|---|---|---|
| Initial Reading | $R_0$ | 8663.2 | digits |
| Current Reading | $R_1$ | 8663.2 | digits |
| Barometric Pressures | $S_0$ | 14.6488 | psi |
| | $S_1$ | 14.6488 | psi |
| Temperatures | $T_0$ | 25.6 | °C |
| | $T_1$ | 25.6 | °C |
| Calibration Factc | G | -0.02536 | psi/digit |
| Polynomial Gage Factors | A | -7.293E-08 | |
| | B | -0.02437 | |
| | C | 216.6 | |
| Thermal Factor | K | 0.003047 | psi/°C |
| | | | |
| Calculated Pressure | | | |
| Linear | 0.0 | psf | |
| Polynomial | 0.0 | psf | |

| Pressure | | | |
|---|---|---|---|
| Initial Reading | $R_0$ | 8663.2 | digits |
| Current Reading | $R_1$ | 8663.2 | digits |
| Barometric Pressures | $S_0$ | 101 | kPa |
| | $S_1$ | 101 | kPa |
| Temperatures | $T_0$ | 25.6 | °C |
| | $T_1$ | 25.6 | °C |
| Calibration Factc | G | -0.1748 | kPa/digit |
| Polynomial Gage Factors | A | -5.028E-07 | |
| | B | -0.168 | |
| | C | 1493.2 | |
| Thermal Factor | K | 0.02101 | kPa/°C |
| | | | |
| Calculated Pressure | | | |
| Linear | 0.0 | kPa | |
| Polynomial | 0.0 | kPa | |

**Table A-29: Coosa County M2 - Serial Number 1606035**

| Pressure | | | |
|---|---|---|---|
| Initial Reading | $R_0$ | 8707.5 | digits |
| Current Reading | $R_1$ | 8707.5 | digits |
| Barometric Pressures | $S_0$ | 14.6488 | psi |
| | $S_1$ | 14.6488 | psi |
| Temperatures | $T_0$ | 28 | °C |
| | $T_1$ | 28 | °C |
| Calibration Factc | G | -0.02649 | psi/digit |
| Polynomial Gage Factors | A | -8.114E-08 | |
| | B | -0.02536 | |
| | C | 227.0 | |
| Thermal Factor | K | 0.002548 | psi/°C |
| | | | |
| Calculated Pressure | | | |
| Linear | 0.0 | psf | |
| Polynomial | 0.0 | psf | |

| Pressure | | | |
|---|---|---|---|
| Initial Reading | $R_0$ | 8707.5 | digits |
| Current Reading | $R_1$ | 8707.5 | digits |
| Barometric Pressures | $S_0$ | 101 | kPa |
| | $S_1$ | 101 | kPa |
| Temperatures | $T_0$ | 28 | °C |
| | $T_1$ | 28 | °C |
| Calibration Factc | G | -0.1827 | kPa/digit |
| Polynomial Gage Factors | A | -5.594E-07 | |
| | B | -0.1748 | |
| | C | 1564.5 | |
| Thermal Factor | K | 0.01757 | kPa/°C |
| | | | |
| Calculated Pressure | | | |
| Linear | 0.0 | kPa | |
| Polynomial | 0.0 | kPa | |

**Table A-30: Coosa County T2 - Serial Number 1606034**

| Pressure | | | |
|---|---|---|---|
| Initial Reading | $R_0$ | 8828.2 | digits |
| Current Reading | $R_1$ | 8828.2 | digits |
| Barometric Pressures | $S_0$ | 14.6488 | psi |
| | $S_1$ | 14.6488 | psi |
| Temperatures | $T_0$ | 27.2 | °C |
| | $T_1$ | 27.2 | °C |
| Calibration Factc | G | -0.02545 | psi/digit |
| Polynomial Gage Factors | A | -8.294E-08 | |
| | B | -0.02431 | |
| | C | 221.1 | |
| Thermal Factor | K | 0.005792 | psi/°C |
| | | | |
| Calculated Pressure | | | |
| Linear | 0.0 | psf | |
| Polynomial | 0.0 | psf | |

| Pressure | | | |
|---|---|---|---|
| Initial Reading | $R_0$ | 8828.2 | digits |
| Current Reading | $R_1$ | 8828.2 | digits |
| Barometric Pressures | $S_0$ | 101 | kPa |
| | $S_1$ | 101 | kPa |
| Temperatures | $T_0$ | 27.2 | °C |
| | $T_1$ | 27.2 | °C |
| Calibration Factc | G | -0.1755 | kPa/digit |
| Polynomial Gage Factors | A | -5.719E-07 | |
| | B | -0.1676 | |
| | C | 1524.2 | |
| Thermal Factor | K | 0.03993 | kPa/°C |
| | | | |
| Calculated Pressure | | | |
| Linear | 0.0 | kPa | |
| Polynomial | 0.0 | kPa | |

## Raw Measurements

## Chambers County

### Table A-31: Chambers County Raw Measurements B1

| | | | Linear | | Polynomial | |
|---|---|---|---|---|---|---|
| Date | $R_1$ | $T_1$ | psf | kPa | psf | kPa |
| 6/29/15 9:52 AM | 8899.5 | 22.8 | -13.4 | -0.6 | -13.5 | -0.6 |
| 6/30/15 12:15 PM | 8911.3 | 25.5 | -54.2 | -2.6 | -54.7 | -2.6 |
| 6/30/15 2:34 PM | 8847.0 | 32.1 | 172.4 | 8.3 | 174.1 | 8.3 |
| 6/30/15 3:02 PM | 8845.6 | 32.1 | 177.3 | 8.5 | 179.0 | 8.6 |
| 6/30/15 3:30 PM | 8841.1 | 32.1 | 193.0 | 9.2 | 195.0 | 9.3 |
| 6/30/15 4:02 PM | 8845.6 | 32.2 | 177.3 | 8.5 | 179.1 | 8.6 |
| 7/1/15 8:01 AM | 8835.9 | 40.1 | 212.8 | 10.2 | 214.9 | 10.3 |
| 7/1/15 9:11 AM | 8896.5 | 37.6 | 0.0 | 0.0 | 0.0 | 0.0 |
| 7/1/15 10:03 AM | 8902.3 | 35.3 | -20.8 | -1.0 | -21.0 | -1.0 |
| 7/6/15 11:49 AM | 8897.7 | 23.3 | -7.0 | -0.3 | -7.0 | -0.3 |
| 7/6/15 5:17 PM | 8865.7 | 24.9 | 105.5 | 5.1 | 106.5 | 5.1 |
| 7/9/15 1:14 PM | 8863.4 | 27.2 | 114.0 | 5.5 | 115.1 | 5.5 |
| 7/14/15 5:57 AM | 8865.0 | 26.0 | 108.1 | 5.2 | 109.2 | 5.2 |
| 7/21/15 10:39 AM | 8886.9 | 27.1 | 31.6 | 1.5 | 31.9 | 1.5 |
| 7/28/15 8:45 AM | 8899.2 | 25.9 | -11.7 | -0.6 | -11.8 | -0.6 |
| 8/5/15 12:02 PM | 8891.7 | 25.6 | 14.5 | 0.7 | 14.7 | 0.7 |
| 8/13/15 6:14 AM | 8902.8 | 24.2 | -24.7 | -1.2 | -24.9 | -1.2 |
| 8/24/15 12:42 PM | 8892.5 | 24.5 | 11.5 | 0.6 | 11.6 | 0.6 |
| 9/1/15 9:42 AM | 8913.9 | 22.2 | -63.9 | -3.1 | -64.5 | -3.1 |
| 9/15/15 8:45 AM | 8913.1 | 17.5 | -62.0 | -3.0 | -62.6 | -3.0 |
| 10/20/15 10:40 AM | 8914.9 | 10.4 | -69.7 | -3.3 | -70.4 | -3.4 |
| 1/12/16 2:46 PM | 8774.1 | 6.0 | 422.7 | 20.2 | 427.0 | 20.4 |
| 3/31/16 12:40 PM | 8695.5 | 15.0 | 699.9 | 33.5 | 706.6 | 33.8 |
| 4/19/16 1:06 PM | 8660.3 | 14.8 | 823.1 | 39.4 | 831.0 | 39.8 |
| 6/15/16 9:05 AM | 8701.0 | 23.5 | 682.2 | 32.7 | 688.8 | 33.0 |
| 9/13/16 12:00 PM | 8890.6 | 23.5 | 18.0 | 0.9 | 18.2 | 0.9 |
| 11/17/16 9:00 AM | 8923.8 | 10.7 | -100.8 | -4.8 | -101.8 | -4.9 |

**Table A-32: Chambers County Raw Measurements M1**

| | | | Linear | | Polynomial | |
|---|---|---|---|---|---|---|
| Date | $R_1$ | $T_1$ | psf | kPa | psf | kPa |
| 6/29/15 9:52 AM | 8886.7 | 23.1 | -28.1 | -1.3 | -28.3 | -1.4 |
| 6/30/15 12:15 PM | 8895.3 | 27.2 | -56.5 | -2.7 | -57.1 | -2.7 |
| 6/30/15 2:34 PM | 8886.2 | 32.2 | -19.6 | -0.9 | -19.8 | -0.9 |
| 6/30/15 3:02 PM | 8895.2 | 32.2 | -52.5 | -2.5 | -53.1 | -2.5 |
| 6/30/15 3:30 PM | 8903.8 | 32.4 | -83.7 | -4.0 | -84.7 | -4.1 |
| 6/30/15 4:02 PM | 8904.8 | 32.6 | -87.2 | -4.2 | -88.2 | -4.2 |
| 7/1/15 8:01 AM | 8879.0 | 41.6 | 13.5 | 0.6 | 13.6 | 0.7 |
| 7/1/15 9:11 AM | 8882.1 | 38.6 | 0.0 | 0.0 | 0.0 | 0.0 |
| 7/1/15 10:03 AM | 8890.0 | 36.5 | -30.4 | -1.5 | -30.7 | -1.5 |
| 7/6/15 11:49 AM | 8897.7 | 23.2 | -68.1 | -3.3 | -68.8 | -3.3 |
| 7/6/15 5:17 PM | 8862.8 | 25.2 | 60.6 | 2.9 | 61.5 | 2.9 |
| 7/9/15 1:14 PM | 8869.4 | 28.4 | 38.9 | 1.9 | 39.5 | 1.9 |
| 7/14/15 5:57 AM | 8858.8 | 27.0 | 76.5 | 3.7 | 77.6 | 3.7 |
| 7/21/15 10:39 AM | 8880.1 | 28.2 | -0.3 | 0.0 | -0.2 | 0.0 |
| 7/28/15 8:45 AM | 8893.8 | 26.9 | -51.2 | -2.5 | -51.7 | -2.5 |
| 8/5/15 12:02 PM | 8901.3 | 26.8 | -78.6 | -3.8 | -79.5 | -3.8 |
| 8/13/15 6:14 AM | 8896.5 | 25.0 | -62.4 | -3.0 | -63.1 | -3.0 |
| 8/24/15 12:42 PM | 8903.8 | 26.1 | -88.3 | -4.2 | -89.3 | -4.3 |
| 9/1/15 9:42 AM | 8899.5 | 22.5 | -75.2 | -3.6 | -76.0 | -3.6 |
| 9/15/15 8:45 AM | 8913.1 | 17.5 | -128.4 | -6.1 | -129.9 | -6.2 |
| 10/20/15 10:40 AM | 8898.8 | 9.6 | -82.0 | -3.9 | -82.8 | -4.0 |
| 1/12/16 2:46 PM | 8804.0 | 4.3 | 259.9 | 12.4 | 263.4 | 12.6 |
| 3/31/16 12:40 PM | 8795.5 | 16.1 | 299.5 | 14.3 | 303.4 | 14.5 |
| 4/19/16 1:06 PM | 8748.5 | 15.9 | 470.8 | 22.5 | 476.7 | 22.8 |
| 6/15/16 9:05 AM | 8798.6 | 25.6 | 295.1 | 14.1 | 298.8 | 14.3 |
| 9/13/16 12:00 PM | 8901.5 | 24.5 | -81.0 | -3.9 | -81.9 | -3.9 |
| 11/17/16 9:00 AM | 8907.3 | 8.9 | -113.6 | -5.4 | -114.7 | -5.5 |

**Table A-33: Chambers County Raw Measurements T1**

| | | | Linear | | Polynomial | |
|---|---|---|---|---|---|---|
| Date | $R_1$ | $T_1$ | psf | kPa | psf | kPa |
| 6/29/15 | 8780.4 | 23.9 | -153.3 | -7.3 | -155.5 | -7.4 |
| 6/30/15 | 8671.2 | 26.9 | 230.9 | 11.1 | 234.4 | 11.2 |
| 6/30/15 | 8643.0 | 32.0 | 333.2 | 16.0 | 338.1 | 16.2 |
| 6/30/15 | 8640.0 | 32.0 | 343.7 | 16.5 | 348.7 | 16.7 |
| 6/30/15 | 8637.4 | 32.0 | 352.8 | 16.9 | 358.0 | 17.1 |
| 6/30/15 | 8641.8 | 32.2 | 337.5 | 16.2 | 342.5 | 16.4 |
| 7/1/15 | 8668.5 | 39.5 | 249.2 | 11.9 | 252.8 | 12.1 |
| 7/1/15 | 8739.2 | 36.9 | 0.0 | 0.0 | 0.0 | 0.0 |
| 7/1/15 | 8744.7 | 35.0 | -20.6 | -1.0 | -20.9 | -1.0 |
| 7/6/15 | 8757.0 | 23.1 | -72.0 | -3.4 | -72.9 | -3.5 |
| 7/6/15 | 8741.9 | 25.2 | -17.6 | -0.8 | -17.8 | -0.9 |
| 7/9/15 | 8744.3 | 28.4 | -23.8 | -1.1 | -24.1 | -1.2 |
| 7/14/15 | 8747.5 | 26.8 | -36.1 | -1.7 | -36.6 | -1.8 |
| 7/21/15 | 8732.1 | 28.1 | 18.7 | 0.9 | 19.0 | 0.9 |
| 7/28/15 | 8737.3 | 26.8 | -0.4 | 0.0 | -0.3 | 0.0 |
| 8/5/15 | 8748.5 | 26.7 | -39.7 | -1.9 | -40.2 | -1.9 |
| 8/13/15 | 8746.0 | 25.0 | -32.1 | -1.5 | -32.5 | -1.6 |
| 8/24/15 | 8743.6 | 25.9 | -23.1 | -1.1 | -23.3 | -1.1 |
| 9/1/15 | 8747.6 | 22.4 | -39.6 | -1.9 | -40.0 | -1.9 |
| 9/15/15 | 8758.7 | 17.2 | -82.0 | -3.9 | -83.1 | -4.0 |
| 10/20/15 | 8749.7 | 9.5 | -55.9 | -2.7 | -56.5 | -2.7 |
| 1/12/16 | 8723.6 | 4.1 | 31.6 | 1.5 | 32.4 | 1.6 |
| 3/31/16 | 8748.6 | 16.0 | -47.5 | -2.3 | -48.0 | -2.3 |
| 4/19/16 | 8705.9 | 15.8 | 101.7 | 4.9 | 103.5 | 5.0 |
| 6/15/16 | 8730.9 | 25.5 | 21.1 | 1.0 | 21.5 | 1.0 |
| 9/13/16 | 8747.5 | 24.3 | -37.9 | -1.8 | -38.3 | -1.8 |
| 11/17/16 | 8762.7 | 8.8 | -101.9 | -4.9 | -103.1 | -4.9 |

**Table A-34: Chambers County Raw Measurements B2**

| | | | Linear | | Polynomial | |
|---|---|---|---|---|---|---|
| Date | $R_1$ | $T_1$ | psf | kPa | psf | kPa |
| 7/6/15 9:50 AM | 8804.5 | 25.3 | 57.0 | 2.7 | 57.7 | 2.8 |
| 7/6/15 11:41 AM | 8820.0 | 25.3 | 0.0 | 0.0 | 0.0 | 0.0 |
| 7/6/15 5:34 PM | 8765.7 | 26.0 | 200.0 | 9.6 | 202.5 | 9.7 |
| 7/9/15 1:21 PM | 8765.5 | 27.8 | 201.4 | 9.6 | 203.9 | 9.8 |
| 7/14/15 6:07 AM | 8767.0 | 26.5 | 195.4 | 9.4 | 197.8 | 9.5 |
| 7/21/15 10:48 AM | 8799.3 | 27.3 | 76.9 | 3.7 | 77.8 | 3.7 |
| 7/28/15 9:02 AM | 8831.2 | 26.3 | -40.8 | -2.0 | -41.4 | -2.0 |
| 8/5/15 12:10 PM | 8830.5 | 25.8 | -38.5 | -1.8 | -38.9 | -1.9 |
| 8/13/15 6:22 AM | 8832.5 | 24.5 | -46.3 | -2.2 | -46.8 | -2.2 |
| 8/24/15 12:44 PM | 8834.5 | 25.2 | -53.4 | -2.6 | -54.0 | -2.6 |
| 9/1/15 9:49 AM | 8831.7 | 22.5 | -44.1 | -2.1 | -44.6 | -2.1 |
| 9/15/15 8:53 AM | 8826.9 | 16.8 | -28.4 | -1.4 | -28.8 | -1.4 |
| 10/20/15 10:48 AM | 8829.2 | 10.4 | -39.2 | -1.9 | -39.6 | -1.9 |
| 1/12/16 2:53 AM | 8787.9 | 5.9 | 111.1 | 5.3 | 112.6 | 5.4 |
| 3/31/16 12:43 PM | 8794.2 | 15.4 | 91.4 | 4.4 | 92.5 | 4.4 |
| 4/19/16 1:08 PM | 8784.3 | 15.4 | 127.8 | 6.1 | 129.4 | 6.2 |
| 6/15/16 10:40 AM | 8802.6 | 24.0 | 63.6 | 3.0 | 64.3 | 3.1 |
| 9/13/16 12:00 PM | 8845.6 | 24.0 | -94.7 | -4.5 | -95.8 | -4.6 |
| 11/17/16 9:25 AM | 8844.7 | 10.0 | -96.4 | -4.6 | -97.5 | -4.7 |

**Table A-35: Chambers County Raw Measurements M2**

| | | | Linear | | Polynomial | |
|---|---|---|---|---|---|---|
| Date | $R_1$ | $T_1$ | psf | kPa | psf | kPa |
| 7/6/15 | 8825.0 | 23.7 | 70.2 | 3.4 | 73.2 | 3.5 |
| 7/6/15 | 8845.2 | 26.0 | 0.0 | 0.0 | 0.0 | 0.0 |
| 7/6/15 | 8813.2 | 26.5 | 117.2 | 5.6 | 121.9 | 5.8 |
| 7/9/15 | 8790.3 | 28.9 | 204.0 | 9.8 | 212.1 | 10.2 |
| 7/14/15 | 8793.6 | 26.8 | 188.9 | 9.0 | 196.6 | 9.4 |
| 7/21/15 | 8849.6 | 27.8 | -13.4 | -0.6 | -14.1 | -0.7 |
| 7/28/15 | 8847.5 | 27.4 | -6.3 | -0.3 | -6.7 | -0.3 |
| 8/5/15 | 8847.1 | 26.6 | -6.0 | -0.3 | -6.3 | -0.3 |
| 8/13/15 | 8845.8 | 25.2 | -3.3 | -0.2 | -3.4 | -0.2 |
| 8/24/15 | 8849.3 | 25.7 | -15.4 | -0.7 | -16.0 | -0.8 |
| 9/1/15 | 8844.5 | 22.7 | -2.2 | -0.1 | -2.1 | -0.1 |
| 9/15/15 | 8838.1 | 16.9 | 12.6 | 0.6 | 13.7 | 0.7 |
| 10/20/15 | 8834.5 | 8.9 | 14.1 | 0.7 | 15.7 | 0.8 |
| 1/12/16 | 8845.3 | 3.3 | -33.3 | -1.6 | -33.3 | -1.6 |
| 3/31/16 | 8862.1 | 16.4 | -75.4 | -3.6 | -78.0 | -3.7 |
| 4/19/16 | 8857.0 | 16.1 | -57.3 | -2.7 | -59.1 | -2.8 |
| 6/15/16 | 8861.3 | 25.8 | -58.9 | -2.8 | -61.3 | -2.9 |
| 9/13/16 | 8859.3 | 24.6 | -53.3 | -2.6 | -55.4 | -2.7 |
| 11/17/16 | 8851.6 | 8.2 | -49.1 | -2.4 | -50.1 | -2.4 |

**Table A-36: Chambers County Raw Measurements T2**

| | | | Linear | | Polynomial | |
|---|---|---|---|---|---|---|
| Date | $R_1$ | $T_1$ | psf | kPa | psf | kPa |
| 7/6/15 | 8780.1 | 23.8 | -46.0 | -2.2 | -46.8 | -2.2 |
| 7/6/15 | 8768.2 | 27.0 | 0.0 | 0.0 | 0.0 | 0.0 |
| 7/6/15 | 8766.6 | 25.2 | 4.5 | 0.2 | 4.6 | 0.2 |
| 7/9/15 | 8751.3 | 29.1 | 63.5 | 3.0 | 64.6 | 3.1 |
| 7/14/15 | 8758.2 | 27.0 | 36.6 | 1.8 | 37.3 | 1.8 |
| 7/21/15 | 8763.2 | 27.8 | 18.9 | 0.9 | 19.3 | 0.9 |
| 7/28/15 | 8763.4 | 27.6 | 18.0 | 0.9 | 18.4 | 0.9 |
| 8/5/15 | 8763.2 | 26.6 | 18.0 | 0.9 | 18.3 | 0.9 |
| 8/13/15 | 8763.0 | 25.2 | 17.7 | 0.8 | 18.0 | 0.9 |
| 8/24/15 | 8765.8 | 25.5 | 7.6 | 0.4 | 7.8 | 0.4 |
| 9/1/15 | 8761.7 | 22.8 | 20.6 | 1.0 | 21.0 | 1.0 |
| 9/15/15 | 8764.2 | 16.9 | 6.9 | 0.3 | 7.2 | 0.3 |
| 10/20/15 | 8766.4 | 8.9 | -7.3 | -0.3 | -7.2 | -0.3 |
| 1/12/16 | 8778.8 | 3.4 | -56.9 | -2.7 | -57.6 | -2.8 |
| 3/31/16 | 8788.5 | 16.5 | -82.4 | -3.9 | -83.7 | -4.0 |
| 4/19/16 | 8783.5 | 16.2 | -64.3 | -3.1 | -65.3 | -3.1 |
| 6/15/16 | 8785.0 | 25.9 | -62.4 | -3.0 | -63.5 | -3.0 |
| 9/13/16 | 8783.3 | 24.7 | -57.1 | -2.7 | -58.1 | -2.8 |
| 11/17/16 | 8784.8 | 8.4 | -75.1 | -3.6 | -76.2 | -3.6 |

**Table A-37: Chambers County Raw Measurements B3**

| | | | Linear | | Polynomial | |
|---|---|---|---|---|---|---|
| Date | $R_1$ | $T_1$ | psf | kPa | psf | kPa |
| 8/25/15 | 8815.0 | 25.2 | 0.0 | 0.0 | 0.0 | 0.0 |
| 9/1/15 | 8763.0 | 23.0 | 179.5 | 8.6 | 182.3 | 8.7 |
| 9/15/15 | 8765.8 | 16.2 | 161.7 | 7.7 | 164.4 | 7.9 |
| 10/20/15 | 8809.7 | 9.7 | 0.3 | 0.0 | 0.6 | 0.0 |
| 1/12/16 | 8766.6 | 10.3 | 152.0 | 7.3 | 154.6 | 7.4 |
| 3/31/16 | 8718.5 | 16.1 | 327.2 | 15.7 | 332.4 | 15.9 |
| 4/19/16 | 8731.8 | 15.6 | 280.1 | 13.4 | 284.5 | 13.6 |
| 6/15/16 | 8748.8 | 24.4 | 230.9 | 11.1 | 234.5 | 11.2 |
| 9/13/16 | 8823.2 | 25.1 | -28.8 | -1.4 | -29.3 | -1.4 |
| 11/17/16 | 8824.1 | 12.6 | -46.7 | -2.2 | -47.2 | -2.3 |

**Table A-38: Chambers County Raw Measurements M3**

| | | | Linear | | Polynomial | |
|---|---|---|---|---|---|---|
| Date | $R_1$ | $T_1$ | psf | kPa | psf | kPa |
| 8/25/15 | 8722.0 | 24.2 | 0.0 | 0.0 | 0.0 | 0.0 |
| 9/1/15 | 8689.4 | 23.2 | 122.0 | 5.8 | 123.6 | 5.9 |
| 9/15/15 | 8590.8 | 16.4 | 486.1 | 23.3 | 492.3 | 23.6 |
| 10/20/15 | 8662.2 | 8.6 | 206.0 | 9.9 | 208.9 | 10.0 |
| 1/12/16 | 8688.0 | 8.5 | 108.3 | 5.2 | 110.0 | 5.3 |
| 3/31/16 | 8641.7 | 17.1 | 294.5 | 14.1 | 298.4 | 14.3 |
| 4/19/16 | 8665.3 | 16.5 | 204.5 | 9.8 | 207.3 | 9.9 |
| 6/15/16 | 8663.7 | 26.5 | 223.4 | 10.7 | 226.3 | 10.8 |
| 9/13/16 | 8725.7 | 26.1 | -11.5 | -0.6 | -11.7 | -0.6 |
| 11/17/16 | 8748.8 | 10.7 | -118.7 | -5.7 | -120.1 | -5.7 |

**Table A-39: Chambers County Raw Measurements T3**

| | | | Linear | | Polynomial | |
|---|---|---|---|---|---|---|
| Date | $R_1$ | $T_1$ | psf | kPa | psf | kPa |
| 8/25/15 | 8757.4 | 24.7 | 0.0 | 0.0 | 0.0 | 0.0 |
| 9/1/15 | 8672.6 | 23.3 | 312.1 | 14.9 | 317.3 | 15.2 |
| 9/15/15 | 8494.5 | 16.4 | 966.4 | 46.3 | 981.7 | 47.0 |
| 10/20/15 | 8644.4 | 8.6 | 411.8 | 19.7 | 418.6 | 20.0 |
| 1/12/16 | 8736.3 | 8.6 | 73.1 | 3.5 | 74.4 | 3.6 |
| 3/31/16 | 8650.6 | 17.0 | 391.3 | 18.7 | 397.8 | 19.0 |
| 4/19/16 | 8700.1 | 16.5 | 208.8 | 10.0 | 212.3 | 10.2 |
| 6/15/16 | 8702.9 | 26.3 | 201.3 | 9.6 | 204.7 | 9.8 |
| 9/13/16 | 8729.4 | 26.0 | 103.6 | 5.0 | 105.3 | 5.0 |
| 11/17/16 | 8738.1 | 10.5 | 67.0 | 3.2 | 68.2 | 3.3 |

**Table A-40: Chambers County Raw Measurements B4**

| | | | Linear | | Polynomial | |
|---|---|---|---|---|---|---|
| Date | $R_1$ | $T_1$ | psf | kPa | psf | kPa |
| 8/25/15 | 8737.5 | 28.3 | 0.0 | 0.0 | 0.0 | 0.0 |
| 9/1/15 | 8671.4 | 23.1 | 240.9 | 11.5 | 243.0 | 11.6 |
| 9/15/15 | 8733.0 | 16.2 | 4.0 | 0.2 | 4.2 | 0.2 |
| 10/20/15 | 8736.2 | 9.6 | -14.8 | -0.7 | -14.8 | -0.7 |
| 1/12/16 | 8704.6 | 10.4 | 103.8 | 5.0 | 104.9 | 5.0 |
| 3/31/16 | 8703.3 | 16.8 | 115.4 | 5.5 | 116.5 | 5.6 |
| 4/19/16 | 8699.8 | 18.7 | 130.4 | 6.2 | 131.6 | 6.3 |
| 6/15/16 | 8741.0 | 25.1 | -16.4 | -0.8 | -16.5 | -0.8 |
| 9/13/16 | 8748.1 | 25.8 | -42.1 | -2.0 | -42.5 | -2.0 |
| 11/17/16 | 8747.3 | 11.9 | -53.8 | -2.6 | -54.1 | -2.6 |

**Table A-41: Chambers County Raw Measurements M4**

| | | | Linear | | Polynomial | |
|---|---|---|---|---|---|---|
| Date | $R_1$ | $T_1$ | psf | kPa | psf | kPa |
| 8/25/15 | 8814.2 | 27.6 | 0.0 | 0.0 | 0.0 | 0.0 |
| 9/1/15 | 8798.2 | 23.6 | 57.0 | 2.7 | 57.6 | 2.8 |
| 9/15/15 | 8798.0 | 16.7 | 52.8 | 2.5 | 53.4 | 2.6 |
| 10/20/15 | 8821.0 | 8.7 | -39.0 | -1.9 | -39.3 | -1.9 |
| 1/12/16 | 8824.8 | 8.5 | -53.4 | -2.6 | -53.8 | -2.6 |
| 3/31/16 | 8826.4 | 16.9 | -53.3 | -2.6 | -53.8 | -2.6 |
| 4/19/16 | 8819.4 | 19.3 | -25.4 | -1.2 | -25.6 | -1.2 |
| 6/15/16 | 8819.7 | 26.6 | -21.3 | -1.0 | -21.5 | -1.0 |
| 9/13/16 | 8817.6 | 27.1 | -13.1 | -0.6 | -13.2 | -0.6 |
| 11/17/16 | 8828.9 | 9.9 | -67.7 | -3.2 | -68.2 | -3.3 |

**Table A-42: Chambers County Raw Measurements T4**

| | | | Linear | | Polynomial | |
|---|---|---|---|---|---|---|
| Date | $R_1$ | $T_1$ | psf | kPa | psf | kPa |
| 8/25/15 | 8784.0 | 27.2 | 0.0 | 0.0 | 0.0 | 0.0 |
| 9/1/15 | 8740.0 | 23.6 | 164.0 | 7.9 | 165.7 | 7.9 |
| 9/15/15 | 8723.3 | 16.8 | 223.9 | 10.7 | 226.2 | 10.8 |
| 10/20/15 | 8756.4 | 9.0 | 96.0 | 4.6 | 97.1 | 4.6 |
| 1/12/16 | 8766.8 | 9.0 | 56.9 | 2.7 | 57.5 | 2.8 |
| 3/31/16 | 8768.2 | 17.5 | 55.3 | 2.6 | 55.9 | 2.7 |
| 4/19/16 | 8762.2 | 20.0 | 78.9 | 3.8 | 79.8 | 3.8 |
| 6/15/16 | 8762.2 | 26.7 | 81.8 | 3.9 | 82.6 | 4.0 |
| 9/13/16 | 8758.7 | 27.1 | 95.2 | 4.6 | 96.1 | 4.6 |
| 11/17/16 | 8772.1 | 10.4 | 37.6 | 1.8 | 38.0 | 1.8 |

## Table A-43: Chambers County Modulus of Elasticity Data

| | Pour | Break | Pour | Break | Pour | Break | Pour | Break |
|---|---|---|---|---|---|---|---|---|
| Date | 6/2/2015 | 6/30/2015 | 6/8/2015 | 7/6/2015 | 6/16/2015 | 7/14/2015 | 7/1/2015 | 7/29/2015 |
| First Break ($lb_f$) | 130965 | | 132850 | | 118130 | | 125220 | |
| Initial Target ($lb_f$) | 52386 | | 53140 | | 47252 | | 50088 | |
| | Load ($lb_f$) @ 0.00005 | Strain @ Target | Load ($lb_f$) @ 0.00005 | Strain @ Target | Load ($lb_f$) @ 0.00005 | Strain @ Target | Load ($lb_f$) @ 0.00005 | Strain @ Target |
| Trial 2 | 3295 | 0.00950 | 3885 | 0.00880 | 4250 | 0.00815 | 2950 | 0.00875 |
| Trial 3 | 3100 | 0.00955 | 3550 | 0.00880 | 4525 | 0.00820 | 2940 | 0.00910 |
| $E_c$ (ksi) | 3200 | | 3500 | | 3300 | | 3300 | |
| Second Break ($lb_f$) | 119450 | | 136150 | | 127710 | | 125025 | |
| Second Target ($lb_f$) | 50083 | | 53800 | | 49168 | | 50049 | |
| | Load ($lb_f$) @ 0.00005 | Strain @ Target | Load ($lb_f$) @ 0.00005 | Strain @ Target | Load ($lb_f$) @ 0.00005 | Strain @ Target | Load ($lb_f$) @ 0.00005 | Strain @ Target |
| Trial 2 | 4975 | 0.00895 | 3220 | 0.00880 | 2600 | 0.00875 | 4995 | 0.00815 |
| Trial 3 | 4875 | 0.00890 | 2635 | 0.00885 | 2325 | 0.00875 | 5090 | 0.00815 |
| $E_c$ (ksi) | 3150 | | 3600 | | 3350 | | 3450 | |
| Third Break ($lb_f$) | 120700 | | 139145 | | 122065 | | 135680 | |
| $E_c$ (ksi) | 3200 | | 3550 | | 3350 | | 3400 | |
| $f'_c$ (psi) | 4380 | | 4810 | | 4340 | | 4550 | |

## Table A-44: Chambers County Modulus of Elasticity Data

| | Pour | Break | Pour | Break | Pour | Break |
|---|---|---|---|---|---|---|
| Date | 8/24/2015 | 9/23/2015 | 8/27/2015 | 9/24/2015 | 9/9/2015 | 10/7/2015 |
| First Break ($lb_f$) | 93960 | | 110385 | | 137740 | |
| Initial Target ($lb_f$) | 37584 | | 44154 | | 55096 | |
| | Load ($lb_f$) @ 0.00005 | Strain @ Target | Load ($lb_f$) @ 0.00005 | Strain @ Target | Load ($lb_f$) @ 0.00005 | Strain @ Target |
| Trial 2 | 2315 | 0.00700 | 3845 | 0.00745 | 3495 | 0.00940 |
| Trial 3 | 2225 | 0.00700 | 3540 | 0.00790 | 3855 | 0.00960 |
| $E_c$ (ksi) | 3200 | | 3350 | | 3350 | |
| Second Break ($lb_f$) | 88430 | | 111155 | | 120620 | |
| Second Target ($lb_f$) | 36478 | | 44308 | | 51672 | |
| | Load ($lb_f$) @ 0.00005 | Strain @ Target | Load ($lb_f$) @ 0.00005 | Strain @ Target | Load ($lb_f$) @ 0.00005 | Strain @ Target |
| Trial 2 | 4230 | 0.00650 | 3075 | 0.00720 | 2675 | 0.00870 |
| Trial 3 | 4285 | 0.00655 | 2925 | 0.00725 | 2750 | 0.00865 |
| $E_c$ (ksi) | 3200 | | 3650 | | 3500 | |
| Third Break ($lb_f$) | 96840 | | 117066 | | 133465 | |
| $E_c$ (ksi) | 3200 | | 3500 | | 3450 | |
| $f'_c$ (psi) | 3290 | | 3990 | | 4620 | |

## Lee County

### Table A-45: Lee County Raw Measurements B1

| | | | Linear | | Polynomial | |
|---|---|---|---|---|---|---|
| Date | $R_1$ | $T_1$ | psf | kPa | psf | kPa |
| 3/8/16 9:00 AM | 8832.7 | 19.4 | 0.0 | 0.0 | 0.0 | 0.0 |
| 3/22/16 11:00 AM | 8824.5 | 8.9 | 18.7 | 0.9 | 19.1 | 0.9 |
| 4/19/16 2:40 PM | 8732.5 | 16.4 | 347.8 | 16.6 | 353.1 | 16.9 |
| 6/15/16 9:00 AM | 8754.1 | 24.8 | 280.2 | 13.4 | 284.4 | 13.6 |
| 8/29/16 3:15 PM | 7737.5 | 27.0 | 3839.6 | 183.8 | 3883.4 | 185.9 |
| 8/30/16 8:15 AM | 8091.1 | 25.8 | 2601.1 | 124.5 | 2634.2 | 126.1 |
| 8/30/16 10:30 AM | 8054.7 | 25.6 | 2728.3 | 130.6 | 2762.6 | 132.3 |
| 8/31/16 9:00 AM | 8096.1 | 25.7 | 2583.5 | 123.7 | 2616.4 | 125.3 |
| 9/1/16 2:25 PM | 8054.7 | 26.3 | 2728.9 | 130.6 | 2763.3 | 132.3 |
| 9/21/16 1:25 PM | 8121.3 | 24.6 | 2494.3 | 119.4 | 2526.3 | 121.0 |
| 9/27/16 9:30 AM | 8160.0 | 23.7 | 2358.0 | 112.9 | 2388.7 | 114.4 |
| 9/28/16 9:40 AM | 8152.0 | 23.9 | 2386.2 | 114.2 | 2417.1 | 115.7 |
| 9/28/16 10:15 AM | 8150.0 | 23.9 | 2393.2 | 114.6 | 2424.2 | 116.1 |
| 9/29/16 10:01 AM | 8134.0 | 23.0 | 2448.3 | 117.2 | 2479.9 | 118.7 |
| 9/29/16 10:48 AM | 8128.5 | 23.0 | 2467.6 | 118.1 | 2499.4 | 119.7 |
| 10/8/16 12:28 PM | 8180.7 | 23.4 | 2285.3 | 109.4 | 2315.2 | 110.9 |
| 10/13/16 10:45 AM | 8228.2 | 18.1 | 2114.0 | 101.2 | 2142.1 | 102.6 |
| 10/19/16 1:30 PM | 8237.5 | 21.6 | 2084.8 | 99.8 | 2112.5 | 101.2 |
| 10/27/16 6:01 PM | 8267.0 | 19.9 | 1980.0 | 94.8 | 2006.5 | 96.1 |
| 11/4/16 11:43 AM | 8283.3 | 18.5 | 1921.6 | 92.0 | 1947.5 | 93.3 |
| 11/9/16 2:00 PM | 8370.7 | 15.4 | 1612.8 | 77.2 | 1635.2 | 78.3 |
| 11/16/16 4:00 PM | 8372.4 | 14.9 | 1606.4 | 76.9 | 1628.7 | 78.0 |
| 12/1/16 9:00 AM | 8272.8 | 13.4 | 1953.5 | 93.5 | 1979.8 | 94.8 |
| 12/6/16 10:43 AM | 8337.2 | 11.7 | 1726.5 | 82.6 | 1750.3 | 83.8 |
| 12/16/16 10:54 AM | 8283.2 | 9.2 | 1913.1 | 91.6 | 1939.0 | 92.8 |
| 1/9/17 12:50 PM | 8199.5 | 6.8 | 2203.7 | 105.5 | 2232.9 | 106.9 |
| 1/19/17 12:50 PM | 8300.5 | 14.8 | 1857.9 | 88.9 | 1883.1 | 90.2 |
| 1/26/17 12:01 PM | 8256.9 | 13.6 | 2009.3 | 96.2 | 2036.3 | 97.5 |
| 2/2/17 4:18 PM | 8307.2 | 13.7 | 1833.4 | 87.8 | 1858.4 | 89.0 |
| 2/7/17 11:52 AM | 8282.7 | 13.5 | 1918.9 | 91.9 | 1944.9 | 93.1 |

**Table A-46: Lee County Raw Measurements M1**

| | | | Linear | | Polynomial | |
|---|---|---|---|---|---|---|
| Date | $R_1$ | $T_1$ | psf | kPa | psf | kPa |
| 3/8/16 9:00 AM | 8915.3 | 22.9 | 0.0 | 0.0 | 0.0 | 0.0 |
| 3/22/16 11:00 AM | 8906.5 | 8.4 | 22.1 | 1.1 | 22.5 | 1.1 |
| 4/19/16 2:40 PM | 8924.1 | 18.1 | -34.8 | -1.7 | -35.2 | -1.7 |
| 6/15/16 9:00 AM | 8914.8 | 26.8 | 4.4 | 0.2 | 4.4 | 0.2 |
| 8/29/16 3:15 PM | 8778.8 | 28.0 | 494.4 | 23.7 | 500.2 | 23.9 |
| 8/30/16 8:15 AM | 8778.0 | 26.0 | 495.9 | 23.7 | 501.8 | 24.0 |
| 8/30/16 10:30 AM | 8769.9 | 26.3 | 525.3 | 25.1 | 531.4 | 25.4 |
| 8/31/16 9:00 AM | 8784.1 | 26.5 | 474.3 | 22.7 | 479.9 | 23.0 |
| 9/1/16 2:25 PM | 8806.8 | 27.4 | 393.3 | 18.8 | 397.9 | 19.1 |
| 9/21/16 1:25 PM | 8807.3 | 24.6 | 389.6 | 18.7 | 394.2 | 18.9 |
| 9/27/16 9:30 AM | 8791.6 | 24.8 | 446.2 | 21.4 | 451.5 | 21.6 |
| 9/28/16 9:40 AM | 8786.9 | 24.9 | 463.2 | 22.2 | 468.7 | 22.4 |
| 9/28/16 10:15 AM | 8789.4 | 24.9 | 454.2 | 21.7 | 459.6 | 22.0 |
| 9/29/16 10:01 AM | 8794.7 | 23.9 | 434.5 | 20.8 | 439.6 | 21.0 |
| 9/29/16 10:48 AM | 8797.2 | 23.9 | 425.5 | 20.4 | 430.5 | 20.6 |
| 10/8/16 12:28 PM | 8835.5 | 23.9 | 287.7 | 13.8 | 291.2 | 13.9 |
| 10/13/16 10:45 AM | 8787.2 | 18.5 | 457.9 | 21.9 | 463.4 | 22.2 |
| 10/19/16 1:30 PM | 8841.2 | 22.0 | 266.0 | 12.7 | 269.2 | 12.9 |
| 10/27/16 6:01 PM | 8808.9 | 20.8 | 381.3 | 18.3 | 385.9 | 18.5 |
| 11/4/16 11:43 AM | 8830.0 | 18.6 | 304.0 | 14.6 | 307.7 | 14.7 |
| 11/9/16 2:00 PM | 8811.5 | 14.8 | 368.0 | 17.6 | 372.5 | 17.8 |
| 11/16/16 4:00 PM | 8823.2 | 14.6 | 325.8 | 15.6 | 329.8 | 15.8 |
| 12/1/16 9:00 AM | 8808.1 | 12.9 | 379.0 | 18.1 | 383.6 | 18.4 |
| 12/6/16 10:43 AM | 8833.5 | 11.7 | 286.9 | 13.7 | 290.4 | 13.9 |
| 12/16/16 10:54 AM | 8791.0 | 7.4 | 436.9 | 20.9 | 442.2 | 21.2 |
| 1/9/17 12:50 PM | 8760.3 | 3.0 | 544.4 | 26.1 | 551.0 | 26.4 |
| 1/19/17 12:50 PM | 8861.8 | 16.1 | 188.0 | 9.0 | 190.3 | 9.1 |
| 1/26/17 12:01 PM | 8828.2 | 13.9 | 307.4 | 14.7 | 311.1 | 14.9 |
| 2/2/17 4:18 PM | 8847.3 | 15.4 | 239.7 | 11.5 | 242.6 | 11.6 |
| 2/7/17 11:52 AM | 8843.0 | 12.9 | 253.5 | 12.1 | 256.6 | 12.3 |

**Table A-47: Lee County Raw Measurements T1**

| | | | Linear | | Polynomial | |
|---|---|---|---|---|---|---|
| Date | $R_1$ | $T_1$ | psf | kPa | psf | kPa |
| 3/8/16 9:00 AM | 8786.4 | 23.9 | 0.0 | 0.0 | 0.0 | 0.0 |
| 3/22/16 11:00 AM | 8772.4 | 8.4 | 49.2 | 2.4 | 50.0 | 2.4 |
| 4/19/16 2:40 PM | 8790.7 | 18.4 | -14.6 | -0.7 | -14.9 | -0.7 |
| 6/15/16 9:00 AM | 8795.1 | 26.9 | -30.3 | -1.5 | -30.7 | -1.5 |
| 8/29/16 3:15 PM | 8800.9 | 28.1 | -50.4 | -2.4 | -51.2 | -2.5 |
| 8/30/16 8:15 AM | 8797.8 | 26.4 | -39.6 | -1.9 | -40.2 | -1.9 |
| 8/30/16 10:30 AM | 8798.2 | 25.9 | -41.0 | -2.0 | -41.6 | -2.0 |
| 8/31/16 9:00 AM | 8800.3 | 26.5 | -48.3 | -2.3 | -49.0 | -2.3 |
| 9/1/16 2:25 PM | 8804.0 | 27.5 | -61.1 | -2.9 | -62.1 | -3.0 |
| 9/21/16 1:25 PM | 8800.0 | 25.6 | -47.2 | -2.3 | -47.9 | -2.3 |
| 9/27/16 9:30 AM | 8800.0 | 24.5 | -47.1 | -2.3 | -47.9 | -2.3 |
| 9/28/16 9:40 AM | 8800.4 | 24.8 | -48.5 | -2.3 | -49.3 | -2.4 |
| 9/28/16 10:15 AM | 8800.3 | 24.8 | -48.2 | -2.3 | -48.9 | -2.3 |
| 9/29/16 10:01 AM | 8798.8 | 23.6 | -42.9 | -2.1 | -43.6 | -2.1 |
| 9/29/16 10:48 AM | 8798.8 | 23.5 | -42.9 | -2.1 | -43.6 | -2.1 |
| 10/8/16 12:28 PM | 8801.7 | 23.9 | -53.0 | -2.5 | -53.8 | -2.6 |
| 10/13/16 10:45 AM | 8793.8 | 17.9 | -25.4 | -1.2 | -25.7 | -1.2 |
| 10/19/16 1:30 PM | 8798.0 | 21.9 | -40.1 | -1.9 | -40.7 | -1.9 |
| 10/27/16 6:01 PM | 8794.4 | 21.1 | -27.6 | -1.3 | -28.0 | -1.3 |
| 11/4/16 11:43 AM | 8795.1 | 18.3 | -29.9 | -1.4 | -30.3 | -1.5 |
| 11/9/16 2:00 PM | 8796.9 | 14.6 | -35.9 | -1.7 | -36.5 | -1.7 |
| 11/16/16 4:00 PM | 8799.0 | 14.6 | -43.2 | -2.1 | -43.9 | -2.1 |
| 12/1/16 9:00 AM | 8808.1 | 12.9 | -74.7 | -3.6 | -75.8 | -3.6 |
| 12/6/16 10:43 AM | 8803.0 | 11.8 | -56.9 | -2.7 | -57.8 | -2.8 |
| 12/16/16 10:54 AM | 8787.7 | 6.8 | -3.7 | -0.2 | -3.8 | -0.2 |
| 1/9/17 12:50 PM | 8777.5 | 2.5 | 31.8 | 1.5 | 32.3 | 1.5 |
| 1/19/17 12:50 PM | 8802.4 | 16.4 | -55.1 | -2.6 | -55.9 | -2.7 |
| 1/26/17 12:01 PM | 8799.5 | 13.8 | -44.9 | -2.2 | -45.6 | -2.2 |
| 2/2/17 4:18 PM | 8798.8 | 16.3 | -42.6 | -2.0 | -43.3 | -2.1 |
| 2/7/17 11:52 AM | 8801.4 | 12.9 | -51.5 | -2.5 | -52.2 | -2.5 |

**Table A-48: Lee County Raw Measurements B2**

| | | | Linear | | Polynomial | |
|---|---|---|---|---|---|---|
| Date | $R_1$ | $T_1$ | psf | kPa | psf | kPa |
| 3/8/16 9:00 AM | 8871.0 | 21.6 | 0.0 | 0.0 | 0.0 | 0.0 |
| 3/22/16 11:00 AM | 8792.5 | 9.7 | 287.9 | 13.8 | 290.3 | 13.9 |
| 4/19/16 2:40 PM | 8771.3 | 17.9 | 373.0 | 17.9 | 376.1 | 18.0 |
| 6/15/16 9:00 AM | 8787.2 | 25.5 | 318.1 | 15.2 | 320.6 | 15.4 |
| 8/29/16 3:15 PM | 8196.7 | 25.9 | 2541.9 | 121.7 | 2559.3 | 122.6 |
| 8/30/16 8:15 AM | 8318.6 | 25.2 | 2082.5 | 99.7 | 2097.2 | 100.4 |
| 8/30/16 10:30 AM | 8280.1 | 25.0 | 2227.3 | 106.6 | 2242.9 | 107.4 |
| 8/31/16 9:00 AM | 8306.0 | 25.1 | 2129.8 | 102.0 | 2144.9 | 102.7 |
| 9/1/16 2:25 PM | 8319.5 | 25.6 | 2079.3 | 99.6 | 2094.0 | 100.3 |
| 9/21/16 1:25 PM | 8450.2 | 24.2 | 1586.3 | 76.0 | 1597.9 | 76.5 |
| 9/27/16 9:30 AM | 8457.2 | 23.5 | 1559.4 | 74.7 | 1570.9 | 75.2 |
| 9/28/16 9:40 AM | 8464.6 | 23.8 | 1531.8 | 73.3 | 1543.1 | 73.9 |
| 9/28/16 10:15 AM | 8466.5 | 23.7 | 1524.5 | 73.0 | 1535.8 | 73.6 |
| 9/29/16 10:01 AM | 8460.3 | 22.8 | 1547.3 | 74.1 | 1558.7 | 74.7 |
| 9/29/16 10:48 AM | 8460.0 | 22.8 | 1548.4 | 74.1 | 1559.9 | 74.7 |
| 10/8/16 12:28 PM | 8515.0 | 22.8 | 1341.3 | 64.2 | 1351.4 | 64.7 |
| 10/13/16 10:45 AM | 8522.0 | 18.5 | 1312.2 | 62.8 | 1322.1 | 63.3 |
| 10/19/16 1:30 PM | 8524.5 | 20.8 | 1304.3 | 62.4 | 1314.1 | 62.9 |
| 10/27/16 6:01 PM | 8535.1 | 19.7 | 1263.6 | 60.5 | 1273.2 | 61.0 |
| 11/4/16 11:43 AM | 8527.9 | 18.7 | 1290.1 | 61.8 | 1299.8 | 62.3 |
| 11/9/16 2:00 PM | 8585.6 | 15.6 | 1070.8 | 51.3 | 1079.1 | 51.7 |
| 11/16/16 4:00 PM | 8595.1 | 14.4 | 1034.3 | 49.5 | 1042.2 | 49.9 |
| 12/1/16 9:00 AM | 8510.7 | 13.6 | 1351.6 | 64.7 | 1361.7 | 65.2 |
| 12/6/16 10:43 AM | 8552.6 | 12.9 | 1193.3 | 57.1 | 1202.4 | 57.6 |
| 12/16/16 10:54 AM | 8500.1 | 9.2 | 1388.6 | 66.5 | 1399.1 | 67.0 |
| 1/9/17 12:50 PM | 8506.9 | 11.3 | 1364.4 | 65.3 | 1374.7 | 65.8 |
| 1/19/17 12:50 PM | 8463.4 | 15.7 | 1531.0 | 73.3 | 1542.4 | 73.9 |
| 1/26/17 12:01 PM | 8462.1 | 15.2 | 1535.6 | 73.5 | 1547.0 | 74.1 |
| 2/2/17 4:18 PM | 8481.6 | 14.9 | 1462.0 | 70.0 | 1472.9 | 70.5 |
| 2/7/17 11:52 AM | 8502.3 | 14.4 | 1383.7 | 66.3 | 1394.1 | 66.8 |

**Table A-49: Lee County Raw Measurements M2**

| | | | Linear | | Polynomial | |
|---|---|---|---|---|---|---|
| Date | $R_1$ | $T_1$ | psf | kPa | psf | kPa |
| 3/8/16 9:00 AM | 8830.5 | 22.9 | 0.0 | 0.0 | 0.0 | 0.0 |
| 3/22/16 11:00 AM | 8831.4 | 9.2 | -19.6 | -0.9 | -37.5 | -0.9 |
| 4/19/16 2:40 PM | 8834.6 | 19.3 | -19.0 | -0.9 | -100.2 | -0.9 |
| 6/15/16 9:00 AM | 8833.2 | 28.2 | -3.3 | -0.2 | -56.8 | -0.2 |
| 8/29/16 3:15 PM | 8358.7 | 27.5 | 1693.1 | 81.1 | 11041.7 | 82.0 |
| 8/30/16 8:15 AM | 8490.1 | 26.5 | 1221.9 | 58.5 | 7966.3 | 59.2 |
| 8/30/16 10:30 AM | 8439.5 | 25.6 | 1401.8 | 67.1 | 9149.0 | 67.9 |
| 8/31/16 9:00 AM | 8478.5 | 26.5 | 1263.4 | 60.5 | 8237.7 | 61.2 |
| 9/1/16 2:25 PM | 8478.6 | 27.0 | 1263.6 | 60.5 | 8235.9 | 61.2 |
| 9/21/16 1:25 PM | 8577.5 | 25.3 | 907.8 | 43.5 | 5920.3 | 44.0 |
| 9/27/16 9:30 AM | 8584.2 | 24.3 | 882.7 | 42.3 | 5762.4 | 42.8 |
| 9/28/16 9:40 AM | 8580.6 | 24.6 | 895.9 | 42.9 | 5847.0 | 43.4 |
| 9/28/16 10:15 AM | 8582.8 | 24.6 | 888.1 | 42.5 | 5795.5 | 43.0 |
| 9/29/16 10:01 AM | 8588.2 | 23.5 | 867.4 | 41.5 | 5667.9 | 42.0 |
| 9/29/16 10:48 AM | 8590.5 | 23.5 | 859.2 | 41.1 | 5614.1 | 41.6 |
| 10/8/16 12:28 PM | 8609.7 | 23.5 | 790.5 | 37.9 | 5165.0 | 38.3 |
| 10/13/16 10:45 AM | 8634.1 | 17.8 | 696.4 | 33.4 | 4587.4 | 33.7 |
| 10/19/16 1:30 PM | 8620.8 | 21.2 | 748.1 | 35.8 | 4902.6 | 36.2 |
| 10/27/16 6:01 PM | 8605.6 | 20.0 | 801.0 | 38.4 | 5256.7 | 38.8 |
| 11/4/16 11:43 AM | 8631.9 | 18.9 | 705.6 | 33.8 | 4640.2 | 34.2 |
| 11/9/16 2:00 PM | 8681.2 | 14.9 | 524.5 | 25.1 | 3482.2 | 25.4 |
| 11/16/16 4:00 PM | 8668.1 | 13.7 | 569.9 | 27.3 | 3787.2 | 27.6 |
| 12/1/16 9:00 AM | 8621.1 | 13.2 | 737.4 | 35.3 | 4886.0 | 35.7 |
| 12/6/16 10:43 AM | 8668.5 | 11.9 | 566.3 | 27.1 | 3775.7 | 27.4 |
| 12/16/16 10:54 AM | 8709.1 | 7.1 | 415.3 | 19.9 | 2820.3 | 20.1 |
| 1/9/17 12:50 PM | 8730.9 | 3.1 | 332.5 | 15.9 | 2305.7 | 16.1 |
| 1/19/17 12:50 PM | 8622.2 | 15.2 | 735.9 | 35.2 | 4862.6 | 35.7 |
| 1/26/17 12:01 PM | 8608.8 | 13.3 | 781.5 | 37.4 | 5173.8 | 37.9 |
| 2/2/17 4:18 PM | 8605.5 | 13.5 | 793.6 | 38.0 | 5251.2 | 38.5 |
| 2/7/17 11:52 AM | 8620.7 | 12.4 | 737.9 | 35.3 | 4894.4 | 35.8 |

**Table A-50: Lee County Raw Measurements T2**

| | | | Linear | | Polynomial | |
|---|---|---|---|---|---|---|
| Date | $R_1$ | $T_1$ | psf | kPa | psf | kPa |
| 3/8/16 9:00 AM | 8748.3 | 23.3 | 0.0 | 0.0 | 0.0 | 0.0 |
| 3/22/16 11:00 AM | 8748.9 | 9.3 | -4.0 | -0.2 | -4.0 | -0.2 |
| 4/19/16 2:40 PM | 8757.4 | 19.0 | -31.8 | -1.5 | -32.1 | -1.5 |
| 6/15/16 9:00 AM | 8754.3 | 28.3 | -19.9 | -1.0 | -20.1 | -1.0 |
| 8/29/16 3:15 PM | 8561.2 | 27.7 | 642.6 | 30.8 | 648.8 | 31.1 |
| 8/30/16 8:15 AM | 8635.5 | 26.5 | 387.5 | 18.6 | 391.3 | 18.7 |
| 8/30/16 10:30 AM | 8574.5 | 26.3 | 596.8 | 28.6 | 602.5 | 28.8 |
| 8/31/16 9:00 AM | 8623.5 | 26.5 | 428.7 | 20.5 | 432.8 | 20.7 |
| 9/1/16 2:25 PM | 8639.0 | 27.2 | 375.6 | 18.0 | 379.2 | 18.2 |
| 9/21/16 1:25 PM | 8651.3 | 25.3 | 333.1 | 16.0 | 336.4 | 16.1 |
| 9/27/16 9:30 AM | 8666.6 | 24.3 | 280.5 | 13.4 | 283.2 | 13.6 |
| 9/28/16 9:40 AM | 8661.3 | 24.6 | 298.7 | 14.3 | 301.6 | 14.4 |
| 9/28/16 10:15 AM | 8663.2 | 24.5 | 292.2 | 14.0 | 295.0 | 14.1 |
| 9/29/16 10:01 AM | 8677.1 | 23.2 | 244.3 | 11.7 | 246.7 | 11.8 |
| 9/29/16 10:48 AM | 8677.2 | 23.2 | 244.0 | 11.7 | 246.4 | 11.8 |
| 10/8/16 12:28 PM | 8648.6 | 23.6 | 342.2 | 16.4 | 345.5 | 16.5 |
| 10/13/16 10:45 AM | 8691.5 | 27.4 | 195.5 | 9.4 | 197.4 | 9.4 |
| 10/19/16 1:30 PM | 8635.4 | 21.3 | 387.1 | 18.5 | 390.9 | 18.7 |
| 10/27/16 6:01 PM | 8584.1 | 20.4 | 563.1 | 27.0 | 568.5 | 27.2 |
| 11/4/16 11:43 AM | 8603.6 | 18.9 | 495.9 | 23.7 | 500.7 | 24.0 |
| 11/9/16 2:00 PM | 8666.4 | 14.6 | 279.9 | 13.4 | 282.6 | 13.5 |
| 11/16/16 4:00 PM | 8675.2 | 13.9 | 249.6 | 11.9 | 252.0 | 12.1 |
| 12/1/16 9:00 AM | 8643.0 | 12.7 | 359.9 | 17.2 | 363.4 | 17.4 |
| 12/6/16 10:43 AM | 8681.1 | 12.0 | 229.1 | 11.0 | 231.3 | 11.1 |
| 12/16/16 10:54 AM | 8691.8 | 6.4 | 191.6 | 9.2 | 193.5 | 9.3 |
| 1/9/17 12:50 PM | 8695.3 | 2.0 | 179.0 | 8.6 | 180.8 | 8.7 |
| 1/19/17 12:50 PM | 8663.0 | 15.5 | 291.7 | 14.0 | 294.5 | 14.1 |
| 1/26/17 12:01 PM | 8644.7 | 13.1 | 354.1 | 17.0 | 357.6 | 17.1 |
| 2/2/17 4:18 PM | 8659.2 | 14.0 | 304.5 | 14.6 | 307.5 | 14.7 |
| 2/7/17 11:52 AM | 8659.5 | 12.6 | 303.3 | 14.5 | 306.3 | 14.7 |

**Table A-51: Lee County Raw Measurements B3**

| | | | Linear | | Polynomial | |
|---|---|---|---|---|---|---|
| Date | R1 | T1 | psf | kPa | psf | kPa |
| 3/22/16 11:00 AM | 8727.6 | 8.6 | 0.0 | 0.0 | 0.0 | 0.0 |
| 4/19/16 2:40 PM | 8633.3 | 16.6 | 359.4 | 17.2 | 364.1 | 17.4 |
| 6/15/16 9:00 AM | 8674.2 | 26.1 | 225.2 | 10.8 | 227.8 | 10.9 |
| 8/29/16 3:15 PM | 8624.6 | 26.1 | 407.2 | 19.5 | 412.3 | 19.7 |
| 8/30/16 8:15 AM | 8695.7 | 25.0 | 144.4 | 6.9 | 146.1 | 7.0 |
| 8/30/16 10:30 AM | 8693.2 | 24.9 | 153.4 | 7.3 | 155.2 | 7.4 |
| 8/31/16 9:00 AM | 8672.8 | 24.9 | 228.3 | 10.9 | 231.1 | 11.1 |
| 9/1/16 2:25 PM | 8674.1 | 25.7 | 224.9 | 10.8 | 227.6 | 10.9 |
| 9/21/16 1:25 PM | 8679.0 | 24.5 | 204.9 | 9.8 | 207.3 | 9.9 |
| 9/27/16 9:30 AM | 8681.6 | 23.4 | 193.5 | 9.3 | 195.8 | 9.4 |
| 9/28/16 9:40 AM | 8681.1 | 23.4 | 195.3 | 9.4 | 197.7 | 9.5 |
| 9/28/16 10:15 AM | 8680.8 | 23.4 | 196.4 | 9.4 | 198.8 | 9.5 |
| 9/29/16 10:01 AM | 8670.1 | 22.4 | 234.0 | 11.2 | 236.9 | 11.3 |
| 9/29/16 10:48 AM | 8676.3 | 22.5 | 211.4 | 10.1 | 214.0 | 10.2 |
| 10/8/16 12:28 PM | 8664.5 | 22.9 | 255.4 | 12.2 | 258.6 | 12.4 |
| 10/13/16 10:45 AM | 8701.1 | 17.2 | 111.6 | 5.3 | 112.9 | 5.4 |
| 10/19/16 1:30 PM | 8673.7 | 20.6 | 217.8 | 10.4 | 220.5 | 10.6 |
| 10/27/16 6:01 PM | 8672.5 | 18.3 | 218.4 | 10.5 | 221.1 | 10.6 |
| 11/4/16 11:43 AM | 8682.4 | 17.9 | 181.4 | 8.7 | 183.7 | 8.8 |
| 11/9/16 2:00 PM | 8712.3 | 14.8 | 66.5 | 3.2 | 67.3 | 3.2 |
| 11/16/16 4:00 PM | 8713.3 | 13.0 | 59.8 | 2.9 | 60.5 | 2.9 |
| 12/1/16 9:00 AM | 8684.6 | 12.9 | 165.0 | 7.9 | 167.1 | 8.0 |
| 12/6/16 10:43 AM | 8695.0 | 12.4 | 126.0 | 6.0 | 127.6 | 6.1 |
| 12/16/16 10:54 AM | 8705.1 | 8.3 | 82.1 | 3.9 | 83.2 | 4.0 |
| 1/9/17 12:50 PM | 8680.1 | 8.3 | 173.8 | 8.3 | 176.2 | 8.4 |
| 1/19/17 12:50 PM | 8665.6 | 14.9 | 238.0 | 11.4 | 241.1 | 11.5 |
| 1/26/17 12:01 PM | 8653.2 | 13.9 | 281.8 | 13.5 | 285.6 | 13.7 |
| 2/2/17 4:18 PM | 8656.5 | 14.2 | 270.2 | 12.9 | 273.8 | 13.1 |
| 2/7/17 11:52 AM | 8664.0 | 13.3 | 241.2 | 11.6 | 244.4 | 11.7 |

**Table A-52: Lee County Raw Measurements M3**

| | | | Linear | | Polynomial | |
|---|---|---|---|---|---|---|
| Date | $R_1$ | $T_1$ | psf | kPa | psf | kPa |
| 3/22/16 | 8743.0 | 9.5 | 0.0 | 0.0 | 0.0 | 0.0 |
| 4/19/16 | 8711.2 | 17.9 | 116.5 | 5.6 | 117.9 | 5.6 |
| 6/15/16 | 8736.5 | 28.4 | 35.0 | 1.7 | 35.3 | 1.7 |
| 8/29/16 | 8691.2 | 27.5 | 192.6 | 9.2 | 194.8 | 9.3 |
| 8/30/16 | 8750.7 | 25.9 | -16.2 | -0.8 | -16.6 | -0.8 |
| 8/30/16 | 8752.3 | 25.8 | -21.9 | -1.0 | -22.3 | -1.1 |
| 8/31/16 | 8743.1 | 25.7 | 10.2 | 0.5 | 10.2 | 0.5 |
| 9/1/16 | 8739.0 | 26.7 | 25.1 | 1.2 | 25.3 | 1.2 |
| 9/21/16 | 8735.4 | 25.3 | 36.8 | 1.8 | 37.1 | 1.8 |
| 9/27/16 | 8742.5 | 23.9 | 11.1 | 0.5 | 11.1 | 0.5 |
| 9/28/16 | 8743.0 | 23.9 | 9.4 | 0.4 | 9.4 | 0.4 |
| 9/28/16 | 8742.6 | 24.0 | 10.8 | 0.5 | 10.8 | 0.5 |
| 9/29/16 | 8740.9 | 22.5 | 15.8 | 0.8 | 15.9 | 0.8 |
| 9/29/16 | 8750.9 | 22.6 | -19.1 | -0.9 | -19.4 | -0.9 |
| 10/8/16 | 8751.4 | 23.2 | -20.4 | -1.0 | -20.8 | -1.0 |
| 10/13/16 | 8764.5 | 16.5 | -70.5 | -3.4 | -71.5 | -3.4 |
| 10/19/16 | 8766.9 | 21.1 | -75.9 | -3.6 | -77.0 | -3.7 |
| 10/27/16 | 8765.0 | 18.4 | -71.0 | -3.4 | -72.0 | -3.4 |
| 11/4/16 | 8765.5 | 17.8 | -73.2 | -3.5 | -74.2 | -3.5 |
| 11/9/16 | 8766.4 | 14.6 | -78.4 | -3.8 | -79.4 | -3.8 |
| 11/16/16 | 8768.4 | 12.2 | -86.9 | -4.2 | -88.0 | -4.2 |
| 12/1/16 | 8765.8 | 12.4 | -77.7 | -3.7 | -78.7 | -3.8 |
| 12/6/16 | 8772.6 | 11.9 | -101.8 | -4.9 | -103.1 | -4.9 |
| 12/16/16 | 8758.5 | 6.2 | -56.3 | -2.7 | -56.9 | -2.7 |
| 1/9/17 | 8750.2 | 3.0 | -29.4 | -1.4 | -29.7 | -1.4 |
| 1/19/17 | 8738.8 | 15.2 | 18.4 | 0.9 | 18.5 | 0.9 |
| 1/26/17 | 8731.5 | 13.0 | 42.4 | 2.0 | 42.9 | 2.1 |
| 2/2/17 | 8721.2 | 13.2 | 78.5 | 3.8 | 79.5 | 3.8 |
| 2/7/17 | 8738.8 | 12.1 | 16.4 | 0.8 | 16.5 | 0.8 |

**Table A-53: Lee County Raw Measurements T3**

| | | | Linear | | Polynomial | |
|---|---|---|---|---|---|---|
| Date | $R_1$ | $T_1$ | psf | kPa | psf | kPa |
| 3/22/16 11:00 AM | 9028.3 | 10.8 | 0.0 | 0.0 | 0.0 | 0.0 |
| 4/19/16 2:40 PM | 9032.1 | 18.1 | -10.9 | -0.5 | -11.0 | -0.5 |
| 6/15/16 9:00 AM | 9043.4 | 28.6 | -47.2 | -2.3 | -47.8 | -2.3 |
| 8/29/16 3:15 PM | 9040.7 | 28.0 | -37.9 | -1.8 | -38.4 | -1.8 |
| 8/30/16 8:15 AM | 9046.0 | 26.3 | -57.2 | -2.7 | -57.9 | -2.8 |
| 8/30/16 10:30 AM | 9046.1 | 26.0 | -57.7 | -2.8 | -58.4 | -2.8 |
| 8/31/16 9:00 AM | 9048.5 | 25.9 | -66.2 | -3.2 | -67.0 | -3.2 |
| 9/1/16 2:25 PM | 9050.4 | 27.0 | -72.6 | -3.5 | -73.4 | -3.5 |
| 9/21/16 1:25 PM | 9047.2 | 25.4 | -61.8 | -3.0 | -62.5 | -3.0 |
| 9/27/16 9:30 AM | 9049.0 | 24.0 | -68.7 | -3.3 | -69.5 | -3.3 |
| 9/28/16 9:40 AM | 9049.5 | 24.1 | -70.4 | -3.4 | -71.2 | -3.4 |
| 9/28/16 10:15 AM | 9049.5 | 24.1 | -70.4 | -3.4 | -71.2 | -3.4 |
| 9/29/16 10:01 AM | 9048.5 | 22.6 | -67.4 | -3.2 | -68.2 | -3.3 |
| 9/29/16 10:48 AM | 9049.4 | 22.7 | -70.5 | -3.4 | -71.4 | -3.4 |
| 10/8/16 12:28 PM | 9051.9 | 23.5 | -79.1 | -3.8 | -80.0 | -3.8 |
| 10/13/16 10:45 AM | 9045.3 | 16.2 | -58.3 | -2.8 | -58.9 | -2.8 |
| 10/19/16 1:30 PM | 9048.2 | 21.3 | -66.8 | -3.2 | -67.5 | -3.2 |
| 10/27/16 6:01 PM | 9043.4 | 18.5 | -50.8 | -2.4 | -51.3 | -2.5 |
| 11/4/16 11:43 AM | 9047.0 | 17.8 | -63.7 | -3.1 | -64.5 | -3.1 |
| 11/9/16 2:00 PM | 9046.1 | 13.9 | -61.9 | -3.0 | -62.6 | -3.0 |
| 11/16/16 4:00 PM | 9047.2 | 12.1 | -66.4 | -3.2 | -67.2 | -3.2 |
| 12/1/16 9:00 AM | 9045.6 | 12.2 | -60.7 | -2.9 | -61.4 | -2.9 |
| 12/6/16 10:43 AM | 9053.6 | 11.9 | -89.2 | -4.3 | -90.2 | -4.3 |
| 12/16/16 10:54 AM | 9040.9 | 5.8 | -46.3 | -2.2 | -46.8 | -2.2 |
| 1/9/17 12:50 PM | 9032.9 | 2.3 | -19.3 | -0.9 | -19.4 | -0.9 |
| 1/19/17 12:50 PM | 9048.2 | 15.3 | -68.9 | -3.3 | -69.6 | -3.3 |
| 1/26/17 12:01 PM | 9047.3 | 13.1 | -66.4 | -3.2 | -67.2 | -3.2 |
| 2/2/17 4:18 PM | 9042.4 | 13.4 | -49.0 | -2.3 | -49.6 | -2.4 |
| 2/7/17 11:52 AM | 9050.1 | 12.2 | -76.7 | -3.7 | -77.5 | -3.7 |

**Table A-54: Lee County Raw Measurements B4**

| | | | Linear | | Polynomial | |
|---|---|---|---|---|---|---|
| Date | $R_1$ | $T_1$ | psf | kPa | psf | kPa |
| 3/22/16 11:00 AM | 8887.0 | 9.0 | 0.0 | 0.0 | 0.0 | 0.0 |
| 4/19/16 2:40 PM | 8699.8 | 18.7 | 687.1 | 32.9 | 691.0 | 33.1 |
| 6/15/16 9:00 AM | 8798.2 | 25.1 | 329.0 | 15.8 | 331.0 | 15.8 |
| 8/29/16 3:15 PM | 8480.9 | 25.6 | 1489.3 | 71.3 | 1497.4 | 71.7 |
| 8/30/16 8:15 AM | 8597.8 | 25.0 | 1061.7 | 50.8 | 1067.7 | 51.1 |
| 8/30/16 10:30 AM | 8508.0 | 24.9 | 1390.0 | 66.6 | 1397.6 | 66.9 |
| 8/31/16 9:00 AM | 8543.0 | 24.6 | 1261.9 | 60.4 | 1268.9 | 60.7 |
| 9/1/16 2:25 PM | 8548.8 | 25.1 | 1240.9 | 59.4 | 1247.8 | 59.7 |
| 9/21/16 1:25 PM | 8598.2 | 23.7 | 1059.9 | 50.8 | 1065.8 | 51.0 |
| 9/27/16 9:30 AM | 8604.1 | 23.3 | 1038.2 | 49.7 | 1044.1 | 50.0 |
| 9/28/16 9:40 AM | 8607.1 | 23.4 | 1027.3 | 49.2 | 1033.1 | 49.5 |
| 9/28/16 10:15 AM | 8606.3 | 23.3 | 1030.2 | 49.3 | 1036.0 | 49.6 |
| 9/29/16 10:01 AM | 8596.5 | 22.2 | 1065.7 | 51.0 | 1071.7 | 51.3 |
| 9/29/16 10:48 AM | 8595.9 | 22.2 | 1067.9 | 51.1 | 1073.9 | 51.4 |
| 10/8/16 12:28 PM | 8626.0 | 22.0 | 957.8 | 45.9 | 963.2 | 46.1 |
| 10/13/16 10:45 AM | 8606.0 | 16.7 | 1029.5 | 49.3 | 1035.3 | 49.6 |
| 10/19/16 1:30 PM | 8619.2 | 20.1 | 982.1 | 47.0 | 987.7 | 47.3 |
| 10/27/16 6:01 PM | 8621.6 | 18.4 | 972.9 | 46.6 | 978.4 | 46.8 |
| 11/4/16 11:43 AM | 8626.5 | 18.1 | 954.9 | 45.7 | 960.3 | 46.0 |
| 11/9/16 2:00 PM | 8628.1 | 14.8 | 948.1 | 45.4 | 953.5 | 45.6 |
| 11/16/16 4:00 PM | 8638.4 | 13.3 | 910.1 | 43.6 | 915.3 | 43.8 |
| 12/1/16 9:00 AM | 8548.5 | 13.3 | 1238.8 | 59.3 | 1245.7 | 59.6 |
| 12/6/16 10:43 AM | 8533.7 | 12.5 | 1292.7 | 61.9 | 1299.8 | 62.2 |
| 12/16/16 10:54 AM | 8486.0 | 8.4 | 1466.0 | 70.2 | 1474.0 | 70.6 |
| 1/9/17 12:50 PM | 8408.9 | 6.1 | 1747.2 | 83.7 | 1756.6 | 84.1 |
| 1/19/17 12:50 PM | 8557.4 | 14.5 | 1206.6 | 57.8 | 1213.3 | 58.1 |
| 1/26/17 12:01 PM | 8498.3 | 13.4 | 1422.3 | 68.1 | 1430.2 | 68.5 |
| 2/2/17 4:18 PM | 8530.6 | 13.1 | 1304.2 | 62.5 | 1311.4 | 62.8 |
| 2/7/17 11:52 AM | 8527.9 | 12.7 | 1313.9 | 62.9 | 1321.2 | 63.2 |

**Table A-55: Lee County Raw Measurements M4**

| | | | Linear | | Polynomial | |
|---|---|---|---|---|---|---|
| Date | $R_1$ | $T_1$ | psf | kPa | psf | kPa |
| 3/22/16 11:00 AM | 8825.0 | 12.3 | 0.0 | 0.0 | 0.0 | 0.0 |
| 4/19/16 2:40 PM | 8842.2 | 18.3 | -54.2 | -2.6 | -54.6 | -2.6 |
| 6/15/16 9:00 AM | 8832.0 | 27.2 | -5.4 | -0.3 | -5.6 | -0.3 |
| 8/29/16 3:15 PM | 8793.3 | 27.6 | 135.1 | 6.5 | 135.8 | 6.5 |
| 8/30/16 8:15 AM | 8807.9 | 26.2 | 80.4 | 3.8 | 80.8 | 3.9 |
| 8/30/16 10:30 AM | 8794.6 | 25.9 | 128.1 | 6.1 | 128.8 | 6.2 |
| 8/31/16 9:00 AM | 8799.0 | 25.8 | 112.0 | 5.4 | 112.7 | 5.4 |
| 9/1/16 2:25 PM | 8804.0 | 26.8 | 95.3 | 4.6 | 95.8 | 4.6 |
| 9/21/16 1:25 PM | 8813.5 | 24.9 | 58.4 | 2.8 | 58.7 | 2.8 |
| 9/27/16 9:30 AM | 8813.0 | 23.9 | 58.9 | 2.8 | 59.2 | 2.8 |
| 9/28/16 9:40 AM | 8813.2 | 24.0 | 58.3 | 2.8 | 58.6 | 2.8 |
| 9/28/16 10:15 AM | 8814.0 | 23.9 | 55.3 | 2.6 | 55.5 | 2.7 |
| 9/29/16 10:01 AM | 8812.4 | 22.5 | 59.2 | 2.8 | 59.5 | 2.8 |
| 9/29/16 10:48 AM | 8813.5 | 22.5 | 55.2 | 2.6 | 55.5 | 2.7 |
| 10/8/16 12:28 PM | 8816.3 | 22.6 | 45.2 | 2.2 | 45.4 | 2.2 |
| 10/13/16 10:45 AM | 8812.2 | 15.6 | 50.7 | 2.4 | 51.0 | 2.4 |
| 10/19/16 1:30 PM | 8814.3 | 20.5 | 49.6 | 2.4 | 49.9 | 2.4 |
| 10/27/16 6:01 PM | 8808.1 | 18.7 | 69.7 | 3.3 | 70.1 | 3.4 |
| 11/4/16 11:43 AM | 8812.2 | 18.3 | 54.3 | 2.6 | 54.6 | 2.6 |
| 11/9/16 2:00 PM | 8816.0 | 14.1 | 34.9 | 1.7 | 35.2 | 1.7 |
| 11/16/16 4:00 PM | 8816.0 | 12.9 | 33.3 | 1.6 | 33.6 | 1.6 |
| 12/1/16 9:00 AM | 8788.9 | 12.4 | 130.7 | 6.3 | 131.5 | 6.3 |
| 12/6/16 10:43 AM | 8791.8 | 11.8 | 119.4 | 5.7 | 120.2 | 5.8 |
| 12/16/16 10:54 AM | 8778.8 | 6.1 | 158.8 | 7.6 | 159.9 | 7.7 |
| 1/9/17 12:50 PM | 8770.0 | 1.9 | 185.0 | 8.9 | 186.3 | 8.9 |
| 1/19/17 12:50 PM | 8795.1 | 14.9 | 111.6 | 5.3 | 112.3 | 5.4 |
| 1/26/17 12:01 PM | 8782.4 | 12.5 | 154.3 | 7.4 | 155.3 | 7.4 |
| 2/2/17 4:18 PM | 8780.2 | 12.7 | 162.5 | 7.8 | 163.6 | 7.8 |
| 2/7/17 11:52 AM | 8782.5 | 11.9 | 153.1 | 7.3 | 154.2 | 7.4 |

**Table A-56: Lee County Raw Measurements T4**

| | | | Linear | | Polynomial | |
|---|---|---|---|---|---|---|
| Date | $R_1$ | $T_1$ | psf | kPa | psf | kPa |
| 3/22/16 11:00 AM | 8801.3 | 14.3 | 0.0 | 0.0 | 0.0 | 0.0 |
| 4/19/16 2:40 PM | 8812.2 | 18.2 | -34.7 | -1.7 | -35.2 | -1.7 |
| 6/15/16 9:00 AM | 8808.4 | 27.3 | -12.2 | -0.6 | -12.5 | -0.6 |
| 8/29/16 3:15 PM | 8794.1 | 27.8 | 38.9 | 1.9 | 39.2 | 1.9 |
| 8/30/16 8:15 AM | 8799.1 | 26.4 | 19.8 | 0.9 | 19.9 | 1.0 |
| 8/30/16 10:30 AM | 8791.5 | 26.0 | 46.3 | 2.2 | 46.8 | 2.2 |
| 8/31/16 9:00 AM | 8793.5 | 26.0 | 39.2 | 1.9 | 39.6 | 1.9 |
| 9/1/16 2:25 PM | 8794.9 | 26.9 | 35.2 | 1.7 | 35.5 | 1.7 |
| 9/21/16 1:25 PM | 8796.2 | 24.8 | 28.5 | 1.4 | 28.7 | 1.4 |
| 9/27/16 9:30 AM | 8798.0 | 24.0 | 21.3 | 1.0 | 21.5 | 1.0 |
| 9/28/16 9:40 AM | 8798.2 | 24.0 | 20.6 | 1.0 | 20.8 | 1.0 |
| 9/28/16 10:15 AM | 8798.5 | 24.0 | 19.5 | 0.9 | 19.7 | 0.9 |
| 9/29/16 10:01 AM | 8799.1 | 22.7 | 16.1 | 0.8 | 16.2 | 0.8 |
| 9/29/16 10:48 AM | 8799.8 | 22.6 | 13.6 | 0.6 | 13.6 | 0.7 |
| 10/8/16 12:28 PM | 8800.4 | 22.6 | 11.4 | 0.5 | 11.5 | 0.5 |
| 10/13/16 10:45 AM | 8799.6 | 15.8 | 7.5 | 0.4 | 7.6 | 0.4 |
| 10/19/16 1:30 PM | 8804.0 | 20.5 | -3.4 | -0.2 | -3.5 | -0.2 |
| 10/27/16 6:01 PM | 8797.5 | 18.5 | 17.6 | 0.8 | 17.8 | 0.9 |
| 11/4/16 11:43 AM | 8802.0 | 18.2 | 1.4 | 0.1 | 1.4 | 0.1 |
| 11/9/16 2:00 PM | 8800.8 | 13.7 | 1.2 | 0.1 | 1.2 | 0.1 |
| 11/16/16 4:00 PM | 8800.4 | 12.9 | 1.8 | 0.1 | 1.8 | 0.1 |
| 12/1/16 9:00 AM | 8785.4 | 12.5 | 54.4 | 2.6 | 55.2 | 2.6 |
| 12/6/16 10:43 AM | 8793.4 | 11.7 | 25.3 | 1.2 | 25.7 | 1.2 |
| 12/16/16 10:54 AM | 8766.3 | 5.6 | 115.1 | 5.5 | 116.8 | 5.6 |
| 1/9/17 12:50 PM | 8759.0 | 1.3 | 136.6 | 6.5 | 138.7 | 6.6 |
| 1/19/17 12:50 PM | 8787.4 | 15.0 | 49.8 | 2.4 | 50.5 | 2.4 |
| 1/26/17 12:01 PM | 8775.0 | 12.4 | 91.1 | 4.4 | 92.4 | 4.4 |
| 2/2/17 4:18 PM | 8772.9 | 12.6 | 98.7 | 4.7 | 100.1 | 4.8 |
| 2/7/17 11:52 AM | 8780.1 | 11.9 | 72.6 | 3.5 | 73.6 | 3.5 |

### Table A-57: Lee County Modulus of Elasticity Data

| | Pour | Break | Pour | Break | Pour | Break |
|---|---|---|---|---|---|---|
| Date | 2/26/2016 | 3/25/2016 | 3/8/2016 | 4/5/2016 | 3/21/2016 | 4/18/2016 |
| | | | | | | |
| First Break ($lb_f$) | 132590 | | 152565 | | 161310 | |
| Initial Target ($lb_f$) | 53036 | | 61026 | | 64524 | |
| | **Load ($lb_f$) @ 0.00005** | **Strain @ Target** | **Load ($lb_f$) @ 0.00005** | **Strain @ Target** | **Load ($lb_f$) @ 0.00005** | **Strain @ Target** |
| Trial 2 | 7795 | 0.00595 | 6430 | 0.00585 | 6550 | 0.00560 |
| Trial 3 | 8000 | 0.00585 | 9750 | 0.00565 | 6720 | 0.00560 |
| **$E_c$ (ksi)** | **5000** | | **6050** | | **6850** | |
| | | | | | | |
| Second Break ($lb_f$) | 124055 | | 144675 | | 167660 | |
| Second Target ($lb_f$) | 51329 | | 59448 | | 65794 | |
| | **Load ($lb_f$) @ 0.00005** | **Strain @ Target** | **Load ($lb_f$) @ 0.00005** | **Strain @ Target** | **Load ($lb_f$) @ 0.00005** | **Strain @ Target** |
| Trial 2 | 6685 | 0.00560 | 8630 | 0.00575 | 6160 | 0.00600 |
| Trial 3 | 6800 | 0.00560 | 8470 | 0.00570 | 5550 | 0.00610 |
| **$E_c$ (ksi)** | **5250** | | **5850** | | **6450** | |
| | | | | | | |
| Third Break ($lb_f$) | 135680 | | 142910 | | 176695 | |
| **$E_c$ (ksi)** | **5150** | | **5950** | | **6650** | |
| **$f'_c$ (psi)** | **4630** | | **5190** | | **5960** | |

## Coosa County

### Table A-58: Coosa County Raw Measurements B1

| | | | Linear | | Polynomial | |
|---|---|---|---|---|---|---|
| Date | $R_1$ | $T_1$ | psf | kPa | psf | kPa |
| 5/5/16 9:00 AM | 8828.2 | 23.3 | 0.0 | 0.0 | 0.0 | 0.0 |
| 6/15/16 12:33 PM | 8744.6 | 24.7 | 301.9 | 14.5 | 305.6 | 14.6 |
| 10/8/16 2:07 PM | 8733.3 | 25.7 | 343.7 | 16.5 | 347.8 | 16.7 |
| 11/7/16 4:20 PM | 8784.0 | 23.7 | 159.3 | 7.6 | 161.2 | 7.7 |
| 1/27/17 5:07 PM | 8687.0 | 13.6 | 496.3 | 23.8 | 502.4 | 24.1 |
| 1/29/17 1:48 PM | 8670.5 | 12.5 | 554.3 | 26.5 | 561.1 | 26.9 |

**Table A-59: Coosa County Raw Measurements M1**

| | | | Linear | | Polynomial | |
|---|---|---|---|---|---|---|
| Date | $R_1$ | $T_1$ | psf | kPa | psf | kPa |
| 5/5/16 9:00 AM | 9012.9 | 20.0 | 0.0 | 0.0 | 0.0 | 0.0 |
| 6/15/16 12:33 PM | 8902.2 | 26.6 | 409.5 | 19.6 | 414.5 | 19.8 |
| 10/8/16 2:07 PM | 8948.6 | 26.7 | 239.3 | 11.5 | 242.3 | 11.6 |
| 11/7/16 4:20 PM | 8939.5 | 24.0 | 271.3 | 13.0 | 274.7 | 13.2 |
| 1/27/17 5:07 PM | 8852.4 | 14.4 | 585.7 | 28.0 | 593.0 | 28.4 |
| 1/29/17 1:48 PM | 8851.7 | 11.7 | 586.9 | 28.1 | 594.1 | 28.4 |

**Table A-60: Coosa County Raw Measurements T1**

| | | | Linear | | Polynomial | |
|---|---|---|---|---|---|---|
| Date | $R_1$ | $T_1$ | psf | kPa | psf | kPa |
| 5/5/16 9:00 AM | 8817.6 | 21.0 | 0.0 | 0.0 | 0.0 | 0.0 |
| 6/15/16 12:33 PM | 8725.7 | 26.9 | 354.3 | 17.0 | 359.3 | 17.2 |
| 10/8/16 2:07 PM | 8830.5 | 27.0 | -35.0 | -1.7 | -35.8 | -1.7 |
| 11/7/16 4:20 PM | 8805.3 | 23.5 | 51.1 | 2.4 | 51.8 | 2.5 |
| 1/27/17 5:07 PM | 8546.9 | 13.6 | 990.2 | 47.4 | 1004.2 | 48.1 |
| 1/29/17 1:48 PM | 8783.0 | 105.5 | 310.4 | 14.9 | 312.3 | 15.0 |

**Table A-61: Coosa County Raw Measurements B2**

| | | | Linear | | Polynomial | |
|---|---|---|---|---|---|---|
| Date | $R_1$ | $T_1$ | psf | kPa | psf | kPa |
| 6/15/16 12:33 PM | 8663.2 | 25.6 | 0.0 | 0.0 | 0.0 | 0.0 |
| 10/8/16 2:07 PM | 8670.5 | 22.6 | -28.0 | -1.3 | -28.3 | -1.4 |
| 11/7/16 4:20 PM | 8689.6 | 18.0 | -99.7 | -4.8 | -100.8 | -4.8 |
| 1/27/17 5:07 PM | 8625.7 | 10.4 | 130.3 | 6.2 | 131.7 | 6.3 |
| 1/29/17 1:48 PM | 8640.0 | 8.5 | 77.2 | 3.7 | 78.1 | 3.7 |

**Table A-62: Coosa County Raw Measurements M2**

| | | | Linear | | Polynomial | |
|---|---|---|---|---|---|---|
| Date | $R_1$ | $T_1$ | psf | kPa | psf | kPa |
| 6/15/16 12:33 PM | 8707.5 | 28.0 | 0.0 | 0.0 | 0.0 | 0.0 |
| 10/8/16 2:07 PM | 8741.5 | 23.0 | -131.5 | -6.3 | -132.9 | -6.4 |
| 11/7/16 4:20 PM | 8769.5 | 18.6 | -240.0 | -11.5 | -242.5 | -11.6 |
| 1/27/17 5:07 PM | 8655.4 | 9.9 | 192.1 | 9.2 | 194.2 | 9.3 |
| 1/29/17 1:48 PM | 8626.4 | 7.5 | 301.8 | 14.5 | 305.1 | 14.6 |

## Table A-63: Coosa County Raw Measurements T2

| | | | Linear | | Polynomial | |
|---|---|---|---|---|---|---|
| Date | $R_1$ | $T_1$ | psf | kPa | psf | kPa |
| 6/15/16 12:33 PM | 8828.2 | 27.2 | 0.0 | 0.0 | 0.0 | 0.0 |
| 10/8/16 2:07 PM | 8841.5 | 23.3 | -52.0 | -2.5 | -52.6 | -2.5 |
| 11/7/16 4:20 PM | 8839.6 | 18.6 | -49.0 | -2.3 | -49.5 | -2.4 |
| 1/27/17 5:07 PM | 8816.1 | 9.6 | 29.7 | 1.4 | 30.2 | 1.4 |
| 1/29/17 1:48 PM | 8829.9 | 7.1 | -23.0 | -1.1 | -23.1 | -1.1 |

## Table A-64: Coosa County Modulus of Elasticity Data

| | Pour | Break | Pour | Break | Pour | Break | Pour | Break |
|---|---|---|---|---|---|---|---|---|
| Date | 4/7/2016 | 5/5/2016 | 4/14/2016 | 5/12/2016 | 5/4/2016 | 6/1/2016 | 5/9/2016 | 6/6/2016 |
| | | | | | | | | |
| First Break ($lb_f$) | 135470 | | 143065 | | 147840 | | 170440 | |
| Initial Target ($lb_f$) | 54188 | | 57226 | | 59136 | | 68176 | |
| | **Load ($lb_f$) @ 0.00005** | **Strain @ Target** | **Load ($lb_f$) @ 0.00005** | **Strain @ Target** | **Load ($lb_f$) @ 0.00005** | **Strain @ Target** | **Load ($lb_f$) @ 0.00005** | **Strain @ Target** |
| Trial 2 | 4470 | 0.00715 | 5540 | 0.00705 | 7270 | 0.00655 | 7980 | 0.00740 |
| Trial 3 | 4400 | 0.00720 | 5835 | 0.00710 | 7025 | 0.00650 | 7650 | 0.00745 |
| **$E_c$ (ksi)** | **4400** | | **4650** | | **5150** | | **5150** | |
| | | | | | | | | |
| Second Break ($lb_f$) | 131380 | | 145135 | | 150475 | | 169470 | |
| Second Target ($lb_f$) | 53370 | | 57640 | | 59663 | | 67982 | |
| | **Load ($lb_f$) @ 0.00005** | **Strain @ Target** | **Load ($lb_f$) @ 0.00005** | **Strain @ Target** | **Load ($lb_f$) @ 0.00005** | **Strain @ Target** | **Load ($lb_f$) @ 0.00005** | **Strain @ Target** |
| Trial 2 | 5480 | 0.00660 | 7210 | 0.00660 | 3820 | 0.00715 | 6315 | 0.00745 |
| Trial 3 | 5240 | 0.00660 | 6240 | 0.00655 | 3445 | 0.00710 | 6445 | 0.00745 |
| **$E_c$ (ksi)** | **4700** | | **5000** | | **5000** | | **5250** | |
| | | | | | | | | |
| Third Break ($lb_f$) | 135355 | | 142360 | | 150940 | | 172575 | |
| **$E_c$ (ksi)** | **4550** | | **4850** | | **5100** | | **5200** | |
| **$f'_c$ (psi)** | **4740** | | **5080** | | **5300** | | **6040** | |